

Universidade de Brasília

Instituto de Geociências

Programa de Pós-Graduação em Geociências Aplicadas e Geodinâmica

Tese no: 089

Variability of the tropical hydroclimate across the Americas: from continental to local scales

Paula Ribeiro Bianchini

Advisor: Prof. Dr. Elder Yokoyama (IG/UnB)

Co-advisor: Prof. Dr. Luciana F. Prado (FAOC/UERJ)

Brasilia/DF

August/2025



Universidade de Brasília

Instituto de Geociências

Programa de Pós-Graduação em Geociências Aplicadas e Geodinâmica

Tese n°: 089

Variability of the tropical hydroclimate across the Americas: from continental to local scales

Variabilidade do hidroclima tropical nas Américas: da escala continental à local

Paula Ribeiro Bianchini

Thesis submitted to the Instituto de Goeciências from the Universidade de Brasília to obtain the title of Doctor in the Programa de Pós Graduação em Geociências e Geodinâmica

Comissão Examinadora:

Prof. Dr. Elder Yokoyama (Advisor - IG/UnB)

Profa. Dra. Marilia Shimizu (INPE)

Prof. Dr. Caio Moraes (FAOC/UERJ)

Prof. Dr. Valdir Novello (IGUnB)

Brasília/DF

August/2025

Ficha catalográfica elaborada automaticamente, com os dados fornecidos pelo(a) autor(a)

Bianchini, Paula

Variability of the tropical hydroclimate across the Americas: from continental to local scales / Paula Bianchini; orientador Elder Yokoyama; co-orientador Luciana Prado. Brasília, 2025.
211 p.

Tese(Doutorado em Geociências Aplicadas) Universidade de Brasília, 2025.

1. Américas Tropicais. 2. Sistema de Monção Americana. 3. Paleoregistros. 4. Comparação dado modelo. 5. Precipitação. I. Yokoyama, Elder, orient. II. Prado, Luciana, co-orient.

Bv

ACKNOWLEDGEMENTS

I would like to thank all the people who contributed to this work, especially:

To my advisor Prof. Dr. Elder Yokoyama, for all the years of work and teaching.

To my advisor Profa. Dra. Luciana Prado for all your patience and for all the teachings. I appreciate each conversation, discussion and learning moment.

To the entire IGD-UnB team and to all my graduate colleagues.

To my family, my base, who have always been there and supported me. I especially thank my mother Márcia, for being my best friend and for all the patience in these last years, my father Paulo and my brother Pedro, for all the support.

To Mateus Augusto for all the affection and patience, for having been my support in difficult times and for standing up when I thought I was not going to make it.

To Coordenação de Aperfeiçoamento de Pessoal de Nível Superior - Brasil (CAPES) for the partial financial support - Finance Code 001 001 (88887.642819/2021-00).

Variabilidade do hidroclima tropical nas Américas: da escala continental à local

Resumo

A variabilidade climática desempenhou um papel fundamental na formação das sociedades e ecossistemas humanos ao longo da história, com os padrões de precipitação nas Américas Tropicais (AT) sendo especialmente importantes devido ao seu papel central no sistema climático global. Esta tese investiga a variabilidade hidroclimática na região AT durante o Holoceno (~11.700 anos AP) em três escalas espaciais — continental, regional e local destacando a influência do Sistema de Monções Americano (SMA), da Zona de Convergência Intertropical (ZCIT) e da Zona de Convergência do Atlântico Sul (ZCAS). Utilizando uma combinação de proxies paleoclimáticos (por exemplo, sedimentos lacustres, espeleotemas), dados observacionais e dados da simulação TraCE-21ka, o estudo identifica as principais variações nos padrões de precipitação na região, incluindo o deslocamento da ZCIT e da ZCAS, o enfraquecimento do Sistema de Monções Norte-Americano (SMNA) e o fortalecimento do Sistema de Monções Sul-Americano (SMSA). Resultados de análises em escala continental revelam tendências amplas nos padrões de precipitação no Holoceno, enquanto estudos regionais refinam essas tendências, destacando a variabilidade espacial na América do Sul (AS), particularmente na Amazônia, no nordeste do Brasil e no Sul da AS. A análise em escala local de testemunho de sedimento lacustre da Lagoa Feia, no Cerrado Brasileiro, fornece evidências detalhadas de mudanças na vegetação, eventos de incêndio e ações humanas. Juntas, essas análises multiescala demonstram a interconexão de fatores climáticos de larga escala e respostas ambientais localizadas. Os resultados enfatizam a importância da integração de dados proxy com a modelagem para aprimorar a compreensão de climas passados, o que é crucial para aprimorar as previsões climáticas futuras, gerenciar recursos hídricos e apoiar estratégias de adaptação climática.

Palavras-chave: Américas Tropicais, América do Sul, Cerrado, precipitação, Sistema de Monção Americana, paleoregistros, comparação dado modelo.

Abstract

Climate variability has played a fundamental role in shaping human societies and ecosystems throughout history, with precipitation patterns in the Tropical Americas (TA) being especially important due to their central role in the global climate system. This thesis investigates hydroclimatic variability in the TA region during the Holocene (~11,700 years BP) at three spatial scales—continental, regional, and local—highlighting the influence of the American Monsoon System (AMS), the Intertropical Convergence Zone (ITCZ), and the South Atlantic Convergence Zone (SACZ). Using a combination of paleoclimatic proxies (e.g., lake sediments, speleothems), observational data, and data from the TraCE-21ka simulation, the study identifies major variations in precipitation patterns in the region, including the shift of the ITCZ and SACZ, the weakening of the North American Monsoon System (NAMS), and the strengthening of the South American Monsoon System (SAMS). Results from continental-scale analyses reveal broad trends in Holocene precipitation patterns, while regional studies refine these trends, highlighting spatial variability in South America (SA), particularly in the Amazon, northeastern Brazil, and southern SA. Localscale analysis of lake sediment cores from Lagoa Feia in the Brazilian Cerrado provides detailed evidence of vegetation changes, fire events, and human actions. Together, these multiscale analyses demonstrate the interconnection of large-scale climate drivers and localized environmental responses. The results emphasize the importance of integrating proxy data with modeling to improve understanding of past climates, which is crucial for improving future climate predictions, managing water resources, and supporting climate adaptation strategies.

Keywords: Tropical Americas, South America, Cerrado, precipitation, American Monsoon System, paleorecords, model comparison.

Summary

ntroduction	1
recipitation patterns and variability in Tropical Americas during the Holocer	1e7
Abstract	7
1. Introduction	8
2. Data and methods	9
2.1. Historical climate	9
2.2. Holocene climate	10
3. Results	14
3.1. Historical climate	14
3.2. Holocene climate	16
4. Discussion	25
4.1. Holocene precipitation reconstruction by paleorecords and model outputs.	25
4.2. Variability	27
5. Conclusions	29
Declaration of competing interest	30
ACKNOWLEDGEMENTS	30
Appendix A.Supplementary data	30
Data availability	31
References	31
fully calibrated and updated mid-Holocene climate reconstruction	n for
astern South America	39
Abstract	39
1. Introduction	40
2. Material and Methods	45
2.1. Proxies and Paleoarchives	45
2.2. Data and material	46

2.3. Calibration	47/
2.4. Quality index	48
3. Results	50
3.1. Age calibration	50
3.2. Precipitation	50
3.3. Temperature, lake levels and salinity	56
4. Discussion	60
4.1. The NSF transition zone	63
5. Conclusion	65
Author Contributions	67
Declaration of competing interest	68
Acknowledgments	68
	68
Appendix A. Supplementary data	
Appendix A. Supplementary data References	68
References	
References Long-and shor-term vegetation change and inferred of	elimate dynamics and
References Long-and shor-term vegetation change and inferred counthropogenic activity in the central Cerrado during the Hole	elimate dynamics and ocene82
References	elimate dynamics and ocene82
References Long-and shor-term vegetation change and inferred counthropogenic activity in the central Cerrado during the Hole	elimate dynamics and ocene82
References	elimate dynamics and ocene
References Long-and shor-term vegetation change and inferred conthropogenic activity in the central Cerrado during the Hole Abstract Introduction	elimate dynamics and ocene
References	82
References Long-and shor-term vegetation change and inferred of anthropogenic activity in the central Cerrado during the Hole Abstract Introduction Material and methods Study area Modern vegetation Sampling and chronology Analytical protocols Results Palynological analyses XRF analyses	climate dynamics and ocene 82

Discussion	99
Expansion of the arboreal cerrado in central Brazil	99
Climatic drivers of vegetation changes in central Brazil	102
Fire events in central Brazil	106
Conclusions	109
Acknowledgements	110
Conflict of interest	110
Author contributions	110
Data availability statement	110
Supporting information	110
Supporting information	111
References	111
Integrative discussion and final remaks	121
References	126
Appendices	137
Appendix I	138
Appendix II	166
Appendix III	189

Introduction

Climate variations have long driven human biological and social evolution, contributing to the rise and collapse of different civilizations throughout human history, as they have influenced humans' ability to produce products at the levels needed to sustain them (Brevik et al., 2018; Gowdy, 2020). These climate variations can alter the spatiotemporal patterns of precipitation over the continents (intensity, frequency, duration and amount of precipitation), and the magnitude of these changes directly affects ecosystems and people's lives around the world (Carvalho, 2020; Jackson et al., 1996; Trenberth & Otto-Bliesner, 2003).

The Tropical Americas (TA) span parts of both hemispheres with a very complex hydrological cycle, and the hydroclimatological conditions in this region play a crucial role in the global climate system (Ait Brahim et al., 2022; Carvalho, 2020). The climate system in the TA is dominated by changes in precipitation that are mainly related to the development of a monsoon system (Geen et al., 2020a), and the regional characteristics of this precipitation imply different levels of vulnerability to extreme events (Costa et al., 2023; Palomino-Lemus et al., 2018).

South America (SA) has a wide variety of climates, soil types and ecological environments (Pinto et al., 2008). As in other regions of the TA, SA has an economy strongly based on agricultural production, is highly dependent on hydroelectric generation and has constantly suffered from extreme weather events that cause enormous socioeconomic damage (Torres & Marengo, 2013).

The Brazilian Cerrado is the second largest biome in SA, occupying approximately 2 million km² (Diniz et al., 2010; Oliveira & Marquiss R. J., 2002). The Cerrado is located, for the most part, in the Central Plateau of Brazil, standing out for its high diversity and degree of endemism, and for playing an important role in the production of water for the Amazon rivers, since numerous hydrographic basins of the Amazon Basin originate in the Cerrado region (Cardoso Da Silva & Bates, 2022; Werneck, 2011). Despite its importance, the Cerrado is the biodiversity hotspot with the highest deforestation rates in Brazil, as well as the largest number of forest fires and burned areas, indicating the accelerated pace of destruction of this ecosystem (Strassburg et al., 2017; Vieira et al., 2022).

The climate system in the TA region is dominated by changes in precipitation that are mainly related to the development of a monsoon system (Geen et al., 2020b). These systems are characterized by a rainy summer and drier winter, are accompanied by a seasonal reversal of the prevailing winds and occur in response to seasonal changes in the thermal contrast between the continent and adjacent oceanic regions (Geen et al., 2020b; Vera et al., 2006). In the American continent, the present monsoon system is called the American Monsoon System (AMS), which is composed of the North American Monsoon System (NAMS) (Figure 1. a) and the South American Monsoon System (SAMS) (Figure 1. b) (Figueroa & Nobre, 1990; Higgins et al., 1997; Vera et al., 2006).

The AMS is responsible for more than 50% of the total annual precipitation during the summer in the respective hemispheres, although precipitation values in the Southern Hemisphere (SH) are slightly higher (Figueroa & Nobre, 1990; Higgins et al., 1997; Vera et al., 2006). This system encompasses the Intertropical Convergence Zone (ITCZ) in both hemispheres and the South Atlantic Convergence Zone (SACZ) in the SH (Fu et al., 2016; Mechoso et al., 2004; S. Silva & E., 2012). The influence of the AMS on the rainfall regime of this region and the regional characteristics of this precipitation implies different levels of vulnerability to extreme events (Costa et al., 2023; Palomino-Lemus et al., 2018).

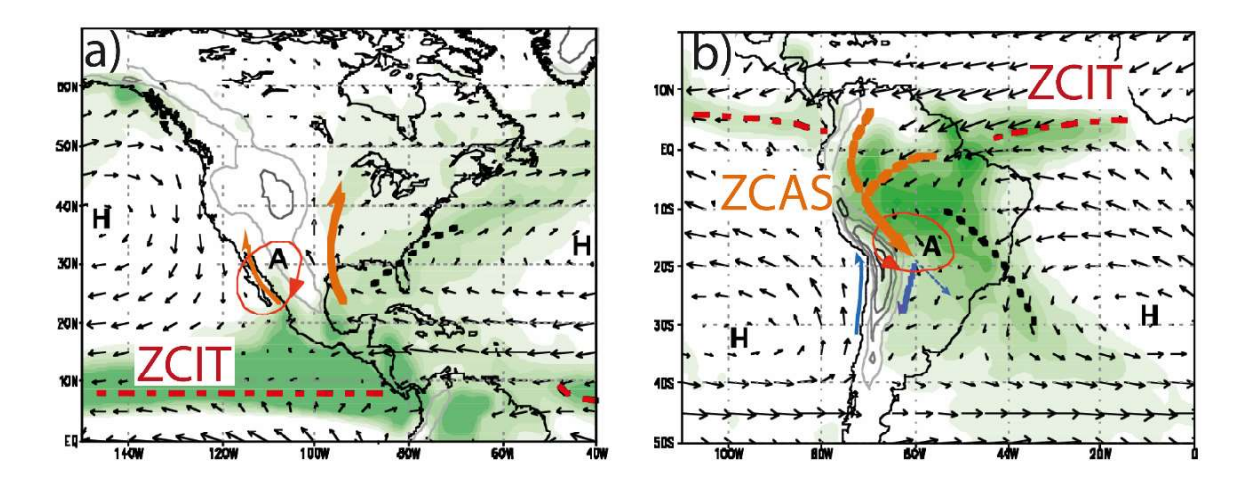


Figure 1. Schematic illustration of a) North American Monsoon System; and b) South American Monsoon System. "H" indicates the subtropical high pressure at the surface, and an "A" indicates the upper-level anticyclone related to the monsoon (adapted from Mechoso et al., 2004).

The study of climate variations in the TA, in the SA and in the Brazilian Cerrado allows a better understanding of the influence of the AMS, the ITCZ and the SACZ on continental, regional and local scales, respectively. Study on a continental scale is essential to understand the complexity of the climate system in this region, while study on regional and local scales is essential to develop and/or implement strategies for adapting to climate change, since such adaptation is limited by the degree of confidence in the changes projected at these scales (Marengo et al., 2010).

During the Holocene period (~12,000 years Before Present (BP)), several climate changes occurred on a global scale, mainly due to changes in insolation related to variations in the Earth's orbital parameters and solar variability (Mayewski et al., 2004). During this period there was a decrease (increase) in summer insolation in the Northern (Southern) Hemisphere, generating opposite hemispheric trends of summer insolation that promoted a redistribution of energy (Wanner et al., 2011). This redistribution promoted different global climate changes during the Holocene, as the variation of the seasonal migration area of the ITCZ and of the SACZ, and the weakening of summer monsoon systems in the Northern Hemisphere (NH). (Braconnot et al., 2007).

Based on the prominent occurrence of abrupt climatic events on a global scale, the Holocene has been divided into three subseries: the Early Holocene (EH), from $\sim 11,700$ to 8,200 years BP; the Middle Holocene (MH), from ~ 8,200 to 4,200 years BP; and the Late Holocene (LH), from ~ 4,200 years BP to the present (Walker et al., 2019). The EH initiated with the occurrence of the Younger Dryas (YD) event, an abrupt event that characterized the last glacial cold period (Dansgaard et al., 1989). Since the end of the YD, the global mean surface temperature showed an increasing trend during the EH, which was disturbed by a series of abrupt climatic events, the most pronounced of which occurred at ~9,300 years BP and ~8,200 years BP (Porinchu et al., 2019). The 9.3 event (~9,300 years BP) consisted of a decrease in the surface temperature of the North Atlantic Ocean and lasted about 110 years (Blockley et al., 2012; Came et al., 2007; Yu et al., 2010). The 8.2 event (\sim 8,200 – 6,800 yr BP) consisted of a widespread cooling associated with the sudden drainage of the Lake Agassiz-Ojibway glacial complex across Hudson Strait and lasted ~150 yr (Alley et al., 1997; Barber et al., 1999; Thomas et al., 2007). This was a unique event during the Holocene, the most abrupt and of greatest magnitude, which considered the most significant climate perturbation of the last 10,000 yr BP (Kobashi et al., 2007). This event had global effects and culminated in the beginning of the collapse of large ice sheets in the NH, such as the Laurentide Ice Sheet (Barber et al., 1999), in addition to resulting in a decrease in the annual global mean temperature of ~3.3°C (Porinchu et al., 2019).

The MH initiated with the 8.2 event and was characterized by a bigger (smaler) amount of continuous insolation in the NH (SH). This warmer period is commonly called the Mid-Holocene Climatic Optimum (Charpentier Ljungqvist, 2011). During this period there was a reorganization in the variability of the global climate system, since the change from colder to warmer conditions and the collapse of the North Atlantic ice sheets altered ocean circulation and increased climate variability in the Atlantic Ocean and, consequently, climate across the globe (Wirtz et al., 2010). During the MH, some notable temperature drop events occurred, with the 5,300 and 4,200 year BP events standing out (Wanner et al., 2015). The 5.3 event (~5,300 yr BP) consisted of a climate reversal in which cooler and wetter climatic conditions prevailed (Magny & Haas, 2004). The 4.2 event lasted for about 300 years and consisted of an abrupt (mega)drought and/or cooling event of global extent that has been recorded in a variety of archives worldwide (Bond et al., 2001; Thompson et al., 2002; Zhang et al., 2018). This climatic event was very important and has been the subject of several studies in recent years because it is associated with the collapse of different ancient civilizations and with human migration in different regions of the world (such as India, Egypt, Mesopotamia and China) (e.g. Drysdale et al., 2006; Ruan et al., 2016; Zhang et al., 2018).

The LH initiated with the 4.2 event (~4,200 years BP) and was characterized by a drop in mean temperatures in the NH due to a decline in summer insolation in that hemisphere (Denton & Karlén, 1973; Wanner et al., 2008). Several notable events occurred during the LH, including the 2.8 event, the Medieval Climate Anomaly (MCA) and the Little Ice Age (LIA) (Chambers et al., 2007; Mann et al., 2009). The 2.8 event (~2,800 years BP) was characterized by an abrupt global cooling, related to a rapid reduction in solar activity, or Grand Solar Minimum (Chambers et al., 2007; Plunkett & Swindles, 2008). This event is associated with the transformation of pre-existing social patterns in different ways in different parts of the world (such as in China, Greece and the Mediterranean region), including population migration and new subsidence strategies (Jia et al., 2022; Raspopov et al., 2013). The MCA (~950 to 1250 Common Era – CE) was a pre-industrial period of natural climate change associated with elevated temperatures and hydroclimatic variability in different parts of the world (Lüning et al., 2018, 2019; Mann

et al., 2009). The LIA (~1400 to 1700 CE) was characterized by cooling of the NH continents but warming in the Middle East, central North Atlantic, Africa, tropical Eurasia, and extratropical Pacific (Mann et al., 2009). The LIA was the coldest period since the 2.8 event and was strongly influenced by covariation between groups of large volcanic eruptions and four notable Grand Solar Minima (PAGES 2k Consortium, 2013).

Understanding the variability of the atmosphere, oceans and air-sea interaction processes, as well as their effects on global climate, both present and past, constitutes a powerful tool for predicting future climate (Reboita et al., 2021). Observational data are essential for characterizing the present climate system and variability, but the length of observational climates' time series is relatively short (~150 years) when it comes to past climate, which limits a better understanding of past climate variability. In this context, paleorecords have been used as indirect indicators of environmental conditions (proxybased records), becoming interesting tools in paleoclimatic studies (Gornitz, 2009; Hernández et al., 2020; Marcott et al., 2013). Among the most used archives in paleoclimatic reconstructions, we can highlight, for example, ice, marine, lake and soil cores, as well as speleothems, corals and tree rings (Bradley, 1999).

In addition to paleorecords, climate models have been increasingly used in the reconstruction of past climate, because once a relationship is identified, paleorecords can be confronted with results from numerical simulations to explain the possible physical mechanisms involved in the observed climate changes, quantifying the relative importance of one factor in relation to another, or even testing climate sensitivity to different forcings (Bradley, 1999). In this way, the use of observational data together with paleorecords and climate models allows the reproduction of past climates, contributing to more reliable future projections. (e.g., Prado et al., 2013).

Therefore, the main objective of this project is to <u>investigate hydroclimate</u> variability in the domain of the current American monsoon (TA region), at different <u>spatial scales</u>. To meet the general objective of the project, the following specific objectives were defined:

- Determine hydroclimatological variations in the TA on a continental scale;
- Determine hydroclimatological relationships in the TA on a regional scale; and
- Determine hydroclimatological relationships in the TA on a local scale.

A deeper understanding of hydroclimatic variations in the TA across different scales can improve extreme event predictability, enhance water resource management, and provide valuable support for decision-making.

This doctoral thesis consists of three scientific articles that were published. Each article consists of a chapter that stands alone but complement each other. For a better understanding of this thesis, below is a brief description of each chapter:

Precipitation patterns and variability in Tropical Americas during the Holocene. Article by Bianchini et al. (2025), published in the *Palaeogeography*, *Palaeoclimatology*, *Palaeoecology* journal - This article analyzes precipitation trends in the TA during the Holocene using paleorecords from lake sediments and speleothems, along with output data from the Transient Climate Simulation of the Last 21,000 Years (TraCE-21ka).

A fully calibrated and updated mid-Holocene climate reconstruction for Eastern South America. Article by Gorenstein et al. (2022), published in the *Quaternary Science Reviews* journal - This article is an update in the compilation made by Prado et al. (2013) with the addition of new records and with the calibration of the uncalibrated ¹⁴C age models showing the difference between the use of calibrated and uncalibrated ¹⁴C age models in paleoclimatic studies.

Long- and short-term vegetation change and inferred climate dynamics and anthropogenic activity in central Cerrado during the Holocene. Article by Escobar-Torrez et al. (2022), published in the *Journal of Quaternary Science* - This article presents a palynological study using pollen, macrocharcoal, and trace elements from a lake sediment core in the Central Cerrado to assess vegetation, fire, and climate interactions influenced by natural and anthropogenic disturbances during the Holocene.

Integrative discussion and final remaks. Brief integrative discussion that synthesizes the main findings of this research.

Integrative discussion and final remaks. Brief integrative discussion that synthesizes the main findings of this research.

Appendix I. Supplementary Material from "Precipitation patterns and variability in Tropical Americas during the Holocene".

Appendix II. Supplementary Material from "A fully calibrated and updated mid-Holocene climate reconstruction for Eastern South America".

Appendix III. Supplementary Material from "Long- and short-term vegetation change and inferred climate dynamics and anthropogenic activity in central Cerrado during the Holocene".



Contents lists available at ScienceDirect

Palaeogeography, Palaeoclimatology, Palaeoecology



Precipitation patterns and variability in Tropical Americas during the Holocene

Paula R. Bianchini ^{a, *}, Luciana F. Prado ^b, Elder Yokoyama ^a, Ilana Wainer ^c, Iuri Gorenstein ^c, Francesco S. R. Pausata ^d

a Laboratório de Estudos Magnéticos em Geociências (LEMAG), Instituto de Geociências, Universidade de Brasília, Brasília, Brazil

b Faculdade de Oceanografia, Universidade do Estado do Rio de Janeiro, Rio de Janeiro, Brazil c Instituto Oceanográfico, Universidade de São Paulo, São Paulo, Brazil

d Centre ESCER (Etude et la Simulation du Climat a; l'Echelle Regionale) and GEOTOP (Research Center on the Dynamics of the Earth System), Department of Earth and Atmospheric Sciences, University of Quebec in Montreal, Montreal, OC, Canada

Abstract

The Tropical Americas (TA) have monsoons as the dominant feature of their hydroclimate. Precipitation in this region is influenced by the American Monsoon System (AMS). Throughout the Holocene, several global climate changes occurred that modified precipitation patterns in this region. Here we identify a general trend of increasing precipitation in the TA over the last 11,700 years. We analyzed different precipitation datasets, as paleorecords from lake sediments and speleothems, and Transient Climate Simulation of the Last 21,000 Years (TraCE-21ka) model results. We also identified occasional shifts in the TA's precipitation during the Holocene, with variations in the pattern of precipitation anomalies around 9,000 to 8,000 years, corroborated by high-energy wavelet analysis signals detected before 7,710 years. These results show that TA's precipitation was influenced by the final collapse of the North American ice sheets, accelerated by increased summer insolation in Northern Hemisphere (NH).

Keywords: Lake sediments, Speleothems, Data-model comparison, America Monsoon System, compilation, TraCE-21ka.

1. Introduction

The hydrological cycle in the Tropical Americas (TA) (40°N-40°S; 120°-30°W) is influenced by a complex interplay of physical processes at various spatial and temporal scales, resulting in intricate patterns. This region is characterized by its unique ecosystems, diverse cultures, and rich traditions (Carvalho, 2020). However, there is a significant disparity in economic development among the nations within this region (Carvalho, 2020). Recent studies indicate that heavy precipitation events in this region are projected to increase in intensity and frequency, with varying levels of confidence (Seneviratne et al., 2021). Despite advancements in weather forecasting and seasonal forecasts, populations, and governments in both developed and developing countries in TA have shown a lack of preparedness in dealing with extreme climatic events (Pelling, 2010).

Tropical regions experience monsoons as a dominant feature of their hydroclimate. These monsoons are humid summer circulations that provide most of the annual precipitation in their regions of operation, being characterized by rainy summers and dry winters, accompanied by a seasonal inversion of prevailing winds (Geen et al., 2020; Zhou and Lau, 1998). The TA region is influenced by the American Monsoon System (AMS), which consist of the North American Monsoon System (NAMS) and the South American Monsoon System (SAMS) (Fu et al., 2016; Mechoso et al., 2004; Vera et al., 2006).

The NAMS plays a crucial role in the climate of the region between the southwestern United States (USA) and the extreme north of South America, being responsible for producing 50 % to 70 % of the summer rainfall in this region (Fu et al., 2016; Mitchell et al., 2002; Sheppard et al., 2002). The SAMS constitutes the most significant climatic feature in South America, being responsible for most of the annual precipitation in the continent (Gan et al., 2004; Marengo et al., 2012).

Over the course of the Holocene, there have been several global climate changes primarily caused by variations in Earth's orbital parameters affecting insolation (Mayewski et al., 2004). The opposite hemispheric trend in summer insolation during this period was characterized by a decrease in Northern Hemisphere (NH) summer insolation and an increase in Southern Hemisphere (SH) summer insolation. This led to changes in the distribution of energy across the globe (Wanner et al., 2011). The distribution of energy in the atmosphere primarily occurs through the transport of water vapor (Mayewski et al., 2004). Changes in summer insolation promoted several global climatic

changes during the Holocene, including the narrowing of the Intertropical Convergence Zone (ITCZ) seasonal migration range, the weakening of the NAMS, the strengthening of the SAMS and the southward migration of the South Atlantic Convergence Zone (SACZ) (Braconnot et al., 2007; Campos et al., 2022; Chiessi et al., 2021; Custodio et al., 2024).

Gaining insights into hydroclimate variability, both past and present, is a valuable tool to help understand future climate changes (Reboita et al., 2021; Tierney et al., 2020). This study aims to investigate the hydroclimate variability in the TA throughout the Holocene and how it differed relative to today's climate. In doing so, we will use a combination of observational and reanalysis datasets, paleoclimate archives (lake sediments and speleothems) and outputs from the Transient Climate Simulation of the Last 21,000 Years (TraCE-21ka). Finally, we conducted a regional analysis of Holocene precipitation in five key areas to identify changes in variability.

2. Data and methods

2.1. Historical climate

We analyzed data from observational and reanalysis datasets from the National Oceanic and Atmospheric Administration (NOAA) to understand the current precipitation patterns and variability in the TA. The data is publicly available on the NOAA website (https://psl.noaa.gov/data/gridded/index.html, last accessed on 22 February 2023).

The monthly mean rainfall data were calculated from four observational datasets: CPC Merged Analysis of Precipitation (CMAP), with gridded monthly precipitation data available from 1979 to 2022 and spatial resolution of 0.25° (Xie and Arkin, 1997); Global Precipitation Climatology Centre (GPCC), with gridded monthly precipitation data available from 1891 to 2022 and spatial resolution of 0.25° (Schneider et al., 2016); NOAA's Precipitation Reconstruction over Land (PREC/L), with gridded monthly precipitation data available from 1948 to 2022 and spatial resolution of 0.25° (Chen et al., 2002); and Global Precipitation Climatology Project (GPCP) Monthly Precipitation Climate Data Record (CDR), with gridded monthly precipitation data available from 1979 to 2015 and spatial resolution of 0.25° (Adler et al., 2018).

We analyzed precipitation outputs from two versions of the National Oceanic and Atmospheric Administration Cooperative Institute for Research in Environmental Sciences (NOAA-CIRES) 20th Century Reanalysis. The first version, NOAA-CIRES 20th Century Reanalysis version 2 (NOAA-20Cv2), provides gridded monthly precipitation rates from 1871 to 2012 with a spatial resolution of 0.2° (Compo et al., 2011). The second version, NOAA-CIRES 20th Century Reanalysis version 3 (NOAA-20Cv3), provides gridded monthly precipitation rates from 1836 to 2015 with a spatial resolution of 0.1° (Slivinski et al., 2019).

Observational and reanalysis datasets were used to calculate mean precipitation and its standard deviation (SD) during the four seasons: December to February (DJF), March to May (MAM), June to August (JJA) and September to November (SON) within the study area. The data covers a 30-year time series starting in 1982. These calculations were made to measure variability during the period from January 1982 to December 2012. This time is common to all observational and reanalysis data used in the study.

2.2. Holocene climate

2.2.1. Paleorecords

We conducted a comprehensive analysis of precipitation patterns and variability in the TA during the Holocene, as recorded by paleorecords. Our study compiled data from 83 lake sediment records and 19 speleothem records in the study area. These findings are based on scientific journal publications up until April 2023. We chose to use lake sediments and speleothems as they are paleoclimatic archives that provide proxies for precipitation. In this compilation, we use data from the NOAA's Paleoclimatology Program (https://www.ncei.noaa.gov/maps/paleo/, last accessed on 01 May 1, 2023). The data sources included paleolimnology, lake level Paleo Networks, and speleothem. We supplemented our compilation with the study by Gorenstein et al. (2022) since there are only a few studies available in South America.

The selection of studies for this compilation was based on three main criteria. The first domain is the spatial domain. The latitudinal limits used are 40°N to 40°S, and the longitudinal limits used are 120°W to 30°W, as shown in Fig. 1. These limits determine the area of influence of the NAMS and SAMS, constituting the area of action of the AMS in TA (Pinchinat et al., 2015; Vera et al., 2006).

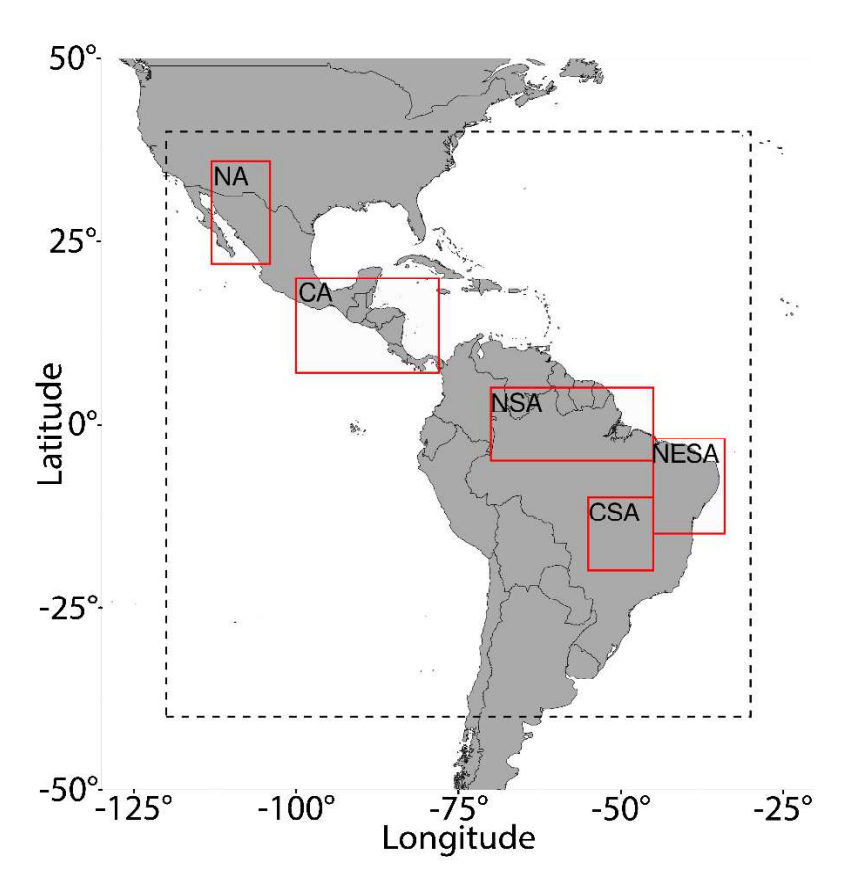


Fig. 1. Domain of the present study. The dashed line indicates the study area (40°N-40°S; 120°-30°W). The five solid red boxes indicate the key areas selected for assessing climate metrics and trends in this study (for further details on the typicality and necessity of each area, refer to Section 2.2.3): the North America region (NA, 36°-22°N; 113°-104°W), the Central America region (CA, 20°-7°N; 100°-78°W), the Northern South America region (NSA, 5°N-5°S; 70°-45°W), the Northeastern South America region (NESA, 2°-15°S; 45°-34°W) and the Central South America region (CSA, 10°-20°S; 55°-45°W). (For interpretation of the references to colour in this figure legend, the reader is referred to the web version of this article.)

Studies carried out during the Holocene period were examined, which spans from 11,700 years to the present (Walker et al., 2019). We selected studies that covered the time between 12,000 and 100 years before present (BP) (1,850 years CE) to exclude any anthropic signals from the historical period. The criteria were established to ensure temporal and spatial consistency in the paleorecords regarding precipitation patterns in TA during the Holocene.

Only studies with calibrated ages were considered, as calibration accounts for the error caused by the conventional half-life (Libby ages) and the temporal variability of

atmospheric 14C content (Hajdas, 2008). Calibrated ages can also serve as a linear age scale that can be used in conjunction with other chronologies, such as 210Pb and 137Cs (Birks and Birks, 2006).

Various types of proxies were analyzed from selected paleoarchives, with a focus on precipitation records. The information on precipitation extracted from paleorecords was obtained by compiling various studies qualitatively. These studies indicate periods of both drier and wetter conditions than the present, as reported in their respective publications. Table S.1 provides additional details about the lakes and speleothems that were analyzed in this compilation. The precipitation reconstruction from paleorecords during the Holocene period was compared to the results obtained from the analyzed models, as will be discussed later.

2.2.2. Model outputs

We analyzed data from the TraCE-21ka to gain insight into past precipitation patterns and variability in TA. This simulation provides estimates of seasonal precipitation and temperature changes over the last 21,000 years (He, 2011). We utilized the complete TraCE simulation (Main TraCE dataset), which incorporates transient forcing changes in greenhouse gases, variations in insolation driven by orbital factors, ice sheets, and meltwater flux (Liu et al., 2009). We analyzed precipitation data from the "TraCE paleoclimate simulation, Atmosphere Post Processed Data, Decadal Mean Seasonal Averages, version 1" (https://www.earthsystemgrid.org/dataset/ucar.cgd.ccsm.trace.atm.proc. seasonal_ave.html, last accessed on February 22, 2023).

The TraCE-21ka model utilized the Community Climate System Model version 3 (CCSM3) from the National Center of Atmospheric Research (NCAR). This model is a global coupled climate model that includes the interactions between the ocean, atmosphere, sea ice, and land surface, and does not require flux adjustment (Collins et al., 2006). The atmospheric-land model used in this study is the Community Atmospheric Model 3 (CAM3), which has 26 levels of hybrid coordinates in vertical resolution and approximately 3.75 degrees in horizontal resolution. The ocean model employed is the Parallel Ocean Program (POP) from NCAR, which has 25 levels in vertical z coordinate. The sea ice model utilized is the Community Sea Ice Model (CSIM) from NCAR, which has the same resolution as POP (He, 2011). The simulations were conducted using the T31 gx3v5 resolution (Yeager et al., 2006), and the dynamic global vegetation models

CLM-DGVM (Yeager et al., 2006). The simulation begins at 22,000 years and ends in 1990 CE.

The model output data is used to calculate the SD during DJF, MAM, JJA and SON. It also calculates the difference between mean precipitation during the Holocene period before the pre-industrial period (11,700 years – 1,850 years Common Era (CE)) and during the pre- industrial period (1,850 years CE – 1,990 years CE) for the same seasons (1,850 years CE is equivalent to the "0 year" in the model, and the 1,990 years CE is equivalent to "-40 years" in the model). This calculation was performed for three subseries of the Holocene (Table 1) and the results were compared to information obtained from paleorecords regarding precipitation. This comparison will be discussed further.

Table 1

Formal subdivision of the Holocene Stage/Age and their corresponding Subseries/Subepoch (based on Walker et al. (2019)).

Stage/Age	Subseries/Subepoch	Years Before Present (BP)
Greenlandian	Early Holocene (EH)	~11,700 – 8,200
Northgrippian	Middle Holocene (MH)	~8,200 – 4,200
Meghalayan	Late Holocene (LH)	~4,200 - present

2.2.3. Key areas

By calculating the SD for different subseries of the Holocene, we found five significant regions that showed higher variability in precipitation during the study period. Key areas were defined based on previous studies that identified different seasonal precipitation patterns in those areas (Fig. 1), as explained in more detail below.

The North America region (NA) extends from the southern region of the USA to northern Mexico (36°-22°N; 113°-104°W). Cavazos et al. (2020) delimited this region because of the significant influence of the NAMS on its precipitation.

The Central America region (CA) is in Southern Mexico and Central America (20°-7°N; 100°-78°W). This region highlighted by Corrales- Suastegui et al. (2020) is characterized by a climatic phenomenon known as summer drought, typically occurring from June to September.

The Northern South America region (NSA) is primarily situated in the northern region of Brazil (5°N-5°S; 70°-45°W), while the Northeastern South America region

(NESA) is in the northeast region of Brazil (2°-15°S; 45°-34°W) and the Central South America region (CSA) is in the central region of Brazil (10°-20°S; 55°-45°W). Alves et al. (2021) defined these regions based on their distinct seasonal precipitation patterns and their significance in studying biomes, climate, hydrological systems, and social systems in Brazil.

We used TraCE-21ka output data to calculate the annual cycle for each area during the Holocene period and for the entire period. We calculated the mean time series precipitation anomaly for each box by comparing the Holocene period before the preindustrial period (11,700 years -1,850 years CE) with the subsequent period (1,850 years CE -1,990 years CE).

2.2.4. Wavelet analysis

Wavelet analysis was conducted using TraCE-21ka output data to estimate variations in the power spectrum of precipitation anomaly time series (Torrence and Compo, 1998). We utilize a Morlet wave function for our continuous wavelet transform, following the approach outlined in Torrence and Compo (1998). This method decomposes the time series into a time-frequency space to identify the dominant variability modes and their temporal variations (Prado et al., 2021; Torrence and Compo, 1998). We applied this method to our data using the WaveletComp package in the R Statistics Software (R"osch and Schmidbauer, 2018). Wavelet analyses were applied to standardized and detrended anomalies from key areas throughout the Holocene period.

3. Results

3.1. Historical climate

To analyze current precipitation patterns in the TA, we used observational and reanalysis datasets. The results from the observational datasets (CMAP, GPCC, GPCP-CDR, and PRECL) in the analyzed periods, DJF and JJA, show that the monthly precipitation averages in the study region range approximately from 0 to 400 \pm 35 mm/month in the observational datasets (Figs. S.1, S.2, S.3, and S.4 - a, b, c, and d). The DJF season (Figs. S.1 and S.3 - a, b, c, and d) is marked by dry conditions in southern North America and most of Central America, with precipitation below 100 \pm 40 mm/month, except for the southern portion of Central America, with precipitation ranging from 100 to 200 \pm 100 mm/month. Most of South America experiences wetter conditions,

with precipitation ranging from 100 to 350 \pm 100 mm/month, except for northeastern Brazil and southern South America, where precipitation is below 100 \pm 50 mm/month. The JJA season (Figs. S.2 and S.4 - a, b, c, and d) is marked by wetter conditions from southern North America to northern South America, with precipitation ranging from 100 to 450 \pm 100 mm/month. Central and southern South America are drier, with precipitation below 100 \pm 50 mm/month, except for northeast and south of Brazil, with precipitation ranging from 100 to 200 \pm 100 mm/ month.

The results from the reanalysis datasets (NOAA CIRES V2 NOAA CIRES V3) in the analyzed periods, DJF and JJA, show that the monthly precipitation averages in the study region range approximately from 0 to 500 ±45 mm/month in the reanalysis datasets (Figs. S.1, S.2, S.3, and S.4 - e and f). The DJF season (Figs. S.1 and S.3 - e and f) is marked by dry conditions in southern North America and most of Central America, with precipitation below 200 ±30 mm/month, except for the southern portion of Central America, with precipitation ranging from 200 to 300 ± 150 mm/month. Most of South America experiences wetter conditions, with precipitation ranging from 200 to 500 ± 150 mm/month, except for northeastern Brazil and southern South America, where precipitation is below 100 ± 30 mm/month. The JJA season (Figs. S.2 and S.4 - e and f) is marked by wetter conditions from southern North America to northern South America, with precipitation ranging from 300 to 500 ±150 mm/month. Central and southern South America are drier, with precipitation below 200 ±50 mm/month, except for south of Brazil, with precipitation ranging from 200 to 300 ± 100 mm/ month in the NOAA-20Cv2 dataset, and with no variation in the NOAA-20Cv3 dataset.

It is possible to observe that the observational data sets show agreement in the patterns and mean values observed for the monthly averages of precipitation and SD in both periods. Reanalysis datasets, on the other hand, have some disagreements. The monthly precipitation averages in DJF have higher values in the western part of South America in the NOAA_CIRES_V2 dataset (Fig. S.1.e), and in JJA these values are higher across the entire area in the NOAA_CIRES_V3 dataset (Fig. S.2.f). The SD in DJF have higher values in western South America and western Central America in the NOAA_CIRES_V2 dataset (Fig. S.3.e), and in JJA both datasets show agreement in the patterns and mean values. Therefore, the observational datasets represented the current precipitation patterns in the TA satisfactorily, while the reanalysis datasets represented the data with divergences and overestimated values.

3.2. Holocene climate

3.2.1. Paleorecords and model outputs

We compiled data from 83 lacustrine studies and 19 speleothems studies. The compilation showed that there were more records from South America (147 records) than from Central America (23 records) and Southern North America (47 records). Furthermore, there were more records from the LH (93 records) compared to the EH (50 records) and MH (74 records) (Table S.2). The records considered are proxy for precipitation that record an average rainfall value, used in paleoclimate reconstructions. We assume that most of the precipitation recorded by these proxies refers to summer rains, which reflects the behavior of the AMS. Therefore, we performed an analysis of paleorecords during the summer in each portion of the study area, at JJA (DJF) in the northern (southern) portion of the study area.

Climatic reconstruction using these paleorecords suggests that during the EH, in DJF, drier than present conditions prevailed in most of South America, except for south of Peru and east center of Brazil, which present more than one record indicating wetter than present conditions (Fig. 2a). In JJA, wetter than present conditions prevailed in almost all Central and North America (Fig. 2b). During the MH, drier conditions were prevalent in most of South America during the DJF season, except for the southern, southeastern, and northwestern regions of Brazil, as well as the western region of Peru, which showed evidence of wetter conditions than present (Fig. 2c). In JJA, drier than present conditions prevailed in northern South America and west center North America, and wetter than present conditions prevailed in almost all Central America and south of North America (Fig. 2d). During the LH, in DJF, wetter than present conditions prevailed in most of South America, except for the islands west of the Equator and east central of Brazil, which present more than one record indicating drier than present conditions (Fig. 2e). In JJA, wetter than present conditions prevailed in northern South America and in almost all Central and North, except for the north of Central America and the south of North America, which present more than one record indicating wetter than present conditions (Fig. 2f).

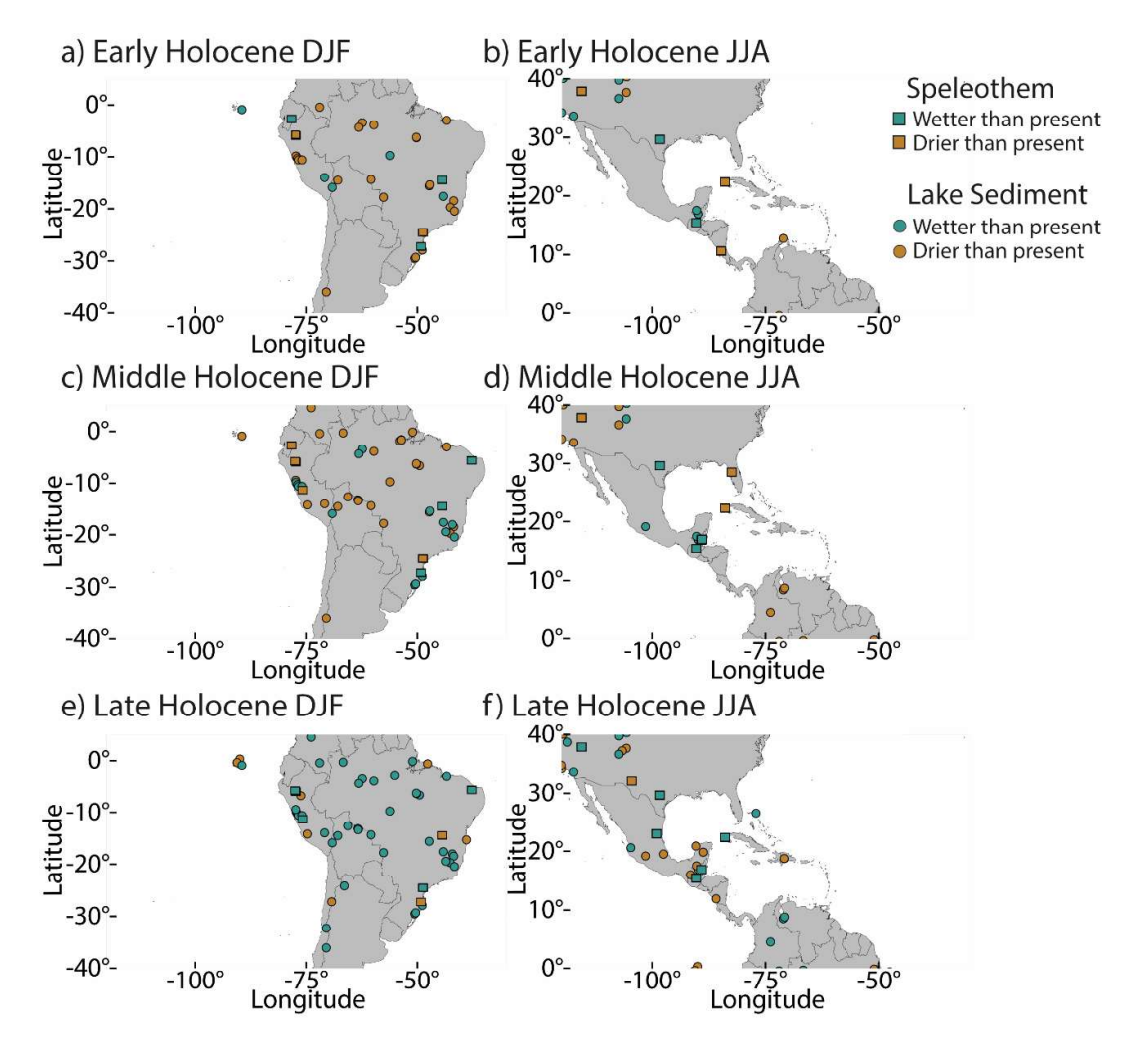


Fig. 2. Map with precipitation climate reconstruction for the Holocene periods and its separation by proxy type. Reconstruction from EH period at: a) DJF and b) JJA. Reconstruction from MH period at: c) DJF and d) JJA. Reconstruction from LH period at: e) DJF and f) JJA. Squares represent data from speleothems and circles represent data from lake sediments. Green squares/circles indicate higher than present precipitation and brown squares/circles indicate lower than present pre-cipitation. (For interpretation of the references to colour in this figure legend, the reader is referred to the web version of this article.)

The results of the difference between mean precipitation during the Holocene period before the pre-industrial period (11,700 years -1,850 years CE) and during the pre-industrial period (1,850 years CE -1,990 years CE) derived from TraCE-21ka model outputs show that during EH, in DJF, drier than present conditions prevailed in almost all South America (-60 to -10 mm/month), except for northeast Brazil, which shows wetter than present conditions (10 to 70 mm/month) (Fig. 3a). In JJA, drier than present

conditions prevailed in northeastern South America, Central America, and southeast North America (– 70 to – 10 mm/month), and wetter than present conditions prevailed in northwestern South America and southwestern North America (10 to 70 mm/ month) (Fig. 3b). During MH, in DJF, drier than present conditions prevailed in almost all South America (– 50 to – 5 mm/month), except for northeast Brazil, which shows wetter than present conditions (10to 50 mm/month) (Fig. 3c). In JJA, wetter than present conditions prevailed in almost all South, Central and North America (10 to 60 mm/ month), except for northeastern USA, which shows drier than present conditions (– 70 to – 10 mm/month) (Fig. 3d). During LH, in DJF, drier than present conditions prevailed in central and northwestern South America (– 30 to – 5 mm/month), and wetter than present conditions prevailed in northeastern and southern South America (10 to 30 mm/ month) (Fig. 3e). In JJA, wetter than present conditions prevailed in South and Central America, and in almost all North America (– 20 to 30 mm/month), except for south USA and north Mexico, which show drier than present conditions (– 15 to – 5 mm/month) (Fig. 3f).

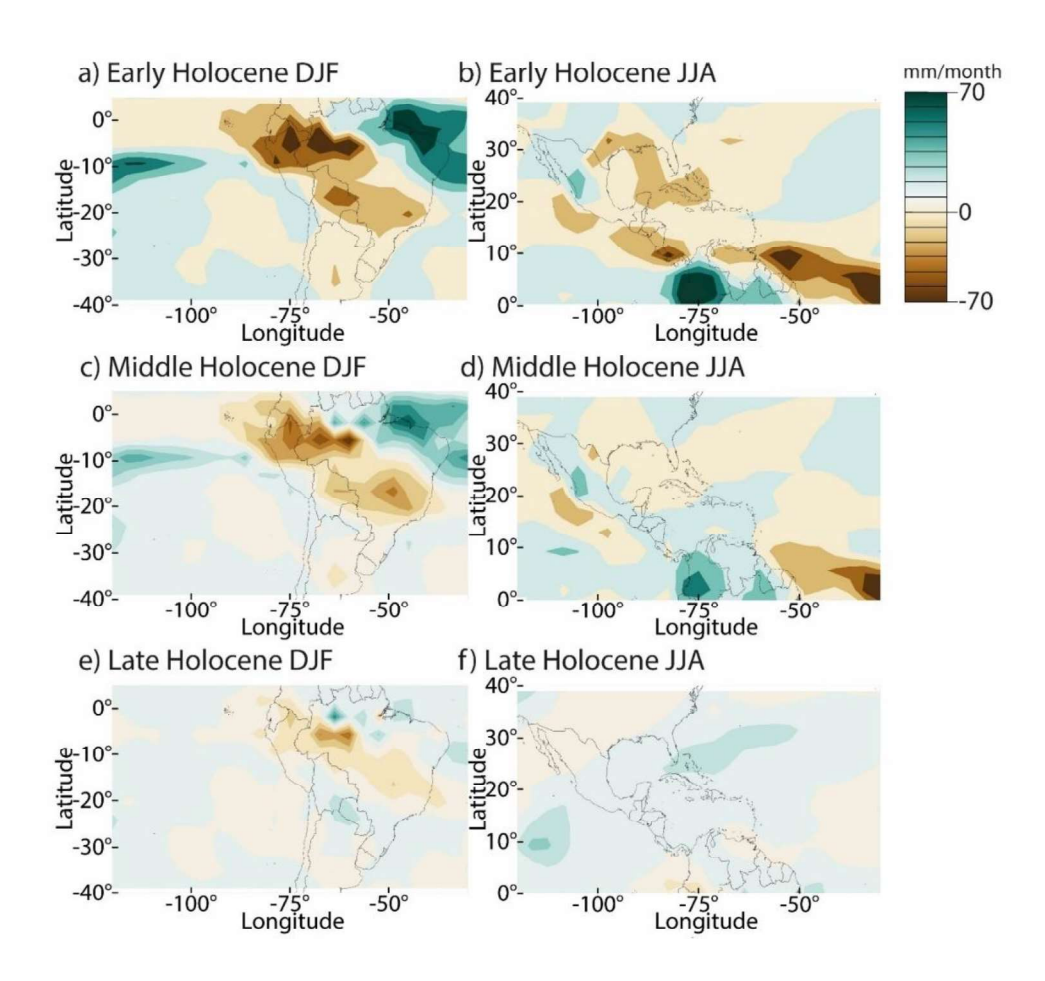


Fig. 3. Map of the difference between mean precipitation during the Holocene period before the pre-industrial period (11,700 years - 1,850 years CE) and during the pre-

industrial period (1,850 years CE – 1,990 years CE), derived from TraCE-21ka model outputs. Reconstruction from EH period at: a) DJF and b) JJA. Reconstruction from MH period at: c) DJF and d) JJA. Reconstruction from LH period at: e) DJF and f) JJA. Brown (green)-shaded areas correspond to drier (wetter) Holocene conditions if compared to the pre-industrial (control run) and are expressed in millimeters per month (mm/month). (For interpretation of the references to colour in this figure legend, the reader is referred to the web version of this article.)

3.2.2. Key areas

Results from the NA are shown in Fig. 4 (the reader is referred to Section 2.2.3. for more details on the areas' domains). Precipitation varied between 0 and 65 mm/month. The wet season occurred from September to February in the past, differing from today's wet season (June–October). DJF was wetter during the Early Holocene (EH) (~61 mm/month), decreasing through the Middle Holocene (MH) (~55 mm/ month) and Late Holocene (LH) (~53 mm/month). JJA followed a similar trend but with lower values.

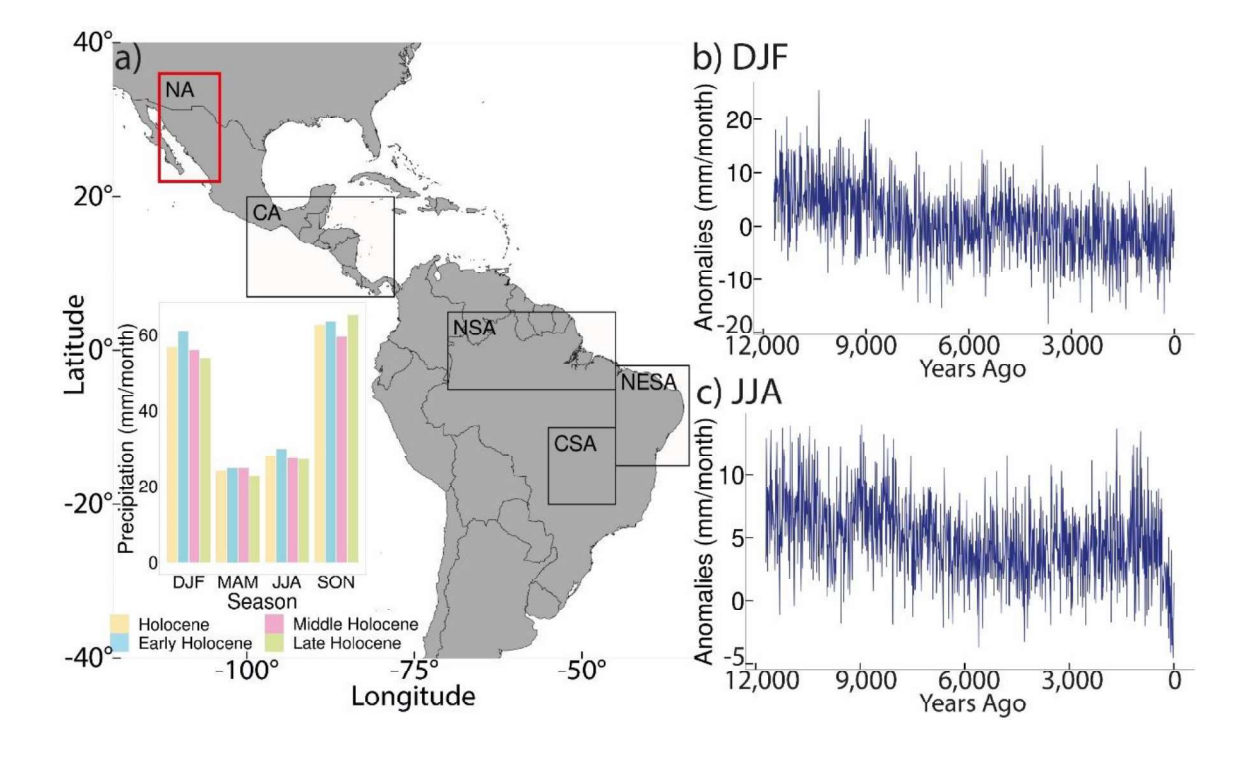


Fig. 4. Results from NA. a) Annual cycle of precipitation according to the seasons and according to the period: yellow bars for the entire Holocene, blue bars for the EH, pink bars for the MH and green bars for the LH. b) Precipitation anomaly during DJF relative to its original time series. c) Precipitation anomaly during JJA relative to its original time

series. As the magnitude of the variation of the anomaly in the season during JJA is much smaller when compared to DJF, we chose to use different scales to be possible to observe the variations. (For interpretation of the references to colour in this figure legend, the reader is referred to the web version of this article.)

Results from the CA are shown in Fig. 5. Precipitation varied between 0 and 140 mm/month. The MH was the wettest period (~90 mm/month in DJF), while the LH was the driest (~15 mm/month). JJA remained wetter than DJF, with a peak during the MH and LH (~135 mm/month). The wet season followed the current pattern (May–October).

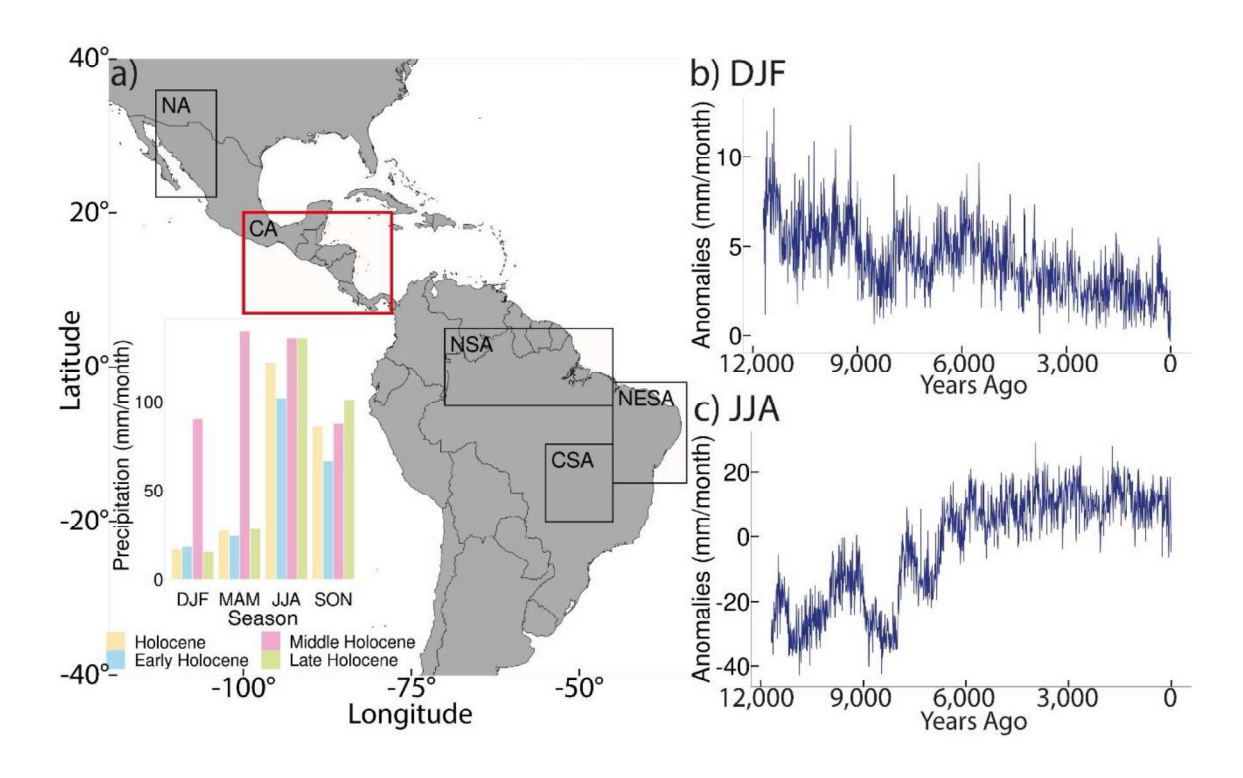


Fig. 5. Results from CA. a) Annual cycle of precipitation according to the seasons and according to the period: yellow bars for the entire Holocene, blue bars for the EH, pink bars for the MH and green bars for the LH. b) Precipitation anomaly during DJF relative to its original time series. c) Precipitation anomaly during DJF relative to its original time series. As the magnitude of the variation of the anomaly in the season during JJA is much smaller when compared to DJF, we chose to use different scales to be possible to observe the variations. (For interpretation of the references to colour in this figure legend, the reader is referred to the web version of this article.)

Results from the NSA are shown in Fig. 6. Precipitation ranged from 0 to 160 mm/month. DJF precipitation declined from EH (~90 mm/ month) to LH (~75 mm/month). JJA followed the same trend, decreasing from EH (~135 mm/month) to LH (~117 mm/month). The past wet season (March–August) differs from today's (December–April).

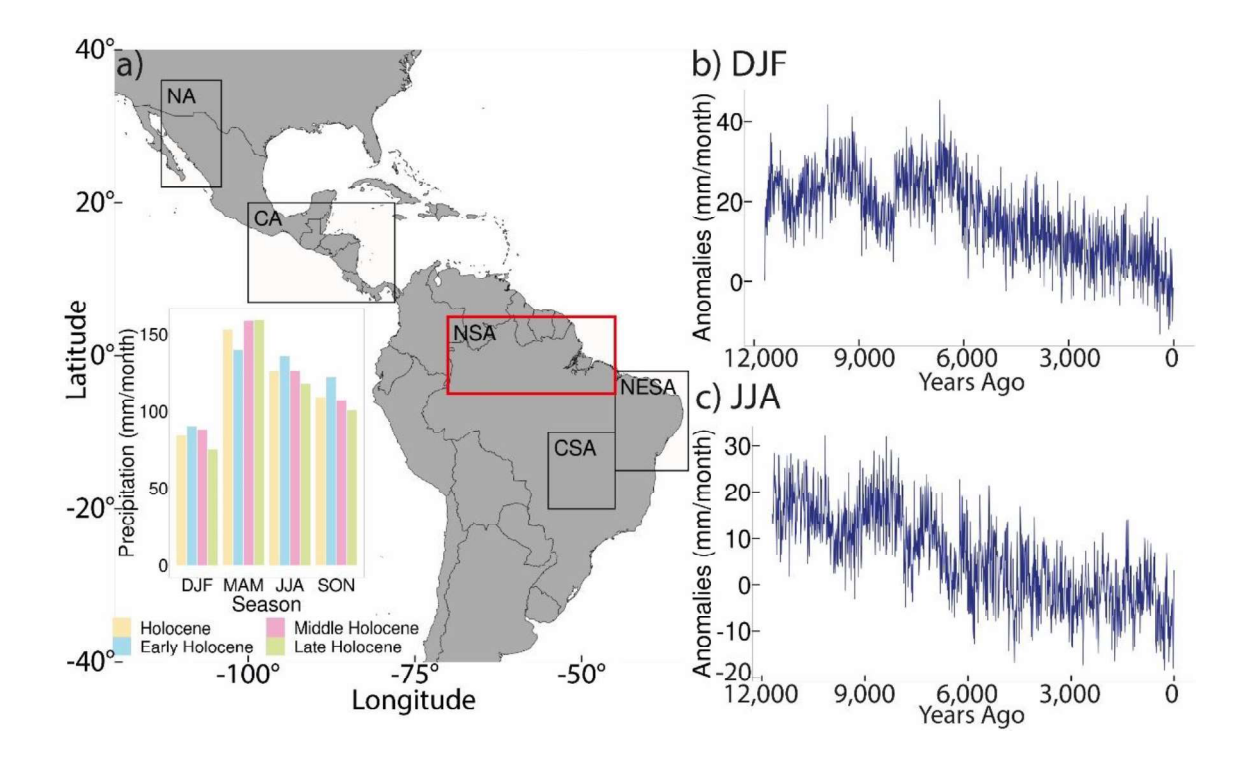


Fig. 6. Results from NSA. a) Annual cycle of precipitation according to the seasons and according to the period: yellow bars for the entire Holocene, blue bars for the EH, pink bars for the MH and green bars for the LH. b) Precipitation anomaly during DJF relative to its original time series. c) Precipitation anomaly during JJA relative to its original time series. As the magnitude of the variation of the anomaly in the season during JJA is much smaller when compared to DJF, we chose to use different scales to be possible to observe the variations. (For interpretation of the references to colour in this figure legend, the reader is referred to the web version of this article.)

Results from the NESA are shown in Fig. 7. Precipitation varied between 0 and 210 mm/month. DJF precipitation was highest during EH (~208 mm/month) and decreased through MH (~183 mm/month) and LH (~169 mm/month). JJA showed little

variation (~10–11 mm/ month). The wet season (January–May) aligns with present-day patterns.

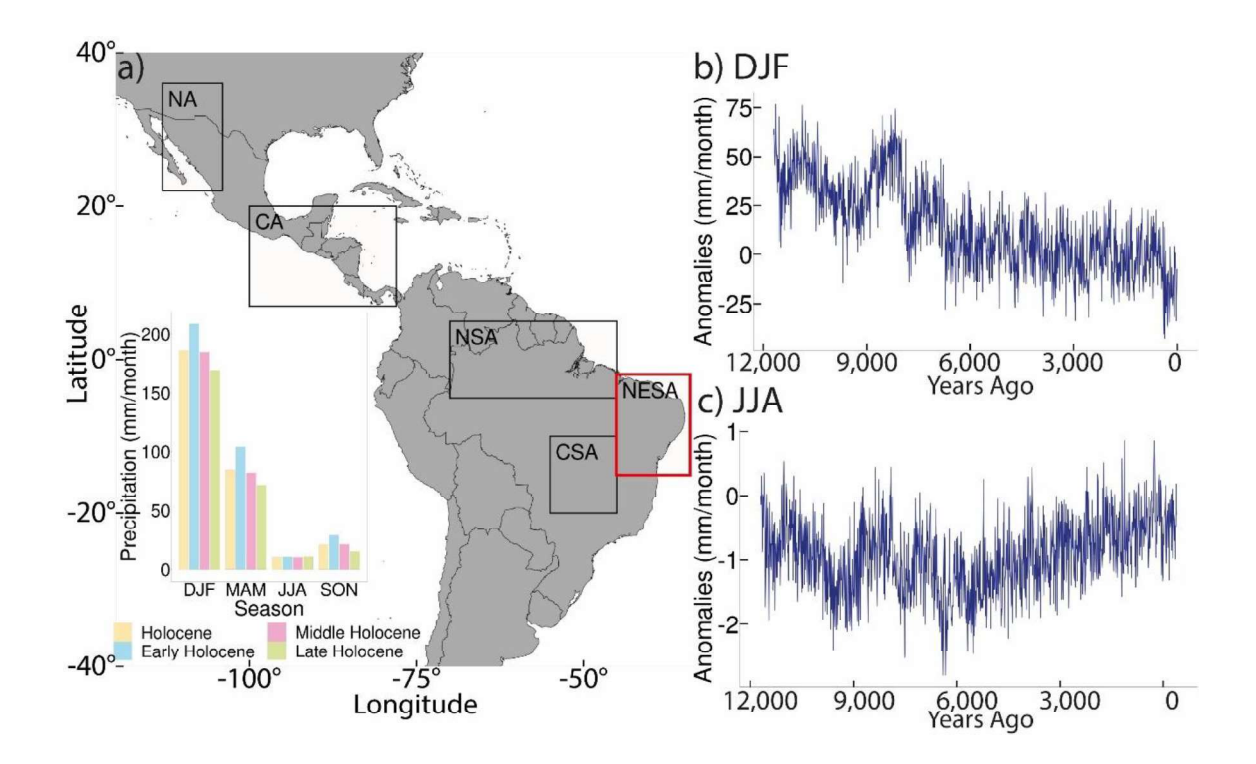


Fig. 7. Results from NESA. a) Annual cycle of precipitation according to the seasons and according to the period: yellow bars for the entire Holocene, blue bars for the EH, pink bars for the MH and green bars for the LH. b) Precipitation anomaly during DJF relative to its original time series. c) Precipitation anomaly during JJA relative to its original time series. As the magnitude of the variation of the anomaly in the season during JJA is much smaller when compared to DJF, we chose to use different scales to be possible to observe the variations. (For interpretation of the references to colour in this figure legend, the reader is referred to the web version of this article.)

Results from the CSA are shown in Fig. 8. Precipitation ranged from 0 to 245 mm/month. DJF followed a fluctuating pattern, with the highest precipitation in EH (~240 mm/month), a decrease in MH (~229 mm/month), and a rise again in LH (~242 mm/month). JJA remained relatively dry, with minor variations. The wet season (October–March) matches current climate trends. Throughout all regions, precipitation anomalies showed significant fluctuations, with abrupt changes associated with major

climatic events such as the Younger Dryas (YD) and the 8,200-year event. A more detailed analysis of each key area is provided in the supplementary material.

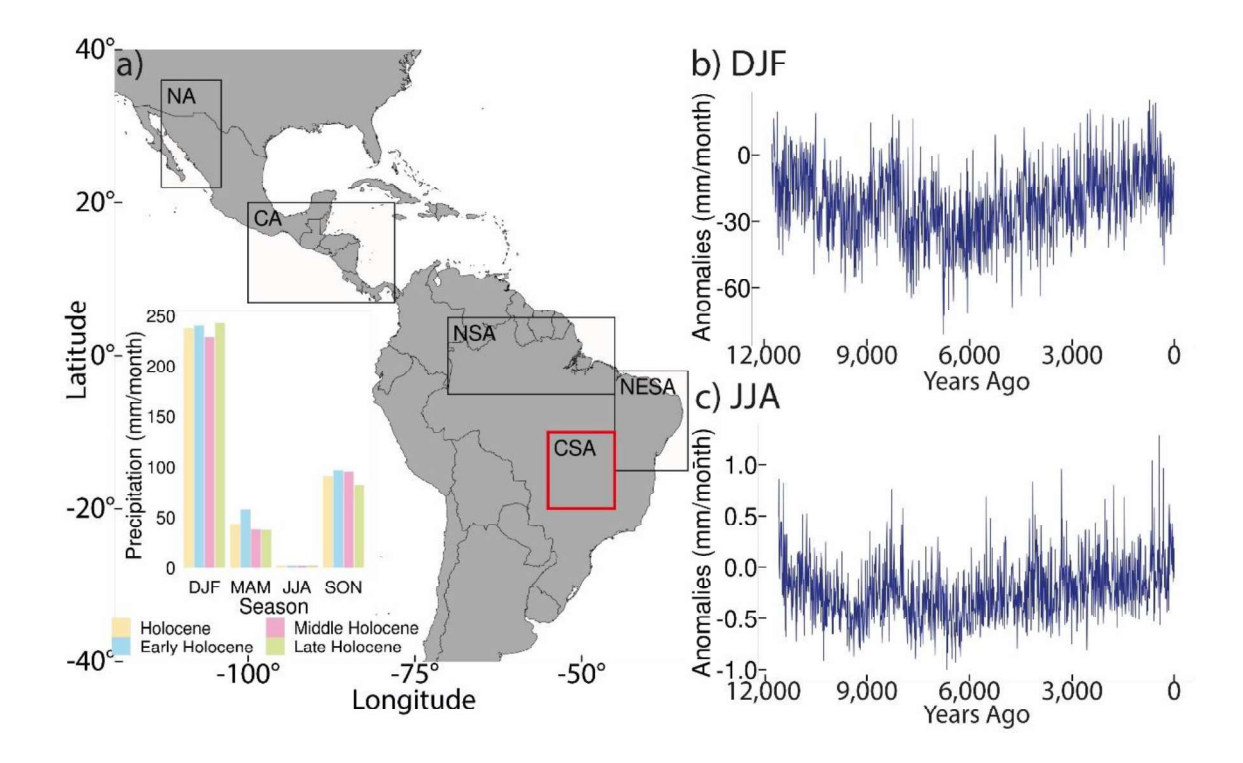


Fig. 8. Results from CSA. a) Annual cycle of precipitation according to the seasons and according to the period: yellow bars for the entire Holocene, blue bars for the EH, pink bars for the MH and green bars for the LH. b) Precipitation anomaly during DJF relative to its original time series. c) Precipitation anomaly during JJA relative to its original time series. As the magnitude of the variation of the anomaly in the season during JJA is much smaller when compared to DJF, we chose to use different scales to be possible to observe the variations. (For interpretation of the references to colour in this figure legend, the reader is referred to the web version of this article.)

3.2.3. Wavelet analysis

We examined the spectral behavior of DJF and JJA precipitation in each of the key areas throughout the Holocene by applying wavelet analysis to the standardized anomalies time series. Figs. 9 and 10 show that wavelet power levels as a function of period and integration time for DJF and JJA, respectively. Wavelet spectrum in DJF reveals that, in the NA, a high energy at low frequencies (above ~5,000 years) is the predominant frequency feature from 11,700 to 4,800 years (Fig. 9a). In the CA, there are two periods with higher power, one at intermediate frequencies (~1,550 years) from 9,710

to 7,710 years, and another at higher frequencies (~360 years) from 10,350 to 9,710 years (Fig. 9b). In the NSA, power is maximum at low frequencies (~3,100 years) is predominant from 9,710 to 7,710 years (Fig. 9c). In the NESA, power concentrates at intermediate frequencies (~2,200 years) from 11,700 to 9,710 years (Fig. 9d). In CSA, a high energy values at intermediate frequencies (~1,280 years) is the predominant power from 8,710 to 7,710 years (Fig. 9e).

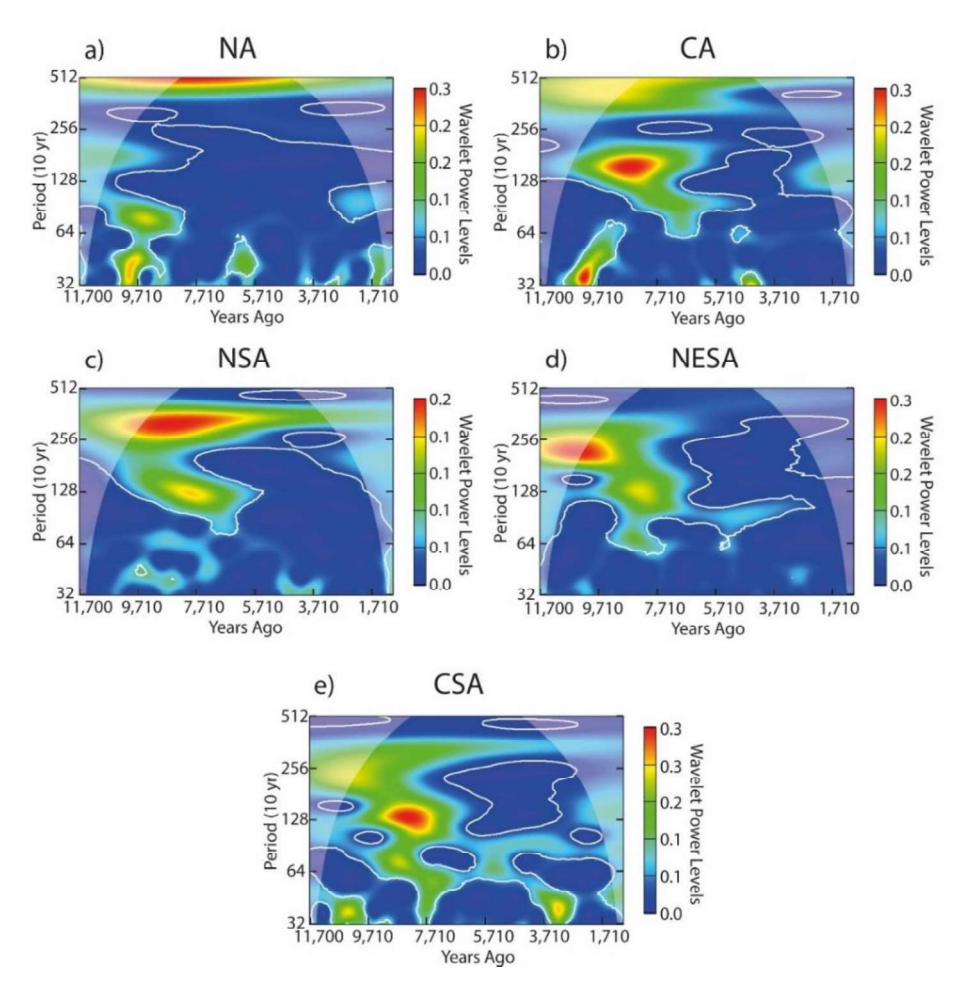


Fig. 9. Wavelet power levels of DJF precipitation anomalies (non-dimensional) of: a) NA; b) CA; c) NSA; d) NESA; and e) CSA. White solid line indicates 95 % significance.

Wavelet spectrum in JJA reveals that in the NA, CA and NSA, higher power at intermediate frequencies (~2,000 years) from 11,700 to 9,710 years (Fig. 10a, b and c), which may be related to the variation in insolation throughout of the Holocene. In the NSA, a secondary power peak occurs at intermediate frequencies (~1,000 years) from 8,240 to 6,910 years, and tertiary peak occurs at high frequencies (~480 years) from 6,910 to 6,040 years (Fig. 10c). In the NESA, power concentrates at intermediate frequencies

(~1,050 years) from 8,180 to 6,780 years (Fig. 10d). In the CSA, maximum power values occur at intermediate frequencies (~900 years) from 4,910 to 3,980 years (Fig. 10e).

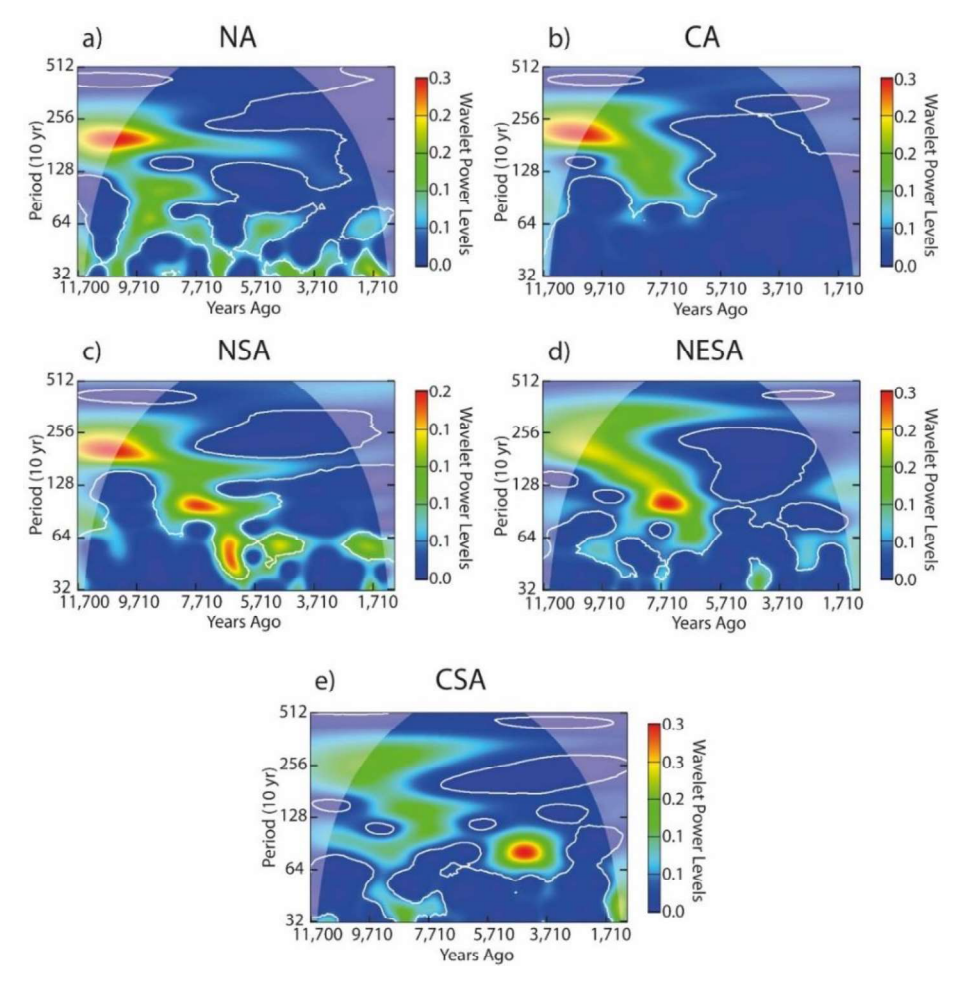


Fig. 10. Wavelet power levels of JJA precipitation anomalies (non-dimensional) of: a) NA; b) CA; c) NSA; d) NESA; and e) CSA. White solid line indicates 95 % significance.

4. Discussion

4.1. Holocene precipitation reconstruction by paleorecords and model outputs

To understand the precipitation patterns and variability in TA during the Holocene we used paleorecords compilation and output data from TraCE-21ka. While both datasets broadly indicate a progressive increase in humidity in TA from EH to LH, both in DJF and JJA, some discrepancies emerge at regional and temporal scales (Figs. 2 and 3).

Paleorecord reconstructions indicate that during the EH, lacustrine and speleothem records show drier than present conditions during the DJF in most of South America, except for northeast Brazil and southern Peru (Fig. 2a). They also show wetter than present conditions during the JJA in Central and North America (Fig. 2b). During the LH,

the paleorecords show wetter than present conditions during DJF dominating South America, with localized drying in east-central Brazil (Fig. 2e).

Reconstructions from TraCE-21ka outputs indicate that during the EH, conditions are drier than present during the DJF in South America (-60 to - 10 mm/month), except over northeastern Brazil (10 to 70 mm/month; Fig. 3a). During the LH, conditions are drier than present during DJF in central/northwestern South America (-30 to - 5 mm/month); Fig. 3e), contrasting with proxy evidence of wetter than present conditions.

The occurrence of paleorecords with opposed climatic signals in the same region may occur because proxies work as system filters and operate at different spatial and temporal scales (Birks and Birks, 2006), which means that climatic events may not be registered in the same way by different proxies (Gorenstein et al., 2022). Another possibility is that the proxies are recording events of different scales, since it is not always clear the scale of the event that a given record reflects (Sorooshian and Martinson, 1995). For example, in northeast Brazil (EH), lacustrine records indicate wetter conditions, whereas speleothems suggest intermittent aridity, reflecting short-term droughts unresolved in lake sediments (Gorenstein et al., 2022).

The conflicting results between the paleorecords and the model output do not come as a surprise (Laepple et al., 2023). It may occur due to resolution differences between the paleorecords and the model. TraCE-21ka's coarse grid (~2°) smooths localized features. In LH during DJF, the model fails to capture wetter than present conditions in southern Peru (Fig. 2e vs. Fig. 3e), likely due to unresolved orographic rainfall (Nowacki et al., 2019).

Another possibility is that paleorecords often reflect centennial-scale trends, while TraCE-21ka outputs average 100-year intervals. For instance, in MH during JJA drying in Central America (Fig. 2d) contrasts with model-simulated wetter conditions (Fig. 3d), potentially due to decadal droughts "averaged out" in the model (Laepple et al., 2023).

A final possibility for the discrepancies found is regional sampling bias. There is a geographic imbalance in the paleorecords, with South America dominating our proxy dataset (147 records vs. 23 in Central America; Table S2). The sparse coverage of Central America may amplify apparent mismatches (e.g., in the LH, a drying during JJA in the southern US; Fig. 3f).

4.2. Variability

Five key areas were selected, in which we examined the precipitation variability in each one, considering both the seasonal variation (annual cycle) and the variability over time (precipitation anomalies time series), and applied wavelet analysis to the detrended and standardized anomalies time series of each key area. All these analyses were performed using the TraCE-21ka outputs.

The annual cycle of precipitation shows consistent patterns in the key areas, with distinct dry and rainy periods observed in the CA, NESA and CSA. However, there were some variations in the NA and NSA. In the NH (NA and CA), there is a general decrease in precipitation anomaly during the Holocene in DJF and contrasting trends between these areas during JJA. In the SH (NSA, NESA and CSA), there is a general tendency for precipitation anomalies to decrease in DJF, except for the CSA, and to increase in JJA, except for the NSA.

The Laurentide Ice Sheet (LIS) had a significant impact on North American climate variation during the EH (Feng et al., 2011). Since the Last Glacial Maximum (LGM; ~21,00 years), the LIS began collapsing, resulting in the release of meltwater pulses during the Late Pleistocene and EH (Tushingham and Peltire, 1991). Four meltwater pulses from the LIS were identified in the Gulf of Mexico between 9,900 and 8,900 years (Aharon, 2003). The Gulf of Mexico is a significant source of moisture for the monsoon system in the region. The introduction of this water has led to a decrease in sea surface temperature (SST) and reduced precipitation in the area (Rasmussen and Thomsen, 2012). This may have contributed to the observed decline in the NA around 9,000 years (Fig. 4). Around 4,000 years, there was a significant change in the climate of southern North America. This change was caused by a decrease in summer and autumn insolation in the NH, which led to the displacement of the ITCZ to the south (Metcalfe et al., 2015). This change may be related to the observed decrease in trend in the NA around 4,000 years (Fig. 4).

The LIS collapse between 11,000 and 7,000 years is also associated with the deceleration of the Atlantic Meridional Overturning Circulation (AMOC) due to the decrease in SST and salinity in the North Atlantic Ocean. This has led to the narrowing of the seasonal migration range of the ITCZ, causing a strengthening of the SAMS (Campos et al., 2022; Chiessi et al., 2021; Strikis et al., 2011; T"ornqvist and Hijma, 2012), and the increasing trend observed around 8,500 years in CSA (Fig. 8). This deceleration of the AMOC causes the heat to concentrate in the South Atlantic Ocean and

weakens the trade winds in the SH, contributing to a greater concentration of heat in the east of the South Atlantic Ocean and taking more moisture to the northeast of South America and strengthening the SAMS (Strikis et al., 2011), which may have caused the increase trend observed around 8,500 years in NESA during JJA (Fig. 7). The progressive increase in autumnal insolation in NH along the MH and LH led to increases in SST in the Caribbean Sea increasing precipitation in the Central American region (Duarte et al., 2021), which may explain the change in the trend observed around 8,500 years in CA (Fig. 5). The narrowing of the ITCZ seasonal migration range from the MH caused a decrease in precipitation in the northern region of South America, since the meridional migration from the ITCZ towards the differentially warmer hemisphere exerts a strong control of the annual precipitation cycle in this region (Poveda et al., 2006), which may explain the change in the trend observed around 8,500 years in NSA (Fig. 6).

Wavelet analysis shows that in the NA and CSA the power spreads from the lowest frequencies (~3,800 years) to the highest ones (~320 years) and presents a "funnel shape", both in DJF and JJA (Figs. 9. a, e and 10. a, e). In the NA this "funnel shape" shows higher energy in JJA than in DJF and is the predominant forcing feature between 11,700 and 9,710 years approximately (Figs. 9. a, and 10. a). In the CSA, the opposite occurs, this "funnel" shape presents higher energy in DJF than in JJA and is the predominant forcing feature between 11,700 and 7,710 years approximately (Figs. 9. e and 10. e). This "funnel shape" in the wavelet spectrum indicates a sudden and marked change in the time series, since it is a large amplitude artifact that occurs when there is a sharp discontinuity in the signal (e.g., Addison, 2018; Wainer et al., 2021). Therefore, spectra from the NA and CSA show an artifact related to the sharp discontinuities in the signal that may correspond to the meltwater pulses that occurred probably because of the end of the YD (~11,700 years), which was an reglaciating event (e.g. Sowers and Bender, 1995), and because of the 8,200 years event, which consisted of a widespread cooling associated with the sudden draining of the Lake Agassiz-Ojibway glacial complex across the Hudson Strait (Alley et al., 1997; Barber et al., 1999). This event had global effects and culminated in the beginning of the collapse of large ice sheets in the NH, such as the LIS (Barber et al., 1999). In other key areas these meltwater pulses seem to be related to the presence of a high energy at middle and low frequencies (about 640 to 5,120 years) as the predominant forcing feature before 7,710 years, both in DJF and JJA, except for CSA in JJA.

The decrease in insolation in the NH and the increase in insolation in the SH from the Holocene onwards promoted a change in the long-term precipitation trends in both hemispheres, with the increase in the migration range of the ITCZ and the southward displacement of the SACZ in the end of LH (Chiessi et al., 2021; Cust'odio et al., 2024). This trend is identified in the wavelet analysis as a continuous power peak along the Holocene in the lower frequencies (Fig. 9).

These results are very important because they show that all key areas had their annual cycle and precipitation anomalies during the Holocene influenced in some way by the melting of the LIS and the change in the insolation pattern during this period, and that this influence can be observed with the change in the trend that occurs in these areas around 9,000 to 8,000 years and by the high energy signals as the predominant forcing feature before 7,710 years in the wavelet analyses.

5. Conclusions

Here, we investigated precipitation patterns and variability in the TA in the past to examine whether there was variation from the present and how this relates to Holocene climate variations and events. We used precipitation records from different observational and reanalysis datasets to understand precipitation patterns and variability in the TA today, and we used paleorecords from studies in lake sediments and speleothems and model outputs from TraCE-21ka to understand these patterns during the Holocene. Based on these results, we delimited five key areas and did a regional analysis of the variability of precipitation during the period of interest.

Although both paleorecord and TraCE-21ka outputs climate reconstructions agree on long-term wetting trends, proxy sensitivities (temporal resolution) and model limitations (spatial smoothing) are the main drivers of regional discrepancies. Lake sediments and speleothems signals conflict in northeastern Brazil (EH), reflecting their different response timescales, while model-data mismatches in southern Peru (LH) highlight unresolved topography-driven rainfall. Future work should prioritize proxysystem modeling to isolate these factors.

Analysis of precipitation variability in key areas shows that in all areas a change in the trend of the precipitation anomaly was recorded around 9,000 to 8,000 years and the wavelet analysis shows that the Holocene precipitation was strongly influenced by events that generated high energy signals as the predominant forcing feature before 7,710

years. These records around 7,710 years are possibly related to the final collapse of the North American ice sheets and the reorganization of the global climate, i.e., the 8,200 years event. This collapse was accelerated by the increase in summer insolation in the NH during the EH (Walker et al., 2012; Walker et al., 2018). The entry of freshwater into the North Atlantic from this meltwater pulses weakened the AMOC from the MH and that, associated with changes in the insolation pattern in that period, contributed to the displacement of the ITCZ and the SACZ to the south, weakening the NAMS and strengthening the SAMS (Cust'odio et al., 2024; Strikis et al., 2011). This set of factors contributed to a change in the pattern of precipitation in the TA during the Holocene, influencing both the seasonal variation (annual cycle) and the variability over time (precipitation anomaly) in key areas.

Although in recent years more studies have been carried out on rainfall variation in the TA, more detailed studies on climate variation in this region during the Holocene are needed to properly assess observed trends. This is necessary since these trends influence the unique ecosystems of the TA and the socioeconomic activities of different countries, some of which have a large part of their economy dependent on agriculture. Understanding how precipitation patterns in this area have varied in the past under nonanthropogenic forcings can help predict future changes, allowing governments of countries in this region to prepare for these changes to mitigate their impacts.

Declaration of competing interest

The authors declare that they have no known competing financial interests or personal relationships that could have appeared to influence the work reported in this paper.

ACKNOWLEDGEMENTS

P. R. B. thanks Coordenação de Aperfeiçoamento de Pessoal de Nível Superior – Brasil (CAPES) for her PhD scholarship – Finance Code 001: 88887.642819/2021-00. The authors are also thankful to FAPDF: 0193.001374/2016; FAPESP: 2019/08247-1; FAPERJ: E-26/210.291/2024; CNPq-Universal 405607/2023-7.

Appendix A.Supplementary data

Supplementary data to this article can be found online at https://doi. org/10.1016/j.palaeo.2025.112935.

Data availability

Data will be made available on request.

References

- Addison, P.S., 2018. Introduction to redundancy rules: the continuous wavelet transform comes of age. Philos. Trans. R. Soc. A Math. Phys. Eng. Sci. 376 (2126), 20170258. https://doi.org/10.1098/rsta.2017.0258.
- Adler, R.F., Sapiano, M.R.P., Huffman, G.J., Wang, J.J., Gu, G., Bolvin, D., Chiu, L., Schneider, U., Becker, A., Nelkin, E., Xie, P., Ferraro, R., Shin, D. Bin, 2018. The global precipitation climatology project (GPCP) monthly analysis (New Version 2.3) and a review of 2017 global precipitation. Atmosphere 9 (4). https://doi.org/10.3390/atmos9040138.
- Aharon, P., 2003. Meltwater flooding events in the Gulf of Mexico revisited: Implications for rapid climate changes during the last deglaciation. Paleoceanography 18 (4). https://doi.org/10.1029/2002PA000840.
- Alley, R.B., Mayewski, P.A., Sowers, T., Stuiver, M., Taylor, K.C., Clark, P.U., 1997. Holocene climatic instability: a prominent, widespread event 8200 yr ago. Geology 25 (6), 483. https://doi.org/10.1130/0091-7613(1997)025<0483:HCIAPW>2.3. CO;2.
- Alves, L.M., Chadwick, R., Moise, A., Brown, J., Marengo, J.A., 2021. Assessment of rainfall variability and future change in Brazil across multiple timescales. Int. J. Climatol. 41 (S1), E1875–E1888. https://doi.org/10.1002/joc.6818.
- Barber, D.C., Dyke, A., Hillaire-Marcel, C., Jennings, A.E., Andrews, J.T., Kerwin, M.W., Bilodeau, G., McNeely, R., Southon, J., Morehead, M.D., Gagnon, J.-M., 1999. Forcing of the cold event of 8,200 years ago by catastrophic drainage of Laurentide lakes. Nature 400 (6742), 344–348. https://doi.org/10.1038/22504.
- Birks, H.H., Birks, H.J.B., 2006. Multi-proxy studies in palaeolimnology. Veg. Hist. Archaeobotany 15 (4), 235–251. https://doi.org/10.1007/s00334-006-0066-6.

- Braconnot, P., Otto-Bliesner, B., Harrison, S., Joussaume, S., Peterchmitt, J.-Y., Abe-Ouchi, A., Crucifix, M., Driesschaert, E., Fichefet, Th., Hewitt, C.D., Kageyama, M., Kitoh, A., Laîn'e, A., Loutre, M.-F., Marti, O., Merkel, U., Ramstein, G., Valdes, P., Weber, S.L., Zhao, Y., 2007. Results of PMIP2 coupled simulations of the mid-holocene and last glacial maximum part 1: experiments and large-scale features. Clim. Past 3 (2), 261–277. https://doi.org/10.5194/cp-3-261-2007.
- Campos, M.C., Chiessi, C.M., Novello, V.F., Crivellari, S., Campos, J.L.P.S., Albuquerque, A.L.S., Venancio, I.M., Santos, T.P., Melo, D.B., Cruz, F.W., Sawakuchi, A.O., Mendes, V.R., 2022. South American precipitation dipole forced by interhemispheric temperature gradient. Sci. Rep. 12 (1), 10527. https://doi.org/10.1038/s41598-022-14495-1.
- Carvalho, L.M.V., 2020. Assessing precipitation trends in the Americas with historical data: a review. In: Wiley Interdisciplinary Reviews: Climate Change Vol. 11. Wiley-Blackwell. https://doi.org/10.1002/wcc.627.
- Cavazos, T., Luna-Ni˜no, R., Cerezo-Mota, R., Fuentes-Franco, R., M'endez, M., Pineda Martínez, L.F., Valenzuela, E., 2020. Climatic trends and regional climate models intercomparison over the CORDEX-CAM (Central America, Caribbean, and Mexico) domain. Int. J. Climatol. 40 (3), 1396–1420. https://doi.org/10.1002/joc.6276.
- Chen, M., Xie, P., Janowiak, J.E., Arkin, P.A., 2002. Global land precipitation: A 50-yr monthly analysis based on gauge observations. J. Hydrometeorol. 3 (3), 249–266.
- Chiessi, C.M., Mulitza, S., Taniguchi, N.K., Prange, M., Campos, M.C., H¨aggi, C., Schefuß, E., Pinho, T.M.L., Frederichs, T., Portilho-Ramos, R.C., Sousa, S.H.M., Crivellari, S., Cruz, F.W., 2021. Mid- to late holocene contraction of the intertropical convergence zone over Northeastern South America. Paleoceanogr. Paleoclimatol. 36 (4). https://doi.org/10.1029/2020PA003936.
- Collins, W.D., Bitz, C.M., Blackmon, M.L., Bonan, G.B., Bretherton, C.S., Carton, J.A., Doney, S.C., Hack, J.J., Henderson, T.B., Kiehl, J.T., Large, W.G., Mckenna, D.S., Santer, B.D., Smith, R.D., 2006. The Community Climate System Model Version 3 (CCSM3). www.ccsm.ucar.edu/models.

- Compo, G.P., Whitaker, J.S., Sardeshmukh, P.D., Matsui, N., Allan, R.J., Yin, X., Gleason, B.E., Vose, R.S., Rutledge, G., Bessemoulin, P., Br¨onnimann, S., Brunet, M., Crouthamel, R.I., Grant, A.N., Groisman, P.Y., Jones, P.D., Kruk, M.C., Kruger, A.C., Marshall, G.J., Worley, S.J., 2011. The twentieth century reanalysis project. Q. J. R. Meteorol. Soc. 137 (654), 1–28. https://doi.org/10.1002/qj.776.
- Corrales-Suastegui, A., Fuentes-Franco, R., Pavia, E.G., 2020. The mid-summer drought over Mexico and Central America in the 21st century. Int. J. Climatol. 40 (3), 1703–1715. https://doi.org/10.1002/joc.6296.
- Cust'odio, I.S., da Silva Dias, P.L., Wainer, I., Prado, L.F., 2024. Changes in the South American Monsoon system components since the last glacial maximum: a TraCE-21k perspective. Clim. Dyn. https://doi.org/10.1007/s00382-024-07139-9.
- Duarte, E., Obrist-Farner, J., Correa-Metrio, A., Steinman, B.A., 2021. A progressively wetter early through middle Holocene climate in the eastern lowlands of Guatemala. Earth Planet. Sci. Lett. 561, 116807. https://doi.org/10.1016/j.epsl.2021.116807.
- Feng, S., Hu, Q., Oglesby, R.J., 2011. Influence of Atlantic Sea surface temperatures on persistent drought in North America. Clim. Dyn. 37 (3–4), 569–586. https://doi.org/10.1007/s00382-010-0835-x.
- Fu, R., Arias, P.A., Wang, H., 2016. The connection between the North and South American monsoons. In: Springer Climate. Springer, pp. 187–206. https://doi.org/10.1007/978-3-319-21650-8 9.
- Gan, M.A., Kousky, V.E., Ropelewski, C.F., 2004. The South America Monsoon circulation and its relationship to rainfall over west-central Brazil. J. Clim. 17 (1), 47–66. https://doi.org/10.1175/1520-0442(2004)017<0047:TSAMCA>2.0.CO;2.
- Geen, R., Bordoni, S., Battisti, D.S., Hui, K., 2020. Monsoons, ITCZs, and the concept of the global monsoon. Rev. Geophys. 58 (4). https://doi.org/10.1029/2020RG000700.
- Gorenstein, I., Prado, L.F., Bianchini, P.R., Wainer, I., Griffiths, M.L., Pausata, F.S.R., Yokoyama, E., 2022. A fully calibrated and updated mid-Holocene climate reconstruction for Eastern South America. Quat. Sci. Rev. 292. https://doi.org/10.1016/j.quascirev.2022.107646.
- Hajdas, I., 2008. Radiocarbon Dating and its Applications in Quaternary Studies.

- He, F., 2011. Simulating Transient Climate Evolution of the Last Deglaciation with CCSM3. Thesis University of Wisconsin-Madison.
- Laepple, T., Ziegler, E., Weitzel, N., H'ebert, R., Ellerhoff, B., Schoch, P., Martrat, B., Bothe, O., Moreno-Chamarro, E., Chevalier, M., Herbert, A., Rehfeld, K., 2023. Regional but not global temperature variability underestimated by climate models at supradecadal timescales. Nat. Geosci. 16 (11), 958–966. https://doi.org/10.1038/s41561-023-01299-9.
- Liu, Z., Otto-Bliesner, B.L., He, F., Brady, E.C., Tomas, R., Clark, P.U., Carlson, A.E., Lynch-Stieglitz, J., Curry, W., Brook, E., Erickson, D., Jacob, R., Kutzbach, J., Cheng, J., 2009. Transient simulation of last deglaciation with a new mechanism for bølling-allerød warming. Science 325 (5938), 310–314. https://doi.org/10.1126/science.1171041.
- Marengo, J.A., Liebmann, B., Grimm, A.M., Misra, V., Silva Dias, P.L., Cavalcanti, I.F.A., Carvalho, L.M.V., Berbery, E.H., Ambrizzi, T., Vera, C.S., Saulo, A.C., Nogues-Paegle, J., Zipser, E., Seth, A., Alves, L.M., 2012. Recent developments on the south American monsoon system. Int. J. Climatol. 32 (1), 1–21. https://doi.org/10.1002/joc.2254.
- Mayewski, P.A., Rohling, E.E., Curt Stager, J., Karl'en, W., Maasch, K.A., Meeker, L.D.,
 Meyerson, E.A., Gasse, F., van Kreveld, S., Holmgren, K., Lee-Thorp, J., Rosqvist,
 G., Rack, F., Staubwasser, M., Schneider, R.R., Steig, E.J., 2004. Holocene climate
 variability. Quat. Res. 62 (3), 243–255. https://doi.org/10.1016/j. yqres.2004.07.001.
- Mechoso, C.R., Robertson, A.W., Ropelewski, C.F., Grimm, A.M., 2004. The American Monsoon Systems.
- Metcalfe, S.E., Barron, J.A., Davies, S.J., 2015. The Holocene history of the north American Monsoon: 'known knowns' and 'known unknowns' in understanding its spatial and temporal complexity. Quat. Sci. Rev. 120, 1–27. https://doi.org/10.1016/j.quascirev.2015.04.004.
- Mitchell, D.L., Ivanova, D., Rabin, R., Brown, T.J., Redmond, K., 2002. Gulf of California Sea surface temperatures and the north American Monsoon: mechanistic implications from observations. J. Clim. 15 (17), 2261–2281. https://doi.org/ 10.1175/1520-0442(2002)015<2261:GOCSST>2.0.CO;2.

- Nowacki, D., Langan, C.C.M., Kadereit, A., Pint, A., Wunderlich, J., 2019. 'Lake Gorgana'-A paleolake in the lower Danube valley revealed using multi-proxy and regionalisation approaches. Quat. Int. 511, 107–123.
- Pelling, M., 2010. Adaptation to Climate Change: From Resilience to Transformation, New York, NY. Routledge.
- Pinchinat, A.M., Soria, J., Bazan, R., 2015. Multiple Cropping in Tropical America, pp. 51–61. https://doi.org/10.2134/asaspecpub27.c4.
- Poveda, G., Waylen, P.R., Pulwarty, R.S., 2006. Annual and inter-annual variability of the present climate in northern South America and southern Mesoamerica.
- Palaeogeogr. Palaeoclimatol. Palaeoecol. 234 (1), 3–27. https://doi.org/10.1016/j. palaeo.2005.10.031.
- Prado, L.F., Wainer, I., Yokoyama, E., Khodri, M., Garnier, J., 2021. Changes in summer precipitation variability in Central Brazil over the past eight decades. Int. J. Climatol. 41 (8), 4171–4186. https://doi.org/10.1002/joc.7065.
- Rasmussen, T.L., Thomsen, E., 2012. Changes in planktic foraminiferal faunas, temperature and salinity in the Gulf Stream during the last 30,000 years: influence of meltwater via the Mississippi River. Quat. Sci. Rev. 33, 42–54. https://doi.org/10.1016/j.quascirev.2011.11.019.
- Reboita, M.S., Ambrizzi, T., Crespo, N.M., Dutra, L.M.M., de Ferreira, G.W.S., Rehbein, A., Drumond, A., da Rocha, R.P., de Souza, C.A., 2021. Impacts of teleconnection patterns on South America climate. Ann. N. Y. Acad. Sci. 1504 (1), 116–153. https://doi.org/10.1111/nyas.14592.
- R"osch, A., Schmidbauer, H., 2018. WaveletComp 1.1: A Guided Tour Through the R Package. Available at https://cran.r-project.org/web/packages/WaveletComp/WaveletComp.pdf[Accessed 20th June 2023].
- Schneider, U., Ziese, M., Meyer-Christoffer, A., Finger, P., Rustemeier, E., Becker, A., 2016. The new portfolio of global precipitation data products of the Global Precipitation Climatology Centre suitable to assess and quantify the global water cycle and resources. Proc. Int. Assoc. Hydrol. Sci. 374, 29–34. https://doi.org/10.5194/piahs-374-29-2016.

- Seneviratne, S.I., Zhang, X., Adnan, M., Badi, W., Dereczynski, C., Di Luca, A., Ghosh,
 S., Iskandar, I., Kossin, J., Lewis, S., Otto, F., Pinto, I., Satoh, M., Vicente-Serrano,
 S.M., Wehner, M., Zhou, B., 2021. Weather and climate extreme events in a changing climate. In: Climate Change 2021: The Physical Science Basis. Contribution of Working Group I to the Sixth Assessment Report of the Intergovernmental Panel on Climate Change. Cambridge University Press, Cambridge, United Kingdom and New York, NY, USA, pp. 1513–1766.
- Sheppard, P.R., Comrie, A.C., Packin, G.D., Angersbach, K., Hughes, M.K., 2002. The climate of the U.S. southwest. Clim. Res. 21, 219–238.
- Slivinski, L.C., Compo, G.P., Whitaker, J.S., Sardeshmukh, P.D., Giese, B.S., McColl, C., Allan, R., Yin, X., Vose, R., Titchner, H., Kennedy, J., Spencer, L.J., Ashcroft, L., Br"onnimann, S., Brunet, M., Camuffo, D., Cornes, R., Cram, T.A., Crouthamel, R., Wyszy'nski, P., 2019. Towards a more reliable historical reanalysis: improvements for version 3 of the Twentieth Century reanalysis system. Q. J. R. Meteorol. Soc. 145 (724), 2876–2908. https://doi.org/10.1002/qj.3598.
- Sorooshian, S., Martinson, D.G., 1995. Proxy indicators of climate, an essay. In: Natural Climate Variability on Decade-to-Century Time Scales. The National Academies Press, Washington D.C., pp. 489–494
- Sowers, T., Bender, M., 1995. Climate records covering the last deglaciation. Science 269 (5221), 210–214. https://doi.org/10.1126/science.269.5221.210.
- Strikis, N.M., Cruz, F.W., Cheng, H., Karmann, I., Edwards, R.L., Vuille, M., Wang, X., de Paula, M.S., Novello, V.F., Auler, A.S., 2011. Abrupt variations in south American monsoon rainfall during the holocene based on a speleothem record from Central- Eastern Brazil. Geology 39 (11), 1075–1078. https://doi.org/10.1130/G32098.1.
- Tierney, J.E., Zhu, J., King, J., Malevich, S.B., Hakim, G.J., Poulsen, C.J., 2020. Glacial cooling and climate sensitivity revisited. Nature 584 (7822), 569–573. https://doi.org/10.1038/s41586-020-2617-x.
- T"ornqvist, T.E., Hijma, M.P., 2012. Links between early Holocene ice-sheet decay, sealevel rise and abrupt climate change. Nat. Geosci. 5 (9), 601–606. https://doi.org/10.1038/ngeo1536.

- Torrence, C., Compo, G.P., 1998. A practical guide to wavelet analysis. Bull. Am. Meteorol. Soc. 79 (1), 61–78. https://doi.org/10.1175/1520-0477(1998)079<0061: APGTWA>2.0.CO;2.
- Tushingham, A.M., Peltire, W.R., 1991. Ice-3G' a new global model of late pleistocene deglaciation based upon geophysical predictions of post-glacial relative sea level change. J. Geophys. Res. 96, 4497–4523.
- Vera, C., Higgins, W., Amador, J., Ambrizzi, T., Garreaud, R., Gochis, D., Gutzler, D., Lettenmaier, D., Marengo, J., Mechoso, C.R., Nogues-Paegle, J., Dias, P.L.S., Zhang, A.C., 2006. Toward a Unified View of the American Monsoon Systems.
- Wainer, I., Prado, L. F., Khodri, M., & Otto-Bliesner, B. (2021). The South Atlantic subtropical dipole mode since the last deglaciation and changes in rainfall. Clim. Dyn., 56(1–2), 109–122. doi:https://doi.org/10.1007/s00382-020-05468-z.
- Walker, M.J.C., Berkelhammer, M., Bj"orck, S., Cwynar, L.C., Fisher, D.A., Long, A.J., Lowe, J.J., Newnham, R.M., Rasmussen, S.O., Weiss, H., 2012. Formal subdivision of the holocene series/epoch: a discussion paper by a Working Group of INTIMATE (integration of ice-core, marine and terrestrial records) and the subcommission on quaternary stratigraphy (international commission on stratigraphy). J. Quat. Sci. 27 (7), 649–659. https://doi.org/10.1002/jqs.2565.
- Walker, M., Head, M.J., Berkelhammer, M., Bj"orck, S., Cheng, H., Cwynar, L., Fisher, D., Gkinis, V., Long, A., Lowe, J., Newnham, R., Rasmussen, S.O., Weiss, H., 2018. Formal ratification of the subdivision of the holocene series/epoch (quaternary system/period): two new global boundary stratotype sections and points (GSSPs) and three new stages/subseries. Episodes 41 (4), 213–223. https://doi.org/10.18814/epiiugs/2018/018016.
- Walker, M., Gibbard, P., Head, M.J., Berkelhammer, M., Bj"orck, S., Cheng, H., Cwynar,
 L. C., Fisher, D., Gkinis, V., Long, A., Lowe, J., Newnham, R., Rasmussen, S.O.,
 Weiss, H., 2019. Formal subdivision of the holocene series/epoch: a summary. J.
 Geol. Soc. India 93 (2), 135–141. https://doi.org/10.1007/s12594-019-1141-9.
- Wanner, H., Solomina, O., Grosjean, M., Ritz, S.P., Jetel, M., 2011. Structure and origin of holocene cold events. Quat. Sci. Rev. 30 (21 □ 22), 3109–3123. https://doi.org/10.1016/j.quascirev.2011.07.010.

- Xie, P., Arkin, P.A., 1997. Global precipitation A 17-year monthly analysis based on gauge observations, satellite estimates, and numerical model outputs. Bull. Am. Meteorol. Soc. 78 (11), 2539–2558.
- Yeager, S.G., Shields, C.A., Large, W.G., Hack, J.J., 2006. The Low-Resolution CCSM3.
- Zhou, J., Lau, K.-M., 1998. Does a monsoon climate exist over South America? J. Clim. 11 (5), 1020–1040. https://doi.org/10.1175/1520-0442(1998)011<1020: DAMCEO>2.0.CO;2.



Contents lists available at ScienceDirect

Quaternary Science Reviews



A fully calibrated and updated mid-Holocene climate reconstruction for Eastern South America



Iuri Gorenstein a, *, Luciana F. Prado a, b, Paula R. Bianchini b, Ilana Wainer a,

Michael L. Griffiths c, Francesco S.R. Pausata d, Elder Yokoyama b

Abstract

Investigating the extent and climate implications of the mid-Holocene (MH - around 6000 years ago) is essential in better understanding the uncertainties associated with the ongoing and future projections of global warming. South America (SA) contains the biome with the largest biodiversity in the world, its population exceeds 400 million people, and its economy is mainly agricultural. Thus, studies involving South America's climate variability have become a subject of significant importance over the years. Paleoclimate archives provide unique indirect measurements, helping us to characterize past climates. However, the derived radiometric ages from several paleoarchives in SA published before the 2000s have not yet been calibrated, which represents a large source of uncertainty. In this article, we present a climate reconstruction for eastern SA during the MH with fully calibrated age models. We compiled 173 paleoclimate records, where 50 of them were calibrated in this study using Bayesian methods. Through this multiproxy approach and the elaboration of a new homogeneous quality index for proxies, our novel

^a Instituto Oceanogra fico, Universidade de Sa~o Paulo, Sa~o Paulo, Brazil

^b Instituto de Geoci[^]encias, Universidade de Brasília, Brasília, Brazil

^c Department of Environmental Science, William Paterson University, Wayne, NJ, USA

^d Centre ESCER (Etude et la Simulation du Climat a` l'Echelle Regionale) and GEOTOP (Research Center on the Dynamics of the Earth System), Department of Earth and Atmospheric Sciences, University of Quebec in Montreal, Montreal, QC, Canada

climate reconstruction sheds new light on the regional climate of SA climate during MH. All high quality (higher than 1) paleoarchives agree at regional scale. Compiled paleodata confirms reduced rainfall in Amazonia and a warmer and drier Southern SA, indicating an overall weakening of the South American Summer Monsoon during the MH. North East Brazil coast show higher than present moisture during the MH, while the border between Northeast Brazil and Southern SA shows divergent behavior, pointing to a local erratic rainfall regime with inputs of higher than present moisture conditions, most likely caused by changes in precipitation over the South Atlantic Convergence Zone, and a weaker than present South Atlantic Subtropical High during MH.

Keywords: Mid-Holocene, Proxy data, South America Compilation, Precipitation, Lake levels, Surface temperature, Sea surface temperature, Sea surface salinity, Quality index

1. Introduction

Investigating rainfall changes in SA has become a subject of significant importance considering that the impact of recent global warming trends can present a serious threat to its population, particularly in regions such as Northeast Brazil (NE) that already face severe water shortages (Souza et al. (2005); Rojas et al. (2014); Cunha et al. (2019)). Recently the IPCC Sixth Assessment Report (AR6) showed projections for 1.5 or 2 °C global warming and a local increase even higher, of at least +0.5 °C, in almost the entire South American continent (Ajjur and Al-Ghamdi (2021); Torres et al. (2021)). This temperature rise implicate in projections with an increased precipitation in the southern region of Brazil and in the northern portion of the Brazilian Northeast, in northern Argentina, Uruguay, and parts of Peru, Ecuador, Colombia and Venezuela; while the areas between the south of Chile and Argentina and the extreme north of South America are expected to suffer precipitation reductions (Torres et al. (2021)).

Paleorecords have the potential to provide valuable insights into how the climate system operates on a range of timescales beyond the instrumental historical period (Bradley (1999)). Together with model-based climate simulations, the paleodata can help elucidate the mechanisms and feedbacks associated with global climate change that cannot be provided by direct observation of the modern climate (Pausata et al. (2016, 2017)); Lu et al. (2018); Hernández et al. (2020); Kaufman et al. (2020); Tabor et al. (2020)). Consid- ering both: the MH as an analog for current and near-future global

warming; and the small number of paleoclimate reconstruction studies for South America (Prado et al., 2013a; Smith and Mayle (2017)), having a reliable and relatively well populated data set is fundamental to reduce uncertainties related to the understanding of South American climate. The work from Prado et al. (2013a) and Smith and Mayle (2017) were the last two published multi-proxy full climate and dynamic vegetation reconstructions for Eastern SA, respectively. Although Smith & Mayle's focus was not the MH epoch per se, their discussions and conclusions were essential for the following compilation update and made the elaboration of the climate reconstruction maps, with the regional subdivision, possible.

The mid-Holocene (MH, period between 5000 and 7000 years Before Present) was characterized by lower summer insolation in the Southern Hemisphere and higher summer insolation in the Northern Hemisphere, resulting in the so-called "Holocene Ther- mal Maximum" (Berger (1988); Liu et al. (2002); Bova et al. (2021)). While it may be seen as a conceivable geological analog for the future (Burkea et al. (2018); Kaufman et al. (2020)), the warming associated with these changes was neither global nor year-round, with large differences across the hemispheres and seasons (Berger, 1978; Zhao and Harrison (2012); Huo et al. (2021)).

Climate changes during the MH vary across the globe. While the direct effects of the MH insolation pattern produced an enhance- ment in the Northern Hemisphere monsoon, the Southern Hemi- sphere precipitation experienced a reduction when compared to present day (Liu et al. (2004); Wanner et al. (2008); Smith and Mayle (2017)). Other MH climate forcings, such as the presence of vegetation on contemporary deserted locations in North Africa and Asia, have been associated to changes in globalmean surface temperature, global precipitation and to an increase of the Atlantic Meridional Overturning Circulation (Harrison and Bartlein (2012); Pausata et al. (2017); Griffiths et al. (2020); Ding et al. (2021); Huo et al. (2021); Zhang et al., 2021). In South America (SA - Fig. 1) climate is not fully monsoonal in the classical definition (i.e. the low-level winds never reverse their direction). However, the shift from winter's maximum continental rainfall over the ITCZ to the austral summer precipitation extending through the southern half of the Amazon Basin to northern Argentina, next to the South Atlantic Convergence Zone (SACZ), is sometimes described as 'monsoon-like' and is defined as the South America Monsoon System (Zhou and Lau (1998); Vera et al. (2006); Garreaud et al. (2009); Marengo et al. (2012)). MH climate conditions have been linked to vegetation changes in Southwest Amazonia and southeast Brazil, regions more reliant on

South American summer monsoon (SASM) derived precipitation (Smith and Mayle (2017)). It may have also been responsible for southeast Brazil demographic shifts and migration to more buffered climates where agricultural activities could be more predictable (Raczka et al. (2013); Riris and Arroyo- Kalin (2019)). In addition, lower precipitation causing weaker river runoffs have been linked to a weaker Brazil Current, resulting in saltier sea surface conditions in Brazil's Coast during the MH (Prado et al., 2013a).

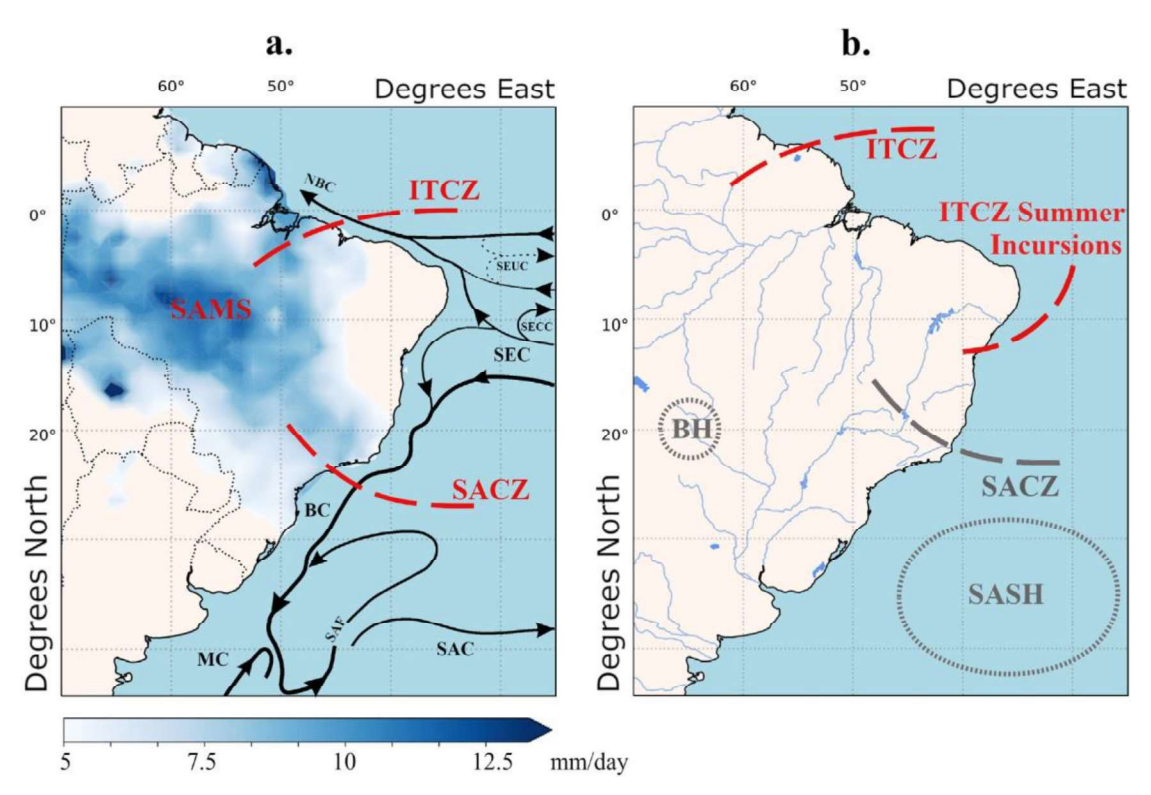


Fig. 1. a) South American mean precipitation over land during summer (December, January and February mean from 1891 to 2019) from the Global Precipitation Climatology Center (GPCC) in mm/day (Schneider et al. (2015)). The Intertropical and South Atlantic Convergence Zones (ITCZ and SACZ, respectively), associated with the South American Summer Monsoon (SASM) are highlighted in red. Black arrows represent the upper-level barotropic currents and fronts on the Brazilian continental margin, western South Atlantic Ocean: BC e Brazil Current; MC e Malvinas Current; NBC e North Brazil Current; SAF - South Atlantic Current; SEUC e South Equatorial Under Current; SECC e South Equatorial Countercurrent; SEC e South Equatorial Current; SAF e Subantarctic Front; adapted from Peterson and Stramma (1991). b) South America's rivers and lakes present distribution with its climate features from the mid-Holocene. In red, the ITCZ northward shift and its increased Summer incursions

during the Southern Hemisphere's summer. In Grey the features which showed weakening during the mid-Holocene: The Bolivian High (BH) causing lower moisture transport inside the continent; The South Atlantic Convergence Zone (SACZ) which also may have suffered a northerly displacement due to the weakening of the South Atlantic Subtropical High (SASH) (Dias et al. (2009); Prado et al., 2013a, 2013b; Maksic et al. (2019)).

Different paleoclimate data provide information on distinct climate variables. For example, pollen data reflect both temperature and precipitation changes (Behling and Costa (1997a); Ledru et al. (2009)). Oxygen isotope (δ^{18} O) records in cave deposits are commonly interpreted as changes in the intensity of local and regional monsoon activity (Wang et al. (2017); Wong et al. (2021)) while other geochemical tracers, such as 87Sr/86Sr which can reflect relative changes in local karstic hydrology and productivity (soil production/erosion), also have been used to retrieve indirect information of wet/dry conditions (Ward et al. (2019)). Charcoal analysis can reveal changes in sedimentation rates and fire history linked to a specific time period, giving indirect information on past rainfall variability and even human activity (Brugger et al. (2016); Riris and Arroyo-Kalin (2019)). Meanwhile, the abundance from a specific chemical element in a sediment sample brought only by rain to a lake site or ocean basin can also be an indicator of past rainfall activity in that area (Haug et al. (2001)). The foraminiferal δ^{18} O and Mg/Ca records and other biological dependent organic compounds found in marine sediment cores are used to evaluate water-mass influence on planktonic activity. Changes in these proxies can suggest variations in the sea surface salinity (SSS) or sea surface temperature (SST), suggesting the strengthening from a specific Ocean current or even changes the low-atmospheric cir- culation, water formation and river discharges (Howe et al. (2018)). In a continent such as SA proxy records interpretation can signifi- cantly change from a place to another. Therefore, each excavation's site characteristics must be analyzed and the proxy information interpreted accordingly.

Calibration of radiocarbon ages used to generate age models is critical to multiproxy analyses as the uncertainties from a sample's age are responsible for attributing (or not) a specific characteristic or climate change to a geologic period (Lowe and Walker (1997)). Conventions for calibrating terrestrial samples have evolved over time, radiocarbon dating began being used to calibrate paleo- archive ages in 1940s (Wood (2015)). Radiocarbon dates now dominate the vast majority of archaeological and palaeoenvironmental chronologies. Publications from this research field have been provided with a specific journal (Radiocarbon) and their methods and applications are discussed in regular conferences (e.g. AMS, Radiocarbon, Radiocarbon and the Environment, Radiocarbon and Archaeology). Particularly, in the last couple of decades radiocarbon dating of any paleorecord has become indispensable for more robust reconstructions of past climate (Hogg et al. (2013)). Other than paleo-reconstructions, previous studies used climate model simulations to analyze the MH climate and vegetation in South America (Prado et al., 2013b; Maksic et al. (2019); Tabor et al. (2020)). In a numerical simulation for the Holocene, Maksic et al. (2019) discussed climate and vegetation changes over SA. The model simulated conditions drier than present over most of SA, with a gradual strengthening of the SASM toward the present day. By contrast, the models show that northern NE Brazil was wetter because of the southward migration of the ITCZ. The results of Maksic et al. (2019) suggest NE Brazil was replaced with savanna or dense shrubland and the Amazonian tropical forest was smaller in area than today, although western Amazonia persisted as a tropical forest throughout the Holocene. In another recent study, Tabor et al. (2020) used an Earth system model that simulates water isotopologues in mid-Holocene climate. Focusing on speleothems δ^{18} O values from the South American and Asian monsoon regions, the authors found that the presence of a vegetated Sahara during the mid-Holocene leads to global warming and generally amplifies the orbital-driven changes in the δ^{18} O values in South America, further increasing the rainfall deficit from this region in MH.

This study reviews and updates the paleorecords compilation of Prado et al. (2013a, 2013b) by including recently published records, and calibrating age models that were not previously calibrated. The paleo precipitation, temperature, lake levels, SST and SSS from SA during the MH are mapped. From our new climate reconstructions, we then discuss South America's MH precipitation signals in detail, particularly the Northeast Brazil frontier with Southern SA (14-20S and 40e48W) where precipitation and temperature paleoarchives information from the MH diverge the most. This region belongs to the center of the SASM and its rainy season is mainly controlled by the South Atlantic Convergence Zone (Mahiques et al. (2009); Wong et al. (2021)). Interpreting the paleorecords in regional context, including their inherent limitations are discussed for this region. The age calibrations were obtained using Bayesian statistics described in the Methods Section.

2. Material and Methods

2.1. Proxies and Paleoarchives

We compiled 173 (total) studies, consisting of different paleo- archives: 19 speleothems, 145 sediment cores (13 marine, 63 lacustrine, and 69 terrestrial) and 8 soil samples from South America, published in scientific journals and dissertations until mid-2021. The proxy classification description is shown in Table 1 and the proxies used in this study are exemplified and detailed in Table S.1.

Table 1Description of proxy types used in this study (modified from Wirtz et al., 2010).

Code	Proxy Type	Description
ĪF	Isotopic fraction	$d^{18}O, d^{13}C, d^{15}N, d^{87}Sr.$
PC	Physico-chemical	Mg/Ca, Ti/Ca, Fe/Ca, Fe/Sr,
BI	Biological	Al/Si, Si/Ca, C/N, Grain size, Alkenone, Mineralogy, Magnetic susceptibility Pollen, Diatoms, Spores, Algae,
		Molluscs, Sponge, Organic Matter, Charcoal, Relative abundance

From those paleoarchives, a large variety of proxy types have been analyzed. Table 1 describes the main proxy types used in this study. Our methodology is similar to Prado et al. (2013a, 2013b). Oxygen, carbon, strontium and nitrogen stable isotopic ratios are the fractionation-dependent proxies. The physico-chemical proxies comprise all geochemical ratios and physico-chemical approaches, whilst all information derived from organisms is classified as bio- logical (Prado et al., 2013a; Wirtz et al. (2010)).

The analysis made in each proxy study compiled here is not extensively discussed, however, nearby study sites with conflicting information are examined in detail. Table 2 displays the coordinates from the proxies corresponding to each record. The same paleoclimate archive can sometimes present one or even all three different proxy analyses. In total there are 137 paleo archives that contain biological proxies, 93 with isotopic fraction proxies and 56 presenting physico-chemical (Table S.1).

Due to uncertainties in the age models, we defined the MH as the period from 7000 to 5000 calibrated years before present (cal yr BP). This 2000-year window is

necessary to correctly fit the climate data in the desired time interval without losing any valuable in- formation from the MH.

Table 2

Number and quality index mean (Q mean) from each compiled paleoarchive (speleothem,nsediment and soil samples) and proxy types (IF: Isotopic fraction; BIO: Biological; PC: Physico-chemical) in the precipitation reconstruction.

Eastern South America Precipitation				
Paleoarchives	Number	Q mean		
Speleothem	18	2.09		
Sediment	116	0.57		
Soil Samples	11	0.61		
Proxies	Number	Q mean		
IF	39	1.24		
BIO	118	0.48		
PC	36	0.56		

2.2. Data and material

The 173 records compiled in this study, assembled in Table S.1 (respective locations can be found in Fig. S.3), include proxies for precipitation, air temperature, lake level, SST and SSS.

In Prado et al. (2013a, 2013b), 69 of the 120 paleoclimatic re- cords had calibrated age models. We calibrated the ages of the remaining 51, and from those records 5 could not be used in this compilation anymore. After calibration their ages were out of the MH time interval defined in this study. Those records include: Lago do Pires (Behling (1995)), Lago Calado (Behling et al. (2001)), Lagoa da Confusa~o (Behling (2002)), Lake Geral (Bush et al. (2000)) and Empalme Querandies (Prieto (1996)). Their age modeled curves are shown in Fig. S.1.

From the 173 records compiled 50 are newly calibrated, 46 from Prado et al. (2013a, 2013b) and 4 newly added. All the records calibrated by this study are shown in Fig. S.2 and have been marked with an asterisk in Table S.1.

2.3. Calibration

Age calibration is one of the main sources of uncertainty in paleoclimate reconstructions. This is because many mechanisms, such as the geomagnetic field strength, the solar activity, the increased burning of fossil fuels, and the nuclear tests in the 1950s, can alter the production rate and/or exchange rate between carbon reservoirs. These mechanisms' operation culminates in variations of the radiocarbon (¹⁴C) content in the atmosphere over time (Van der Plicht (2015)). These variations affect ¹⁴C dating and limit the accuracy of age estimates (Hajdas (2008)), thus resulting in misleading reconstructions for those generated from uncalibrated age models. Since ¹⁴C ages do not provide absolutely dated chro-nologies for archaeological or paleoenvironmental studies directly they must be converted to calendar age equivalents, compensating for fluctuations in the atmospheric concentration of ¹⁴C (Reimer et al. (2020); McDonald et al. (2019)).

Building on the work of Prado et al. (2013a, 2013b), we compiled only calibrated age data for the climate reconstruction, and calibrated the ages from those that were not. Therefore, all paleoarchive's age samples were dated in the MH using their calendar years (cal yr). Calibrating the ages has not only simplified the definition of our quality index but made it a more homogeneous source of uncertainty identification. We calibrated the ¹⁴C by processing the paleoarchive ages to estimate the depth and age models. The uncertainty intervals and the best age model, both calculated using Bayesian methods, can influence the age calibration if there is any event that disturbs the sediment deposition (Boudreau (1998)). In addition, contamination of the material during the coring process can increase the age-heterogeneity of material at a given depth (Boudreau (1998); Guinasso and Schink (1975)) and/or generate plateaus and age reversals in radiocarbon calibration curves (Reimer et al. (2004)). This bias can cause problems in the interpretation of the calibrated age models (Dolman et al. (2021); Hubay et al. (2018)).

The calculations were made by using Bayesian statistics with the BACON software. BACON estimates the accumulation rates (years/cm) via Markov Chain Monte Carlo (MCMC) iterations by dividing the core into a predetermined number of vertical sections (Blaauw and Christen (2011)). Cores containing several ¹⁴C dates were processed semi-automatically in order to obtain age-depth models. In this process, the ¹⁴C dates were calibrated, after which age-depth curves were repeatedly drawn through point estimates sampled from the dates. In this case, for each date, the probability of a calendar year being sampled is proportionate to its calibrated probability (Blaauw (2010)). The

uncertainty ranges as well as a 'best' age-model were also calculated. Here, we used the default thickness of 5 cm. To calibrate the age models, we used the SHCal13 calibration curve for the Southern Hemisphere (Hogg et al. (2013)), and considered the post-bomb period using the curve number 4 for the Southern Hemisphere Zone 1e2 (Blaauw and Christen (2013)). BACON's calendar scale is calendar or calibrated years before AD 1950.

To interpolate the accumulation rates from the most recent date to the top, the core-top sample date was assigned as the core collection year, when there was no information about the sample collection date. Fig. S.2 shows the spatial distribution of the records with age models calibrated by the present study. The age models calibration was performed with the BACON package from the R Statistics software, available at: https://cran.r-project.org/web/packages/rbacon/index.html.

2.4. Quality index

The quality index (Q) of each proxy point used in the climate reconstructions (Fig. 2, 4 and S.1) was adapted from Prado et al. (2013a, 2013b). Here we consider the sum of the resolution (R) from the paleoarchive (number of samples per centimeter) and the number of datings (D) in MH divided by ten as shown by the equation (1). However, we did not use the number of calibrated ages in the index calculation, as done in Prado et al. (2013a, 2013b), since we calibrated all compiled data.

Speleothems have higher resolution when compared with other records and therefore can have very high Q. As a consequence, we capped the Quality index to a maximum value of 3 for all proxies with a Q value equal or exceeding 3. The Quality index from every proxy present in this compilation can be seen in Table S.1.

$$Q = \begin{cases} 3 & \text{if } R + \frac{D}{10} \ge 3 \\ R + \frac{D}{10} & \text{if } R + \frac{D}{10} < 3 \end{cases}$$
 (1)

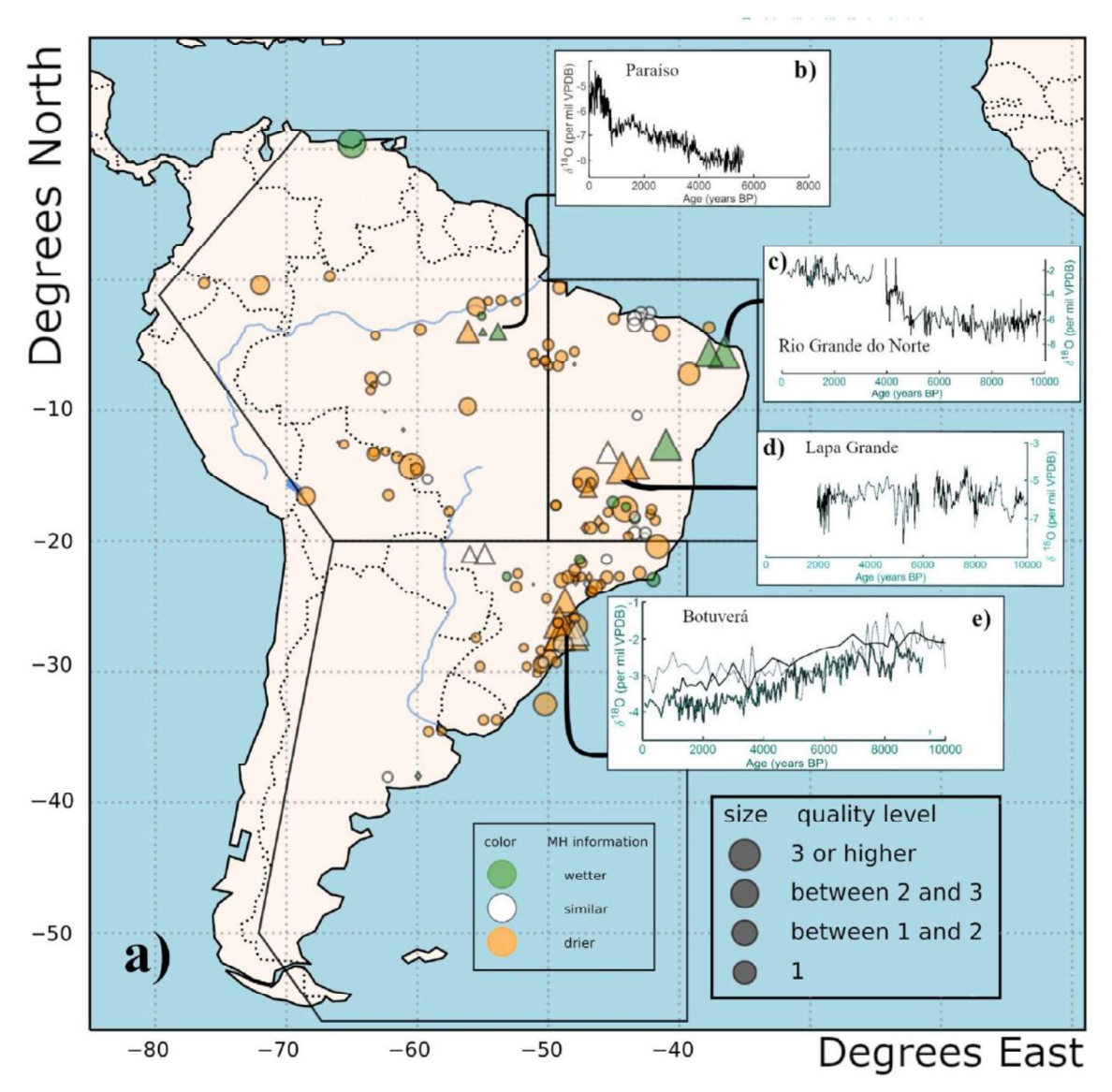


Fig. 2. South America precipitation climate reconstruction for the MH and its highest quality paleo-data history. a) Green indicates higher than present precipitation during MH, white similar and orange lower precipitation. Circles for sediment, triangles for speleothems and diamonds for soil samples. The size from each point resembles the quality from the paleoarchive and its definition is in the Material and Methods section while the large continent boxes defined by the IPCC AR5 are the North East Brazil (top right), the Amazonia (top left) and Southern South America (bottom) regions. b) Paraíso Cave record, adapted from (Ward et al. (2019)). c) Rio Grande do Norte site record, adapted from (Ward et al. (2019)). d) Lapa Grande Cave record, adapted from (Ward et al. (2019)).

The quality from a paleoarchive is a measurement of its resolution during the MH. It must not be mistaken with the intensity of precipitation/temperature/salinity anomalies during MH in comparison to the present. Focusing in higher quality paleoarchives ($Q \ge 1$) sheds light into South America's regional climate response to the MH forcing. Nevertheless, it is important not to discard any proxy information. Even when the proxy shows lower quality, comparing divergent information that may arise can improve the separation of regional and local responses.

3. Results

3.1. Age calibration

The calibrated age model represents a correct paleoarchive's evolution in time if the generated age model presents an adequate adjustment that encompasses the uncalibrated ages and that it is coherent with the ages initially considered. An adequate adjustment is characterized by a constant accumulation rate as a result of a continuous and uniform deposition process (Ramsey (2008)). The accumulation rate may change when the deposition process experiences different climate regimes (e.g., drier or wetter conditions), but it will remain constant while one mode of deposition persists (Ramsey (2008)). Any change or discontinuities in deposition modes will be clearly apparent in the sediments themselves and this does not invalidate the age models, but indicates the deposition mode may have changed. Adjustments made to generate the age model can present problems as well as the age calibrations. This seems to be the case for the Lago do Pires, Lago Calado (LCB1), Lagoa da Confus~ao, Lago Geral (GER) and Empalme Querandies age models (Fig. S3). These are the records from Prado et al. (2013a, 2013b) compilation that could no longer be used in this compilation. The calculated age models for these records do not cover the majority of uncalibrated ages. In some paleoarchives these adjustment problems may have occurred due to hiatuses, gaps, erosion or redeposition during the deposition causing the calibrated age models to extrapolate the range of interest of this study."

3.2. Precipitation

Pollen assemblages represent the most abundant proxy in Eastern South America during MH, providing indirect information for precipitation and/or moisture change in the region (Fig. 2). A regional interpretation of the results was obtained by following the

IPCC AR5 Reference Regions (IPCC (2014)) dividing Eastern SA into 3 regions. Southern SA, Amazonia, and NE Brazil. Regarding the latter, NE Brazil was divided into three different sectors shown in Fig. 3: its eastern and interior influenced by the ITCZ; and its southern frontier under the influence of SACZ (Fig. 1). This NE Brazil subdivision has already been proposed similarly by Smith and Mayle (2017) when exploring regional differences within the South East Brazil paleoclimate. Individual reconstructions for each proxy type are shown in Fig. 5 in the Supplementary Material section.

3.2.1. Amazonia

In the Amazonia region, the MH was overall drier than present. It is characterized by 37 precipitation proxy records: 30 data studies, mainly with biological proxy analysis, point to a drier MH; 4 data suggest wetter than present MH; and 3 similar to present (Fig. 2) (see Table 3).

Table 3Number and quality index mean (Q mean) from each compiled paleoarchive (speleothem, sediment and soil samples) and proxy types (IF: Isotopic fraction; BIO: Biological; PC: Physico-chemical) inside the Amazonia region box (IPCC (2014)) precipitation reconstruction.

Amazonia Precipitation				
Paleoarchives	Number	Q mean		
Speleothem	3	0.67		
Sediment	31	0.57		
Soil Samples	3	0.11		
Proxies	Number	Q mean		
IF	5	0.66		
BIO	30	0.47		
PC	9	0.80		

The Cariaco Basin (Table S.1, No: 156), which is in the northernmost part of the Amazonia region, is one paleoclimate archive that suggests a wetter MH relative to present climate based on high Ti and Fe values brought by precipitation to the sediment survey site (Haug et al. (2001)). This has been linked with a local moisture variation due to ITCZ displacement during the MH. This wetter than presentMHinformation is in agreement with theMHdrier Amazon scenario since its precipitation is expected to be in

opposition with the south of the equator part of Amazonia. There is an apparent inverse rainfall response between the South and North of the Equator parts of Amazonia to the meridional shifts of the ITCZ.

The other three records pointing to higher MH moisture are from Paraíso Cave (Table S.1, No: 117 and 118) and Tapajós Lake (Table S.1, No: 46). The Paraíso cave studies contain two oxygen isotopic records pointing to a substantial increase in convection intensity and rainfall at the cave site (Wang et al. (2017)). According to Ward et al. (2019), speleothem δ¹⁸O values from interior cave sites do not co-vary with 87Sr/86Sr (a proxy for localwater balance) from the same specimens, indicating that regional monsoon intensity is not necessarily tied to local hydroclimate. This indicates disconnected local and regional monsoon responses. The Tapajós lake pollen and carbon isotope data (Table S.1, No:46) points to a decline in Cecropia pollen abundance (from 40% during the MH to 10% after 4600 BP). Other studies have interpreted the same Cecropia behavior as a decrease in the frequency and/or intensity of drought events, signaling more of a climate transition during MH (Weng et al. (2002); Irion et al. (2006)).

The border region of Amazonia and NE Brazil (50_W from 20_S to the Equator) presents 11 proxy data points, all indicating a drier than present MH.

3.2.2. Northeast Brazil

There are 43 precipitation proxy records for the NE Brazil region with 6 data pointing to a wetter than present MH, 11 similar to present, and 26 indicating a drier MH in comparison to present (Fig. 2) (see Table 4).

Three speleothems located on the NE Brazilian coast point to a wetter climate during MH (Fig. 3) due to lower δ^{18} O values (Table S.1, Numbers: 71,72 and 114). Since the rainfall regime from this region is directly controlled by the ITCZ, those records indicate more southern incursions of the ITCZ across the continent during the MH (e.g. Prado et al., 2013a, 2013b).

Table 4

Number and quality index mean (Q mean) from each compiled paleoarchive (speleothem, sediment and soil samples) and proxy types (IF: Isotopic fraction; BIO: Biological; PC: Physico-chemical) inside the Northeast Brazil region box (IPCC (2014)) precipitation reconstruction.

Northeast Brazil Precipitation				
Paleoarchives	Number	Q mean		
Speleothem	6	2.58		
Sediment	35	0.53		
Soil Samples	2	0.50		
Proxies	Number	Q mean		
IF	9	1.88		
BIO	34	0.53		
PC	6	0.48		

The interior sites of NE Brazil present the same drier than present pattern as Amazonia and Southern SA during MH (Fig. S2). Precipitation in Amazonia and interior sites of NE is mostly controlled by the ITCZ, even though its effects are more important in the coastal NE Brazil. A drier Amazonia agrees with numerical models that suggest a northerly displacement of the ITCZ during MH (Novello et al. (2018); Brierley et al. (2020); Brown et al. (2020)). The present-day precipitation dipole between the NE Brazil coast (dry climate) and Amazonia (wet climate) is largely controlled by the strength of the SASM and associated features. The paleo compilation of Smith and Mayle (2017) argues that the drier west SASM region (interior sites) and wetter NE coast during MH is due to a weaker South Atlantic subtropical high and weaker convective activity in the core of the SASM region reducing the strength of the Nordeste Low and subsidence over the region (Cruz et al. (2009); Cheng et al. (2013)). Weaker El Ni~no Southern Oscillation (ENSO) activity during the MH may also have reduced severe drought events in the NE coast and the NE Brazil/Southern SA frontier (NSF, 14-20S and 40e48W, Fig. 3) (Raczka et al. (2013); Wang et al. (2017); Smith and Mayle (2017); Pausata et al. (2017)).

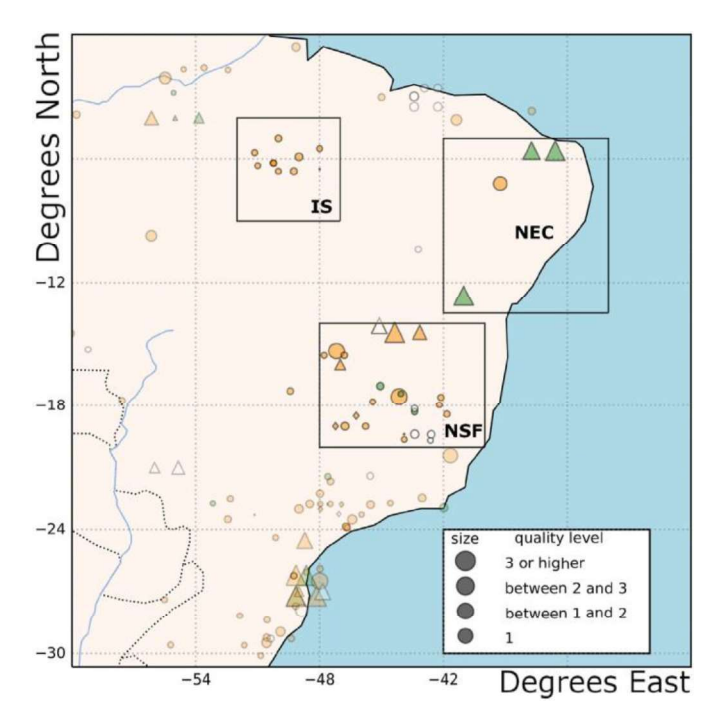


Fig. 3. North East Brazil regional division precipitation climate reconstruction for the MH. Green indicates higher than present precipitation during MH, white similar and orange lower precipitation. Circles for sediment, triangles for speleothems and diamonds for soil samples. The size from each point resembles the quality from the paleoarchive and its definition is in the Material and Methods section while the large boxes are the North East Brazil coast (NEC), the interior sites (IS) and North East/Southern South America Frontier (NSF) regions.

The remaining paleoarchives that indicate a higher than present moisture during the MH (Table S.1, Numbers: 75, 127, 160) are sediments near NSF. This region is influenced by changes in the SACZ position through time and the SASM southerly summer displacement (Garreaud et al. (2009); Dias et al. (2009); Shimizu et al. (2020); Cassino et al. (2020)). These are all biological proxies, which found either an increase or an abundance of different vegetation pollen (palm swamp, Mauritia flexuosa in the first two studies and Ceratophyllum leafs, Zygnema zygospore in the last one). Raczka et al. (2013) describe erratic rainfall in Lagoa Olhos D'água (Table S.1, No: 141) where changes in lake level were inferred from variability in ferns, algae and wetland plants, reinforcing the high precipitation variability and conflicting data present within this region during the MH (Cassino (2011); Raczka et al. (2013); Cassino et al. (2018, 2020); Hor_ak-Terra et al. (2020)). CMIP5 and PMIP4/ CMIP6 MHmodel simulations suggest aweakening and contraction of the SASM during the MH (Brierley et al. (2020); Shimizu

et al. (2020)), consistent with Cassino et al. (2020) who discuss the centennial-scale fluctuations from dry to wet conditions throughout the early and MH associated with a weakening of the SASM during summer and repeated shifts of its belt position during this time range. Different types of proxies in this region could have different timescales of response to changes in precipitation, creating this inhomogeneous precipitation pattern on the NSF during MH (Wang et al. (2017); Riris and Arroyo-Kalin (2019); Tabor et al. (2020)).

3.2.3. Southern South America

For the Southern SA region there are 60 precipitation proxy records with 3 of them pointing to a wetter than present MH, 8 similar to present, and 49 indicating a drier MH in comparison to present (Fig. 2) (see Table 5).

Table 5Number and quality index mean (Q mean) from each compiled paleoarchive (speleothem, sediment and soil samples) and proxy types (IF: Isotopic fraction; BIO: Biological; PC: Physico-chemical) inside the Southern South America region box (IPCC (2014)) precipitation reconstruction.

Southern South America Precipitation				
Paleoarchives	Number	Q mean		
Speleothem	9	2.24		
Sediment	46	0.50		
Soil Samples	5	0.28		
Proxies	Number	Q mean		
IF	25	1.08		
BIO	47	0.48		
PC	19	0.66		

Two sediment studies (spread from 22S to 27S) from interior sites point to a wetter MH. Stevaux. (2000) conducted a pollen analysis on Paran_a River sediment cores (Table S.1, No: 94), although, similar to present when compared to other dry event periods (from 40,000 to 8000 BP and from 3500 to 1500 BP), the MH was characterized by a wetter than present climate. At Tamanduá River, Turcq et al. (1997) found pollen samples pointing to forest development and reduction of slope erosion, also indication of a wetter than present MH (Table S.1, No: 171). Multiple cores and a mammal archaeology record

far south in Argentina pampeon region (i.e Table S.1 No:155) found a variety of data that indicates a humid phase during the MH and, finally, a marine sediment core pointing to an increase in sand and productivity, higher values of C/N and a decrease in carbonate contents also points to a wetter than present MH (i.e Table S.1 No:58).

The quality level from those records (Numbers: 58, 94, 155 and 171) that show wetter than present MH proxies in the Southern SA region are low (no higher than Q = 0.5), indicating a local response with respect to the moisture condition, probably beyond the regional monsoon. Also, two of them (Table S.1, No: 58 and 171) are located close to the NSF, agreeing with other wetter than present MH records cited before when describing the NE region (Table S.1, Numbers: 75, 127, 160), suggesting that the SACZ belt position was not constant during the MH. Since the majority of the proxies from Southern SA points otherwise (over 70% points to a drier MH), it is more likely to assume that the regional response is in fact a drier than present scenario during MH.

3.3. Temperature, lake levels and salinity

Across the Amazonia region only one paleoarchive (Table S.1 No: 3) indicates a higher than present water level while 12 sediment archives in this region point to lower lake levels (Table S.1 Numbers: 8, 12, 13, 26, 35, 128, 129, 130, 164, 166, 167 and 170). In Southern SA and its border with the NE Brazil three proxy data (Table S.1 Numbers: 32,38 and 103) also show a lower than present lake level (see Table 6).

Table 6Number and quality index mean (Q mean) from each compiled paleoarchive (sediment) and proxy types (IF: Isotopic fraction; BIO: Biological; PC: Physicochemical) in the lake level reconstruction.

Lake Level			
Paleoarchives	Number	Q mean	
Sediment	16	0.50	
Proxies	Number	Q mean	
IF	2	0.62	
BIO	16	0.50	
PC	9	0.47	

The sea surface temperature (SST) reconstruction (Fig. 4 c), mainly from studies using δ^{18} O or biological proxies, gives a similar to present temperature during MH on

Eastern South America's coast above 20S (Table S.1 Numbers: 52, 60, 62, 157 and 158), with a warmer than present region close to the equator line (Table S.1 Numbers: 54, 56 and 126) and, below 20_S, three proxy data point instead to a cooling pattern (Table S.1 Numbers: 51, 53, 59) (see Table 7).

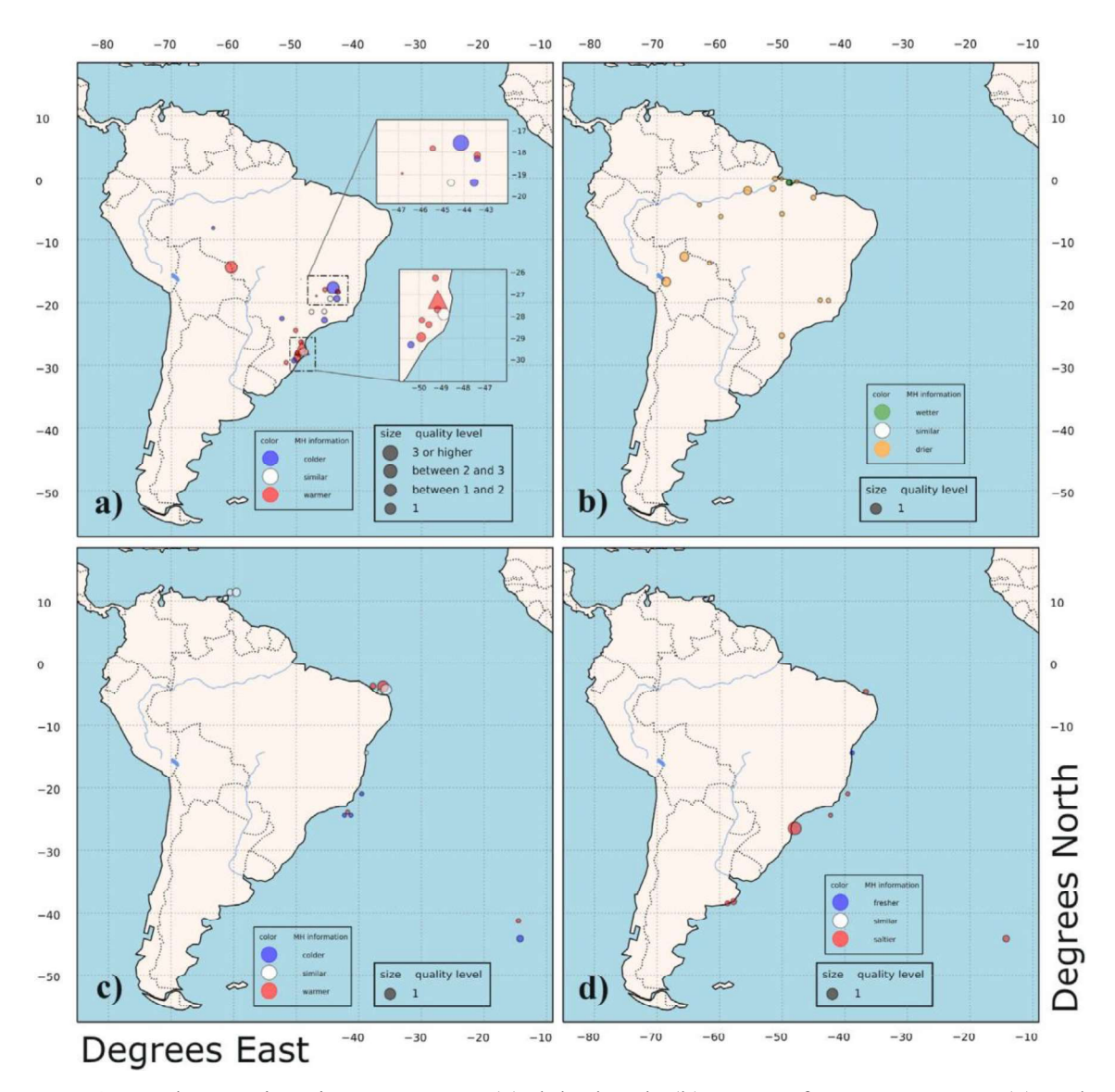


Fig. 4. South America air temperature (a), lake levels (b), sea surface temperature (c) and sea surface salinity (d) climate reconstructions for the MH. The size from each point reflects the quality of the paleoarchive. For more details on how the size of each proxy has been calculated please see the Material and Methods section.

Table 7

Number and quality index mean (Q mean) from each compiled paleoarchive (speleothem and sediment) and proxy types (IF: Isotopic fraction; BIO: Biological; PC: Physicochemical) in the surface temperature and sea surface temperature reconstructions.

Surface Temperature			Sea Surface Temperature		
Paleoarchives	Number	Q mean	Paleoarchives	Number	Q mean
Speleothem	1	3	Sediment	14	0.60
Sediment	22	0.52			
Proxies	Number	Q mean	Proxies	Number	Q mean
Proxies IF	Number 3	Q mean 1.77	Proxies IF	Number 9	Q mean 0.52
	Number 3 20				

Below 15_S, marine sediment SAN-76 was used in three different studies (Table S.1, Numbers: 51,57 and 59) with a total of four different proxy analyses. Two isotopic fraction (Table S.1, Numbers: 51,59) and one biological record (Table S.1, Numbers: 59) pointed to lower SST during the MH. By contrast, in the other record (Table S.1, Numbers: 57) the lower biological marker ratio (G. bulloides/ G. ruber) during the MH (relative to Late Holocene - LH) was attributed to a stronger Brazil Current (more intense ITCZ) and in turn warmer SSTs (Toledo et al. (2007, 2008); Pivel et al. (2010)).

Above 15_S, two δ^{18} O proxy studies indicate warmer SSTs north of the NE Brazil coast (Table S.1, Numbers: 54 and 56). Four records gave similar to present SSTs during MH: at the North Hemisphere a proxy study of Fe/Ti metal concentration in Cariaco and a pollen analysis from a sediment core in Tobago Basin (Table S.1, Numbers: 156 and 157); and Ti/Ca, Mg/Ca and δ^{18} O concentrations from three different sediment cores in NE Brazil coast (Table S.1, Numbers: 60 and 62, sediment cores GeoB3129, GeoB3911 and GeoB3910-2).

The SSS reconstruction has 8 data points, with only one (based on planktonic foraminifera as a proxy for vertical mixing of surface waters) pointing to fresher than present conditions during the MH (Toledo et al. (2007)). The other 6 data points (Table S.1, Numbers:34, 50, 51, 53, 60, 123), spread across the South American coast, exhibit saltier than present sea surface. The highest quality level proxy data indicates a lower sedimentation rate allied with a higher than present sea level at the southeast coast of Brazil (Table S.1, No: 126). Since the sedimentation in this region is mainly determined by the Rio de La Plata plume water flow (which carries sediments from the Rio de La Plata) and from the southern Brazilian coastal lagoons, both sources of fresh and cold

water, this indicates saltier than present conditions during the MH (Mahiques et al. (2009)). A study involving δ^{18} O and Mg/Ca measurements on the benthic foraminifera Uvigerina spp. from MD07-3076 sediment core, located at the middle of the South Atlantic Ocean Ridge (Table S.1, No: 159), also points to higher than present SSS during the MH (Roberts et al. (2016)) (see Tables 8 and 9).

Table 8Number and quality index mean (Q mean) from each compiled paleoarchive (sediment) and proxy types (IF: Isotopic fraction; BIO:Biological; PC: Physicochemical) in the sea surface salinity reconstruction.

Sea Surface Salinity				
Paleoarchives	Number	Q mean		
Sediment	8	0.54		
Proxies	Number	Q mean		
IF	3	0.37		
BIO	8	0.54		
PC	3	0.70		

Table 9
- Acronyms.

Acronyms	Full Name
SA	South America
MH	Northeast
NE	Northeast
NEC	Northeast Brazil coast
IS	Interior Sites
ITCZ	Intertropical Convergence Zone
SACZ	South Atlantic Convergence Zone
SASH	South Atlantic Subtropical High
SASM	South American Summer Monsoon
NSF	NE Brazil/Southern SA frontier
SST	Sea Suface Temperature
SSS	Sea Suface Salinity
BI	Biological
IF	Isotopic Fractions
PC	Physico-chemical

4. Discussion

Different paleoarchives reflect different environments, providing evidence for the same processes or cascades of processes (Nowacki et al. (2019)) in addition to operating at different spatial and temporal scales (Birks and Birks (2006); Nowacki et al. (2019)). Moreover, different types of proxy have relative sensitivities that can delay their responses to rapid climate change (Bush et al. (2004); Birks and Birks (2006); Urrego et al. (2009); Costa et al. (2018)). Fig. 5 helps elucidate the range of different proxy analysis that can be interpreted based on their locality and quality index. Pollen, which is the main proxy used in the SA MH studies, is derived from vegetation that can take a few hundred years to adjust to abrupt changes in climate having a minimal sampling interval of two decades, recording long-term climate changes (Bradley (1999); Prado et al., 2013a). Speleothems, which are mineral formations occurring in limestone caves, most commonly known as stalagmites or stalactites, have annual to decadal resolution of climatic fluctuations in the temporal range of thousands of years (Bradley (1999)). Therefore, the response time of each type of proxy must be considered in paleoclimatic studies to avoid misinterpretations.

While proxy records are essential for climate reconstruction it should be noted that it is not always clear whether a proxy record signal reflects only local, regional or global conditions (Sorooshian and Martinson (1995)). In most cases analyzed in this study, the analysis of different proxies from proximal climate archives produced similar results. However, we noticed conflicting information obtained from some proximal climatic archives, such as in studies carried out in Paraíso Cave (Wang et al. (2017); Ward et al. (2019)). In this case, analysis of speleothems from the same cave provided opposite climatic information for the same period. Furthermore, conflicting information can also be noticed in the analysis of sediments from nearby sites (Barberi et al. (2000); Turcq et al. (2002); Cassino et al. (2020)).

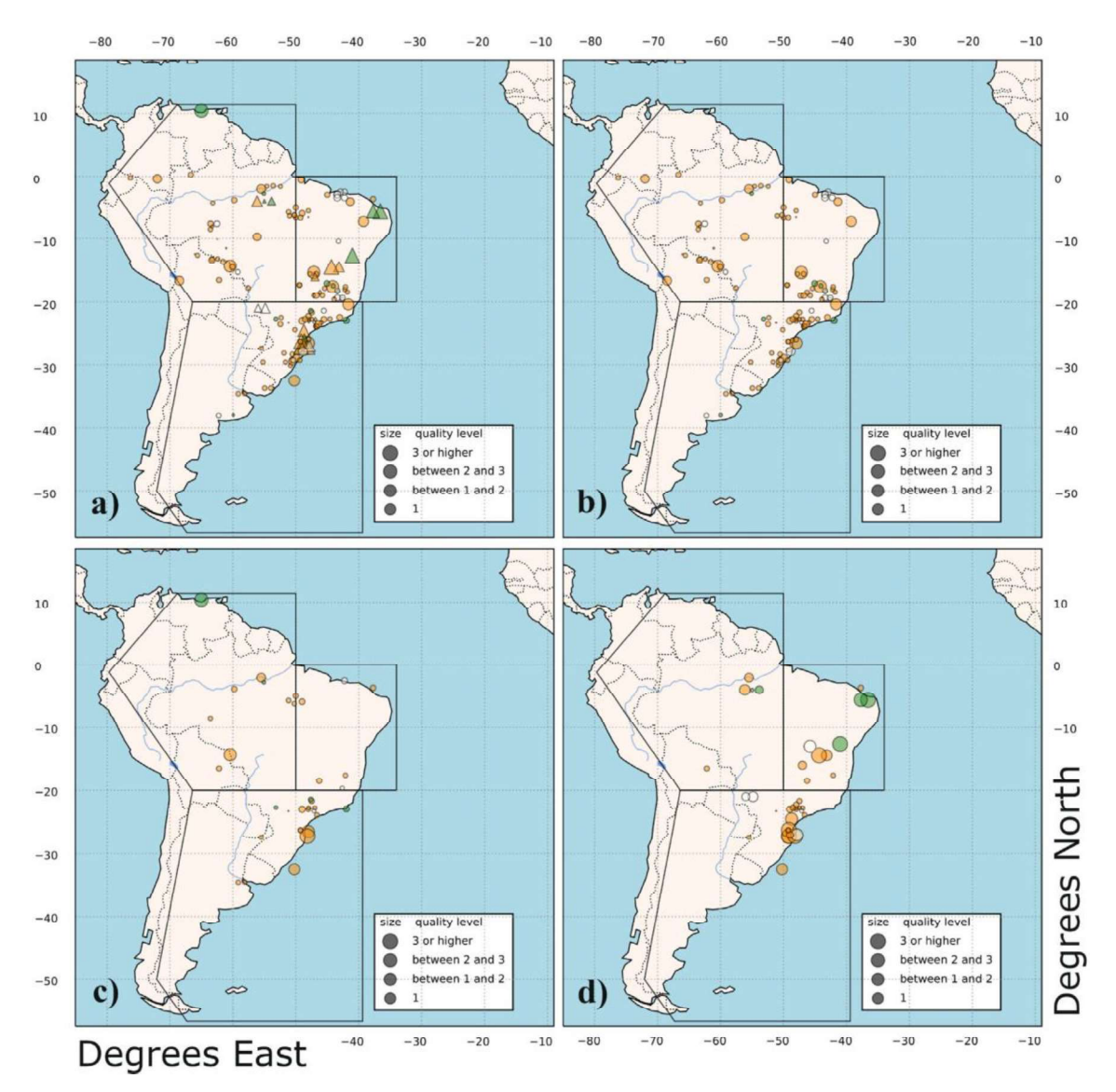


Fig. 5. South America precipitation climate reconstruction for the MH and its separation by proxy types. Green indicates higher than present precipitation during MH, white similar and orange lower precipitation. The size from each point resembles the quality from the paleoarchive and its definition is in the Material and Methods section while the large continent boxes defined by the IPCC AR5 are the North East Brazil (top right), the Amazonia (top left) and Southern South America (bottom) regions. a) Circles for sediment, triangles for speleothems and diamonds for soil samples b) Biological proxies. c) Physical-Chemical proxies. d) Isotopic Fraction proxies.

Speleothems are mineral deposits formed in caves, being typical of karstified host rocks, having a greater capacity for highresolution preservation of continuous or semi-continuous weather signals for prolonged periods when compared to other archives such as pollen and sediments (Gunn (2004); Wong and Breecker 2015; Atsawawaranunt et al.

(2018)). Furthermore, the characteristic vegetation of karstic terrains allocates more biomass to the roots, retaining more water and promoting a more humid environment than in the surrounding regions (Ni et al. (2015)). This is why speleothems can sometimes record wetter conditions while sediments from nearby regions register drier conditions. Another source of divergence that may arise are due to hiatuses in speleothem samples, making the precise onset of dry and wet conditions impossible to assign (Ward et al. (2019)). This may have been the case in the diverging results from studies in Paraíso Cave (Wang et al. (2017)). Although the majority of proxies in the Amazon region and nearby sites point to a drier MH, Wang et al. (2017) found indication of a wetter than present Amazon during MH (Fig. 2; Table S.1 No: 117 and 118). Their study was based on highresolution speleothem $\delta^{18}O$ analysis of seven calcite specimens, which were broken and columnar in shape when collected from the site. Even though their focus was during the Last Glacial Maximum period (around 21.000 years ago), this approach also gave insight over the past 45.000 years. Ward et al. (2019) studied several speleothems 87Sr/86Sr and oxygen-isotope variability as a proxy of local moisture conditions, including the ones used by Wang et al. (2017) to track the MH precipitation in Paraíso Cave (PAR01, PAR03 and PAR16, Table S.1, No: 116). In their study, Ward et al. (2019) state that Paraíso's Cave δ^{18} O records notably contain hiatuses during much of the MH. What is more, the speleothem record shows a dry interval within the 87Sr/86Sr proxy framework that is consistent with the much higher δ^{13} C of the Paraíso's Cave records (Extended Data Fig. 9 in Wang et al., 2017), also a potential indication of decreased cave recharge. This intervalwas coincident with slower speleothem growth but is not reflected in δ^{18} O values. The Paraíso 87Sr/86Sr values then increase, suggesting recovery from the dry interval (Ward et al. (2019)).

Another possible explanation for conflicting outcomes between different proxy types may be the result of changes that have taken place at the local scale. Proxies work as climate system filters and operate at different spatial and temporal scales (Birks and Birks (2006); Khatiwala et al. (2001)), hence weather events may not be registered in the same way by different proxies. When interpreting the results of analysis from different proxies, one should try to differentiate the recording of large-scale events from local ones. One way to make this differentiation is by comparing the results found with studies carried out in adjacent regions. If there is an equivalence of records, there may be an indication of larger scale climate events and, if not, there may be an indication of smaller scale climate events. The Southern SA region, where an overwhelming number of

different proxy types (Biological, Physical-Chemical and Isotopic Fraction) and paleoarchives (sediments, speleothems and soil samples) indicate a drier than present MH (Fig. 2 and S1). This is an example of a larger scale climate response. Even though it is possible to make past climatic reconstructions using only one proxy, multi-proxy compilations are necessary to produce more robust reconstructions (Prado et al. (2013a)).

4.1. The NSF transition zone

Most of the studies assembled in this compilation agree on a regional scale. Although, the Amazon's ecoregion classification during the MH was no different from the evergreen forest present classification (Smith and Mayle (2017)); the lower summer insolation pattern in the Southern Hemisphere during the MH is responsible for weaker and fewer ITCZ incursions in the region, contributing to a drier and warmer Amazon during MH in comparison to the present. Southern SA also displays a drier than present MH, whereas NE Brazil shows a transition behavior in its border with Southern SA. The NSF is the principal region where paleoarchive studies appear to disagree (Fig. S.2). There are three speleothems (Table S.1, Numbers: 66, 65 and 115), two soil (Table S.1, Numbers: 77 and 83) and fifteen sediment core samples pointing to a drier MH (Table S.1, Numbers: 1, 6, 14, 32, 39, 76, 86, 93, 102, 104, 112, 113, 130, 140 and 161), while three biological proxies located at the center of NSF region box (Table S.1, Numbers: 75, 127 and 160. Fig. S.2) are in disagreement showing a wetter climate during the MH. This indication of awetter than present NSF during the MH was supported by the presence of different wet climate plants (palm swamp, Mauritia flexuosa, Ceratophyllum leaf spines, Sagittaria and Nymphaeaceae) in the respective sediment samples during the MH interval (Cassino (2011); Cassino et al. (2018)).

Precipitation proxy and numerical modeling studies argue that ENSO variability during the MH was lower than modern (Sandweiss et al. (2009); Raczka et al. (2013); Zhang et al., 2014; Wang et al. (2017); Smith and Mayle (2017); Pausata et al. (2017)). ENSO's impact on SA is dependent on a number of factors, from other modes of climate variability to inter-basin interactions between the Pacific and the Atlantic oceans (Marengo et al. (2012)). Each ENSO event has its own characteristics, such as location of maximum amplitude and magnitude of the signal, generating a unique response of precipitation anomalies in SA (Cai et al. (2020)). In particular, anomalous convection over central and tropical Pacific during El Ni~no events is associated with anomalies in

the Walker circulation cell and extra tropical Rossbywave trains correlating the ENSO signal with precipitation anomaly episodes in eastern SA (Kousky et al. (1984); Ropelewski and Bell (2008); Irving and Simmonds (2016); Barreiro (2010); Sasaki et al. (2015); Cai et al. (2020)). The water deficit scenario in Southern SA during the MH is associated with the weaker SASM activity induced by a weaker ENSO variability. The SASM belt shifted significantly during the MH, causing erratic precipitation patterns in the NSF region (Raczka et al. (2013); Smith and Mayle (2017)). One way to explain the presence of these inhomogeneous moisture patterns retrieved from the biological proxies in this region (Table S.1, Numbers: 76, 160 and 171) could be a higher variability of the SACZ belt position (Turcq et al. (1997); Dias et al. (2009); Cassino (2011); Raczka et al. (2013); Maksic et al. (2019); Cassino et al. (2018)) creating the inputs of wetter NSF during MH when compared to the present. Climate models reproducing South America's MH climate also found the NSF to be colder and drier than present (Dias et al. (2009); Maksic et al. (2019)). Both Dias et al. (2009) and Prado et al. (2013b) related this regional response to a possible insolation effect on the SACZ changing its position and intensity during MH. However, recent model experiments conducted by Maksic et al. (2019) could not identify which forcing was more important for the austral summer rainfall anomalies in this region.

Another possibility comes from the proxy records that point to a similar to present MH precipitation in this region (Table S.1, Numbers: 92, 141, 142, 152 and 173). In their most recent work, Wong et al. (2021) analyses Angelica's cave speleothem (Table S.1, No: 173) and concludes that the low variability from δ^{18} O proxy record in the last 7.000 years points to a constant SACZ belt position, including during the MH. Although the speleothem sample AG4 shows a linear growth of δ^{18} O from 7.000 to 6.000 cal yrs BP, Wong et al. argues that the SACZ core is mostly dependent on the subtropical insolation and the South Atlantic Subtropical High. Therefore, the NSF's precipitation would not have been influenced by the lower summer insolation in the south hemisphere during the MH (Wong et al. (2021)). The records that point to drier climate in this region would be reflecting the lower than present moisture transport from Amazonia to Southern SA (Prado et al. (2013a)), while the higher than present precipitation inputs could be interpreted as local only information, not representing the regional monsoon.

5. Conclusion

Past climate reconstructions contain important information about our planet's climate history and are essential when learning how physical variables, such as precipitation or temperature, respond to external forcings. Improving the number of paleoarchives and calculating their calibrated age-models are the most straightforward way to improve climate reconstructions and reduce their uncertainties (Blaauw (2010)). This study presents a MH multi-proxy reconstruction from Eastern South America climate using 173 calibrated-only paleoarchives. We have calculated the calibrated agemodels of 55 paleoarchives (Table 2 sites marked with an asterisk) and defined a newquality index (equation (1)) to quantify each paleoarchive uncertainty. After calibration, five from those age models (Fig. S.1) were no longer in the range of MH epoch (7000e5000 cal yr BP), discarding possible misleading information from the climate reconstruction. Five maps of precipitation, temperature, lake-levels, SST and SSS (Figs. 2 and 3) present a full view of SA climate during the MH compared to the present day. A more detailed discussion concerning the NE Brazil region (Fig. S2) and paleoarchives particularities were used to draw robust conclusions on SA climate during the MH.

Precipitation remains the most robust climatic parameter to study the MH in eastern South America, mainly because of the large diversity of proxies that capture changes in this parameter. The Amazonia and Southern SA proxies show an overall agreement in terms of precipitation; less than 20% of the different proxy archives disagree with an overall drier than present climate during the MH, agreeing with the previous paleocompilations and climate models (Smith and Mayle (2017); Maksic et al. (2019); Tabor et al. (2020)). Rainfall variability for these regions are SASM-derived, so vegetation here is likely to be susceptible to long-term changes in SASM strength (Smith and Mayle (2017)). Previous studies have documented that both SACZ and ITCZ positions have shifted in the past in response to abrupt millennial-scale events (Dias et al. (2009); Prado et al. (2013a); Smith and Mayle (2017); Cassino et al. (2020)), including in the MH, thereby significantly affecting precipitation over the SA continent.

NE Brazil is the region with most conflicting paleodata in terms of their MHclimate signal; 60% of the different proxy archives point to a drier MH, 14% point to wetter and 26% to a similar to present climate during the MH. Therefore, a regional sector division from this NE Brazil box (Fig. 3) helps elucidate the climate features from the MH. Southern incursions of the ITCZ as well as the trade winds, which are associated

with the position and intensity of the South Atlantic subtropical high, most heavily influenced coastal areas showing wetter conditions during the MH (Prado et al. (2013a); Wainer et al. (2014)). Another possibility is the perseverance of the modern eastewest precipitation dipole between northeastern Brazil (dry climate) and the central South American tropics (wet climate), which was inverted during the MH (dry Amazon/Interior sites and wet NE coast) (Smith and Mayle (2017)).

The NSF is located in the core of the SASM, inside the NE region box (14-20S and 40e48W). Its rainy season is mostly controlled by the SACZ and inner continent moisture transport from Amazonia to Southern SA (Mahiques et al. (2009); Smith and Mayle (2017); Wong et al. (2021)). There are two possibilities to explain the behavior from the proxy records found in this region. Both hypotheses agree with CMIP5 and PMIP4/CMIP6 model simulations that suggest a contraction of the SASM during MH (Brierley et al. (2020); Shimizu et al. (2020)) creating lower than present precipitation in the region. The first hypothesis argues that the instability seen in different NSF proxy records could be explained by a weaker and northward displaced SACZ during MH, while the lower than present ENSO variability during MH could be responsible for positive precipitation anomalies in local areas of the region. This first hypothesis agrees with Raczka et al. (2013), who found erratic precipitation and unstable climates to have affected local human settlements during MH, as drought and flood would have caused migration relative to more stable climates. It also agrees with climate models that relate the MH forcings to weaker convection on the SACZ influence area (Dias et al. (2009); Prado et al. (2013a, 2013b); Maksic et al. (2019)). The second hypothesis argues that the SACZ belt region is mostly dependent on the subtropical South Atlantic SSTs, which remained largely stable over the mid-to-late Holocene (Wong et al. (2021)). Similar to present, proxy records in the NSF region point to no major shifts from the SACZ latitudinal position or intensity in the last 7.000 years (Wong et al. (2021)). In this case, the lower than present precipitation proxies in this region would be reflecting weaker continent moisture transport. This compilation's precipitation reconstruction (Fig. 2) supports a drier than present Southern SA and NSF during the MH. The majority of proxies in the SACZ influence area presented precipitation anomalies in this epoch, indicating changes in SACZ during the MH. Nevertheless, more studies are needed to fully understand the impact of MH's insolation patterns on the SACZ intensity and position.

It is possible to relate the NSF as colder than present during the MH, while Southern SA presented warmer and drier climate, concurring with model studies that suggest a SASM contraction during MH (Maksic et al. (2019); Tabor et al. (2020)). The scarcity of air temperature proxies in the Amazonia region hampers any assumptions about its temperature during MH. Nevertheless, the precipitation and lower lake levels proxies clearly point to a drier than present MH climate.

The SST reconstructions suggest a dipole pattern for the SA coast during the MH relative to the late-Holocene. Above 15_S a warmer/ similar to present SST indicates a strong Brazil Current due to a more intense ITCZ while the decrease in summer insolation in the Southern Hemisphere during the MH could have been responsible for colder than present SSTs below 15_S.

With the exception of one record (Toledo et al. (2007)) (Table S.1 No:52), the SSS studies reach an almost unanimous scenario showing a saltier ocean mixed layer during the MH western South Atlantic. This pattern is supported by lower than present lake levels and river discharges in the coastal region suggesting overall drier and warmer conditions during the MH.

Although there are open questions about what was the local response of specific regions with diverging proxy information (such as NSF), the highest quality proxies (higher than 1) all agree at regional scale. High levels of the quality index are reached by sediments containing BI analyzes (ranging up to 1.30 - Table S.1, no:140), but they are more scarce in BI proxy analyses from sediments than in IF analysis taken from speleothems. Nevertheless, the new quality indexes as defined here give perspective to the climate reconstructions. The focus of further studies regarding Eastern SA's climate responses to MH forcings should be the SACZ. Both model and paleoarchive studies may increase our knowledge of how the SACZ position and intensity changed (or not) due to insolation anomalies or other forcings present during the MH.

Author Contributions

We would like to declare that all authors have made substantial contributions to this submission. Iuri Gorenstein, Luciana F. Prado and Paula R. Bianchini were responsible for compiling the information and creating the figures of the manuscript. All the remaining authors were essential in the process of orienting, reviewing and correcting sections in the manuscript corresponding to their unique area of expertise. All authors have contributed to the writing process.

Declaration of competing interest

The authors declare that they have no known competing financial interests or personal relationships that could have appeared to influence the work reported in this paper.

Acknowledgments

The Data used in this study is available in the studies cited in the references and through the link next to this manuscripts file.

This study was supported in part by the grants CAPES: 88882.383622/2019-01, 88887.495715/2020-00, 88887.614636/2021-00; FAPESP: 2019/08247-1; FAPDF: 0193.001374/2016 and CNPq: 130927/2021-0.

Appendix A. Supplementary data

Supplementary data related to this article can be found at https://doi.org/10.1016/j.quascirev.2022.107646.

References

- Ajjur, S.B., Al-Ghamdi, S.G., 2021. Global hotspots for future absolute temperature extremes from cmip6 models. Earth Space Sci. 8. https://doi.org/10.1029/2021EA001817.
- Atsawawaranunt, K., Comas-Bru, L., Amirnezhad Mozhdehi, S., Deininger, M., Harrison, S.P., Baker, A., et al., 2018. The sisal database: a global resource to document oxygen and carbon isotope records from speleothems. Earth Syst. Sci. Data 10 (3), 1687e1713. https://doi.org/10.5194/essd-10-1687-2018. Retrieved from. https://essd.copernicus.org/articles/10/1687/2018/.
- Barberi, M., Salgado-Labouriau, M.L., Suguio, K., 2000. Paleovegetation and paleoclimate of "vereda de aguas emendadas". Cent. Braz. J. S. Am. Earth Sci. 13, 241e254. https://doi.org/10.1016/S0895-9811(00)00022-5.
- Barreiro, M., 2010. Influence of enso and the south atlantic ocean on climate predictability over southeastern south America. Clim. Dynam. 35, 1493e1508. https://doi.org/10.1007/s00382-009-0666-9.

- Behling, H., 1995. Investigations into the late pleistocene and holocene history of vegetation and climate in santa catarina (Brazil). Veg. Hist. Archaeobotany 4, 127e152.
- Behling, H., 2002. Late quaternary vegetation and climate dynamics in southeastern amazonia inferred from lagoa da confusao in tocantins state, northern Brazil. Amazoniana 17, 27e39.
- Behling, H., Cohen, M.C.L., Lara, R.J., 2001. Studies on holocene mangrove ecosystem dynamics of the bragança peninsula in north-eastern para, Brazil. Palaeogeogr. Palaeocl. 167, 225e242. https://doi.org/10.1016/S0031-0182(00)00239-X.
- Behling, H., Costa, M.L., 1997. Studies on holocene tropical vegetation mangrove and coast environments in the state of maranhao, ne Brazil. J. Quat. S. Am. A. 10, 93e118.
- Berger, 1988. Milankovitch theory and climate. AGU. Res. Lett. https://doi.org/10.1029/RG026i004p00624.
- Berger, A., 1978. Long-term variations of daily insolation and quaternary climatic changes. J. Atmos. Sci. 35, 2362e2367. https://doi.org/10.1175/1520-0469(1978)035;2362:LTVODI;2.0.CO;2.
- Birks, H.H., Birks, H.J.B., 2006. Multi-proxy studies in palaeolimnology. Veg. Hist. Archaeobotany 15, 235e251. https://doi.org/10.1007/s00334-006-0066-6.
- Blaauw, M., 2010. Methods and code for 'classical' age-modelling of radiocarbon sequences. Quat. Geochronol. 5 (5), 512e518. https://doi.org/10.1016/j.quageo. 2010.01.002. Retrieved from. https://www.sciencedirect.com/science/article/pii/S1871101410000038.
- Blaauw, M., Christen, J., 2011. Flexible paleoclimate age-depth models using an autoregressive gamma process. Bayesian Anal. 6, 457e474. https://doi.org/10.1214/11-BA618.
- Blaauw, M., Christen, J., 2013. Bacon Manual V2, 3.3.
- Boudreau, B.P., 1998. Mean mixed depth of sediments: the wherefore and the why. Limnol. Oceanogr. 43 (3), 524e526. https://doi.org/10.4319/lo.1998.43.3.0524.

- Bova, S., Rosenthal, Y., Liu, Z., Godad, S.P., Yan, M., 2021. Seasonal origin of the thermal maxima at the holocene and the last interglacial. Nature 589, 548e553. https://doi.org/10.1038/s41586-020-03155-x.
- Bradley, R.S., 1999. Paleoclimatology: Reconstructing Climates of the Quaternary. Elsevier Brierley, C.M., Zhao, A., Harrison, S.P., Braconnot, P., Williams, C.J.R., Thornalley, D.J.R., et al., 2020. Large-scale features and evaluation of the pmip4cmip6 midholocene simulations. Clim. Past 16, 1847e1872. https://doi.org/10.5194/cp-16-1847-2020.
- Brown, J.R., Brierley, C.M., Ana, S.-I., Guarino, M.-V., Stevenson, S., Williams, C.J.R., et al., 2020. Comparison of past and future simulations of enso in cmip5/pmip3 and cmip6/pmip4 models. Clim. Past 16, 1777e1805. https://doi.org/10.5194/cp-16-1847-2020.
- Brugger, S.O., Gobet, E., van Leeuwen, J.F., Ledru, M.-P., Colombaroli, D., van der Knaap, W., et al., 2016. Long-term maneenvironment interactions in the bolivian amazon: 8000 years of vegetation dynamics. Quat. Sci. Rev. 132, 114e128. https://doi.org/10.1016/j.quascirev.2015.11.001.
- Burkea, K.D., Williams, J.W., Chandler, M.A., Haywood, A.M., Lunt, D.J., Otto-Bliesner, B.L., 2018. Pliocene and eocene provide best analogs for nearfuture climates. PNAS. https://doi.org/10.1073/pnas.1809600115.
- Bush, M.B., Miller, M.C., De Oliveira, P.E., Colinvaux, P., 2000. Two histories of environmental change and human disturbance in eastern lowland amazonia. Holocene 10, 543e553. https://doi.org/10.1191/095968300672647521.
- Bush, M.B., Silman, M.R., Urrego, D.H., 2004. 48,000 years of climate and forest change in a biodiversity hot spot. Science 303, 827e829. https://doi.org/10.1126/science.1090795.
- Cai, W., McPhaden, M.J., Grimm, A., Rodrigues, R.R., Taschetto, R.D., Andr_ea, S., Garreaud, Dewitte, B., et al., 2020. Climate impacts of the el ni~noesouthern oscillation on south America. Nat. Rev. Earth Environ. 1, 215e231. https://doi.org/10.1038/s43017-020-0040-3.

- Cassino, R.F., 2011. Reconstituiç~ao da vegetaç~ao e do clima do chapad~ao dos gerais durante o holoceno, a partir da analise palinol_ogica da vereda laçador. Av. Pres. Antonio Carlos, 6627 Pampulha, Belo Horizonte MG, Brazil.
- Cassino, R.F., Ledru, M.-P., de Almeida Santos, R., Favier, C., 2020. Vegetation and fire variability in the central cerrados (Brazil) during the pleistocene-holocene transition was influenced by oscillations in the sasm boundary belt. Quat. Sci. Rev. 232. https://doi.org/10.1016/j.quascirev.2020.106209.
- Cassino, R.F., Martinho, C.T., Caminha, S.A.S., 2018. A late quaternary palynological record of a palm swamp in the cerrado of central Brazil interpreted using modern analog data. Palaeogeogr. Palaeocl. 490, 1e16. https://doi.org/10.1016/j.palaeo.2017.08.036.
- Cheng, H., Sinha, A., Cruz, F., Wang, X., Edwards, R., d'Horta, F., et al., 2013. Climate change patterns in amazonia and biodiversity. Nat. Commun. 4, 1411. https://doi.org/10.1038/ncomms2415.
- Costa, G., Hampe, A., Ledru, M.-P., Martinez, P., Mazzochini, G., Shepard, D., et al., 2018. Biome stability in south America over the last 30 kyr: inferences from long-term vegetation dynamics and habitat modelling. Global Ecol. Biogeogr. 3 (27), 285e297. https://doi.org/10.1111/geb.12694.
- Cruz, F.W., Vuille, M., Wang, X., Cheng, H., Werner, M., Lawrence Edwards, R., et al., 2009. Orbitally driven east-west antiphasing of south american precipitation. Nat. Geosci. 2, 210e214. https://doi.org/10.1038/NGEO444.
- Cunha, A.P.M.A., Leal, M.Z.K.D., Costa, L., Cuarta, L.A., Marengo, J.A., Tomasella, J., et al., 2019. Extreme drought events over Brazil from 2011 to 2019. Atmosphere. https://doi.org/10.3390/atmos10110642.
- Dias, P.L.S., Turcq, B., Silva Dias, M.A.F., Braconnot, P., Jorgetti, T., 2009. Midholocene climate of tropical south America: a model-data approach. In: Vimeux, F., Sylvestre, F., Khodri, M. (Eds.), Past Climate Variability in South america and Surrounding Regions: from the Last Glacial Maximum to the Holocene. Springer Netherlands, Dordrecht, pp. 259e281. https://doi.org/10.1007/978-90-481-2672-9_11 doi: 10.1007/978-90-481-2672-9_11.

- Ding, Z., Lu, R., Wang, L., Yu, L., Liu, X., Liu, Y., et al., 2021. Early-mid holocene climatic changes inferred from colors of eolian deposits in the mu us desert. Geoderma 401, 115172. https://doi.org/10.1016/j.geoderma.2021.115172. Retrieved from. https://www.sciencedirect.com/science/article/pii/S0016706121002524.
- Dolman, A.M., Groeneveld, J., Mollenhauer, G., Ho, S.L., Laepple, T., 2021. Estimating bioturbation from replicated small-sample radiocarbon ages. Paleoceanogr. Paleoclimatol. 36 (7). https://doi.org/10.1029/2020PA004142.
- Garreaud, R.D., Vuille, M., Compagnucci, R., Marengo, J., 2009. Present-day south american climate. Palaeogeogr. Palaeoclimatol. Palaeoecol. 281. https://doi.org/10.1016/j.palaeo.2007.10.032.
- Griffiths, M.L., Johnson, K.R., Pausata, F.S.R., White, J.C., Henderson, G.M., Wood, C.T., et al., 2020. End of green sahara amplified mid- to late holocene megadroughts in mainland southeast asia. Nat. Commun. 11, 4204. https://doi.org/10.1038/s41467-020-17927-6.
- Guinasso, N.L.G., Schink, D.R., 1975. Quantitative estimates of biological mixing rates in abyssal sediments. J. Geophys. Res. 80 (21), 3032e3043. https://doi.org/10.1029/JC080i021p03032.
- Gunn, J., 2004. Encyclopedia of Caves and Karst Science. Fitzroy Dearborn, New York.
- Hajdas, I., 2008. Radiocarbon dating and its applications in quaternary studies. E&G Quat. Sci. J. 57 (1/2), 2e24. https://doi.org/10.3285/eg.57.1-2.1. Retrieved from. https://egqsj.copernicus.org/articles/57/2/2008/.
- Harrison, S.P., Bartlein, P., 2012. Chapter 14 records from the past, lessons for the future: what the palaeorecord implies about mechanisms of global change. In: Henderson-Sellers, A., McGuffie, K. (Eds.), The Future of the World's Climate, second ed. Elsevier, Boston, pp. 403e436. https://doi.org/10.1016/B978-0-12-386917-3.00014-2. Retrieved from. https://www.sciencedirect.com/science/article/pii/B9780123869173000142.
- Haug, G.H., Hughen, K.A., Sigman, D.M., Peterson, L.C., R€ohl, U., 2001. Southwar migration of the intertropical convergence zone through the holocene. Science 293, 1304e1308. https://doi.org/10.1126/science.1059725.

- Hern_andez, A., Martin-Puertasb, C., Moffa-S_anchezc, P., Moreno-Chamarro, E., Ortega, P., Blockley, S., et al., 2020. Modes of climate variability: synthesis and review of proxy-based reconstructions through the holocene. Earth Sci. Rev. 209. https://doi.org/10.1016/j.earscirev.2020.103286.
- Hogg, A.G., Hua, Q., Blackwell, P.G., Niu, M., Buck, C.E., Guilderson, T.P., et al., 2013. Shcal13 southern hemisphere calibration, 0e50,000 years cal bp. Radiocarbon 55 (4), 1889e1903. https://doi.org/10.2458/azu_js_rc.55.16783.
- Hor_ak-Terra, I., Cortizas, A.M., Luz, C.F.P.D., Silva, A.C., Mighall, T., Camargo, P.B.D., et al., 2020. Late quaternary vegetation and climate dynamics in central-eastern Brazil: insights from a 35k cal a bp peat record in the cerrado biome. JQS. https://doi.org/10.1002/jqs.3209.
- Howe, J.N.W., Piotrowski, A.M., Oppo, D.W., Huang, K.-F., Mulitza, S., Chiessi, C.M., Blusztajn, J., 2018. Antarctic Intermediate Water Circulation in the South Atlantic over Thepast 25,000 Years. American Geophysical Union. https://doi.org/10.1002/2016PA002975.
- Hubay, K., Moln_ar, M., Orb_an, I., Braun, M., Bír_o, T., Magyari, E., 2018. Ageedepth relationship and accumulation rates in four sediment sequences from the retezat mts, south carpathians (Romania). Quat. Int. 477, 7e18. https://doi.org/10.1016/j.quaint.2016.09.019. Providing long environmental records of Late Quaternary climatic oscillations in the South Carpathian Retezat Mountains (PROLONG).
 - https://www.sciencedirect.com/science/article/pii/S1040618216301380.
- Huo, Y., Peltier, W.R., Chandan, D., 2021. Mid-holocene monsoons in south and southeast asia: dynamically downscaled simulations and the influence of the green sahara. Clim. Past 17, 1645e1664. https://doi.org/10.5194/cp-17-1645-2021.
- IPCC, 2014. Ar5 Reference Regions. Retrieved from. https://www.ipcc-data.org/guidelines/pages/ar5%5c regions.html.
- Irion, G., Bush, M.B., Nunes de Mello, J.A., Stuben, D.N., Muller, G., Morais de, J.O., Junk, J.W., 2006. A multi proxy palaeoecological record of holocene lake sediments from the rio tapajos, eastern amazonia. Palaeogeogr. Palaeocl. 240, 523e535. https://doi.org/10.1016/j.palaeo.2006.03.005.

- Irving, D., Simmonds, I., 2016. A new method for identifying the pacificesouth american pattern and its influence on regional climate variability. AMS 29 (17), 6109e6125. https://doi.org/10.1175/JCLI-D-15-0843.1.
- Kaufman, D., McKay, N., Routson, C., Erb, M., Davis, B., Heiri, O., et al., 2020. A global database of holocene paleotemperature records. Sci. Data. https://doi.org/10.6084/m9.figshare.11967924.
- Khatiwala, S., Visbeck, M., Schlosser, P., 2001. Age tracers in an ocean gcm. Deep Sea Res. Oceanogr. Res. Pap. 48 (6), 1423e1441. https://doi.org/10.1016/S09670637(00)00094-7. Retrieved from. https://www.sciencedirect.com/science/article/pii/S0967063700000947.
- Kousky, V.E., Kagano, M.T., Cavalcanti, I.F.A., 1984. A review of the southern oscillation: oceanic-atmospheric circulation changes and related rainfall anomalies. Tellus 36A, 490e504. https://doi.org/10.1111/j.1600-0870.1984.tb00264.x.
- Ledru, M.-P., Mourguiart, P., Riccomini, C., 2009. Related changes in biodiversity, insolation and climate in the atlantic rainforest since the last interglacial. Palaeogeogr. Palaeoclimatol. Palaeoecol. 271 (1), 140e152. https://doi.org/10.1016/j.palaeo.2008.10.008.https://www.sciencedirect.com/science/article/pii/S0031018208005786.
- Liu, Z., Harrison, S.P., Kutzbach, J., Otto-Bliesner, B., 2002. Global monsoons in the midholocene and oceanic feedback. Clim. Dynam. 22, 157e182. https://doi.org/10.1007/s00382-003-0372-y.
- Liu, Z., Harrison, S.P., Kutzbach, J., Otto-Bliesner, B., 2004. Global monsoons in the mid-holocene and oceanic feedback. Clim. Dynam. 22, 157e182. https://doi.org/10.1007/s00382-003-0372-y.
- Lowe, J.J., Walker, M.J.C., 1997. Reconstructing Quaternary Environments, second ed. Prentice Hall. Lu, Z., Miller, P.A., Zhang, Q., Wårlind, D., Nieradzik, L., Sjolte, J., Smith, B., 2018. Dynamic vegetation simulations of the mid-holocene green sahara. Geophys. Res. Lett. https://doi.org/10.1029/2018GL079195.
- Mahiques, M.M., Wainer, I.K.C., Burone, L., Nagai, R., de Mello e Sousa, S.H., Figueira, R.C.L., et al., 2009. A high-resolution holocene record on the southern brazilian

- shelf: paleoenvironmental implications. Quat. Int. 206, 52e61. https://doi.org/10.1016/j.quaint.2008.09.010.
- Maksic, J., Shimizu, M.H., de Oliveira, G.S., Venancio, I.M., Cardoso, M., Ferreira, F.A., 2019. Simulation of the holocene climate over south America and impacts on the vegetation. Holocene 29. https://doi.org/10.1177/0959683618810406.
- Marengo, J.A., Liebmann, B., Alice, G., Misra, V., Dias, P.L.S., Cavalcanti, I.F.A., et al., 2012. Recent developments on the south american monsoon system. Int. J. Climatol. 32, 1e21. https://doi.org/10.1002/joc.2254.
- McDonald, L., Chivall, D., Miles, D., Bronk Ramsey, C., 2019. Seasonal variations in the 14c content of tree rings: influences on radiocarbon calibration and singleyear curve construction. Radiocarbon 61 (1), 185e194. https://doi.org/10.1017/RDC.2018.64.
- Ni, J., Luo, D.H., Xia, J., Zhang, Z.H., Hu, G., 2015. Vegetation in karst terrain of southwestern China allocates more biomass to roots. Solid Earth 6 (3), 799e810. https://doi.org/10.5194/se-6-799-2015. Retrieved from. https://se.copernicus.org/articles/6/799/2015/.
- Novello, V.F., Cruz, F.W., Vuille, M., Stríkis, N.M., Edwards, R.L., Cheng, H., et al., 2018. A high-resolution history of the south american monsoon from last glacial maximum to the holocene. Sci. Rep. 7, 44267. https://doi.org/10.1038/srep44267.
- Nowacki, D., Langan, C.C.M., Kadereit, A., Pint, A., Wunderlich, J., 2019. 'lake gorgana' a paleolake in the lower danube valley revealed using multi-proxy and regionalisation approaches. Quat. Int. 511, 107e123. https://doi.org/10.1016/j.quaint.2018.09.021.https://www.sciencedirect.com/science/article/pii/S1040618217315926.
- Pausata, F.S.R., Messori, G., Zhang, Q., 2016. Impacts of dust reduction on the northward expansion of the african monsoon during the green sahara period. Earth Planet Sci. Lett. 434, 298e307. https://doi.org/10.1016/j.epsl.2015.11.049.
- Pausata, F.S.R., Zhang, Q., Muschitiello, F., Lu, Z., Chafik, L., Niedermeyer, E.M., et al., 2017. Greening of the sahara suppressed enso activity during the mid-holocene. Nat. Commun. 8, 16020. https://doi.org/10.1038/ncomms16020.

- Peterson, R.G., Stramma, L., 1991. Upper-level circulation in the south atlantic ocean.

 Prog. Oceanogr. 26 (1), 1e73. https://doi.org/10.1016/0079-6611(91)90006-8.

 Retrieved from.

 https://www.sciencedirect.com/science/article/pii/0079661191900068.
- Pivel, M.A.G., Toledo, F.A.L., Costa, K.B., 2010. Foraminiferal record of changes in summer monsoon precipitation at the southeastern brazilian continental margin since the last glacial maximum. Rev. Bras. Palaontol. 13, 79e88. https://doi.org/10.4072/rbp.2010.2.01.
- Prado, L., Wainer, I., Chiessi, C.M., 2013b. Mid-holocene pmip3/cmip5 model results: intercomparison for the south american monsoon system. Palaeogeogr. Palaeocl. 23. https://doi.org/10.1177/0959683613505336.
- Prado, L., Wainer, I., Chiessi, C.M., Ledru, M.-P., Turcq, B., 2013a. A mid-holocene climate reconstruction for eastern south America. Clim. Past 9, 2117e2133. https://doi.org/10.5194/cp-9-2117-2013.
- Prieto, A.R., 1996. Late quaternary vegetational and climatic changes in the pampa grassland of Argentina. Quat. Res. 45, 75e88. https://doi.org/10.1006/qres.1996.0007.
- Raczka, M.F., Oliveira, P.E.D., Bush, M., McMichael, C.H., 2013. Two paleoecological histories spanning the period of human settlement in southeastern Brazil. JQS. https://doi.org/10.1002/jqs.2597.
- Ramsey, C.B., 2008. Deposition models for chronological records. Quat. Sci. Rev. 27 (1), 42e60. https://doi.org/10.1016/j.quascirev.2007.01.019 (INTegration of Icecore, Marine and Terrestrial records (INTIMATE): Refining the record of the Last Glacial-Interglacial Transition). https://www.sciencedirect.com/science/article/pii/S0277379107003617.
- Reimer, P.J., Austin, W.E.N., Bard, E., Bayliss, A., Blackwell, P.G., Bronk Ramsey, C., et al., 2020. The intcal20 northern hemisphere radiocarbon age calibration curve (0e55 cal kbp). Radiocarbon 62 (4), 725e757. https://doi.org/10.1017/RDC.2020.41.
- Reimer, P.J., Baillie, M.G.L., Bard, E., Bayliss, A., Beck, J.W., Bertrand, C.J.H., et al., 2004. Intcal04: terestrial radiocarbon age calibration, 0-26 cal kyr bp. radiocarbon. Radiocarbon 46 (4), 1029e1058. https://doi.org/10.1017/RDC.2020.41.

- Riris, P., Arroyo-Kalin, M., 2019. Widespread population decline in south America correlates with mid-holocene climate change. Sci. Rep. 9, 6850. https://doi.org/10.1038/s41598-019-43086-w.
- Roberts, J., Gottschalk, J., Skinner, L.C., Peck, V.L., Kender, S., Elderfield, H., et al., 2016. Evolution of south atlantic density and chemical stratification across the last deglaciation. Proc. Natl. Acad. Sci. 113 (3), 514e519. https://doi.org/10.1073/pnas.1511252113. https://www.pnas.org/content/113/3/514.
- Rojas, O., YanYun, L., Cumani, R., 2014. Understanding the Drought Impact of El Nino on the Global Agricultural Areas: an Assessment Using Fao's Agricultural Stress Index (Asi). Environment and Natural Resources Management Series, Climate Change.
- Ropelewski, C.F., Bell, M.A., 2008. Shifts in the statistics of daily rainfall in south America conditional on enso phase. J. Clim. 21, 849e865. https://doi.org/10.1175/2007JCLI1617.1.
- Sandweiss, D.H., Solís, R.S., Moseley, M.E., Keefer, D.K., Ortloff, C.R., 2009. Environmental change and economic development in coastal Peru between 5,800 and
- 3,600 years ago. Proc. Natl. Acad. Sci. 106 (5), 1359e1363. https://doi.org/10.1073/pnas.0812645106. Retrieved from. https://www.pnas.org/content/106/5/1359.
- Sasaki, W., Doi, T., Richards, K.J., Masumoto, Y., 2015. The influence of enso on the equatorial atlantic precipitation through the walker circulation in a cgcm. Clim. Dynam. 44, 191e202. https://doi.org/10.1007/s00382-014-2133-5.
- Schneider, U., Becker, A., Finger, P., Meyer-Christoffer, A., Rudolf, B., Ziese, M., 2015. Gpcc full data reanalysis version 6.0 at 2.5_: monthly land-surface precipitation from rain-gauges built on gts-based and historic data, 10 September 2020. https://psl.noaa.gov/data/gridded/data.gpcc.html.
- Shimizu, M.H., Sampaio, G., Venancio, I.M., Maksic, J., 2020. Seasonal changes of the south american monsoon system during the mid-holocene in the cmip5 simulations. Clim. Dynam. 54, 2697e2712. https://doi.org/10.1007/s00382-020-05137-1.

- Smith, Mayle, F.E., 2017. Impact of mid- to late holocene precipitation changes on vegetation across lowland tropical south America: a paleo-data synthesis. Quat. Res. 1e22. https://doi.org/10.1017/qua.2017.89.
- Sorooshian, S., Martinson, D.G., 1995. Proxy Indicators of Climate, an Essay in: Natural Climate Variability on Decade-To-Century Time Scales. The National Academies Press, Washington D.C., pp. 489e494
- Souza, E., Kayano, M.T., Ambrizzi, T., 2005. Intraseasonal and submonthly variability over the eastern amazon and northeast Brazil during the autumn rainy season. Theor. Appl. Climatol. https://doi.org/10.1007/s00704-004-0081-4.
- Tabor, C., Otto-Bliesner, B., Liu, Z., 2020. Speleothems of south american and Asian monsoons influenced by a green sahara. Geophys. Res. Lett. 47. https://doi.org/10.1029/2020GL089695.
- Toledo, F.A.L., Costa, K.B., Pivel, M.A.G., 2007. Salinity changes in the western tropical south atlantic during the last 30 kyr. Global Planet. Change 57, 383e395. https://doi.org/10.1016/j.gloplacha.2007.01.001.
- Toledo, F.A.L., Costa, K.B., Pivel, M.A.G., Campos, E.J.D., 2008. Tracing past circulation changes in the western south atlantic based on planktonic foraminifera. Rev. Bras. Palaontol. 11, 169e178. https://doi.org/10.4072/rbp.2008.3.03.
- Torres, R.R., Benassi, R.B., Martins, F.B., Lapola, D.M., 2021. Projected impacts of 1.5 and 2_c global warming on temperature and precipitation patterns in south America. Int. J. Climatol. https://doi.org/10.1002/joc.7322.
- Turcq, B., Albuquerque, A.L.S., Cordeiro, R.C., Sifeddine, A., Simoes Filho, F.F.L., Souza, A.G., et al., 2002. Accumulation of organic carbon in five brazilian lakes during the holocene. Sediment. Geol. 148, 319e342. https://doi.org/10.1016/S0037-0738(01)00224-X.
- Turcq, B., Pressinotti, M.M., Martin, L., 1997. Paleohydrology and paleoclimate of the past 33,000 years at the tamandu_a river, central Brazil. Quat. Res. 47 (3), 284e294. https://doi.org/10.1006/qres.1997.1880. Retrieved from. https://www.sciencedirect.com/science/article/pii/S0033589497918809.

- Urrego, D.H., Bush, M.B., Silman, M.R., Correa-Metrio, A.Y., Ledru, M.-P., Mayle, F.E., et al., 2009. Millennial-scale ecological changes in tropical south America since the last glacial maximum. In: Vimeux, F., Sylvestre, F., Khodri, M. (Eds.), Past Climate Variability in South america and Surrounding Regions: from the Last Glacial Maximum to the Holocene. Springer Netherlands, Dordrecht, pp. 283e300. https://doi.org/10.1007/978-90-481-2672-9_12 doi: 10.1007/978-90-481-2672-9 12.
- Van der Plicht, J., 2015. Variations in Atmospheric 14c. Reference Module in Earth Systems and Environmental Sciences, 2923e2931. Elsevier Reference Module in Earth Systems and Environmental Sciences. https://doi.org/10.1016/B978-0-12-409548-9.09564-6.
- Vera, C., Higgins, W., Amador, J., Ambrizzi, T., Garreaud, R., Gochis, D., et al., 2006. Towards a unified view of the american monsoon system. J. Clim. 19, 4977e5000. https://doi.org/10.1175/JCLI3896.1.
- Wainer, I., Prado, L., Khodri, M., Otto-Bliesner, B., 2014. Reconstruction of the south atlantic subtropical dipole index for the past 12,000 years from surface temperature proxy. Sci. Rep. 4, 5291. https://doi.org/10.1038/srep05291.
- Wang, X., Augusto, R.L.E., Auler, S., Cheng, H., Kong, X., Wang, Y., et al., 2017. Hydroclimate changes across the amazon lowlands over the past 45,000 years. Nature 541, 204e207. https://doi.org/10.1038/nature20787.
- Wanner, H., Beer, J., Bütikofer, J., Crowley, T.J., Cubasch, U., Flückiger, J., et al., 2008. Mid- to late holocene climate change: an overview. Quat. Sci. Rev. 27 (19), 1791e1828. https://doi.org/10.1016/j.quascirev.2008.06.013. Retrieved from. https://www.sciencedirect.com/science/article/pii/S0277379108001479.
- Ward, B.M., Wong, C.I., Novello, V.F., Gee, D.M., Santos, R.V., Silva, L.C.R., et al., 2019. Reconstruction of holocene coupling between the south american monsoon system and local moisture variability from speleothem d 180 and 87sr/86sr records. Quat. Sci. Rev. 210, 51e63. https://doi.org/10.1016/j.quascirev.2019.02.019.
- Weng, C., Bush, M.B., Athens, J., 2002. Holocene climate change and hydrarch succession in lowland amazonian Ecuador. Rev. Palaeobot. Palynol. 120 (1), 73e90.

- https://doi.org/10.1016/S0034-6667(01)00148-8. Retrieved from. https://www.sciencedirect.com/science/article/pii/S0034666701001488.
- Wirtz, K.W., Lohmann, G., Bernhardt, K., Lemmen, C., 2010. Midholocene regional reorganization of climate variability: analyses of proxy data in the frequency domain. Palaeogeogr. Palaeocl. 298, 189e200. https://doi.org/10.1016/j.palaeo.2010.09.019.
- Wong, Wang, X., Latrubesse, E.M., He, S., Bayer, M., 2021. Variations in the South atlantic convergence zone over the mid-to-late holocene inferred from speleothem d 180 in central Brazil. Quat. Sci. Rev. 270, 107178. https://doi.org/10.1016/j.quascirev.2021.107178. Retrieved from. https://www.sciencedirect.com/science/article/pii/S0277379121003851.
- Wong, C., Breecker, D., 2015. Advancements in the use of speleothems as climate archives. Quat. Sci. Rev. 127, 1e18. https://doi.org/10.1016/j.quascirev.2015.07.019. Novel approaches to and new insights from speleothembased climate reconstructions.https://www.sciencedirect.com/science/article/pii/S0277379115300 585.
- Wood, R., 2015. From revolution to convention: the past, present and future of radiocarbon dating. J. Archaeol. Sci. 56, 61e72. https://doi.org/10.1016/j.jas.2015.02.019 (Scoping the Future of Archaeological Science: Papers in Honour of Richard Klein. https://www.sciencedirect.com/science/article/pii/S0305440315000576.
- Zhang, M., Liu, Y., Zhang, J., Wen, Q., 2021. Amoc and climate responses to dust reduction and greening of the sahara during the mid-holocene. J. Clim. 34, 4893e4912. https://doi.org/10.1175/JCLI-D-20-0628.1.
- Zhang, Z., Leduc, G., Sachs, J.P., 2014. El ni~no evolution during the holocene revealed by a biomarker rain gauge in the gal_apagos islands. Earth Planet Sci. Lett. 404, 420e434.https://doi.org/10.1016/j.epsl.2014.07.013.https://www.sciencedirect.com/science/article/pii/S0012821X14004634.
- Zhao, Y., Harrison, S., 2012. Mid-holocene monsoons: a multi-model analysis of the
- interhemispheric differences in the responses to orbital forcing and ocean feedbacks. Clim. Dynam. 39, 1457e1487. https://doi.org/10.1007/s00382-011-1193-z.

Zhou, J., Lau, K., 1998. Does a monsoon climate exist over south America? J. Clim. 11, 1020e1040. https://doi.org/10.1175/1520-0442(1998)011<1020: DAMCEO>2.0.CO;2.

JQS

Journal of Quaternary Science



Long-and shor-term vegetation change and inferred climate dynamics and anthropogenic activity in the central Cerrado during the Holocene

KATERINE ESCOBAR-TORREZ,^{1,2*} MARIE-PIERRE LEDRU,¹ RAQUEL FRANCO CASSINO,² PAULA RIBEIRO BIANCHINI³ and ELDER YOKOYAMA³

¹Institut des Sciences de l'Evolution de Montpellier (ISEM), Université de Montpellier-CNRS-IRD-EPHE, France

²Departamento de Geologia, Universidade Federal de Ouro Preto, Brazil

Abstract

A paleoecologic analysis of pollen, macrocharcoal and trace elements from a lacustrine sediment core located at Lake Feia, central Cerrado (Goiás State, Brazil), was used to evaluate the relationship between vegetation, fire and climate during the Holocene. The development of cerrado vegetation appears to have begun 6000 years ago, initially with the establishment of an open cerrado, followed from 4800 cal a BP by a change to a woody cerrado driven by an increase in summer insolation. The increases in precipitation levels in the central Cerrado during the last 5000 years are related to the increased influence of the Amazon in central Brazil, which has facilitated biomass burning and anthropogenic activities in the region of Lake Feia. Multi - centennial - scale changes in water level - related and gallery forest pollen assemblages indicate three main dry episodes, at 3440–2760, 2700–1690 and 1330–1150 cal a BP, linked to regional shifts between northern and southern South American summer monsoon boundaries. The presence of low continuous fire activity does not appear to have affected vegetation recovery, whereas two intervals with increased fire activity, at ~3300 and ~1300 cal a BP, indicated a slower recovery.

Keywords: fire, insolation, pollen, South American summer monsoon, Tropics

³Instituto de Geociências, Universidade de Brasília, Brazil

Introduction

The Cerrado biome in central Brazil covers about 2 million km². It represents a diverse ecosystem, harboring 4800 endemic plant and vertebrate species (Strassburg et al., 2017), and, as most of the Brazilian basins originate in central Brazil, is an important source of freshwater (Lima et al., 2011). However, despite its high biodiversity and socioeconomic importance, the destruction of this ecosystem is continuing at an accelerated rate (Vieira et al., 2022). Intensive human disturbance, including deforestation and the use of fire, has destabilized natural processes within the ecosystem, thereby increasing hydric stress (Hofmann et al., 2021) and the frequency and severity of fire events (Colli et al., 2020). Future projections for the Cerrado indicate a loss of plant diversity (Velazco et al., 2019), underlining the importance of implementing integrated fire management practices, and combining scientific research with traditional knowledge to address fire management problems (Schmidt and Eloy, 2020).

Floral distribution patterns vary widely across the Cerrado domain (Vieira et al., 2022), the landscape being characterized by vegetation physiognomies ranging from open grassland to dense woodland (Ribeiro and Walter, 2008), with close relationships between vegetation, climate, soil condition and fire frequency (Henriques, 2005; Bueno et al., 2018). Today, two main climatic features, the seasonal South American summer monsoon (SASM) and the spatial shifts of the intertopical convergence zone (ITCZ), result in bimodal rainfall seasonality, with high rainfall from October to March and low rainfall from April to August (Reboita et al., 2010; Marengo et al., 2012).

In the tropical lowlands of South America, paleoclimatic studies indicate a trend toward more wet conditions during the Last Glacial Maximum (21000 cal a BP) and the Younger Dryas (12 700–11 000 cal a BP) in western Amazonia, north-eastern Brazil (NEB), and central and south-eastern Brazil (SEB) (Cruz et al., 2009; Deininger et al., 2019). During the early and mid-Holocene, the presence of a precipitation dipole between NEB and SEB in response to northern/southern hemisphere summer insolation was characterized by longer wet and dry seasons, respectively (Cruz et al., 2009). However, speleothem records have also revealed that the central Cerrado underwent numerous fluctuations in wet and dry episodes between 11 000 and 4000 cal a BP (Ward et al., 2019; Azevedo et al., 2021, Wong et al., 2021), with longer wetter episodes in the last 4000 cal a BP (Strikis et al., 2011; Campos et al., 2019), implying both regional and local influences on seasonality. Paleoecologic studies of the Cerrado are rare and discontinuous in space and time. They also show a wide range of responses depending on location, with

cerrado vegetation undergoing several episodes of expansion and retreat from 11000 cal a BP, in response to the variability of local climatic conditions from east to west, and north to south (Ferraz-Vicentini and Salgado-Labouriau, 1996; Behling, 2002; Ledru et al., 2006; Horák-Terra et al., 2020). In the northern and central Cerrado, floristic changes from cooler to warmer assemblages characterize the transition from the last glacial to the Holocene (Cassino et al., 2018, 2020; Horák-Terra et al., 2020; Ledru et al., 2006). More contrasted responses have been observed during the early Holocene, with centennial-scale fluctuations in wet and dry conditions in the central region until 6000 cal a BP (Cassino et al., 2018, 2020), the full expansion of the Cerrado in northern Brazil from 11 000 cal a BP (Ledru et al., 2006), and the persistence of wet and cold conditions in the north-eastern region of the central Cerrado (Horák-Terra et al., 2020; Sabino et al., 2021).

During the mid-Holocene the vegetation became drier (Salgado-Labouriau et al., 1998; Barberi et al., 2000; Cassino et al., 2020), responding to a weaker SASM influence over eastern Brazil (Prado et al., 2013a and Prado et al., 2013b). During the late Holocene, multi-centennial fluctuations between wet and dry conditions in northern Minas Gerais indicate the expansion of a drier Cerrado after 4000 cal a BP (Cassino et al., 2018), and two drier episodes at 2900 and 900 cal a BP (Sabino et al., 2021). However, the low resolution of the analyses (e.g. Barberi et al., 2000), the absence of macrocharcoal analyses (e.g. Horák-Terra et al., 2020) and the loss of sediment from the upper levels (e.g. Ledru et al., 2006) have prevented a reconstruction of the relationship between vegetation, fire and climate for the last 5000 years, as well as the process of cerrado vegetation recovery after the mid-Holocene dry episode. Moreover, the Cerrado region has been inhabited for at least 15 000 years (Prous and Fogaça, 1999), with archeological sites indicating a decrease in human occupation during the early to mid-Holocene in the southern Cerrado (Araujo et al., 2005), followed by an increase in the late Holocene (Barbosa et al., 2020). Human occupation in the Cerrado is associated with fire activity (Pivello et al., 2021), and deciphering wild from anthropogenic fire is critical to understanding the relationship between fire and climate, and its role in the distribution and composition of cerrado vegetation (Schmidt and Eloy, 2020).

Lake Feia is located in the central Cerrado, where pollen analyses have revealed a high sensitivity to climate change between 19 000 and 5000 cal a BP (Ferraz-Vicentini, 1999; Cassino et al., 2020). The LFB1 and LFB2 sediment cores were collected in 1990 (Turcq et al., 2002), while the LF 15-2 corewas collected in 2015. Pollen and microchacoal analyses have been conducted on 20 samples covering the upper part of

core LFB2 (375 cm deep,) representing the last 6000 years, with a resolution of ~260 years between samples (Ferraz-Vicentini, 1999). Pollen and macrocharcoal analyses have been conducted on core LF15-2 (500 cm deep), dating from 19 000 to 5000 cal a BP (Cassino et al., 2020). Core LFB2 has revealed the expansion of a woody cerrado, with two drier intervals, from 5280 to 4850 and 3010 to 2100 cal a BP, and a gradual reduction in more humid conditions until the present (1990 AD) (Ferraz-Vicentini, 1999). Abundant charred particles have been observed throughout the record until 770 a BP (Ferraz-Vicentini, 1999). However, the low sampling resolution does not allow a comparison of the vegetation changes with other paleoclimatic studies based on, for example, speleothems. Thus, to improve our knowledge of the Cerrado biome during the late Holocene, and more particularly our understanding of the relationships between fire, climate, biodiversity and human activity, we performed highresolution pollen, charcoal and geochemical analyses on the upper 310 cm of core LFB1, representing the last 5000 years. We then compared the results with other sediment and speleothem records, and reconstructed a synthetic framework for the responses of the central Cerrado to climatic and anthropogenic effects during the late Holocene.

Material and methods

Study area

Lake Feia (15°34′20″S, 47°18″20″W, altitude 871 m) is located in the vicinity of the city of Formosa, Goiás State, in the central Cerrado (Fig. 1a), Brazil. It is 3.5 km long, elongated in a north-east (NE)–south-west (SW) direction, 5 m deep (Fig. 1b), and probably of tectonic origin (Ferraz-Vicentini, 1999). Preto River crosses Lake Feia, entering in the NE and exiting in the SW (Fig. 1b). Currently, macrophytes (Nymphaea, Sagittaria and Eichornia) can be observed from the shore and continuing toward the center of the lake, in a water column of 2–3 m.

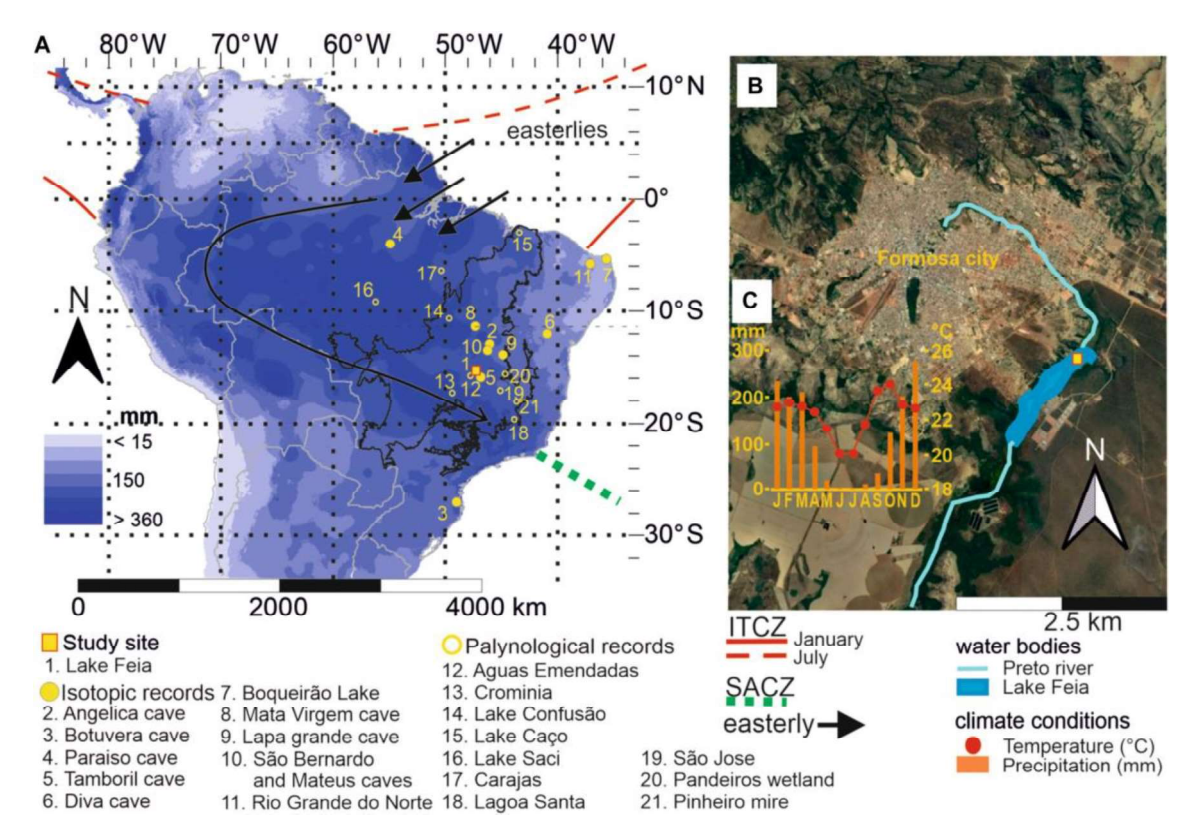


Figure 1. (A) Map of the mean austral summer precipitation levels, showing the position of the ITCZ, the core region of the summer monsoon today (dark blue), the limit of the Cerrado biome (black line), and the location of Lake Feia and the pollen and isotopic records discussed in the text. (B) Satellite view of Lake Feia (source Google Earth) showing its location relative to Formosa and Preto River. (C) Climate diagram for the city of Formosa (INMET, 2022). [Color figure can be viewed at wileyonlinelibrary.com]

Mean annual temperature at Lake Feia is 18–20°C, while mean annual precipitation ranges from 1450 to 1850 mm; 50–70% of the rain falls between November and March, exceeding 400–600 mm from December to February, with a 150–250 mm hydric deficit during the other five months (May to September) characterizing the dry season (Fig. 1c). The rainfall regime in central Brazil is modulated by the position of the South American convergence zone (SACZ) in the southern Atlantic, which influences the intensity of the SASM. The SASM is also influenced by the ITCZ, which moves across the equator following the seasonal insolation cycle (Fig. 1a) (Garreaud et al., 2008). The rainfall in Brazil therefore presents an anti-phased pattern, with high rainfall over Amazonia and central Brazil and low rainfall over northeastern Brazil in austral summer (December to February), and the opposite pattern in austral winter (June to August) (Reboita et al., 2010; Marengo et al., 2012). During the austral summer, when the ITCZ

is in its southernmost position, the incursion of North Atlantic Ocean trade winds over the continent is blocked by the Andes (Insel et al., 2010), thus increasing convective moisture over Amazonia. The flux of moist air generated follows a NE–SW trajectory along the south-western boundary of the Amazon basin, before being redirected toward the Atlantic Ocean at the location where the SACZ activates the SASM (Marengo et al., 2004). Consequently, in January, when the SACZ reaches its southernmost position (26°S), an increase in precipitation is observed in the core region of the monsoon system, in central and south-eastern Brazil (Fig. 1a) (Marengo et al., 2012; Sulca et al., 2016).

Modern vegetation

The Cerrado biome comprises diverse types of vegetation and physiognomy, based on plant structure and growth form (Oliveira-Filho and Ratter, 1995, 2002), which are classified according to soil fertility, water availability and fire occurrence (Bueno et al., 2018). Cerrado physiognomies range from open grassland to dense woodlands. The open cerrado is characterized by a grassland physiognomy with a canopy cover of less than 5%; the cerrado sensu stricto by trees and shrubs 3–8 m in height, with the tree species Astronium fraxinifolium, Byrsonima cocolobifolia, Caryocar basiliense and Roupala montana accounting for 30% of the total crown cover (Ribeiro and Walter, 2008); and the woody cerrado by trees 8–12 m or more in height and a crown cover of 50–90% (Oliveira Filho & Ratter, 2002; Durigan et al., 2022). The gallery forest physiognomy of the Cerrado biome is usually related to water bodies, and commonly divided into floodplain and swamp gallery forests, the assemblages varying in response to groundwater level dependance and/or adaptation (Durigan et al., 2022). The physiognomies and floristic compositions overall vary depending on topography, drainage and soil properties (Felfili, 1995; Bueno et al., 2018).

The landscape around Lake Feia comprises open cerrado, woody cerrado and gallery forest physiognomies (Cassino et al., 2020). The gallery forest grows from the lake shore to 5 m above the water level on the NE side of the lake. The city of Formosa is located on the western side of the lake (Fig. 1b). A botanical survey carried out 7 km from Lake Feia revealed the dominance of the following families: Anacardiaceae, Araliaceae, Malvaceae, Asteraceae, Cyperaceae, Eriocaulaceae, Poaceae, Lamiaceae, Fabaceae, Lentibulariaceae, Malpighiaceae, Melastomataceae, Myrtaceae, Onagraceae, Orchidaceae, Polygalaceae, Pontederiaceae, Verbenaceae and Xyridaceae (Table 1) (Ferraz-Vicentini, 1999).

Table 1. Key Cerrado species identified near Lake Feia, Brazil (Ferraz-Vicentini, 1999).

Growth form	Common plant list			
Trees	Anacardium sp., Schefflera sp., Waltheria sp.,			
	Tephrosia leptostachya, Byrsonima sp., Cabralea sp.			
Herbs, shrubs and epiphytes	Riencourtia tenifolia, Aristida riparia, Axanofarus sp.,			
	Laersia, Hexandra, Paspalum gardinerianum, P.			
	polyphyllum, P. stellatum, Thrasya petrosa,			
	Trachypogon sp., T. spicatus, Bauhinia, Galactia,			
	Periandra,			
	Utricularia myriocista, Microlicia, Desmoscelis.			
	Epiphytes are represented by Epidendrum,			
	Phragmidium, sp.			
Water level-related	Cyperus haspan, Fivrena sp., Rhynchosphora gigantea,			
	Eriocaulon sp., Hyptis, Polygonum, Pontederia			
	cordate,			
	Xyris jupicae			

Sampling and chronology

The 6-m-long sediment core LFB1 was retrieved from Lake Feia in 1990 using vibracoring, adapted from Martin et al. (1995), and stored at the University of Brasília (Federal District, Brazil). For the present study, we analyzed the top 310 cm, corresponding to the last 5000 years. The core was collected in open water in the northeastern part of the lake at a depth of 1.5 m (Fig. 1b) (Turcq et al., 2002).

Eight bulk sediment samples (Table 2) were sent to the Laboratoire de Mesure du Carbone14 (LMC14)–UMS 2572 (CEA/DSM–CNRS–IRD–IRSN–Ministère de la Culture et de la Communication, Saclay, France) for analysis and radiocarbono dating by accelerator mass spectrometry (AMS). The radiocarbon dates were calibrated using the Southern Hemisphere Terrestrial SHcal20 curve (Hogg et al., 2020) in Calib 7.0 (Stuiver and Reimer, 1993). The age–depth relationship was modeled using Bayesian statistics with the Bacon package in R (Blaauw and Christen, 2011). An extra date of –40 a BP was added at 0 cm, corresponding to the year of coring, i.e. 1990. The parameters were adjusted to SHCal20 with a confidence interval of 0.95 (Fig. 2).

Table 2. Radiocarbon dates for the LFB1 sediment core taken from Lake Feia, Brazil. The 14C dates were calibrated using Calib 7.0 (Stuiver and Reimer, 1993), and values are shown to two standard deviations (2σ) .

Laboratory code	Material dated	Depth (cm)	δ ¹³ C (‰)	¹⁴ C age	Age range
				(a BP)	(cal a BP)
SacA 53907	Lake sediment	14–15	-32.4	220 ± 30	136–232
SacA 60352	Lake sediment	40-41	– 27.5	910 ± 30	739–789
SacA 53908	Lake sediment	60–61	-29.8	870 ± 30	680–775
SacA 60353	Lake sediment	102-103	-25.6	1280 ± 30	1069-1189
SacA 60354	Lake sediment	164–165	-30.2	2160 ± 30	2007–2159
SacA 60355	Lake sediment	218–219	-23.8	2925 ± 30	2919-3082
SacA 60356	Lake sediment	270-271	-25.9	3520 ± 30	3677–3841
SacA 53909	Lake sediment	313–314	-33.3	4405 ± 30	4851-4983

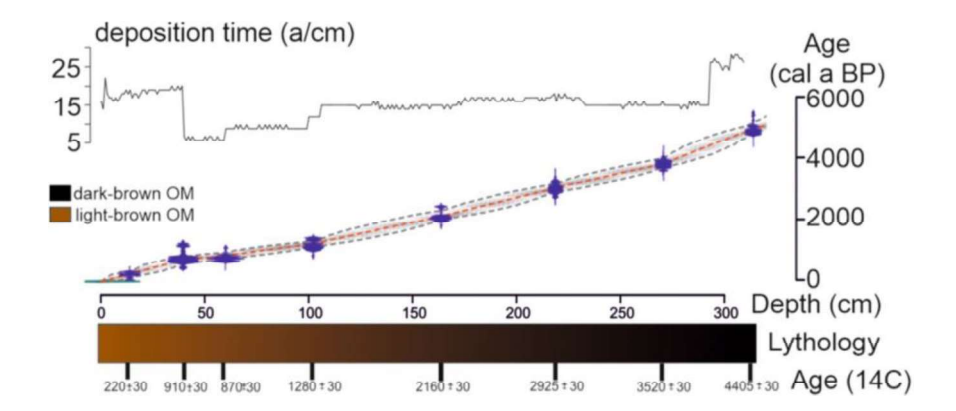


Figure 2. Calibrated age—depth model for the LFB1 core from Lake Feia, with the accumulation rate curve (a cm-1) at the top and the position of the radiocarbon dates (Table 1) along the core lithology (in brown) at the bottom. Standardized errors are indicated by the blue boxes. The black dashed lines show the upper and lowest calibrated ages, the gray band the probability of minor or major dates for each depth, and the red dashed line the most probable age. [Color figure can be viewed at wileyonlinelibrary.com]

Analytical protocols

Pollen was analyzed in 149 sediment subsamples, each measuring 0.5 cm long and 1 cm thick, collected at 2-cm intervals. Pollen was extracted at the ISEM laboratory in France. A spike of two Lycopodium tablets (36 814 Lycopodium clavatum spores per tablet) per sample was added to calculate the concentration of pollen. The samples were first washed in 10% KOH in a hot water bath, before density separation with ZnCl2 (Kummel and Raup, 1965). For samples taken between 309 and 200 cm, a 5-ml 75% HF treatment was performed for 1 h (Faegri and Iversen,1989) to remove silica. Pollen, spores and other non-palynomorphs were identified and counted at 600× magnification.

A total of 175 pollen types was identified using the ISEM pollen reference collection for Cerrado pollen taxa, identification keys and catalogs of pollen types from Brazil (Salgado-Labouriau, 1973; Cassino and Meyer, 2011; Bush and Weng, 2007; RCPol, 2021). Pollen percentages were based on the total sum of terrestrial pollen grains. Additionally, the pollen influx, as grains cm⁻² a⁻¹, was calculated for each taxa. Pollen zones were defined by constrained cluster analysis by sum of squares (CONISS), as proposed by Bennett (1996). Diagrams and pollen zones were created using the rioja package in RStudio. For the selection of pollen taxa, we applied the following process. (i) First, we classified the pollen taxa according to their type of growth (arboreal, nonarboreal) and phytophysiognomy (woody cerrado, cerrado or gallery forest) (Supporting Information Table S1). The Poaceae were then used to characterize open and closed physiognomies, according to Gosling et al. (2005, 2009). (ii) Second, we built a dataset excluding pollen taxa contributing less than 1%, and applied a principal components analysis (PCA) (Table S2). (iii) Third, we used both the frequency (high or low) and the representation (constant or variable) of each pollen taxon selected in the first PCA to constrain the most representative pollen taxa. From a total of 175 identified pollen taxa, 20 were selected based on the three-step process described before.

A second PCA was applied to the most representative pollen taxa to evaluate vegetation variability as a function of time (Table S3). Before each PCA, the dataset was square-root transformed to minimize the heterogeneity and reduce over- or underrepresentation (Becker et al., 1988). The PCA for the selected pollen taxa (Fig. S1) separated them into three groups (Fig. S3), providing information about the environment and climatic conditions based the ecological requirements of each taxon as defined in Table S4.

For palynological interpretation, pollen assemblages were characterized by pollen percentage deposition (pollen influx) and the ecological characteristics such as life form, stratum, light exposure, pollination syndrome and habitat (mostly soil requirements) of each taxon (summarized in Table S4).

For the trace element analysis, 81 sediment samples were dried in a laboratory oven at 50°C for 24 h. Thereafter, sediments were macerated in agate drumsticks, and fractions smaller than 0.180 mm were separated with an 8×2 'INOX ASTM 80 MESH/TYLER 80 by Bertrand sieve'. A sediment volume of 1 cm3 for each subsample was placed in an X-ray fluorescence (XRF) holder cup. The samples were analyzed at the Instituto de Geociências–Uiversidade de Brasilia, using a portable XRF DELTA

(Olympus) in soil mode, with three repetitions of 2 min for each sample and using the mean of the three repetitions to interpret the results. Finally, representative elements were selected, using Ti and Ti/K levels as indicators of erosion (Marshall et al., 2011; Davies et al., 2015). Ti/K ratios were normalized to view the data variation on a homogenized scale.

To reconstruct fire activity, 310 sediment subsamples, each of 0.5 cm3, were collected at 1-cm intervals. The subsamples were deflocculated and bleached with KOH (10%) and NaOC1 (2.6%), and gently passed through a 160-µm mesh under water. The residues were carefully washed into a porcelain evaporating dish, to aid identification and counting of charcoal particles. The material was analyzed at 60× magnification under a Leica microscope, with a camera connected to animage analyzer and Winseedle imageanalysis software (Regent Instruments Canada Inc., 2009), which allowed measurement of total charcoal concentration by number, the area of individual particles and the cumulative sum of charcoal particle area (i.e. the concentration of charcoal by area). The charcoal accumulation rate was calculated by multiplying the total concentration of charcoal number (area) by the sediment accumulation rate (CHAR) (CHAR = particles cm⁻² a ⁻¹ and CHARarea = mm²/ cm⁻² a ⁻¹). In addition, length:width (L:W) was evaluated for each particle. The individual values were then incorporated into a density diagram. The average L:W ratio was used to evaluate the presence and dominance of grass and/or woody charred particles per sample, for which values above 3.5 (below 2.5) suggested charred grass (wood) particles (Vachula et al., 2021).

Results

The age-depth model obtained for the LFB1 core (Fig. 2) provided a chronology for the last 5000 years of vegetation in the Cerrado. The resolution ranged between 12 and 50 years per sample for pollen analysis, and between 6 and 25 years per sample for macrocharcoal analysis. The lowest deposition rate in the whole section was observed between 310 and 270 cm (4830–3800 cal a BP), with an average of 25 a cm–1. Between 269 and 100 cm (3790–1185 cal a BP), the deposition rate was ~15 a cm–1. Between 99 and 40 cm (1180–690 cal a BP), the highest deposition rate ranged from 6 to 10 a cm–1. From 39 to 0 cm (670 to –40 cal a BP) the sedimentation rate was ~20 a cm–1 (Fig. 2). The top of the core was radiocarbon dated to 220 ± 30 14C a BP, corresponding to the last century (Table 2); we therefore considered the top of the core to be modern.

Palynological analyses

Constrained cluster analysis (Bennett, 1996) identified five pollen zones (Fig. S1). PCA showed that temporal changes defined by the individual z-score values, negative values indicated taxa associated with pollen assemblages from gallery forest with seasonal or permanent flooding, while positive values suggested cerrado/gallery forest with well-drained soils (Figs 3, S2A and S2B). Thus, the assemblage Ilex-Myrtaceae-Banisteropsis was associated with swampy gallery forest, with Myrtaceae at the periphery of the swamp and Ilex also present in inundated areas. Both Myrtaceae and Ilex are small trees, forming lower storey forest, while Banisteropsis is a heliophilous woody vine (Araújo et al., 2002). An increase in their pollen frequency/influx associated with a decrease in lake level suggested forest invasion toward the coring site, as their entomophilous pollen cannot travel long distances. The assemblage Alchornea-Apeiba-Casearia-Euterpe-Melastomataceae-Combretaceae-Ouratea-Ternstroemia represented plant taxa generally observed in lower storey strata (>10 m) of gallery forest and woody cerrado (Araújo et al., 2002), associated with moist and fertile soils. The assemblage Poaceae-Anadenanthera-Astronium-Byrsonima-Cecropia-Celtis-Moraceae-Urticaceae–Myrsine–Tapirira–Trema represented cerrado plant taxa generally adapted to dry conditions or reduced water levels (Araújo et al., 2002), with Celtis and Trema being pioneer taxa. These taxa were not very abundant in the pollen record, suggesting that they did not directly influence the coring site (Araújo et al., 2002).

In pollen surface studies, the presence of Byrsonima (<10%), Astronium, Casearia, and Ouratea, accompained by Poaceae (~20–50%), indicated open (Poaceae >50%) and woody or closed (Poaceae <20 %) cerrado physiognomies (Ledru, 2002; Jones et al.,2011). However, a decrease in lake level shifted the gallery forest closer to the coring site, which attenuated the deposition of Poaceae pollen and thus modified the signature for the expansion of open cerrado (Berrio et al., 2000; Gosling et al., 2009).

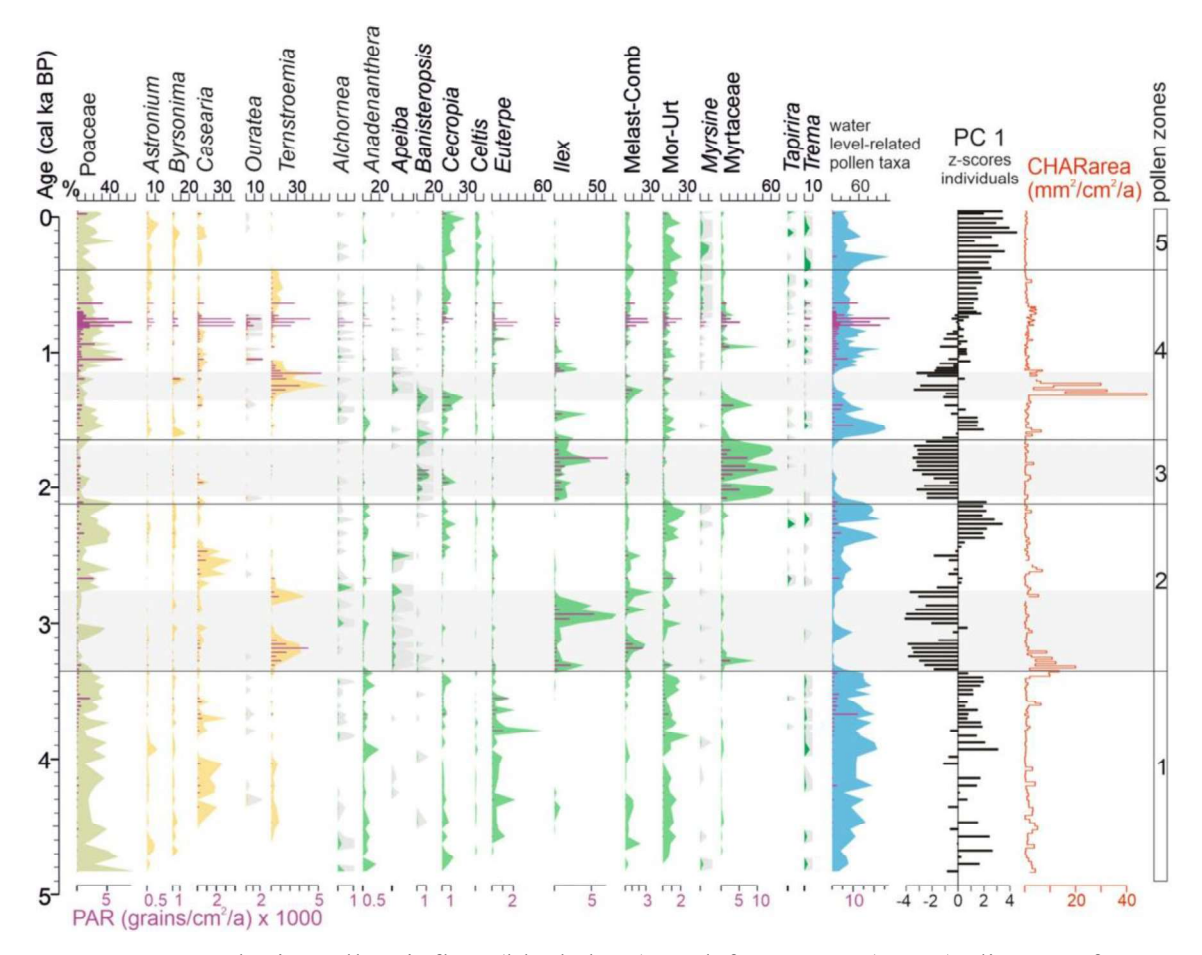


Figure 3. Synthetic pollen influx (black bars) and frequency (curve) diagram for 20 selected pollen taxa from core LFB1, represented by PC1 scores and macrocharcoal accumulation rate (mm² cm⁻² a ⁻¹), respectively, along the time scale. Woody cerrado taxa are shown in yellow, gallery forest taxa in green and water level-related taxa in blue. Gray horizontal bands indicate dry intervals. Exaggeration (×10) curves are in gray. [Color figure can be viewed at wileyonlinelibrary.com]

The assemblage Moraceae–Urticaceae, good pollen producers with an anemophilous syndrome, has been widely used as an indicator of gallery forest when its frequency is more than 40% (Gosling et al., 2005; 2009). However, in the LFB1 record, the frequency of Moraceae–Urticaceae was less than 40%, and other indicators also inferred local changes in moisture levels, such as the water level-related pollen taxa Echinodorus, Eichhornia, Eriocaulon, Myriophyllum and Nymphaea (Fig. S3). In addition, non-pollen palynomorphs, including from ferns and algae, showed similar patterns to water level-related taxa (Fig. S3). Fungi were more or less continuous but, as they were mostly coprophilous (Sordaria, Gelasinospora and Ustulina), while they were associated with continuous fire frequency and dung or organic matter decomposition,

their origins could not be defined as natural or anthropic. Finally, the presence of Sporormiella was not sufficiently frequent to suggest human activity (pastoralism) in the area (Fig. S3).

Zone 1 (309–241 cm, 4830–3370 cal a BP, 33 samples)

Zone 1 was characterized by arboreal pollen (AP) levels varying between 17 and 82%, including Moraceae–Urticaceae, Euterpe, Casearia and Cecropia. High frequencies of Poaceae (69%) were seen at the beginning of zone 1 (depth 309–301 cm; 4830–4620 cal a BP), with the presence of the tree taxa Alchornea (4-8%) and Anadenanthera (4-16%). Above 300 cm Casearia (\sim 1–35%) and Astronium (\sim 1–8%) were present. Levels of Ternstroemia ranged from 3 to 10% between 299 and 279 cm (4570–4030 cal a BP), with Cecropia (~0.5–8%), Anadenanthera (1–16%), Euterpe (~1–61%) and Moraceae– Urticaceae (~1–30%) also present. Moraceae–Urticaceae showed a decrease concomitant with an increase in Euterpe. During this interval, there was a progressive increase in pollen influx from ~46 to 6927 grains cm⁻² a ⁻¹. PC1 values ranged from ~3 to -1.1, with predominantly positive values. The presence of water level-related taxa Sagittaria and Myriophyllum ranged from 1 to 36% and 1 to 70%, respectively. The percentages increased with the appearance of Eichhornia taxa, with a greater frequency at 287 cm (4510 cal a BP). The water level-related taxa followed the same pattern as terrestrial taxa, increasing toward the end of the zone. Pollen influx ranged from 16 to 2893 grains cm⁻² a⁻¹, with a peak of 12 355 grains cm⁻² a⁻¹ at 261 cm (3670 cal a BP). Macrocharcoal was observed from the beginning of the zone and increased toward the end of the zone (values ranging from 0.6 to $9.5 \text{ mm}^2 \text{ cm}^{-2} \text{ a}^{-1}$).

Zone 2 (239–163 cm, 3340–2100 cal a BP, 36 samples)

AP dominated, with frequencies of ~35–90%, mainly of Ilex, Ternstroemia, Melatomataceae–Combretaceae, Moraceae–Urticaceae and Casearia. Levels of Poaceae (36 to ~1%) and Byrsonima (6 to 1%) decreased, while Casearia, Astronium and Ouratea increased (0 to 48%), mostly between 195 and 185 cm (2630–2470 cal a BP). Ternstroemia appeared in two phases, the first from 239 to 219 cm (~4–36%) and the second from 205 to 197 cm (~3–41%) (3340–3030 and 2800–2660 cal a BP, respectively). The percentage of gallery forest taxa ranged from ~7 to 70%, with three distinct phases observed at 239–233 cm (3340–3240 cal a BP), 217–209 cm (3000–2860

cal a BP) and 177–163 cm (2330–2100 cal a BP). The two first phases were dominated by Ilex (7–75%), Apeiba (1–5%) and Moraceae–Urticaceae (1–30%). Euterpe decreased to less than 6%, with less than 3%Myrsine, Celtis and Banisteropsis present. In the third phase, the increase in Moraceae–Urticaceae was accompanied by mixed percentages of Cecropia (~1–17%), Euterpe (1–5%), Myrsine (<2%), Trema (~1–6%) and Celtis (~1–3%), while Apeiba disappeared. The terrestrial pollen frequency ranged from ~900 to 6000 grains cm⁻² a ⁻¹. PC1 values varied from ~ 3.4 to –4.1, with predominantly negative values from a depth of 239–203 cm (3340–2760 cal a BP) and positive values from a depth of 201–163 cm (2730–2100 cal a BP). Macrocharcoal was present throughout the zone from 0.01 to 6 mm² cm⁻² a ⁻¹, with high accumulation rates (8–29 mm² cm⁻² a ⁻¹) from a depth of 239–231 cm (3330–3210 cal a BP).

Zone 3 (161–131 cm, 2070–1630 cal a BP, 16 samples)

The frequency of AP was high (65%) and included Ilex and Myrtaceae. There was less than 2% Poaceae and Byrsonima, and Casearia (10–2%), Astronium and Ouratea (less than 2%), Ternstroemia (<1%), Ilex (\sim 6–44%), Banisteropsis (1–13%), Cecropia (1–17%), Moraceae–Urticaceae and Anadenanthera (1–5%), and Alchornea, Trema, Celtis and Euterpe (<1%) were present. Moraceae–Urticaceae levels increased at the end of the zone (10%). The terrestrial pollen influx was between 314 and 17 789 grains cm⁻² a $^{-1}$. PC1 values ranged from \sim –3.4 to –0.6. Water level-related pollen almost disappeared (from 20 to >1%), with the pollen influx decreasing from 1145 to 11 grains cm⁻² a $^{-1}$. Macrocharcoal was present throughout the zone but accumulation rates were low (0.018–3 mm² cm⁻² a $^{-1}$).

Zone 4 (129–25 cm, 1600–410 cal a BP, 51 samples)

The frequency of AP ranged from 30 and 85%, including Ternstroemia, Ilex and Myrtaceae, followed by Moraceae–Urticaceae (~20%), Cecropia (~1–26%), Poaceae (5–50%) and Byrsonima (~1–19%), with the highest frequencies occurring at the beginning of the zone. Ternstroemia (1–55%) was present, with values above 8% from 111 to 87 cm (1330–1060 cal a BP) and 57 to 25 cm (800–400 cal a BP). The two phases with highest AP frequencies (>8–25%), at 89–81 cm (1080–1010 cal a BP) and 71–45 cm (920–720 cal a BP), included Casearia, Astronium and Ouratea. Moraceae–Urticaceae was present at ~20% throughout the zone. Cecropia levels (1–26%) increased gradually, while Euterpe (1–6%) and Myrsine (1–4%) increased toward the end of the zone, and

Alchornea, Anadenanthera, Apeiba, Celtis and Trema levels (~1–5%) remained low. Ilex displayed high frequencies between 121 and 119 cm (1480–1450 cal a BP) and between 95 and 89 cm (1135–1080 cal a BP). The terrestrial pollen influx ranged from 200 to 38 000 grains cm⁻² a ⁻¹. PC1 values ranged from –3.4 to 1.9, with negative values from a depth of 121–93 cm (1480–1120 cal a BP) and positive values from a depth of 91 cm (1100 cal a BP) toward the end of the zone. Levels of water level-related taxa Eichhornia and Sagittaria ranged from 2 to 20% and from 10 to 40% respectively, with a peak of Sagittaria at the beginning of the zone at 125 cm (1540 cal a BP) (~50%). Myriophyllum increased to ~8%between 73 and 61 cm (930–820 cal a BP). Nymphaeawas present at ~7% from31 cm (515 cal a BP) until the end of the zone. All the water level-related taxa decreased between 111 and 97 cm (1330–1150 cal a BP). The water level related pollen influx ranged from 100 to 24 000 grains cm⁻² a ⁻¹. Macrocharcoal was present throughout the zone from 0.1 to 6 mm² cm⁻² a ⁻¹, with high accumulation rates (15–47 mm² cm⁻² a ⁻¹) from a depth of 111–106 cm (1330–1260 cal a BP).

Zone 5 (23-0 cm, 370 cal a BP to 1990 AD, 13 samples)

AP frequencies ranged from ~40 to 78%, including Moraceae–Urticaceae, Cecropia, Astronium, Celtis and Trema. Byrsonima was present (~10%), while Poaceae was the most frequent taxon (~40–20%). Astronium and Casearia were present (~1–20%), as were Cecropia (5–30%), Moraceae/Urticaceae (5–25%), Celtis (~10%), Trema (~1–10%) and Myrsine (~1–15%). There was less than 5% Alchornea, Anadenanthera, Euterpe and Ilex. The pollen influx decreased from 900 to 200 grains cm⁻² a ⁻¹. PC1 ranged from ~4.5 to 1.2. Overall, the frequencies of water level-related taxa decreased; Eichhornia decreased from 60% at the beginning of the zone (19 cm, 295 cal a BP) to ~10%, while Nymphaea and Sagittaria increased from 1 to ~10% and Myriophyllum almost disappeared (0–3%). The pollen influx ranged from 70 to 2416 grains cm⁻² a ⁻¹, with the lowest values occurring at a depth of 13–15 cm (180–210 cal a BP). Macrocharcoal was continuously present, although this zone had the lowes accumulation rate, ranging from 0.1 to 2 mm² cm⁻² a ⁻¹.

XRF analyses

The XRF results showed contrasting responses, with four main erosive phases indicated by the normalized Ti/K ratio (Fig. 4): from 5000 to 4100, 3330 to 2900, 2100

to 1800 and 1100 to 400 cal a BP. The highest Ti/K ratio was observed 400 years ago (Fig. 4).

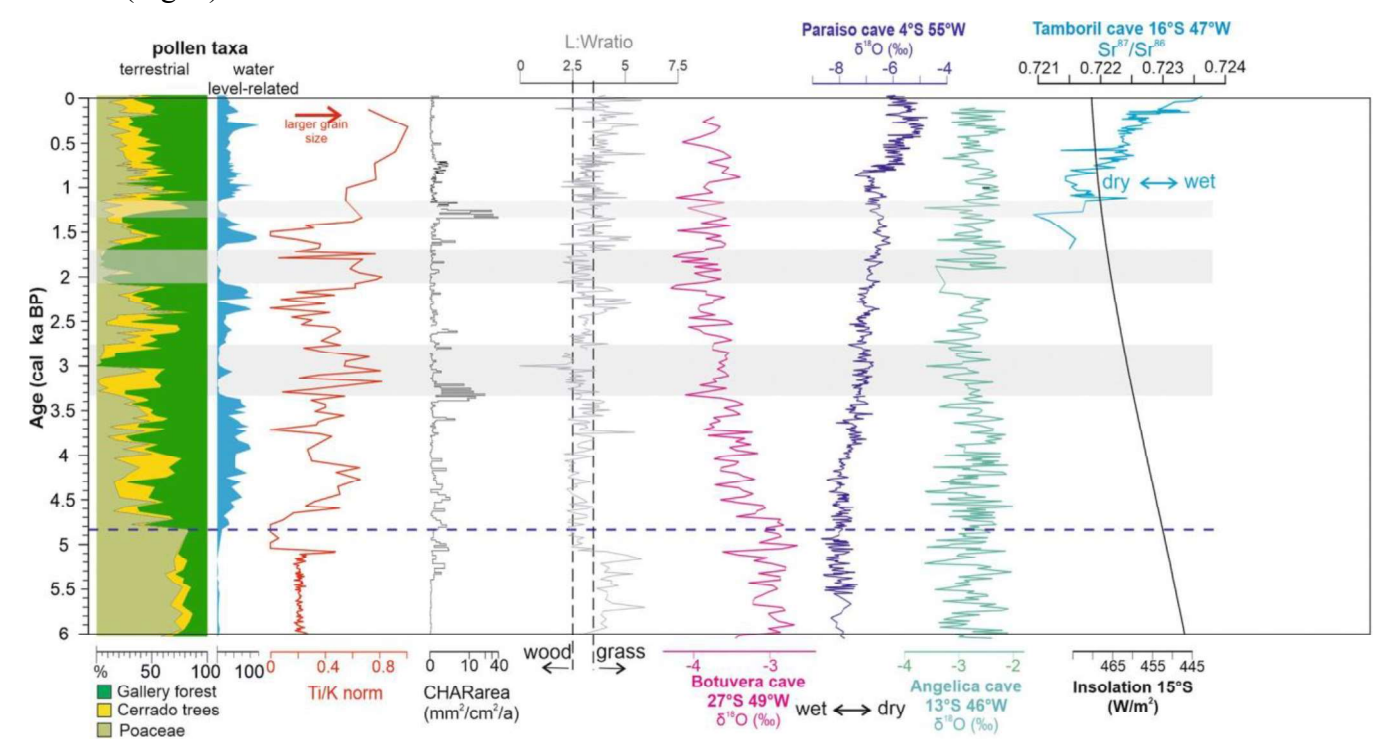


Figure 4. A representation of the last 6000 years in the central region of the Cerrado biome. A synthetic pollen, charcoal and geochemical diagram is shown for Lake Feia (cores LF-15 and LFB1) (Cassino et al., 2020; present study) along with δ18O isotopic ratios from selected speleothem records along a calibrated time scale. The percentages of terrestrial and water level-related taxa, normalized Ti/K ratios, charcoal influxes (CHARarea) and L:W ratio (Vachula et al., 2021) are indicated. The speleothem records come from southern (Botuverá cave; Bernal et al., 2016), northern (Paraiso cave; Wang et al., 2017) and central (Angelica cave; Wong et al., 2021, Wortham et al., 2017) Brazil, with an insolation curve at 15°S (Laskar et al., 2011). The blue dotted line shows the main vegetation observed in the central Cerrado; the gray bands represent dry intervals. [Color figure can be viewed at wileyonlinelibrary.com]

Charcoal analyses

Charcoal analyses showed regular and continuous biomass burning since 5100 cal a BP (Figs 4 and S4), with the charcoal influx ranging from 0 to \sim 40 mm² cm⁻² a ⁻¹, mainly below 10 mm² cm⁻² a ⁻¹ but with two intervals above 10 mm² cm⁻² a ⁻¹, from 3330 to 3210 and 1330 to 1160 cal a BP (Fig. 4). The length and width density analysis (L:W) suggested that since 6000 cal a BP the charred particles originated from grass

vegetation until 5100 cal a BP, then although arboreal particles increases in density the average L:W values remained between 2.5 and 3.5 (Fig. S4), which suggested mixed wood/grass particles until 600 cal a BP, and from grass toward the top of the record (Figs 4 and S4). The increases in wood and grass charred particles during the two episodes of high charcoal deposition and the L:W average values suggest increased intense fire activity during which both types were burned particularly the woody elements from gallery forest, which disappear after the higher fire episodes (Fig. S4).

Interpretation

Our results show that, for the last 5000 years, the landscape in the region of Lake Feia has been characterized by a cerrado with Poaceae (<40%) and the following dominant tree taxa: Astronium (1–10%), Byrsonima (1–15%), Casearia (~1–20%), Ouratea (<5%) and Ternstroemia ($\sim2-40\%$). In the gallery forest, we observed an almost continuous presence of Anadenanthera (0-15%), Euterpe (0-50%), Melastomataceae-Combretaceae (0–30%), Moraceae–Urticaceae (<30%), and the three common pioneer taxa Cecropia (0-30%), Celtis (0-10%) and Trema (0-10%). Changes from a closed to open canopy suggested some reorganization within the gallery forest, as shown by fluctuations in Myrtaceae (0-60%), Ilex (0-70%), Apeiba (0-20%), Banisteropsis (0-20%), Alchornea (0–20%), Myrsine (0–10%) and Tapirira (0–10%). These changes were related to shifts in the position of the gallery forest in the direction of the coring site, indicating a decrease in the lake water column, from 3340 to 2760, 2070 to 1690, and 1330 to 1150 cal a BP. The two first intervals suggested an invasion of the gallery forest toward the coring site, characterized by a decrease in the aquatic taxa, an abrupt increase in Ilex (a tree taxon tolerant of permanent flooding), and an increase in Myrtaceae and Melastomataceae-Combretaceae (two tree taxa associated with groundwater). At the beginning of the first interval and during the third, the reduction in gallery forest elements was accompanied by an increase in the drought-tolerant Ternstroemia, associated with a high fire signal. During the third interval, the disappearance of aquatic taxa suggested a lower lake level. Together, these three intervals suggest drier local climatic conditions. From 4830 to 3370 cal a BP a gradual expansion and stabilization of the arboreal landscape was observed in both gallery forest and woody cerrado.

After each of the dry episodes, the recovery of the arboreal landscape was characterized by an increase in lower storey pioneer tree taxa (Casearia, Cecropia and Trema), while the closure of the canopy was characterized by medium and upper storey

tree pollen taxa (Alchornea, Anadenanthera and Tapirira). During the last 400 years, stabilization of the tree cover has been simultaneous with an increase in the aquatic taxon Nymphaea, commonly found in deep water (Bernhardt and Willard, 2009). Ternstroemia disappeared, while the gallery forest taxa Cecropia, Celtis, Trema, Melastomataceae—Combretaceae and Moraceae—Urticaceae became more frequent, and woody cerrado taxa were well represented by Astronium, Byrsonima and Casearia. Fire activity was low compared with the previous interval.

The two periods of high charcoal influx (deposition) in Lake Feia, at 3350–3200 and 1330–1160 cal a BP, coincided with the observation of two dry intervals in the vegetation, from 3340 to 2760 and from 1330 to 1150 cal a BP. After each event of high fire activity, the recovery of arboreal taxa, mostly gallery forest, took about 30 years. The drier episode from 2070 to 1690 cal a BP showed continuous fire activity and a vegetation recovery of less than 30 years (Figs 4 and S4). During the more humid climatic intervals, the charcoal influx was rarely above 1 mm² cm⁻² a ⁻¹ and no change in the pollen assemblages was observed. Finally, from 813 to 700 cal a BP, the charcoal influx was continuous (~3 mm² cm⁻² a ⁻¹), and the tree taxa recovery period was about 12 years (Figs 4 and S4).

Discussion

Expansion of the arboreal cerrado in central Brazil

To place the vegetational changes within a wider context, we merged our results with those obtained from core LF15-2, dated to between 19 000 and 6000 cal a BP (Cassino et al., 2020) (Figs 4 and 5). The late Pleistocene is characterized by different assemblages, with a dominance of non-arboreal pollen (Poaceae, Asteraceae) and the presence of a Myrsine–Heve–Hedyosmum assemblage characteristic of the high-elevation grassland physiognomy of the Cerrado (Ledru et al., 2007) during the Glacial period. Our study of the last 6000 years suggests a two-step expansion of the Cerrado biome in the region of Lake Feia. First, the interval between 6000 and 5000 cal a BP was characterized by the installation of an open cerrado; second, after 5000 cal a BP, the expansion of a woody cerrado peaked, with the continuous presence of Astronium and Byrsonima, and fluctuating levels of Casearia, Ouratea and Ternstroemia. Three intervals with low water level-related taxa are attributed to drier episodes, from 3340 to 2760, 2070 to 1690, and 1330 to 1150 cal a BP, with a local expansion of the gallery forest toward

the coring site observed during the first and second dry intervals, and a contraction of the gallery forest and expansion of drought-tolerant tree taxa (Ternstroemia) coupled with high fire activity during the third interval (Figs 3 and 4).

The two-step installation of open to woody cerrado is in agreement with two other swamp pollen records, Cromínia and Águas Emendadas (with a resolution of 1000 years per sample for Cromínia and 600 years per sample for Águas Emendadas), located in the central Cerrado (Fig. 1a). The Cromínia record ends at 3500 cal a BP and the Águas Emendadas record at 940 cal a BP (Ferraz-Vicentini and Salgado-Labouriau, 1996; Barberi et al., 2000). The differences in pollen content and Poaceae frequencies (lower at LFB1) can be attributed to the different pollen deposition sites (lake versus swamp).

Two lacustrine pollen records located in the north-western Cerrado (Lake Confusão; Behling, 2002) and northern Cerrado (Lake Caço; Ledru et al., 2006) (Fig. 1a) suggest that the woody cerrado and the gallery forest were established earlier there than in central Brazil, at ~6000 and 8500 a BP, respectively. Cerrado tree taxa are mainly characterized by Byrsonima (5–10%) and Poaceae (<50%), but with differences in other pollen indicators, such as a lower frequency of Curatella (<5%) at Lake Confusão and of Mimosa (10–20%) at Lake Caço. However, the low-resolution analysis at Lake Confusão (~2000 years between samples) and at Caço (~200 years between samples), and the absence of a record after 3000 cal a BP at Caço, makes further detailed comparison impossible.

To the west, in the Amazonia–Cerrado ecotone, the Lake Saci record (Fig. 1a) initially shows a decrease (from 38 to 20%) in the woody cerrado at 7500 cal a BP, with Byrsonima (4%), Curatella (~1%), Poaceae (~18–43%) and Anadenanthera (5%), followed by expansion of the rainforest after 5000 cal a BP (69–95%) (Fontes et al., 2017). A swamp record from the eastern Amazonia–Cerrado ecotone (Carajás) shows an open cerrado, with Poaceae (85%), Byrsonima (≤2%) and Mimosa (0–10%) and the dry forest taxa Anacardiaceae (≤10%) and Bignoniaceae and Zanthoxylum (<2%) from 10 200 to 3400 cal a BP, after which they are replaced by the rainforest taxa Alchornea (30%), Celtis (15%), Melatomataceae–Combretaceae (14%), Moraceae–Urticaceae (19%) and Trema (<5%) (Hermanowski et al., 2012).

In the south-eastern Cerrado, the pollen record at Lagoa Santa (Parizzi et al., 1998) (Fig. 1a) covers the last 5300 cal a BP and shows the presence of the cerrado pollen taxa Poaceae (50%) and Styphnodendron (2–4%). Small changes in humidity have occurred during the last 3000 years, and in the Cerrado–Atlantic Forest ecotone (Horák-Terra et

al., 2020) a record from Pinheiro mire (located at 1240 m asl and spanning the last 6000 years) indicates an open cerrado, with Amaranthus and Borreria (5–10%) present until 3100 cal a BP. The frequency of cerrado tree pollen then increased between 3100 and 740 cal a BP, with Byrsonima, Tabebuia and Smilax (<2%), and grassland has become dominant in the last 740 years (Horák-Terra et al., 2020) at this elevation of the Espinhaço mountain range.

In the north-east, in the Cerrado–Caatinga ecotone, the São José swamp record (at 680 m asl) (Cassino et al., 2018) shows wetter climatic conditions and the expansion of palm swamp until 4400 cal a BP, with Mauritia flexuosa (40%), Poaceae (24–60%), and Ericaceae, Plenkia and Roupala (<3%) present, and an increase in the gallery forest tree taxa Cecropia and Hedyosmum (>20%). After 3500 cal a BP, the expansion of a drier open cerrado is characterized by a regression of the tree pollen taxa and the palm swamp Mauritia flexuosa (<7%), and the expansion of grassland pollen (Poaceae 20%) (Cassino et al., 2018). The Pandeiros wetland record (at 460 m asl) (Sabino et al., 2021) shows the presence of a woody cerrado [mainly Astronium (~5%)] until 2890 cal a BP, when it was replaced by a more open cerrado landscape (Poaceae 18%), with the presence of Asteraceae (5–35%), Euphorbia (5–40%) and Gomphrena (2–25%), during the last part of the Holocene (Sabino et al., 2021).

Notwithstanding the differences in resolution and chronological controls, our review of published Cerrado pollen records reveals a general trend characterized by the expansion of open cerrado until ~5000 a BP and woody cerrado after 5000 a BP, interrupted by a drier episode at ~3500 cal a BP in both central and north-eastern regions. An inverse pattern is seen in the south-eastern and southern regions, with more humid forest being replaced by a drier and more open cerrado physiognomy between 4000 and 3000 cal a BP and a woody cerrado between ~3100 and ~800 cal a BP.

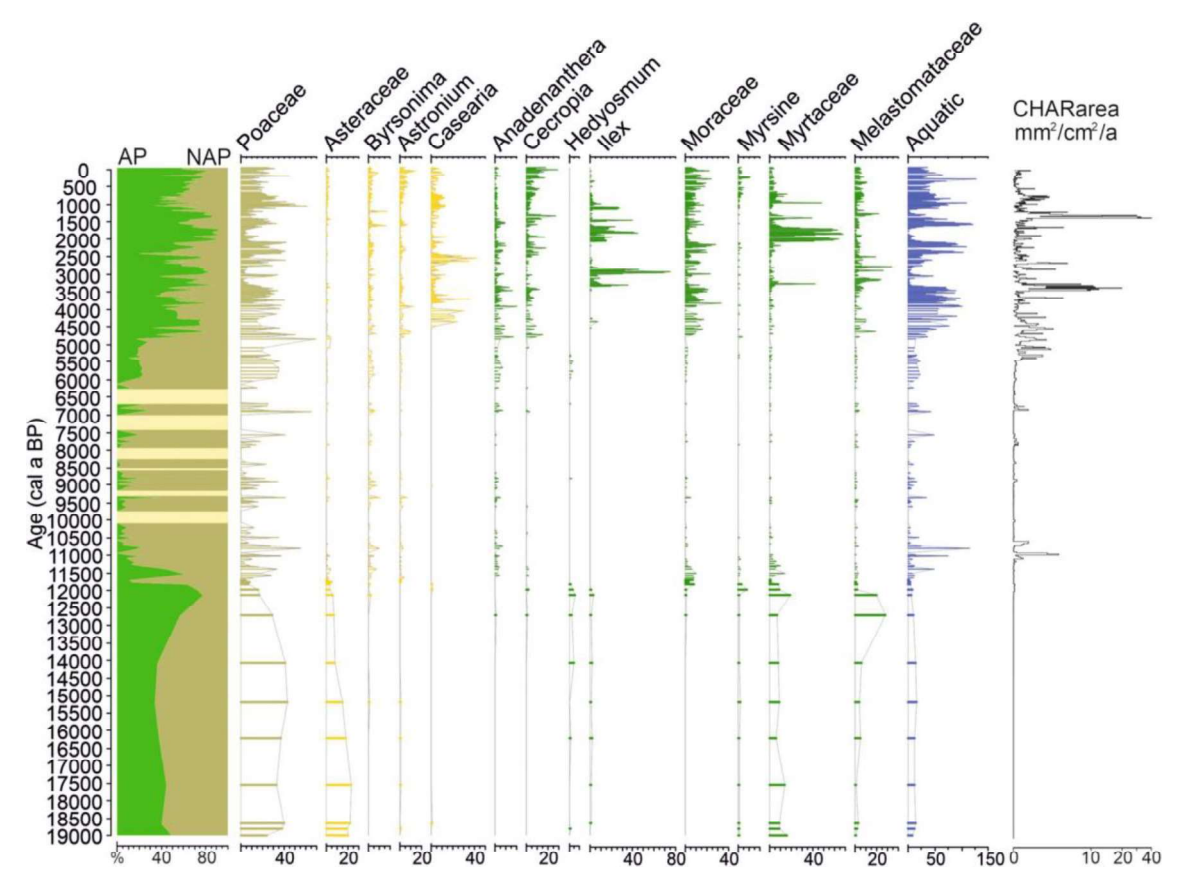


Figure 5. The last 19 000 years in the central Cerrado, as represented by the Lake Feia sediment cores (Cassino et al., 2020; present study). From left to right, a synthetic pollen diagram showing arboreal pollen/non-arboreal pollen frequencies (AP and NAP, respectively), 13 selected pollen taxa, with AP cerrado taxa shown in yellow and gallery forest taxa in green, and water level-related (aquatics) taxa in blue, plus the charcoal influx (CHARarea; mm2 cm-2 a-1). The yellow horizontal bands show the disappearance of Lake Feia during dry episodes (from Cassino et al., 2020). [Color figure can be viewed at wileyonlinelibrary.com]

Climatic drivers of vegetation changes in central Brazil

The Lake Feia pollen record suggests continuous wet conditions, interrupted by three drier intervals, from 3340 to 2760, 2070 to 1690, and 1330 to 1150 cal a BP (Fig. 4). Speleothem records in central Brazil (Fig. 4) show apparently stable climatic conditions during the last 6000 years (Deininger et al., 2019; Wong et al., 2021), compared with southern and northern regions of Brazil at the margins of the monsoon domain, where the establishment of a SW–NE dipole (Novello et al., 2012 and 2019; Deininger et al., 2019) led to abrupt changes in the extent of the monsoon and consequently in seasonality and precipitation (Campos et al., 2019). At Lake Feia, regular

sedimentation and the establishment of the Cerrado started around 6000 cal a BP, suggesting regular regional precipitation. Rainfall stability has also been reported at 7000 a BP in south-eastern Brazil (27°S, 49°W) (Bernal et al., 2016), at 6800 a BP in central Brazil (13°S, 46°W) (Wong et al., 2021) and since the mid-Holocene in northern Brazil (4°S, 55°W) (Wang et al., 2017), as a response to the increase in insolation (Deininger et al., 2019). However, regional differences in the expression of drivers have also been observed, such as the strengthening of the SASM system in the south, which increased rainfall, while in the north the increased rainfall was not directly linked to the SASM but driven by humid convection from the eastern Amazonia (Wong et al., 2021). In central Brazil, both speleothem and pollen records suggest that the SACZ has remained stable, thus allowing a regular SASM trajectory between central and eastern Brazil (Figs. 6 and 7). However, pollen records indicating to a more open landscape between 6000 and 4800 cal a BP suggest lower precipitation levels and a weaker SASM than today, decoupled from the SASM core, while stronger rainfall has prevailed at the northernmost boundary of the SASM zone of influence (Figs. 6 and 7). The location of Lake Feia (15°S, 47°W) was probably too far from the wetter north - east area to be influenced during this period (Fig. 6a). Conditions changed after 4800 cal a BP, with the installation of a dipole between southern and northern Brazil, and the south became wetter and the northeast drier (Bernal et al., 2016; Wang et al., 2017) (Figs 4 and 6b). At Lake Feia the full expansion of the woody cerrado, the abrupt increase in water level - related pollen taxa and the coarse sediment deposition (Ti/K) suggest that the regional wet levels were related to a strengthening and expansion of the SASM boundary at 15°S, and an increase in summer insolation in the southern tropics (Fig. 6b) (Cruz et al., 2009; Deininger et al., 2019). However, despite the trend toward a more stable precipitation regime created by an increase in insolation and the establishment of the modern monsoon regime in the central Cerrado, three drier episodes are indicated by the Lake Feia pollen record: from 3340 to 2760, 2070 to 1690, and 1330 to 1150 cal a BP. We infer that changes in the hydrological system of Preto River, also characterized by an increase in deposition of coarser sediment, are probably related to a reduction of water input into the lake, and consequently in the amount of precipitation at a centennial scale (Figs. 4, 6, and 7). A southward shift of the ITCZ and SASM boundary has been observed between 3700-3400 and ~2700 a BP (Bernal et al., 2016; Cruz et al., 2009; Cassino et al., 2018) (Fig. 6c). The return to wetter conditions at Lake Feia between 2730 and 2100 cal a BP (Fig. 6d) corresponds to several wet events visible in the speleothem records at Diva cave (Novello et al., 2012) and Lapa Grande cave (Strikis et al. 2011). During this interval, the central Cerrado region was wetter because of the expansion of the SASM system (Fig. 6d). Further north, at 5°S, the higher moisture rates observed between 2450 and 1530 cal a BP (Boqueirão lake; Utida et al., 2019) have been related to the northward migration of the ITCZ, which increased the tropical South Atlantic winds into the continent, along with more moisture (Utida et al., 2019). At the equator (Paraiso cave; Wang et al., 2017), convective activity was high and the resulting wet wind flow was driven from eastern Amazonia to the central Cerrado region (Figs 6 and 7).

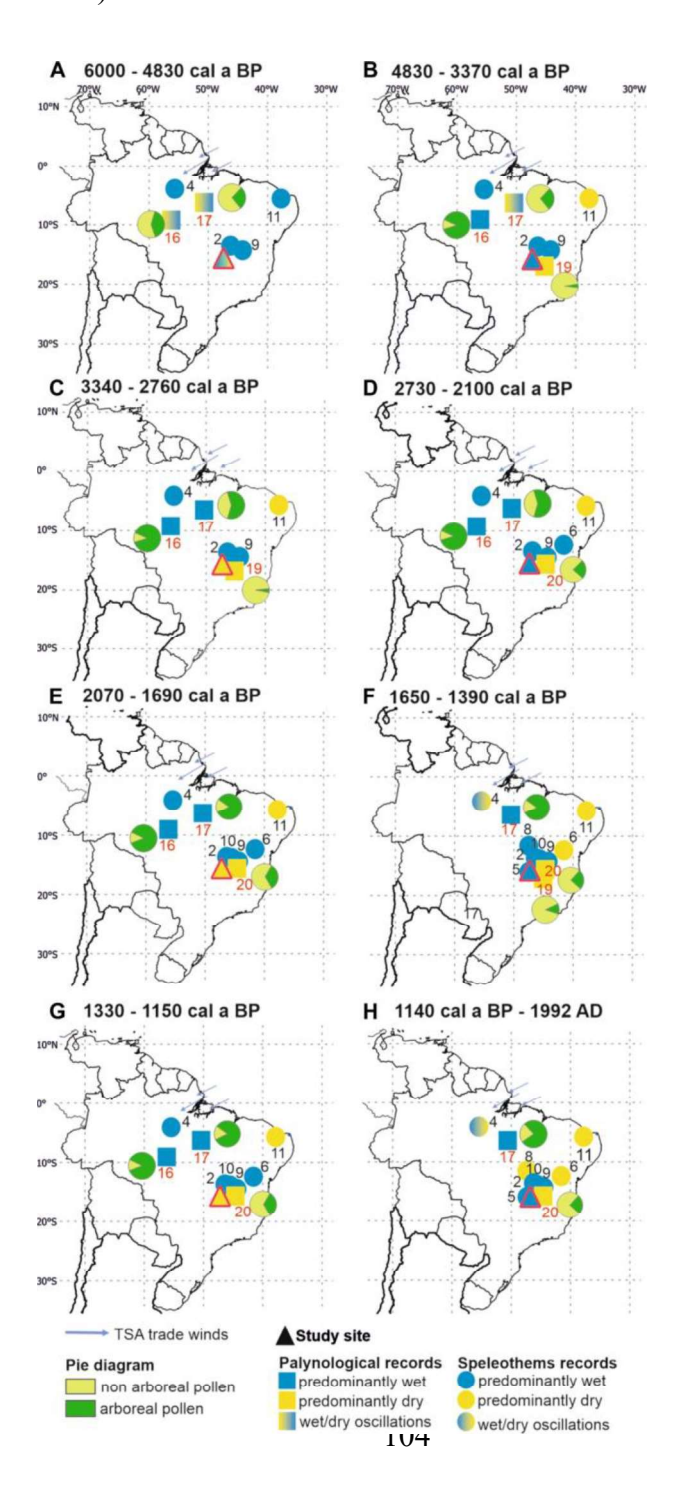


Figure 6. Schematic representation of the eight climate episodes observed during the last 6000 years in the Cerrado biome, with their corresponding latitudinal boundaries. Site numbers are as in Fig. 1. Arboreal pollen/non-arboreal pollen frequencies available from palynological sites are represented as pie diagrams. [Color figure can be viewed at wileyonlinelibrary.com]

During the second and third drier intervals, at 2070–1690 and 1330–1150 cal a BP, a gradual weakening of the SASM system occurred at Lake Feia, when the ITCZ shifted to a more northerly position (Fig. 6e and 6G). The wetter intervals, between 1650 and 1390 cal a BP, and from 1140 cal a BP onwards (Fig. 6f and 6H), was probably the result of instability in the ITCZ core area, which expanded and retracted along its northern edge (Utida et al., 2019). At Lake Feia, this was characterized by an abrupt change in erosion (Ti/K norm) at 1100 cal a BP, when conditions were mostly linked to humid wind flow from eastern Amazonia (Fig. 6f).

Between 1020 and 600 a BP, during the medieval climate anomaly, the ITCZ remained in its northernmost position (Deininger et al., 2019). The northern edge of the SASM core region remained dry (Novello et al., 2012; Utida et al., 2019), while the southern edge received less precipitation as a result of a weaker SAMS trajectory toward the Atlantic Ocean (Bernal et al., 2016; Deininger et al., 2019) (Fig. 7). In the central region, the rainfall regime remained stable after 1140 cal a BP (as indicated at Tamboril cave at 16°S and 47°W; Wortham et al., 2017; Wong et al., 2021) (Fig. 4 and 7), suggesting that the rainfall reduction at the northern and southern boundaries of the SASM did not affect the core monsoon region (Fig. 6h) (Campos et al., 2019). Thus, we infer that, at Lake Feia, a gradual increase in rainfall was mostly linked to its closer position to the core SASM region, with moisture fluxes from eastern Amazonia (Fig. 6h) (Azevedo et al., 2019). In addition, no change in the rainfall regime has been observed at Lake Feia during the last 400 years (corresponding to the Little Ice Age), which is in agreement with a southern shift of the ITCZ, which did not impact the central region (Deininger et al., 2019) but enhanced SASM activity on the southern edge of the SASM zone of influence, and led to drier conditions in the northern region as a result of the establishment of the SW–NE dipole (Novello et al., 2012; Azevedo et al., 2019).

Overall, the Lake Feia pollen record shows that, during the last 6000 years, the floristic composition of the Cerrado has been highly sensitive to small changes in precipitation and seasonality, which has not been observed in neighboring speleothem

records (Figs 6 and S5). The increase in wet climatic conditions was the result of a reduced dry season, as clearly indicated in southern and central Brazil (Azevedo et al., 2019).

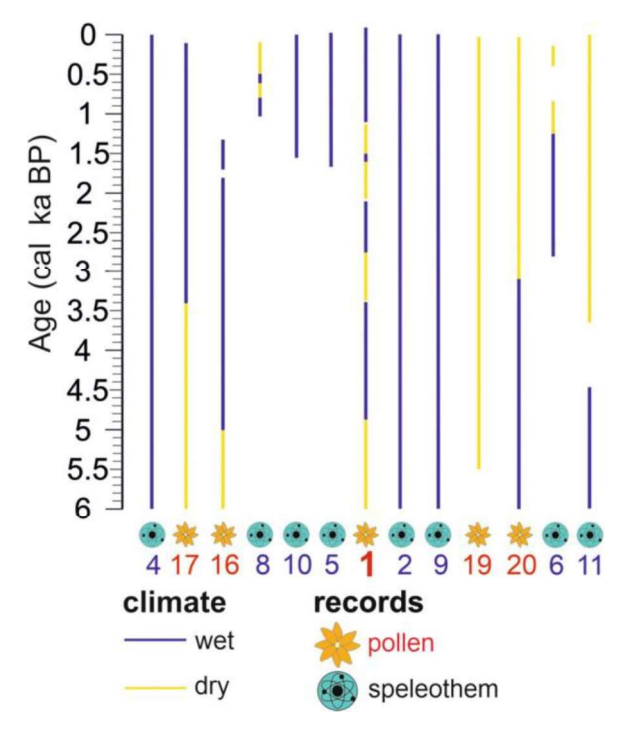


Figure 7. Summary of the main climate changes (wet/dry events) observed in the last 6000 years between the paleo-records shown in Fig. 6, organized according to their latitude and longitude. From left to right: the age scale (cal ka BP), paleo-records from north to south, and finally a summary of the SASM intensity at 15°S, at lake Feia. The blue lines represent wet climate and the yellow lines represent dry climate. The number below each record indicates the name of the record shown in Fig. 1 (pollen records in red and speleothem records in blue). [Color figure can be viewed at wileyonlinelibrary.com]

Fire events in central Brazil

Three main phases of fire activity have been detected at Lake Feia during the last 19 000 years (Fig. 4). The late Pleistocene was characterized by no fire activity, the first biomass burning being observed during the glacial-interglacial transition from ~11 000 to 10 500 cal a BP. Between 10 500 and 5100 cal a BP, the low charcoal influx, and the predominance of burned grass particles usually transported over long distances, suggests a weak, remote and irregular fire activity or surface fire that may leave less charcoal in the sediment (Cassino et al., 2020; Leys et al., 2017). From 5100 cal a BP onward, a higher charcoal influx and continuous fire activity was observed, with two peaks at ~3330

and ~1330 cal a BP (Figs 4, 5, and S4). The increase in charred woody particles (L:W ratio density <2.5) (Fig. S4) is in agreement with the dominance of woody cerrado pollen taxa, which started around 4830 cal a BP (Fig. 5).

The Cerrado is a fire - prone ecosystem where, under natural conditions, fire occurrence varies from 3 to 5–6 years (Pereira Júnior et al., 2014; Schmidt et al., 2017). However, limiting factors for fire occurrence are fuel availability and flammability, and heat (Glasspool et al., 2015). Thus, when a cerrado physiognomy becomes more arboreous, the probability of fire episodes decreases because of a reduction in grass biomass, which is more flammable compared to woody plants (Mistry, 1998; Pereira Júnior et al., 2014). Consequently, fire is more common in an open cerrado physiognomy, where it favors grass species germination (Oliveira et al., 2021; Fidelis and Zirondi, 2021). At Lake Feia, before 5000 cal a BP, the drier climatic conditions and probably the lower temperatures (indicated by the presence of the mountain taxon Hedyosmum) do not appear to have facilitated biomass burning. Experimental studies have shown a positive correlation between charcoal particles and temperature (Leys et al., 2017), suggesting that a reduction in temperature reduces fire activity.

After 5000 cal a BP, an increase in fire events was favored by both an increase in summer insolation and an increase in the length of the wet season (Figs 4 and 5). Natural fires in the modern Cerrado are frequent during the wet season or in the transition between seasons, promoted by lightning, with shortlived fires usually extinguished by subsequent rain, burning small areas and with little effect on vegetation (Ramos - Neto and Pivello, 2000). Two short episodes of intense fire activity (CHARarea 10–40 mm² cm⁻² a⁻¹) (Figs 4 and 5), from 3330 to 3210 cal a BP and 1330 to 1160 cal a BP, were recorded. Three scenarios are proposed to explain the increased charcoal influx during these time periods: (i) a response to drier climatic conditions and lower lake levels, (ii) the presence of fire closer to the study site and (iii) human activity. Regarding the first scenario, the two fire events were reported during the first and third dry intervals, characterized by changes in tree taxa and lower lake levels. A drier climate could favor an expansion of grassland and consequently biomass burning. However, during these two intervals the L:W ratio suggests mixed grass and wood charred particles, probably in response to surface fire where in a grassland and forest mosaic both type of physiognomies are affected. Moreover, if a dry climate could promote an intense fire event, the same pattern should be observed in the second dry interval, from 2070 to 1690 cal a BP. The second interval

in fact shows lower levels of charred particles and fewer changes in assemblages of gallery forest and woody cerrado taxa, with a recovery time of less than 30 years. Consequently, we suggest that drier climatic conditions cannot explain the abrupt increase in fire activity.

For the second scenario, the L:W ratio density suggests that a strong biomass burning reflects a widely burned area, with the fire occurring near the coring site, where tree elements are particularly affected although grasses were also burned, increasing their signal during these two fire episodes. An increase in pollen influx is usually associated with an increase in fire intensity and a shorter distance from its source (Tinner et al., 2006; Duffin et al., 2008). Experimental analysis of charcoal particles has shown that the charcoal area increases with local fire (Leys et al., 2015, 2017), especially when charred wood particles are more abundant (Vachula and Rehn, 2023). From 810 to 730 cal a BP, a mid - magnitude fire event (CHARarea <4 mm² cm⁻² a ⁻¹) with gradual increase in charred grass particles (Figs 4 and S4) was observed after a short dry episode, and did not prevent the expansion of woody cerrado and gallery forest taxa, with a recovery of about 12 years. Thus, for this shorter drier interval, a more regional fire signal that did not impact the local vegetation cover is inferred. The first and second scenarios could represent peaks in biomass burning reflecting climatic and local fire effects. Finally, regarding the third scenario, human activity cannot be discounted as a cause of localized fire, probably on the lake margin, during drought episodes. In the tropical lowlands, the level of human occupation was low until 5000 a BP (Riris and Arroyo - Kalin, 2019), when the climate was unstable and water resources were rare (Cassino et al., 2020). Well - dated archeological studies are missing in the region of Lake Feia, despite its wealth of rock paintings and carvings, which are probably related to year - round abundant freshwater resources. To the west of Lake Feia, and at the same latitude, in the Tocantins-Araguaia river system, an increase in the human population was observed after 4600 cal a BP, as a result of the expansion of the Itaparica civilization (Moreno de Sousa, 2016). During the first and third drier intervals, the higher biomass burning was not concurrent with a gallery forest expansion toward the coring site. Moreover, there was an increase in the tree taxon Ternstroemia related to drier environments. After the high fire events, the recovery time for the expansion of gallery forest toward the coring site was more than 30 years. Considering that forest is less likely to burn, and that gallery forest

usually grows over moist and/or waterlogged soils, the presence of human activity on the lake margin cannot be discounted.

Finally, during the last 4800 years, the three intervals characterized by a decrease in water level - related taxa, at 3400–2700, 2100–1700 and 1350–1200 cal a BP, were associated with multi - centennial drought episodes. During these three drought events, the two higher fire activity events, at 3330–3210 and 1330–1160 cal a BP, which were not associated with an expansion of the gallery forest toward the coring site, suggest both climatic and anthropogenic influences on vegetation cover and fire activity. No fire was observed during the second dry episode at 2070–1690 cal a BP, thus rejecting human influence during this short dry interval, and low fire activity with no evidence of drought suggests remote biomass burning of the Cerrado from 810 to 730 cal a BP.

Conclusions

Our results show that, since the late Pleistocene, the central Cerrado region has been sensitive to local hydrology and changes in regional climate, driven by latitudinal boundaries of the monsoon convection, with changes in the boundaries toward the northern, north-eastern and south-eastern Cerrado at a millennial scale. The long-term expansion of woody cerrado in central Brazil was precluded by the southward shift of the ITCZ, forced by insolation that strengthened the monsoon system and included eastern Amazonia in its zone of influence. Consequently, the development of the cerrado vegetation started 6000 years ago in central Brazil, with the formation of a bimodal climate and an increase in summer insolation. Expansion of the central Cerrado was a two-step process, starting with the establishment of an open cerrado until 4800 cal a BP, which was then replaced by a woody cerrado, perhaps driven by changes in the length of the dry season.

Superimposed on this global trend, multi - centennial shortterm wet/dry episodes are reflected in changes in lake level, floristic composition of the gallery forest and biomass burning. These episodes could be related to small - scale enhancement or weakening of the SACZ, linked to changes in the southernmost and northernmost positions of the ITCZ and consequently driving changes in the SASM zone of influence at the latitude of Lake Feia.

Two fire events, at 3330–3210 and 1330–1160 cal a BP, occurred during drier climatic intervals and could be related to anthropogenic activity near the lake. The full vegetation /recovery period after these events was more than 30 years.

Acknowledgements

This work is part of the 'Cerrados & Fogos' program at IRD. Financial support was provided by IRD, FAPDF (0193.001374/2016), ISEM, DEGEO - UFOP and IG - UnB. K.E.T. benefited from a PhD position funded by the IRD ARTS program and the French Embassy in Bolivia. R.F.C. benefited from a South - North IRD grant during her stay at ISEM. This work has also benefited from an 'Investissement d'Avenir' grant managed by the Agence Nationale de la Recherche (CEBA, ref. ANR - 10 - LABX - 25 - 01). Radiocarbon dating was performed at LMC14 [LSCE (CNRS - CEA - UVSQ) - IRD - IRSN - MC] with IRD financial support. We thank Ludivine Eloy and Michel Brossard for fruitful discussions.

Conflict of interest

The authors have no conflicts of interest to declare.

Author contributions

K.E.T.: conceptualization; formal analysis; investigation; visualization; writing, original draft. M. - P.L.: conceptualization; investigation; funding acquisition; writing, review and editing. R.C.: investigation; writing, review and editing. P.B.: formal analysis; investigation; writing, review and editing. E.Y.: investigation; writing, review and editing.

Data availability statement

Datasets will be available in the open-access database Neotoma after publication.

Supporting information

Additional supporting information can be found in the online version of this article.

Supporting information

Abbreviations. AP, arboreal pollen; ITCZ, inter - topical convergence zone; SASM, South American summer monsoon; NEB, north - eastern Brazil; SEB, central and south - eastern Brazil; AMS, accelerator mass spectrometry; PCA, principal components analysis.

References

- Araujo, A.G.M., Neves, W.A., Piló, L.B. & Atui, J.P.V. (2005) Holocene dryness and human occupation in Brazil during the "Archaic Gap". Quaternary Research, 64, 298–307.
- Araujo, G.M., Barbosa, A.A.A., Arantes, A.A. & Amaral, A.F. (2002) Floristic composition of palm swamp communities near Uberlândia, Minas Gerais, Brazil. Revista Brasil. Bot. 25(4), 475–493.
- Azevedo, V., Strikis, N.M., Novello, V.F., Roland, C.L., Cruz, F.W., Santos, R.V. et al. (2021) Paleovegetation seesaw in Brazil since the Late Pleistocene: A multiproxy study of two biomes. Earth and Planetary Science Letters, 563, 116880.
- Azevedo, V., Stríkis, N.M., Santos, R.A., de Souza, J.G., Ampuero, A., Cruz, F.W. et al. (2019) Medieval climate variability in the Eastern Amazon-Cerrado regions and its archeological implications. Scientific Reports, 9, 20306.
- Barberi, M., Salgado-Labouriau, M.L. & Suguio, K. (2000) Paleovegetation and paleoclimate of "Vereda de Águas Emendadas", central Brazil. Journal of South American Earth Sciences, 13, 241–254.
- Barbosa, J.B., Afonso, M.C. & Rubin, J.C. (2020) Estudio micromofologico en ditios alfareros Uru de la cuenca del rio Araguaia, Gioiás, Brasil. Boletin de Arqueología PUCP, 28, 31–52.
- Becker, R.A., Chambers, J.M. & Wilks, A.R. (1988) The New S Language. Wadsworth & Brooks/Cole.
- Behling, H. (2002) Late Quaternary vegetation and climate dynamics in southeastern Amazonia inferred from Lagoa da Confusão in Tocantins State northern Brazil. Amazoniana, 17, 27–39.

- Bennett, K.D. (1996) Determination of the number of zones in a biostratigraphical sequence. New Phytologist, 132, 155–170.
- Bernal, J.P., Cruz, F.W., Stríkis, N.M., Wang, X., Deininger, M., Catunda, M.C.A. et al. (2016) High-resolution Holocene South American monsoon history recorded by a speleothem from Botuverá Cave, Brazil. Earth and Planetary Science Letters, 450, 186–196.
- Bernhardt, C.E. & Willard, D.A. (2009) Response of the Everglades ridge and slough landscape to climate variability and 20th-century water management. Ecological Applications, 19(7), 1723–1738.
- Berrio, J.C., Hooghiemstra, H., Behling, H. & Van der Borg, K. (2000) Late Holocene history of savanna gallery forest from Carimagua area, Colombia. Review of Palaeobotany and Palynology, 111, 295–308. Available at: https://doi.org/10.1016/S0034-6667(00)00030-0
- Blaauw, M. & Christen, J.A. (2011) Flexible paleoclimate age-depth models using an autoregressive gamma process. Bayesian Analysis, 6, 457–474. Available at: https://doi.org/10.1214/11-BA618
- Bueno, M.L., Dexter, K.G., Pennington, R.T., Pontara, V., Neves, D.M., Ratter, J.A. et al. (2018) The environmental triangle of the Cerrado Domain: Ecological factors driving shifts in tree species composition between forests and savannas. Journal of Ecology, 106, 2109–2120.
- Bush, M.B. & Weng, C. (2007) Introducing a new (freeware) tool for palynology. Journal of Biogeography, 34, 377–380.
- Campos, J.L.P.S., Cruz, F.W., Ambrizzi, T., Deininger, M., Vuille, M., Novello, V.F. et al. (2019) Coherent South American Monsoon Variability During the Last Millennium Revealed Through High-Resolution Proxy Records. Geophysical Research Letters, 46, 8261–8270.
- Cassino, R. & Meyer, K.E. (2011) Morfologia de grãos de pólen e esporos de níveis holocênicos de uma vereda do Chapadão dos Gerais (Buritizeiro, Minas Gerais), Brasil. Gaea Journal of Geoscience, 7, 41–70.

- Cassino, R.F., Ledru, M.-P., Santos, R.A. & Favier, C. (2020) Vegetation and fire variability in the central Cerrados (Brazil) during the Pleistocene-Holocene transition was influenced by oscillations in the SASM boundary belt. Quaternary Science Reviews, 232, 106209.
- Cassino, R.F., Martinho, C.T. & da Silva Caminha, S.A.F. (2018) A Late Quaternary palynological record of a palm swamp in the Cerrado of central Brazil interpreted using modern analog data. Palaeogeography, Palaeoclimatology, Palaeoecology, 490, 1–16.
- Colli, G.R., Vieira, C.R. & Dianese, J.C. (2020) Biodiversity and conservation of the Cerrado: recent advances and old challenges Biodiversity and Conservation, 29, 1465–1475.
- Cruz, F.W., Vuille, M., Burns, S.J., Wang, X., Cheng, H., Werner, M. et al. (2009) Orbitally driven east—west antiphasing of South American precipitation. Nature Geoscience, 2, 210–214. Available at: https://doi.org/10.1038/ngeo444
- Davies, S.J., Lamb, H.F. & Roberts, S.J. (2015) Micro-XRF core scaning in Palaeolimnology: recent developments. In: Croudace, I.W. & Rothwell, R.G. (Eds.) MICRO6XRF studies of sediment cores, developments in Paleoenvironmental research. Cambridge, UK. pp. 189–225.
- Deininger, M., Ward, B.M., Novello, V.F. & Cruz, F.W. (2019) Late Quaternary Variations in the South American Monsoon System as Inferred by Speleothems—New Perspectives Using the SISAL Database. Quaternary, 2, 6. Available at: https://doi.org/10.3390/quat2010006
- Duffin, K.I., Gillson, L. & Willis, K.J. (2008) Testing the sensitivity of charcoal as an indicator of fire events in savanna environments: quantitative predictions of fire proximity, area and intensity. The Holocene, 18, 279–291.
- Durigan, G., Munhoz, C.B., Zakia, M.J.B., Oliveira, R.S., Pilon, N.A.L., Valle, R.S.T. et al. (2022) Cerrado wetlands: multiple ecosystems deserving legal protection as a unique and irreplaceable treasure. Perspectives in ecology and conservation, 20(3), 185–196.

- Faegri, K. & Iversen, J. (1989) Textbook of Pollen Analysis. New York: Hafner. Felfili, J.M. (1995) Diversity, structure and dynamics of a gallery forest in central Brazil. Vegetatio, 117, 1–15.
- Ferraz-Vicentini, K.R. 1999. História do fogo no Cerrado: uma análise palinologicá. Universidade de Brasilia, doctoral thesis, 208.
- Ferraz-Vicentini, K.R. & Salgado-Labouriau, M.L. (1996) Palynological analysis of a palm swamp in Central Brazil. Journal of South American Earth Sciences, 9, 207–219.
- Fidelis, A. & Zirondi, H.L. (2021) And after fire, the Cerrado flowers: A review of post-fire flowering in a tropical savanna. Flora, 280, 151849.
- Fontes, D., Cordeiro, R.C., Martins, G.S., Behling, H., Turcq, B., Sifeddine, A. et al. (2017) Paleoenvironmental dynamics in South Amazonia, Brazil, during the last 35,000 years inferred from pollen and geochemical records of Lago do Saci. Quaternary Science Reviews, 173, 161–180.
- Garreaud, R.D., Vuille, M., Compagnucci, R. & Marengo, J. (2009) Preset-day South American climate. Palaeogeography, Palaeoclimatology, Palaeoecology, 281, 180–195. Available at: https://doi.org/10.1016/j.palaeo.2007.10.032
- Glasspool, I.J., Scott, A.C., Waltham, D., Pronina, N. & Shao, L. (2015) The impact of fire on the Late Paleozoic Earth system. Frontiers in Plant Science, 6, 756.
- Gosling, W.D., Mayle, F.E., Tate, N.J. & Killeen, T.J. (2005) Modern pollen-rain characteristics of tall terra firme moist evergreen forest, southern Amazonia. Quaternary Research, 64, 284–297.
- Gosling, W.D., Mayle, F.E., Tate, N.J. & Killeen, T.J. (2009) Differentiation between Neotropical rainforest, dry forest, and savannah ecosystems by their modern pollen spectra and implications for the fossil pollen record. Review of Palaeobotany and Palynology, 153, 70–85.
- Henriques, R.P.B. (2005) Influência da história, solo e fogo na distribuição e dinámica das fitofisionomias no bioma Cerrado. In: Scariot, A. et al. Cerrado: ecologia, biodiversidade e conservação. Brasília: Ministério do Meio Ambiente. pp. 73–92.

- Hermanowski, B., da Costa, M.L. & Behling, H. (2012) Environmental changes in southeastern Amazonia during the last 25,000 yr revealed from a paleoecological record. Quaternary Research, 77, 138–148.
- Hofmann, G.S., Cardoso, M.F., Alves, R.J.V., Weber, E.J., Barbosa, A.A., Toledo, P.M. et al. (2021) The Brazilian Cerrado is becoming hotter and drier. Global Change Biology, 27, 4060–4073. Available at: https://doi.org/10.1111/gcb.15712
- Hogg, A.G., Heaton, T.J., Hua, Q., Palmer, J.G., Turney, C.S., Southon, J. et al. (2020) SHCal20 Southern Hemisphere Calibration, 0–55,000 Years cal BP. Radiocarbon, 62, 759–778.
- Horák-Terra, I., Cortizas, A.M., da Luz, C.F.P., Silva, A.C., Mighall, T.,
- De Camargo, P.B. et al. (2020) Late Quaternary vegetation and climate dynamics in central-eastern Brazil: insights from a ~35k cal a bp peat record in the Cerrado biome. Journal of Quaternary Science, 35, 664–676. Available at: https://doi.org/10.1002/jqs.3209 INMET. (2022, march 15). Dados Meteorologicos. https://portal.inmet.gov.br/
- Insel, N., Poulsen, C.J. & Ehlers, T.A. (2010) Influence of the Andes Mountains on South American moisture transport, convection, and precipitation. Climate Dynamics, 35, 1477–1492. Available at: https://doi.org/10.1007/s00382-009-0637-1
- Jones, H.T., Mayle, F.E., Pennington, R.T. & Killeen, T.J. (2011) Characterisation of Bolivian savanna ecosystems by their modern pollen rain and implications for fossil pollen records. Review of Palaeobotany and Palynology, 164, 223–237.
- Kummel, B., & Raup D. (1965) Handbook of Paleontological Techniques. San Francisco,
 CA: W. H. Freeman. Laskar, J., Fienga, A., Gastineau, M. & Manche, H. (2011)
 La2010: A new orbital solution for the long-term motion of the Earth.
 ASTRONOMY & ASTROPHYSICS, 532, A89.
- Ledru, M.-P., Ceccantini, G., Gouveia, S.E.M., López-Sáez, J.A., Pessenda, L.C.R. & Ribeiro, A.S. (2006) Millenial-scale climatic and vegetation changes in a northern Cerrado (Northeast, Brazil) since the Last Glacial Maximum. Quaternary Science Reviews, 25, 1110–1126.

- Ledru, M.-P. (2002) Late Quaternary History and Evolution of the Cerrados as revealed by Palynological Recods. In: Marquis, R.J. Oliveira (Ed.) The cerrados of Brazil: ecology and natural history of neotropical savanna. New York: Columbia University Press. pp. 33–50.
- Ledru, M.-P., Salatino, M.L.F., Ceccantini, G., Salatino, A., Pinheiro, F. & Pintaud, J.-C. (2007) Regional assessment of the impact of climatic change on the distribution of a tropical conifer in the lowlands of South America: Tropical conifer and climatic change. Diversity and Distributions, 13, 761–771.
- Leys, B., Brewer, S.C., McConaghy, S., Mueller, J. & McLauchlan, K.K. (2015) Fire history reconstruction in grassland ecosystems: amount of charcoal reflects local area burned. Environmental Research Letters, 10, 114009.
- Leys, B.A., Commerford, J.L. & McLauchlan, K.K. (2017) Reconstructing grassland fire history using sedimentary charcoal: Considering count, size and shape. PLoS One, 12(4), e0176445.
- Lima, J.E.F.W., da Silva, E.M., Oliveira-Filho, E.C., Martins, E.S., Reatto, A. & Bufon, V.B. 2011. The relevance of the Cerrado's water resources to the Brazilian development. IWRA world water Congress, Permambuco Brazil, 11 pag.
- Marengo, J.A., Liebmann, B., Grimm, A.M., Misra, V., Silva Dias, P.L., Cavalcanti, I.F.A. et al. (2012) Recent developments on the South American monsoon system. International Journal of Climatology, 32, 1–21.
- Marengo, J.A., Soares, W.R., Saulo, C. & Nicolini, M. (2004) Climatology of the Low-Level Jet East of the Andes as Derived from the NCEP-NCAR Reanalyses: Characteristics and Temporal Variability. Journal of Climate, 17, 2261–2280.
- Marshall, M.H., Lamb, H.F., Huws, D., Davies, S.J., Bates, C.R., Bloemendahl, J., Boyle, J.F., Leng, M.J., Umer, M. & Bryant, C.L. (2011) Late pleistocene and holocene drought events at lake Tana, the source of the Blue Nile. Glob Plante Change, 78, 147–161.
- Martin, L., Flexor, J.M. & Suguio, K. (1995) Vibrotestemunhador leve. Construção, utilização e potencialidades. Revista do Instituto Geológico, 16, 59–66.

- Mistry, J. (1998) Fire in the Cerrado (savannas), of Brazil: an ecological review. Progress in Physical Geography: Earth and Environment, 22, 425–448.
- Moreno de Sousa, J.C. (2016) Lithic technology of an Itaparica industry archeological site: the Gruta das Araras rockshelter. Midwest Brazil. Journal of Lithis Studies, 3, 1–20. Available at: https://doi.org/10.2218/jls.v3il.1298
- Novello, V.F., Cruz, F.W., Karmann, I., Burns, S.J., Stríkis, N.M., Vuille, M. et al. (2012) Multidecadal climate variability in Brazil's Nordeste during the last 3000 years based on speleothem isotope records: MULTIDECADAL CLIMATE IN BRAZIL. Geophysical Research Letters, 39, n/a.
- Oliveira, U., Soares-Filho, B., de Souza Costa, W.L., Gomes, L., Bustamante, M. & Miranda, H. (2021) Modeling fuel loads dynamics and fire spread probability in the Brazilian Cerrado. Forest Ecology and Management, 482, 118889.
- Oliveira-Filho, A.T. & Ratter, J.A. (1995) A study of the origin of Central Brazilian forests by the analysis of plant species distribution patterns. Edinburgh Journal of Botany, 52(2), 141–194.
- Oliveira-Filho, A.T. & Ratter, J.A. (2002) Vegetation physiognomies and wood flora of the Cerrado biome. In: Oliveira, P.S. & Marquis, R.J., Eds. The Cerrados of Brazil: Ecology and Natural History of a Neotropical Savanna. (91-120). Columbia University, New York.
- Parizzi, M.G., Salgado-Labouriau, M.L. & Kohler, H.C. (1998) Genesis and environmental history of Lagoa Santa, Southeastern Brazil. The Holocene, 8, 311–321.
- Pereira Júnior, A.C., Oliveira, S.L.J., Pereira, J.M.C. & Turkman, M.A.A. (2014) Modelling fire frequency in a Cerrado Savanna Protected area. PLOSone, 9, e102380.
- Pivello, V.R., Vieira, I., Christianini, A.V., Ribeiro, D.B., da Silva Menezes, L., Berlinck, C.N. et al. (2021) Understanding Brazil's catastrophic fires: Causes, consequences and policy needed to prevent future tragedies. Perspectives in Ecology and conservation, 19, 233–255.

- Prado, L.F., Wainer, I. & Chessi, C.M. (2013b) Mid-Holocene PMIP3/ CMIP5 model results: Intercomparison for the South American Monsoon System. The Holocene, 23(12), 1915–1920.
- Prado, L.F., Wainer, I., Chiessi, C.M., Ledru, M.-P. & Turcq, B. (2013a) A mid-Holocene climate reconstruction for eastern South America. Clim. Past, 9, 2117–2133.
- Prous, A. & Fogaça, E. (1999) Archaeology of the Pleistocene-Holocene boundary in Brazil. Quaternary International, 53-54, 21-41.
- Ramos-Neto, M.B. & Pivello, V.R. (2000) Lightning fires in a Brazilian savanna national park: rethinking management strategies. Environmental Management, 26(6), 675–684. RCPol. (2021) october, 20. http://rcpol.org.br
- Reboita, M.S., Gan, M.A., Rocha, R.P. & Ambrizzi, T. (2010) Regimes de precipitação na América do Sul: uma revisão bibliográfica. Revista Brasileira de Meteorologia, 25, 185–204. Regent Instruments Canada Inc. (2009) Image analysis for plant science. https://regent.qc.ca/
- Ribeiro, J.F. & Walter, B.M.T. (2008) As principais fitofisionomias do bioma Cerrado. In: Sano, S.M., Almeida, S.P. & Ribeiro, J.F. (Eds.) Cerrado: Ecologia e Flora. Brasilia, DF: Embrapa Cerrados. pp. 153–212.
- Riris, P. & Arroyo-Kalin, M. (2019) Widespread population decline in South America correlates with mid-Holocene climate change. Scientific Reports, 9, 6850.
- Sabino, S.M.L., Cassino, R.F., Gomes, M.O.S., Sant'Anna, E.M.E., Rocha Augustin, C.H.R. & de Oliveira, D.A. (2021) Late Holocene in central Brazil: vegetation changes and humidity variability in a tropical wetland. Journal of Quaternary Science, 36, 1028–1039.
- Salgado-Labouriau, M.L. (1973) Contribução á Palinologia dos Cerrados. Academia Brasileira de Ciências, Rio de Janeiro, 1, 291.
- Salgado-Labouriau, M.L., Barberi, M., Ferraz-Vicentini, K.R. & Parizzi, M.G. (1998) A dry climatic event during the late Quaternary of tropical Brazil. Review of Palaeobotany and Palynology, 99(2), 115–129. Available at: https://doi.org/10.1016/S0034-6667(97)00045-6

- Schmidt, I.B. & Eloy, L. (2020) Fire regime in the Brazilian Savanna: Recent changes, policy and management. Flora, 268, 151613.
- Schmidt, I.B., Fidelis, A., Miranda, H.S. & Ticktin, T. (2017) How do the wets burn? Fire behavior and intensity in wet grasslands in the Brazilian savanna. Brazilian Journal of Botany, 40, 167–175.
- Strassburg, B.B.N., Brooks, T., Feltran-Barberi, R., Iribarrem, A., Crouzeilles, R., Loyola, R. et al. (2017) Momento f thrut for the Cerrado Hotspot. Nature Ecology & Evolution, 1, 0099.
- Strikis, N.M., Cruz, F.W., Cheng, H., Karmann, I., Edwards, R.L., Vuille, M. et al. (2011) Abrupt variations in South American monsoon rainfall during the Holocene based on a speleothem record from central-eastern Brazil. Geology, 39, 1075–1078. Available at: https://doi.org/10.1130/G32098.1
- Stuiver, M. & Reimer, P.J. (1993) Extended14C Data Base and Revised CALIB 3.014C Age Calibration Program. Radiocarbon, 35, 215–230.
- Sulca, J., Vuille, M., Silva, Y. & Takahashi, K. (2016) Teleconnections between the Peruvian Central Andes and Northeast Brazil during Extreme Rainfall Events in Austral Summer. Journal of Hydrometeorology, 17, 499–515.
- Tinner, W., Hofstetter, S., Zeugin, F., Conedera, M., Wohlgemuth, T., Zimmermann, L. et al. (2006) Long-distance transport of macroscopic charcoal by an intensive crown fire in the Swiss Alps implications for fire history reconstruction. The Holocene, 16, 287–292.
- Turcq, B., Albuquerque, A.L.S., Cordeiro, R.C., Sifeddine, A., Simoes Filho, F.F.L., Souza, A.G., Abrão, J.J., Oliveira, F.B.L., Silva, A.O. & Capitâneo, J. (2002) Accumulation of organic carbon in five Brazilian lakes during the Holocene. Sedimentary Geology, 148, 319–342.
- Utida, G., Cruz, F.W., Etourneau, J., Bouloubassi, I., Schefuß, E., Vuille, M. et al. (2019) Tropical South Atlantic influence on Northeastern Brazil precipitation and ITCZ displacement during the past 2300 years. Scientific Reports, 9, 1698.

- Vachula, R.S. & Rehn, E. (2023) Modeled dispersal patterns for wood and grass charcoal are different: Implications for paleofire reconstruction. The Holocene, 33(2), 159–166.
- Vachula, R.S., Sae-Lim, J. & Li, R. (2021) A critical appraisal of charcoal morphometry as a paleofire fuel type proxy. Quaternary Science Reviews, 262, 106979.
- Velazco, S.J.E., Villalobos, F., Galvão, F. & De Marco Júnior, P. (2019) A dark scenario for Cerrado plant species: Effects of future climate, land use and protected areas ineffectiveness. Diversity and Distributions, 25, 660–673.
- Vieira, L.T.A., Azevedo, T.N., Castro, A.A.J.F. & Martins, F.R. (2022) Reviewing the Cerrado's limits, flora distribution patterns, and conservation status for policy decisions. Land Use Policy, 115, 106038.
- Wang, X., Edwards, R.L., Auler, A.S., Cheng, H., Kong, X., Wang, Y., Cruz, F.W., Dorale, J.A. & Chiang, H.-W. (2017) Hydroclimate changes across the Amazon lowlands over the past 45,000 years. Nature, 541, 204-207.
- Ward, B.M., Wong, C.I., Novello, V.F., McGee, D., Santos, R.V., Silva, L.C.R. et al. (2019) Reconstruction of Holocene coupling between the South American Monsoon System and local moisture variability from speleothem δ18O and 87Sr/86Sr records. Quaternary Science Reviews, 210, 51–63.
- Wong, M.L., Wang, X., Latrubesse, E.M., He, S. & Bayer, M. (2021) Variations in the South Atlantic Convergence Zone over the mid-tolate Holocene inferred from speleothem δ18O in central Brazil. Quaternary Science Reviews, 270, 107178.
- Wortham, B.E., Wong, C.I., Silva, L.C.R., McGee, D., Montañez, I.P., Rasbury, E. T. et al. (2017) Assessing response of local moisture conditions in central Brazil to variability in regional monsoon intensity using speleothem 87Sr/86Sr values. Earth and Planetary Science Letters, 463, 310–322.

Integrative discussion and final remaks

This study focused on investigating the hydroclimate variability in the domain of the current American monsoon (TA region), across multiple spatial scales, including continental, regional, and local scales, along the Holocene (last ~11,000 years). TA are fundamental to the global climate system because they have meteorological and climatic aspects determined by the interaction of different environments, in a complex superposition of physical processes at multiple spatiotemporal scales (Palomino-Lemus et al., 2018). SA is an important part of the TA because it contains unique geographic features that contribute to the regional climate. Central America (CA) has a complex topography of volcanic origin that shapes a narrow isthmus located between the two dynamic ocean systems of the Pacific and Atlantic Oceans (Pérez-Briceño et al., 2016). The migration of the Intertropical Convergence Zone (ITCZ) and associated changes in the strength of the trade winds determine the rhythm of the seasons, the distinct seasonality in precipitation over much of the area, and the sensitivity to climate change (Hidalgo et al., 2015; Maldonado et al., 2018). This is a region particularly vulnerable to the climate disruptions expected due to global warming, with Honduras, Nicaragua, and Guatemala among the 10 countries considered most at risk (Kreft et al., 2013).

The southern United States (US) is a unique region in that it frequently experiences multi-year and multi-annual episodes of severe droughts, as well as frequent flooding (Garfin et al., 2013). This region also experiences changes in the magnitude, timing, and frequency of precipitation (Higgins et al., 1998; Luong et al., 2017; Zhang et al., 2021), which have been associated with changes in soil health (Renard and Simanton, 1975), ecosystem processes (Forzieri et al., 2014), and vegetation in the southwest desert (Khatri-Chhetri et al., 2021). Regional precipitation patterns in the southwestern US are also of great importance, as agricultural exports and livestock production in the region are heavily dependent on them (Garfin et al., 2013).

The SA contains the largest tropical forest in the world, the Amazon rainforest, and the driest desert, the Atacama Desert in Chile, in addition to the central plateau region, where the Cerrado is located, which contains the headwaters of major rivers flowing into the Amazon, La Plata and São Francisco Basins. Those basins contain major agricultural areas and provide most of Brazil's hydroelectric energy production (Silva & Kousky, 2012). A deeper understanding of hydroclimatic variations in the TA across different

scales can improve extreme event predictability, enhance water resource management, and provide valuable support for decision-making.

The continental-scale study "Precipitation patterns and variability in Tropical Americas during the Holocene" by Bianchini et al. (2025) investigates precipitation patterns and variability in the TA region throughout the Holocene. It uses paleoclimate records, such as lake sediments and speleothems, observational and reanalysis data of the current climate, and simulations from the TraCE-21ka experiment. The analysis allows us to identify changes relative to the current climate that allowed the delimitation of five key areas for a detailed regional analysis of precipitation variability.

The results show that despite the general agreement in moisture trends, regional discrepancies arise due to differences in the temporal resolution of the proxies and the spatial limitation of the models. The analysis of precipitation in key areas reveals a significant change in anomalies around 9,000–8,000 years, with a strong influence of high-energy climate events around 7,710 years. These events are linked to the collapse of the North American ice sheets and the weakening of the Atlantic Meridional Overturning Circulation (AMOC), caused by the input of freshwater from the North Atlantic (M. Walker et al., 2018; M. J. C. Walker et al., 2012) which, associated with changes in the insolation pattern in that period, contributed to the displacement of the ITCZ and South Atlantic Convergence Zone (SACZ) to the south, weakening the North American Monsoon System (NAMS) and strengthening the South American Monsoon System (SAMS) (Custódio et al., 2024; Strikis et al., 2011). This caused a reorganization of the monsoon system and changes in precipitation patterns in the TA throughout the Holocene.

The regional-scale study "A fully calibrated and updated mid-Holocene climate reconstruction for Eastern South America" by (Gorenstein et al., 2022) presents a climate reconstruction for eastern SA during the Middle Holocene (MH). It uses paleoclimate records, such as speleothems, lacustrine, marine and terrestrial sediment cores, soil samples, as well as fully calibrated age models. Proxies from the Amazon and southern SA indicate a drier climate during the MH, aligning with previous climate models (Maksic et al., 2019; Smith & Mayle, 2018; Tabor et al., 2020). Precipitation variability in these regions is influenced by the SASM, which also influences vegetation (Smith & Mayle, 2018). In Northeastern Brazil (NEB), conflicting climate data are clarified by regional divides, with ITCZ incursions and trade winds making coastal areas wetter(Prado et al., 2013; Wainer et al., 2014), while another hypothesis suggests a reversal of the

precipitation dipole, with the Amazon dry and the coast wetter in the MH (Smith & Mayle, 2018).

The Northeast/Southern boundary of South America (NSF), located at the core of the SASM, has its rainy season controlled by the SACZ and by moisturizing transport from the Amazon (de Mahiques et al., 2009; Smith & Mayle, 2018; Wong et al., 2021). Two hypotheses explain the observed variability: one suggests a weaker and northward-shifted SACZ during the MH (Raczka et al., 2013), while the other points to the stability of South Atlantic temperatures, keeping the SACZ constant (Wong et al., 2021). Both agree with climate models that indicate a contraction of the SAMS in the MH (Brierley et al., 2020; Shimizu et al., 2020).

During the MH, the Northeast/Southern boundary of SA was cooler, while the south of the region had a warmer and drier climate, with a contracted SAMS (Maksic et al., 2019; Tabor et al., 2020). The lack of temperature indicators in the Amazon limits the analysis, but precipitation records and lake levels indicate drier conditions.

Sea Surface Temperature (SST) reconstructions show a dipolar pattern off the coast of SA during the MH relative to the Late Holocene (LH), with warmer than present waters north of 15°S and cooler than present waters south of 15°S due to a strong ITCZ and reduced summer insolation in the Southern Hemisphere (SH). Sea Suface Salinity (SSS) studies indicate a saltier oceanic mixed layer in the western South Atlantic, with one exception. Lower lake levels and river discharges suggest drier and warmer than present conditions in the coastal region during this period.

Although there is divergence in local responses from regions with conflicting proxies, the highest quality proxies agree at a regional scale. High levels of the quality index are achieved by sediments containing biological analysis, but they are scarcer in biological proxy analyses of sediments than in isotopic fractions analysis obtained from speleothems. Nevertheless, the new quality indices, as defined here, give perspective to climate reconstruction.

Comparison between the paleorecords and the model outputs shows that analyzing different paleorecords in the same region did not always produce similar results, which can be solved with a multiproxy approach associated with differentiating the registration of large-scale events from local events. The multimodel approach is another way of solving these inconsistencies. Furthermore, this study makes it clear that the comparison between different paleorecords and climate model data does not always produce similar results for the same region, which can be resolved with a multiproxy approach associated

with the differentiation of the record of large-scale events from local events, and with the multimodel approach.

The local-scale study "Long- and short-term vegetation change and inferred climate dynamics and anthropogenic activity in central Cerrado during the Holocene" by Escobar-Torrez et al. (2024), investigates the relationship between vegetation, fire and climate in the Central Cerrado region throughout the Holocene. It uses pollen grains, macrocharcoal and trace elements from a lake sediment core located in Lagoa Feia, Goiás State, Brazil. The results show that since the end of the Pleistocene, the central Cerrado region has responded to hydrological and climatic changes driven by variability in monsoon system. The long-term expansion of woody cerrado in central Brazil was prevented by the southward shift of the ITCZ, forced by insolation that strengthened the monsoon system and included eastern Amazonia in its zone of influence. Therefore, the Cerrado vegetation began to develop around 6,000 years, with a bimodal climate and greater insolation.

Its expansion occurred in two phases: first with open cerrado until 4,800 years, and then with wooded cerrado, possibly due to the reduction of the dry season. In addition to these long-term trends, short-term drought and rain events influenced lake level, riparian vegetation and biomass burning. These episodes reflect variations in the intensity of the SACZ and the positioning of the ITCZ. As a result, there were changes in the influence of SAMS in the Lago Feia region. Two fire events, between 3,330–3,210 and 1,330–1,160 calibrated years before present, coincided with drier periods and possibly human activity. Full vegetation recovery took more than 30 years after each event.

During the Holocene, the southward displacement of the ITCZ and SACZ, the weakening of the NAMS and the strengthening of the SAMS in the TA on a continental scale were observed. Regionally, the ITCZ showed weaker and fewer incursions into SA, resulting in a drier and warmer Amazon in the MH. Southern SA was also drier, due to lower SAMS activity and reduced El Niño Southern Oscillation (ENSO) variability. NEB showed transitional behavior, with irregular rainfall and wetter periods than the current one, probably influenced by changes in the ITCZ. Locally, in the Lagoa Feia region in the Brazilian Cerrado, variations in the SACZ and ITCZ positioning and the the strengthening of the SAMS were recorded.

In this thesis it was shown that the general trends in precipitation variation in TA region observed during the Holocene - including the shift of the ITCZ and SACZ, the

weakening of the NAMS, and the strengthening of the SAMS - were recorded by data from the TracE-21ka simulation, by different paleorecords, such as speleothems and sediment cores analyzed in previously published studies, as well as by several proxies extracted from the sediment core from Lagoa Feia. These variations were observed at different scales: continental (in the TA), regional (in the SA, except for isolated records of SAMS weakening, associated with lower ENSO variability), and local (in the Brazilian Cerrado). These changes are associated with the collapse of the North American ice sheets, the weakening of the AMOC, and changes in the insolation pattern throughout the period.

The reconstruction of past global climate change relies on a variety of evidence and many well-distributed records. However, there are few comprehensive databases of continuous proxy records (time series rather than time slices) for different climate variables (Kaufman, 2017). Furthermore, a large proportion of studies on these records are published but not made available through public repositories, which makes their access restricted (Kaufman et al., 2020). All these aspects make the study of past climate through paleorecords challenging. In this context, global and public databases with evidence-based compilations of a wide variety of proxy types, including ecological, geochemical, and biophysical evidence from marine and terrestrial archives, are needed.

Comparing paleorecords and climate model data is a way to reconstruct past climates more robustly. However, the choice and use of each proxy requires prior assessment, considering the entire environmental context, in addition to the pros and cons associated with each proxy (Nowacki et al., 2019). In this context, using a multiproxy and multimodel approach is the best option to expand geographic coverage and avoid the biases inherent to each type of proxy and model. In addition, only data from calibrated age models should be used, since the uncertainties from a sample's age are responsible for attributing or not specific characteristic or climate change to a geologic period (Lowe & Walker, 2014).

Despite recent advances, more detailed studies on climate variability in the TA during the Holocene are needed. Understanding how the climate system varied during the Holocene period and how it varies today allows for better projections of future climate. Studying climate variations at different scales provides complementary insights that are essential for better predictability of extreme events, better management of water resources, and for providing support to decision-makers

References

- Ait Brahim, Y., Peros, M. C., Viau, A. E., Liedtke, M., Pajón, J. M., Valdes, J., Li, X., Edwards, R. L., Reinhardt, E. G., & Oliva, F. (2022). Hydroclimate variability in the Caribbean during North Atlantic Heinrich cooling events (H8 and H9). *Scientific Reports*, 12(1), 20719. https://doi.org/10.1038/s41598-022-24610-x
- Alley, R. B., Mayewski, P. A., Sowers, T., Stuiver, M., Taylor, K. C., & Clark, P. U. (1997). Holocene climatic instability: A prominent, widespread event 8200 yr ago. *Geology*, 25(6), 483. https://doi.org/10.1130/0091-7613(1997)025<0483:HCIAPW>2.3.CO;2
- Barber, D. C., Dyke, A., Hillaire-Marcel, C., Jennings, A. E., Andrews, J. T., Kerwin, M. W., Bilodeau, G., McNeely, R., Southon, J., Morehead, M. D., & Gagnon, J.-M. (1999). Forcing of the cold event of 8,200 years ago by catastrophic drainage of Laurentide lakes. *Nature*, 400(6742), 344–348. https://doi.org/10.1038/22504
- Berger, A., & Loutre, M. F. (1991). Insolation values for the climate of the last 10 million years. *Quaternary Science Reviews*, 10(4), 297–317. https://doi.org/10.1016/0277-3791(91)90033-Q
- Bianchini, P. R., Prado, L. F., Yokoyama, E., Wainer, I., Gorenstein, I., & Pausata, F. S. R. (2025). Precipitation patterns and variability in Tropical Americas during the Holocene. *Palaeogeography, Palaeoclimatology, Palaeoecology*, 669, 112935. https://doi.org/10.1016/j.palaeo.2025.112935
- Blockley, S. P. E., Lane, C. S., Hardiman, M., Rasmussen, S. O., Seierstad, I. K., Steffensen, J. P., Svensson, A., Lotter, A. F., Turney, C. S. M., & Bronk Ramsey, C. (2012). Synchronisation of palaeoenvironmental records over the last 60,000 years, and an extended INTIMATE event stratigraphy to 48,000 b2k. *Quaternary Science Reviews*, *36*, 2–10. https://doi.org/10.1016/j.quascirev.2011.09.017
- Bond, G., Kromer, B., Beer, J., Muscheler, R., Evans, M. N., Showers, W., Hoffmann, S., Lotti-Bond, R., Hajdas, I., & Bonani, G. (2001). Persistent Solar Influence on North Atlantic Climate During the Holocene. *Science*, 294(5549), 2130–2136. https://doi.org/10.1126/science.1065680

- Braconnot, P., Otto-Bliesner, B., Harrison, S., Joussaume, S., Peterchmitt, J.-Y., Abe-Ouchi, A., Crucifix, M., Driesschaert, E., Fichefet, Th., Hewitt, C. D., Kageyama, M., Kitoh, A., Laîné, A., Loutre, M.-F., Marti, O., Merkel, U., Ramstein, G., Valdes, P., Weber, S. L., ... Zhao, Y. (2007). Results of PMIP2 coupled simulations of the Mid-Holocene and Last Glacial Maximum Part 1: experiments and large-scale features. Climate of the Past, 3(2), 261–277. https://doi.org/10.5194/cp-3-261-2007
- Bradley, R. S. (1999). Paleoclimatology: reconstructing climates of the Quaternary. . *Elsevier*, 47.
- Brevik, E. C., Homburg, J. A., & Sandor, J. A. (2018). *Soils, Climate, and Ancient Civilizations* (pp. 1–28). https://doi.org/10.1016/B978-0-444-63865-6.00001-6
- Brierley, C. M., Zhao, A., Harrison, S. P., Braconnot, P., Williams, C. J. R., Thornalley,
 D. J. R., Shi, X., Peterschmitt, J.-Y., Ohgaito, R., Kaufman, D. S., Kageyama, M.,
 Hargreaves, J. C., Erb, M. P., Emile-Geay, J., D'Agostino, R., Chandan, D., Carré,
 M., Bartlein, P. J., Zheng, W., ... Abe-Ouchi, A. (2020). Large-scale features and
 evaluation of the PMIP4-CMIP6 *midHolocene* simulations. *Climate of the Past*,
 16(5), 1847–1872. https://doi.org/10.5194/cp-16-1847-2020
- Came, R. E., Oppo, D. W., & McManus, J. F. (2007). Amplitude and timing of temperature and salinity variability in the subpolar North Atlantic over the past 10 k.y. *Geology*, 35(4), 315. https://doi.org/10.1130/G23455A.1
- Cardoso Da Silva, J. M., & Bates, J. M. (2022). Biogeographic Patterns and Conservation in the South American Cerrado: A Tropical Savanna Hotspot: The Cerrado, which includes both forest and savanna habitats, is the second largest South American biome, and among the most threatened on the continent. *BioScience*, 52(3), 225–234.
- Carvalho, L. M. V. (2020). Assessing precipitation trends in the Americas with historical data: A review. In *Wiley Interdisciplinary Reviews: Climate Change* (Vol. 11, Issue 2). Wiley-Blackwell. https://doi.org/10.1002/wcc.627
- Chambers, F. M., Mauquoy, D., Brain, S. A., Blaauw, M., & Daniell, J. R. G. (2007). Globally synchronous climate change 2800 years ago: Proxy data from peat in South America. *Earth and Planetary Science Letters*, 253(3–4), 439–444. https://doi.org/10.1016/j.epsl.2006.11.007

- Charpentier Ljungqvist, F. (2011). The spatio-temporal pattern of the mid-Holocene thermal maximum. *Geografie–Sborník ČGS*, 116(2), 91–110.
- Costa, A. A., Guimarães, S. O., Sales, D. C., das Chagas Vasconcelos Junior, F., Marinho, M. W. S., Pereira, J. M. R., Martins, E. S. P. R., & da Silva, E. M. (2023). Precipitation extremes over the tropical Americas under RCP4.5 and RCP8.5 climate change scenarios: Results from dynamical downscaling simulations. *International Journal of Climatology*, 43(2), 787–803. https://doi.org/10.1002/joc.7828
- Custódio, I. S., da Silva Dias, P. L., Wainer, I., & Prado, L. F. (2024). Changes in the South American Monsoon System components since the Last Glacial Maximum: a TraCE-21k perspective. *Climate Dynamics*. https://doi.org/10.1007/s00382-024-07139-9
- Dansgaard, W., White, J. W. C., & Johnsen, S. J. (1989). The abrupt termination of the Younger Dryas climate event. *Nature*, *339*(6225), 532–534. https://doi.org/10.1038/339532a0
- de Mahiques, M. M., Coaracy Wainer, I. K., Burone, L., Nagai, R., de Mello e Sousa, S. H., Lopes Figueira, R. C., Almeida da Silveira, I. C., Bícego, M. C., Vicente Alves, D. P., & Hammer, Ø. (2009). A high-resolution Holocene record on the Southern Brazilian shelf: Paleoenvironmental implications. *Quaternary International*, 206(1–2), 52–61. https://doi.org/10.1016/j.quaint.2008.09.010
- Denton, G. H., & Karlén, W. (1973). Holocene Climatic Variations—Their Pattern and Possible Cause. *Quaternary Research*, 3(2), 155–205. https://doi.org/10.1016/0033-5894(73)90040-9
- Diniz, I. R., Marinho Filho, J., Machado, R. B., & Cavalcanti, R. B. (2010). Cerrado: conhecimento científico quantitativo como subsídio para ações de conservação. Brasília: Thesauros Editora.
- Drysdale, R., Zanchetta, G., Hellstrom, J., Maas, R., Fallick, A., Pickett, M., Cartwright, I., & Piccini, L. (2006). Late Holocene drought responsible for the collapse of Old World civilizations is recorded in an Italian cave flowstone. *Geology*, *34*(2), 101. https://doi.org/10.1130/G22103.1
- Escobar-Torrez, K., Ledru, M., Cassino, R. F., Bianchini, P. R., & Yokoyama, E. (2024). Long-and short-term vegetation change and inferred climate dynamics and

- anthropogenic activity in the central Cerrado during the Holocene. *Journal of Quaternary Science*, 39(1), 130–144. https://doi.org/10.1002/jqs.3567
- Figueroa, S. N., & Nobre, C. A. (1990). Precipitation distribution over central and western tropical South America. *Climanálise*, *5*(6), 36–45.
- Fu, R., Arias, P. A., & Wang, H. (2016). The Connection Between the North and South American Monsoons. In *Springer Climate* (pp. 187–206). Springer. https://doi.org/10.1007/978-3-319-21650-8 9
- Geen, R., Bordoni, S., Battisti, D. S., & Hui, K. (2020a). Monsoons, ITCZs, and the Concept of the Global Monsoon. *Reviews of Geophysics*, 58(4). https://doi.org/10.1029/2020RG000700
- Geen, R., Bordoni, S., Battisti, D. S., & Hui, K. (2020b). Monsoons, ITCZs, and the Concept of the Global Monsoon. *Reviews of Geophysics*, 58(4). https://doi.org/10.1029/2020RG000700
- Gorenstein, I., Prado, L. F., Bianchini, P. R., Wainer, I., Griffiths, M. L., Pausata, F. S. R., & Yokoyama, E. (2022). A fully calibrated and updated mid-Holocene climate reconstruction for Eastern South America. *Quaternary Science Reviews*, 292. https://doi.org/10.1016/j.quascirev.2022.107646
- Gornitz, V. (n.d.). Paleoclimate Proxies, An Introduction. In *Encyclopedia of Paleoclimatology and Ancient Environments* (pp. 716–721). Springer Netherlands. https://doi.org/10.1007/978-1-4020-4411-3_171
- Gowdy, J. (2020). Our hunter-gatherer future: Climate change, agriculture and uncivilization. *Futures*, *115*, 102488. https://doi.org/10.1016/j.futures.2019.102488
- Hernández, A., Martin-Puertas, C., Moffa-Sánchez, P., Moreno-Chamarro, E., Ortega, P., Blockley, S., Cobb, K. M., Comas-Bru, L., Giralt, S., Goosse, H., Luterbacher, J., Martrat, B., Muscheler, R., Parnell, A., Pla-Rabes, S., Sjolte, J., Scaife, A. A., Swingedouw, D., Wise, E., & Xu, G. (2020). Modes of climate variability: Synthesis and review of proxy-based reconstructions through the Holocene. *Earth-Science Reviews*, 209, 103286. https://doi.org/10.1016/j.earscirev.2020.103286
- Higgins, R. W., Yao, Y., & Wang, X. L. (1997). Influence of the North American Monsoon System on the U.S. Summer Precipitation Regime. *Journal of Climate*,

- 10(10), 2600–2622. https://doi.org/10.1175/1520-0442(1997)010<2600:IOTNAM>2.0.CO;2
- Jackson, J. B., Budd, A. F., & Coates, A. G. (1996). Evolution and environment in tropical America. *University of Chicago Press*.
- Jia, X., Zhao, D., Storozum, M. J., Shi, H., Bai, G., Liu, Z., Hu, Z., Sun, L., Wang, Q., & Li, H. (2022). The "2.8 ka BP Cold Event" Indirectly Influenced the Agricultural Exploitation During the Late Zhou Dynasty in the Coastal Areas of the Jianghuai Region. Frontiers in Plant Science, 13. https://doi.org/10.3389/fpls.2022.902534
- Kaufman, D. (2017). Bookkeeping or science: what's behind a paleo data compilation.
- Kaufman, D., McKay, N., Routson, C., Erb, M., Davis, B., Heiri, O., Jaccard, S., Tierney,
 J., Dätwyler, C., Axford, Y., Brussel, T., Cartapanis, O., Chase, B., Dawson, A., de
 Vernal, A., Engels, S., Jonkers, L., Marsicek, J., Moffa-Sánchez, P., ... Zhilich, S.
 (2020). A global database of Holocene paleotemperature records. *Scientific Data*,
 7(1), 115. https://doi.org/10.1038/s41597-020-0445-3
- Kobashi, T., Severinghaus, J. P., Brook, E. J., Barnola, J.-M., & Grachev, A. M. (2007). Precise timing and characterization of abrupt climate change 8200 years ago from air trapped in polar ice. *Quaternary Science Reviews*, 26(9–10), 1212–1222. https://doi.org/10.1016/j.quascirev.2007.01.009
- Lowe, J. J., & Walker, M. (2014). Reconstructing quaternary environments. Routledge.
- Lüning, S., Gałka, M., Bamonte, F. P., Rodríguez, F. G., & Vahrenholt, F. (2019). The Medieval Climate Anomaly in South America. *Quaternary International*, *508*, 70–87. https://doi.org/10.1016/j.quaint.2018.10.041
- Lüning, S., Gałka, M., Danladi, I. B., Adagunodo, T. A., & Vahrenholt, F. (2018). Hydroclimate in Africa during the Medieval Climate Anomaly. *Palaeogeography, Palaeoclimatology, Palaeoecology, 495*, 309–322. https://doi.org/10.1016/j.palaeo.2018.01.025
- Magny, M., & Haas, J. N. (2004). A major widespread climatic change around 5300 cal. yr BP at the time of the Alpine Iceman. *Journal of Quaternary Science*, 19(5), 423–430. https://doi.org/10.1002/jqs.850

- Maksic, J., Shimizu, M. H., de Oliveira, G. S., Venancio, I. M., Cardoso, M., & Ferreira, F. A. (2019). Simulation of the Holocene climate over South America and impacts on the vegetation. *The Holocene*, 29(2), 287–299. https://doi.org/10.1177/0959683618810406
- Mann, M. E., Zhang, Z., Rutherford, S., Bradley, R. S., Hughes, M. K., Shindell, D., Ammann, C., Faluvegi, G., & Ni, F. (2009). Global Signatures and Dynamical Origins of the Little Ice Age and Medieval Climate Anomaly. *Science*, *326*(5957), 1256–1260. https://doi.org/10.1126/science.1177303
- Marcott, S. A., Shakun, J. D., Clark, P. U., & Mix, A. C. (2013). A Reconstruction of Regional and Global Temperature for the Past 11,300 Years. *Science*, 339(6124), 1198–1201. https://doi.org/10.1126/science.1228026
- Marengo, J. A., Ambrizzi, T., da Rocha, R. P., Alves, L. M., Cuadra, S. V., Valverde, M. C., Torres, R. R., Santos, D. C., & Ferraz, S. E. T. (2010). Future change of climate in South America in the late twenty-first century: intercomparison of scenarios from three regional climate models. *Climate Dynamics*, 35(6), 1073–1097. https://doi.org/10.1007/s00382-009-0721-6
- Mayewski, P. A., Rohling, E. E., Curt Stager, J., Karlén, W., Maasch, K. A., Meeker, L. D., Meyerson, E. A., Gasse, F., van Kreveld, S., Holmgren, K., Lee-Thorp, J., Rosqvist, G., Rack, F., Staubwasser, M., Schneider, R. R., & Steig, E. J. (2004). Holocene climate variability. *Quaternary Research*, 62(3), 243–255. https://doi.org/10.1016/j.yqres.2004.07.001
- Mechoso, C. R., Robertson, A. W., Ropelewski, C. F., & Grimm, A. M. (2004). *THE AMERICAN MONSOON SYSTEMS*.
- Nowacki, D., Langan, C. C. M., Kadereit, A., Pint, A., & Wunderlich, J. (2019). "Lake Gorgana" A paleolake in the Lower Danube Valley revealed using multi-proxy and regionalisation approaches. *Quaternary International*, 511, 107–123. https://doi.org/10.1016/j.quaint.2018.09.021
- Oliveira, P. S., & Marquiss R. J. (2002). 18. Biodiversity and Conservation Priorities in the Cerrado Region. In *The Cerrados of Brazil* (pp. 351–368). Columbia University Press. https://doi.org/10.7312/oliv12042-019

- PAGES 2k Consortium. (2013). Continental-scale temperature variability during the past two millennia. *Nature Geoscience*, 6(5), 339–346. https://doi.org/10.1038/ngeo1797
- Palomino-Lemus, R., Córdoba-Machado, S., Gámiz-Fortis, S. R., Castro-Díez, Y., & Esteban-Parra, M. J. (2018). High-resolution boreal winter precipitation projections over tropical America from CMIP5 models. *Climate Dynamics*, 51(5–6), 1773–1792. https://doi.org/10.1007/s00382-017-3982-5
- Pinto, J., Bonacic, C., Hamilton-West, C., Romero, J., & Lubroth, J. (2008). Climate change and animal diseases in South America. *Rev Sci Tech*, 27(2), 599–613.
- Plunkett, G., & Swindles, G. T. (2008). Determining the Sun's influence on Lateglacial and Holocene climates: a focus on climate response to centennial-scale solar forcing at 2800cal.BP. *Quaternary Science Reviews*, 27(1–2), 175–184. https://doi.org/10.1016/j.quascirev.2007.01.015
- Porinchu, D. F., MacDonald, G. M., Moser, K. A., Rolland, N., Kremenetski, K., Seppä, H., & Rühland, K. M. (2019). Evidence of abrupt climate change at 9.3 ka and 8.2 ka in the central Canadian Arctic: Connection to the North Atlantic and Atlantic Meridional Overturning Circulation. *Quaternary Science Reviews*, 219, 204–217. https://doi.org/10.1016/j.quascirev.2019.07.024
- Prado, L. F., Wainer, I., Chiessi, C. M., Ledru, M.-P., & Turcq, B. (2013). A mid-Holocene climate reconstruction for eastern South America. *Climate of the Past*, 9(5), 2117–2133. https://doi.org/10.5194/cp-9-2117-2013
- Raczka, M. F., De Oliveira, P. E., Bush, M., & McMichael, C. H. (2013). Two paleoecological histories spanning the period of human settlement in southeastern Brazil. *Journal of Quaternary Science*, 28(2), 144–151. https://doi.org/10.1002/jqs.2597
- Raspopov, O. M., Dergachev, V. A., Zaitseva, G. I., & Ogurtsov, M. G. (2013). Deep solar activity minima, sharp climate changes, and their impact on ancient civilizations. *Geomagnetism and Aeronomy*, 53(8), 917–921. https://doi.org/10.1134/S0016793213080227
- Reboita, M. S., Ambrizzi, T., Crespo, N. M., Dutra, L. M. M., Ferreira, G. W. de S., Rehbein, A., Drumond, A., da Rocha, R. P., & Souza, C. A. de. (2021). Impacts of

- teleconnection patterns on South America climate. *Annals of the New York Academy of Sciences*, 1504(1), 116–153. https://doi.org/10.1111/nyas.14592
- Ruan, J., Kherbouche, F., Genty, D., Blamart, D., Cheng, H., Dewilde, F., Hachi, S., Edwards, R. L., Régnier, E., & Michelot, J.-L. (2016). Evidence of a prolonged drought ca. 4200 yr BP correlated with prehistoric settlement abandonment from the Gueldaman GLD1 Cave, Northern Algeria. *Climate of the Past*, *12*(1), 1–14. https://doi.org/10.5194/cp-12-1-2016
- S. Silva, V. B., & E., V. (2012). The South American Monsoon System: Climatology and Variability. In *Modern Climatology*. InTech. https://doi.org/10.5772/38565
- Shimizu, M. H., Sampaio, G., Venancio, I. M., & Maksic, J. (2020). Seasonal changes of the south american monsoon system during the mid-holocene in the cmip5 simulations. *Clim. Dynam*, *54*, 2697–2712.
- Silva, V. B., & Kousky, V. E. (2012). *Modern climatology* (Shih-Yu (Simon) Wang & Robert R. Gillies, Eds.). IntechOpen.
- Smith, R. J., & Mayle, F. E. (2018). Impact of mid- to late Holocene precipitation changes on vegetation across lowland tropical South America: a paleo-data synthesis. *Quaternary Research*, 89(1), 134–155. https://doi.org/10.1017/qua.2017.89
- Strassburg, B. B. N., Brooks, T., Feltran-Barbieri, R., Iribarrem, A., Crouzeilles, R., Loyola, R., Latawiec, A. E., Oliveira Filho, F. J. B., Scaramuzza, C. A. de M., Scarano, F. R., Soares-Filho, B., & Balmford, A. (2017). Moment of truth for the Cerrado hotspot. *Nature Ecology & Evolution*, 1(4), 0099. https://doi.org/10.1038/s41559-017-0099
- Strikis, N. M., Cruz, F. W., Cheng, H., Karmann, I., Edwards, R. L., Vuille, M., Wang, X., de Paula, M. S., Novello, V. F., & Auler, A. S. (2011). Abrupt variations in South American monsoon rainfall during the Holocene based on a speleothem record from central-eastern Brazil. *Geology*, 39(11), 1075–1078. https://doi.org/10.1130/G32098.1
- Tabor, C., Otto-Bliesner, B., & Liu, Z. (2020). Speleothems of South American and Asian Monsoons Influenced by a Green Sahara. *Geophysical Research Letters*, 47(22). https://doi.org/10.1029/2020GL089695

- Thomas, E. R., Wolff, E. W., Mulvaney, R., Steffensen, J. P., Johnsen, S. J., Arrowsmith, C., White, J. W. C., Vaughn, B., & Popp, T. (2007). The 8.2ka event from Greenland ice cores. *Quaternary Science Reviews*, 26(1–2), 70–81. https://doi.org/10.1016/j.quascirev.2006.07.017
- Thompson, L. G., Mosley-Thompson, E., Davis, M. E., Henderson, K. A., Brecher, H. H., Zagorodnov, V. S., Mashiotta, T. A., Lin, P.-N., Mikhalenko, V. N., Hardy, D. R., & Beer, J. (2002). Kilimanjaro Ice Core Records: Evidence of Holocene Climate Change in Tropical Africa. *Science*, 298(5593), 589–593. https://doi.org/10.1126/science.1073198
- Torres, R. R., & Marengo, J. A. (2013). Uncertainty assessments of climate change projections over South America. *Theoretical and Applied Climatology*, 112(1–2), 253–272.
- Trenberth, K. E., & Otto-Bliesner, B. L. (2003). Toward Integrated Reconstruction of Past Climates. *Science*, 300(5619), 589–590. https://doi.org/10.1126/science.1083122
- Vera, C., Higgins, W., Amador, J., Ambrizzi, T., Garreaud, R., Gochis, D., Gutzler, D., Lettenmaier, D., Marengo, J., Mechoso, C. R., Nogues-Paegle, J., Dias, P. L. S., & Zhang, A. C. (2006). *Toward a Unified View of the American Monsoon Systems*.
- Vieira, L. T. A., Azevedo, T. N., Castro, A. A. J. F., & Martins, F. R. (2022). Reviewing the Cerrado's limits, flora distribution patterns, and conservation status for policy decisions. Land Use Policy, 115, 106038. https://doi.org/10.1016/j.landusepol.2022.106038
- Wainer, I., Prado, L. F., Khodri, M., & Otto-Bliesner, B. (2014). Reconstruction of the South Atlantic Subtropical Dipole index for the past 12,000 years from surface temperature proxy. *Scientific Reports*, 4(1), 5291. https://doi.org/10.1038/srep05291
- Walker, M., Gibbard, P., Head, M. J., Berkelhammer, M., Björck, S., Cheng, H., Cwynar, L. C., Fisher, D., Gkinis, V., Long, A., Lowe, J., Newnham, R., Rasmussen, S. O., & Weiss, H. (2019). Formal Subdivision of the Holocene Series/Epoch: A Summary.
 Journal of the Geological Society of India, 93(2), 135–141. https://doi.org/10.1007/s12594-019-1141-9

- Walker, M., Head, M. J., Berkelhammer, M., Björck, S., Cheng, H., Cwynar, L., Fisher, D., Gkinis, V., Long, A., Lowe, J., Newnham, R., Rasmussen, S. O., & Weiss, H. (2018). Formal ratification of the subdivision of the Holocene Series/Epoch (Quaternary System/Period): two new Global Boundary Stratotype Sections and Points (GSSPs) and three new stages/subseries. *Episodes*, 41(4), 213–223. https://doi.org/10.18814/epiiugs/2018/018016
- Walker, M. J. C., Berkelhammer, M., Björck, S., Cwynar, L. C., Fisher, D. A., Long, A. J., Lowe, J. J., Newnham, R. M., Rasmussen, S. O., & Weiss, H. (2012). Formal subdivision of the Holocene Series/Epoch: a Discussion Paper by a Working Group of INTIMATE (Integration of ice-core, marine and terrestrial records) and the Subcommission on Quaternary Stratigraphy (International Commission on Stratigraphy). *Journal of Quaternary Science*, 27(7), 649–659. https://doi.org/10.1002/jqs.2565
- Wanner, H., Beer, J., Bütikofer, J., Crowley, T. J., Cubasch, U., Flückiger, J., Goosse, H., Grosjean, M., Joos, F., Kaplan, J. O., Küttel, M., Müller, S. A., Prentice, I. C., Solomina, O., Stocker, T. F., Tarasov, P., Wagner, M., & Widmann, M. (2008). Midto Late Holocene climate change: an overview. *Quaternary Science Reviews*, 27(19–20), 1791–1828. https://doi.org/10.1016/j.quascirev.2008.06.013
- Wanner, H., Mercolli, L., Grosjean, M., & Ritz, S. P. (2015). Holocene climate variability and change; a data-based review. *Journal of the Geological Society*, *172*(2), 254–263. https://doi.org/10.1144/jgs2013-101
- Wanner, H., Solomina, O., Grosjean, M., Ritz, S. P., & Jetel, M. (2011). Structure and origin of Holocene cold events. *Quaternary Science Reviews*, 30(21–22), 3109–3123. https://doi.org/10.1016/j.quascirev.2011.07.010
- Werneck, F. P. (2011). The diversification of eastern South American open vegetation biomes: Historical biogeography and perspectives. *Quaternary Science Reviews*, 30(13–14), 1630–1648. https://doi.org/10.1016/j.quascirev.2011.03.009
- Wirtz, K. W., Lohmann, G., Bernhardt, K., & Lemmen, C. (2010). Mid-Holocene regional reorganization of climate variability: Analyses of proxy data in the frequency domain. *Palaeogeography, Palaeoclimatology, Palaeoecology*, 298(3–4), 189–200. https://doi.org/10.1016/j.palaeo.2010.09.019

- Wong, M. L., Wang, X., Latrubesse, E. M., He, S., & Bayer, M. (2021). Variations in the South Atlantic Convergence Zone over the mid-to-late Holocene inferred from speleothem δ18O in central Brazil. *Quaternary Science Reviews*, 270, 107178. https://doi.org/10.1016/j.quascirev.2021.107178
- Yu, S.-Y., Colman, S. M., Lowell, T. V., Milne, G. A., Fisher, T. G., Breckenridge, A., Boyd, M., & Teller, J. T. (2010). Freshwater Outburst from Lake Superior as a Trigger for the Cold Event 9300 Years Ago. *Science*, 328(5983), 1262–1266. https://doi.org/10.1126/science.1187860
- Zhang, H., Cheng, H., Cai, Y., Spötl, C., Kathayat, G., Sinha, A., Edwards, R. L., & Tan, L. (2018). Hydroclimatic variations in southeastern China during the 4.2 ka event reflected by stalagmite records. *Climate of the Past*, *14*(11), 1805–1817. https://doi.org/10.5194/cp-14-1805-2018

Appendices

Appendix I

Supplementary Material

Precipitation patterns and variability in Tropical Americas during the Holocene

Paula R. Bianchini ^{a, *}, Luciana F. Prado ^b, Elder Yokoyama ^a, Ilana Wainer ^c, Iuri Gorenstein ^c, Francesco S. R. Pausata ^d

- a Laboratório de Estudos Magnéticos em Geociências (LEMAG), Instituto de Geociências, Universidade de Brasília, Brasília, Brazil
- b Faculdade de Oceanografia, Universidade do Estado do Rio de Janeiro, Rio de Janeiro, Brazil
- c Instituto Oceanográfico, Universidade de São Paulo, São Paulo, Brazil
- d Centre ESCER (Etude et la Simulation du Climat a; l'Echelle Regionale) and GEOTOP (Research Center on the Dynamics of the Earth System), Department of Earth and Atmospheric Sciences, University of Quebec in Montreal, Montreal, QC, Canada

Table S.1. Complete proxy compilation with the record name, proxy type, coordinates, registered subseries and reference study.

Record name	Proxy type	Lat (°)	Long (°)	EH	МН	LH	Reference
Botuverá cave	Speleothem	-27.22	-49.15	X	X	Х	Bernal et al., 2016
Lapa Grande cave	Speleothem	-14.42	-44.36	X	X	X	Strikis et al., 2011
Majaguas-Cantera Cave	Speleothem	22.38	-83.96	X	x	X	Ait Brahim et al., 2022
El Condor	Speleothem	-5.93	-77.3	X	X	X	Cheng et al., 2013
Cueva del Diamante	Speleothem	-5.73	-77.5	X	x	X	Cheng et al., 2013
Venado Cave	Speleothem	10.6	-84.8	X			Lachniet et al., 2004
Leviathan Cave	Speleothem	37.89	-115.58	X	X	X	Lachniet et al., 2004
Santiago Cave	Speleothem	-2.7	-78.3	X	X		Mosblech et al., 2012
Grutas del Rey Marcos	Speleothem	15.43	-90.28	X	X	X	Winter et al., 2020
Natural Bridge Caverns	Speleothem	29.69	-98.34	X	X	X	Wong et al., 2015
Santana Cave	Speleothem	-24.53	-48.73	X	X	X	Cruz et al., 2006
Rainha Cave	Speleothem	-5.6	-37.73		X	X	Cruz et al., 2009
Macal Chasm	Speleothem	16.883	-89.108		x	X	Akers et al., 2016
Huagapo Cave	Speleothem	-11.27	-75.79		X	X	Kanner et al., 2013
Brown's Cave	Speleothem	28.60	-82.44		X		Pollock et al., 2017
Chen Ha Cave	Speleothem	17	89		X		Pollock et al., 2017
Palestina cave	Speleothem	-5.92	-77.35			X	Apaéstegui et al., 2014

Bat Cave	Speleothem	32.137	-104.54			X	Asmerom et al., 2013
Cueva Bonita	Speleothem	23	-99			х	Wright et al., 2023
Laguna La Gaiba	Lake Sediment	-17.75	-57.58	X	x	х	Whitney et al., 2011
Carajas Serra Norte Lake	Lake Sediment	-6.30	-50.20	х	X	X	Turcq et al., 2002
Caracarana Lake	Lake Sediment	-3.84	-59.78	X	x	х	Turcq et al., 2002
Água Preta de Baixo Lake	Lake Sediment	-18.42	-41.83	x	X	x	Turcq et al., 2002
Dom Helvecio Lake	Lake Sediment	-19.68	-42.59	X	x	х	Turcq et al., 2002
Feia Lake	Lake Sediment	-15.57	-47.30	X	x	х	Turcq et al., 2002
Lagoa do Caçó	Lake Sediment	-2.96	-43.42	X	x	х	Pessenda et al., 2005
Serra do tabuleiro	Lake Sediment	-27.9	-48.87	X	x	X	Jeske-Pieruschka et al., 2013
RdCa	Lake Sediment	-29.48	-50.57	Х	X	х	Jeske-Pieruschka & Behling, 2012
Acará Lake	Lake Sediment	-3.4	62.4	X	x	Х	Horbe et al., 2011
Coari Lake	Lake Sediment	-4.3	-63.2	X	X	х	Horbe et al., 2011
Lake Santa Rosa	Lake Sediment	-14.48	-67.88	X	x	X	Urrego et al., 2013
Pantano de Monica	Lake Sediment	-0.42	-72	X	X	Х	Behling et al., 1999
Lagoa Da Cachoeira	Lake Sediment	-6.21	-50.23	X	X	X	Hermanowski et al., 2015
Pantano da Mauritia	Lake Sediment	-6.21	-50.24	X	x	х	Hermanowski et al., 2012
Huanchaca	Lake Sediment	-14.32	-60.43	X	X	X	Maezumi et al., 2015
Vereda Juquinha	Lake Sediment	-17.56	-44.15	X	x	х	Pires et al., 2016
Alpes de São Francisco	Lake Sediment	-29.29	-50.37	x	X	x	Leonhardt & Lorscheitter, 2010
							Cassino et al., 2020
Lagoa Feia	Lake Sediment	-15.34	-47.18	X	X		
Lago do Saci	Lake Sediment	-9.7	-56.16	X	X	X	Fontes et al., 2017
Lake Peten-Itza	Lake Sediment	16.92	-89.83	X	X	X	Curtis et al., 1998
El Junco	Lake Sediment	-0.895	-89.479	X	X	X	Conroy et al., 2008
Laguna de Los Anteojos	Lake Sediment	12.723	-71.073	X	X	X	Stansell et al., 2010
Laguna Queshquecocha	Lake Sediment	-9.8	-77.3	X	X	Х	Stansell et al., 2013
Laguna Jahuacocha	Lake Sediment	-10.23	-76.93	X	X	X	Stansell et al., 2013
Laguna Lutacocha	Lake Sediment	-10.55	-76.72	X	X	X	Stansell et al., 2013
Yanacocha	Lake Sediment	-13.94	-70.87	X	X	X	Beal et al., 2014
Lake Titicaca	Lake Sediment	-15.85	-69.140	X	X	х	Fornace et al., 2014
Lago Puerto Arturo	Lake Sediment	17.533	-90.183	X	X	х	Wahl et al., 2014
Laguna Yanacocha	Lake Sediment	-10.56	-75.93	X	X	x	Stansell et al., 2015

Laguna La Gaiba	Lake Sediment	-17.75	-57.58	X	x	x	Fornace et al., 2016
8							Frugone-Álvarez et al.,
Laguna del Maule	Lake Sediment	-36.05	-70.5	X	х	X	2020
Lake Elsinore	Lake Sediment	33.66	-117.35	X	X	X	Kirby et al., 2010
Bison Lake	Lake Sediment	39.76	-107.34	X	х	X	Anderson, 2011
Yellow Lake	Lake Sediment	36.66	-107.36	X	X	X	Anderson, 2012
Lower Bear Lake	Lake Sediment	34.24	-119.97	X	x	X	Kirby et al., 2012
San Luis Lake	Lake Sediment	37.67	-105.72	X	х	X	Yuan et al., 2013
Emerald Lake	Lake Sediment	40.30	-105.66	X	X	X	Shuman et al., 2014
Pyramid Lake	Lake Sediment	40.06	-119.6	X	X	X	Benson et al., 2002
Lakes Marcio /Tapera	Lake Sediment	-0.13	-51.08		X	X	De Toledo & Bush, 2007
Lago Aleixo	Lake Sediment	-17.99	-42.12		X	X	Enters et al., 2010
Lake Comprida	Lake Sediment	-1.86	-53.98		X		Bush et al., 2000
Lake Santa Maria	Lake Sediment	-1.58	-53.60		x		Bush et al., 2007
Lake Saracuri	Lake Sediment	-1.68	-53.57		x		Bush et al., 2007
Lake Geral	Lake Sediment	-1.65	-53.59		x		Bush et al., 2007
Carajás	Lake Sediment	-6.58	-49.50		x	x	Sifeddine et al., 2001
Lago Rogaguado	Lake Sediment	-12.6	-65.6		x	х	Brugger et al., 2016
Laguna Orícore	Lake Sediment	-13.2	-63.31		x	х	Carson et al., 2014
Laguna Granja	Lake Sediment	-13.15	-63.42		x	X	Carson et al., 2014; 2015
La Luna	Lake Sediment	-13.35	-63.34		x	x	Carson et al., 2016
Lagoa Olhos D'água	Lake Sediment	-19.38	-43.54		x	X	Raczka et al., 2013
Lagoa dos Mares	Lake Sediment	-19.39	-43.59		x	x	Raczka et al., 2013
Cerro Llamoca	Lake Sediment	-14.16	-74.73		x	х	Schittek et al., 2015
Laguna de Montos	Lake Sediment	8.512	-71.086		х	x	Stansell et al., 2014
Laguna de Mucubají	Lake Sediment	8.797	-70.828		х	X	Stansell et al., 2014
Laguna de Ubaque	Lake Sediment	4.5	-73.9		х	x	Bird et al., 2018
La Alberca maar lake	Lake Sediment	19.21	-101.46	i	х	X	Wogau et al., 2019
Lake Pata	Lake Sediment	-0.29	-66.68		х	х	Nogueira et al., 2021
Laguna Pallcacocha	Lake Sediment	-9.39	-77.37		х	х	Mark et al., 2022
							Behling & Lima da Costa,
Lago Crispim	Lake Sediment	-0.59	-47.65			X	2001
Lago Tapajós	Lake Sediment	-2.79	-55.08			X	Irion et al., 2006
Lake Chichancanab	Lake Sediment	19.86	-88.76			X	Hodell et al., 2005
Laguna Castilla	Lake Sediment	18.79	-70.87			x	Lane et al., 2009
Laguna de Salvador	Lake Sediment	18.795	-70.887			х	Lane et al., 2009
Laguna de Juanacatlán	Lake Sediment	20.62	-104.73			х	Metcalfe et al., 2010

Laguna Pumacocha	Lake Sediment	-10.70	-76.06		x	Bird et al., 2011
Laguna Chepical	Lake Sediment	-32.27	-70.5		X	Jong et al., 2013
Lago El Gancho	Lake Sediment	11.906	-85.918		X	Stansell et al., 2013
Genovesa Crater Lake	Lake Sediment	0.328	-89.96		X	Conroy et al., 2014
maar lake Aljojuca	Lake Sediment	19.533	-97.533		X	Bhattacharya et al., 2015
Cerro Tuzgle peatland	Lake Sediment	-24.15	-66.4		X	Schittek et al., 2016
Lake Kail	Lake Sediment	16	-91.554		X	Stansell et al., 2020
Bainbridge Crater Lake	Lake Sediment	-0.35	-90.57		X	Thompson et al., 2017
Lake Chichancanab	Lake Sediment	19.86	-88.76		X	Evans et al., 2018
Lake Limón	Lake Sediment	-6.71	-76.21		X	Parsons et al., 2018
Lagunillas	Lake Sediment	-27.2	-69.283		X	Kock et al., 2019
Cerro Tuzgle	Lake Sediment	-24.15	-66.4		X	Kock et al., 2019
Lake Petén Itzá	Lake Sediment	-16.92	-89.93		Х	Obrist-Farner & Rice, 2019
Jequitinhonha	Lake Sediment	-15.28	-38.91		X	Bahr et al., 2021
Celestun Lagoon	Lake Sediment	20.90	-90.35		X	Hardage et al., 2022
Walker Lake	Lake Sediment	38.7	-118.72		X	Yuan et al., 2004
Abbott Lake	Lake Sediment	39.02	-121.61		X	Hiner et al., 2016
Zaca Lake	Lake Sediment	34.78	-120.04		X	Kirby et al., 2014

	North America	Central America	South America	Total
EH	10	5	35	50
MH	12	9	53	74
LH	25	9	59	93
Total	47	23	147	217

Table S.2. Number of compiled records according to subcontinent and subseries.

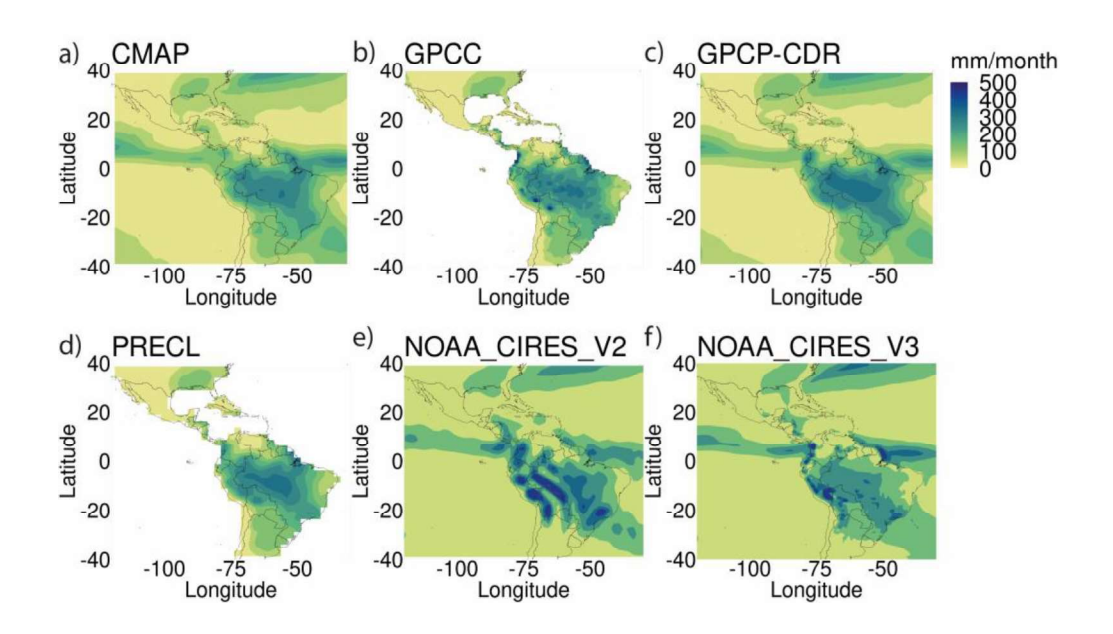


Figure S.1. DJF mean precipitation (mm/month), represented by observational and reanalysis datasets. a) CMAP, b) GPCC, c) GPCP-CDR, d) PRECL, e) NOAA_CIRES_V2, and f) NOAA_CIRES_V3. Reference period for anomalies: 1982 - 2012.

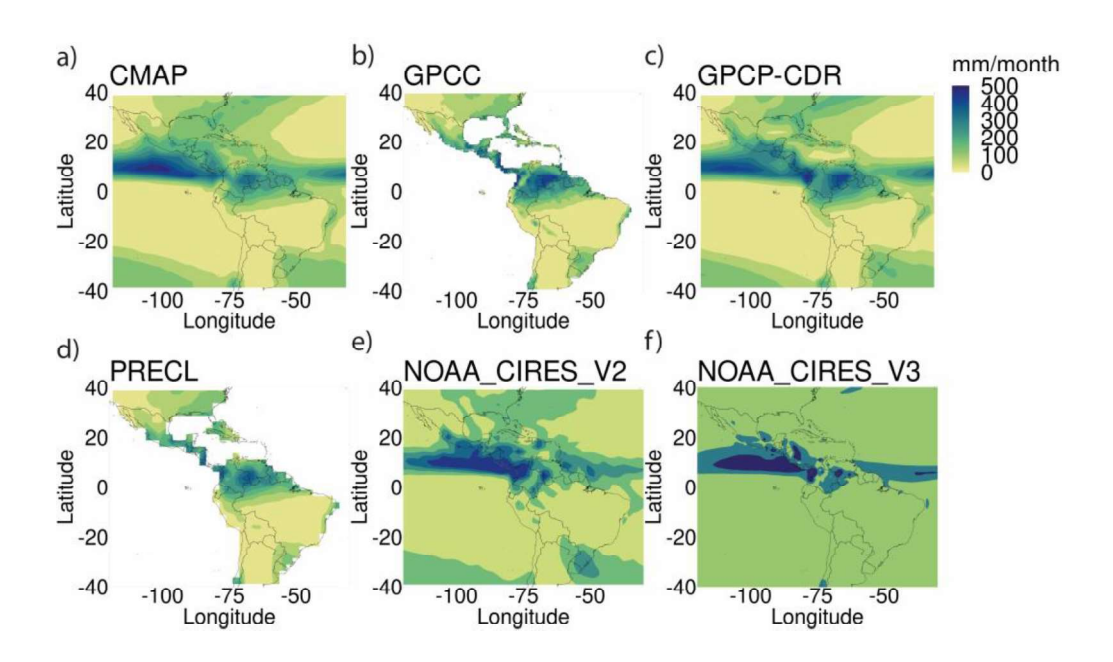


Figure S.2. JJA mean precipitation (mm/month), represented by observational and reanalysis datasets. a) CMAP, b) GPCC, c) GPCP-CDR, d) PRECL, e) NOAA_CIRES_V2, and f) NOAA CIRES V3. Reference period for anomalies: 1982 – 2012.

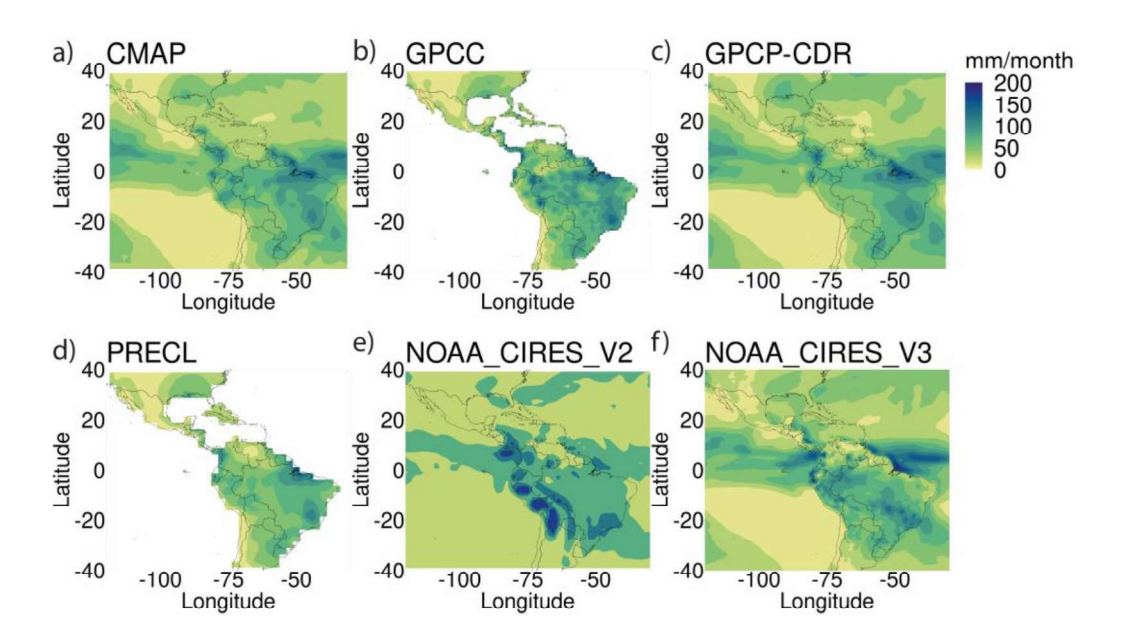


Figure S.3. DJF precipitation variability (SD) (mm/month), represented by observational and reanalysis datasets. a) CMAP, b) GPCC, c) GPCP-CDR, d) PRECL, e) NOAA_CIRES_V2, and f) NOAA_CIRES_V3. Reference period for anomalies: 1982 – 2012.

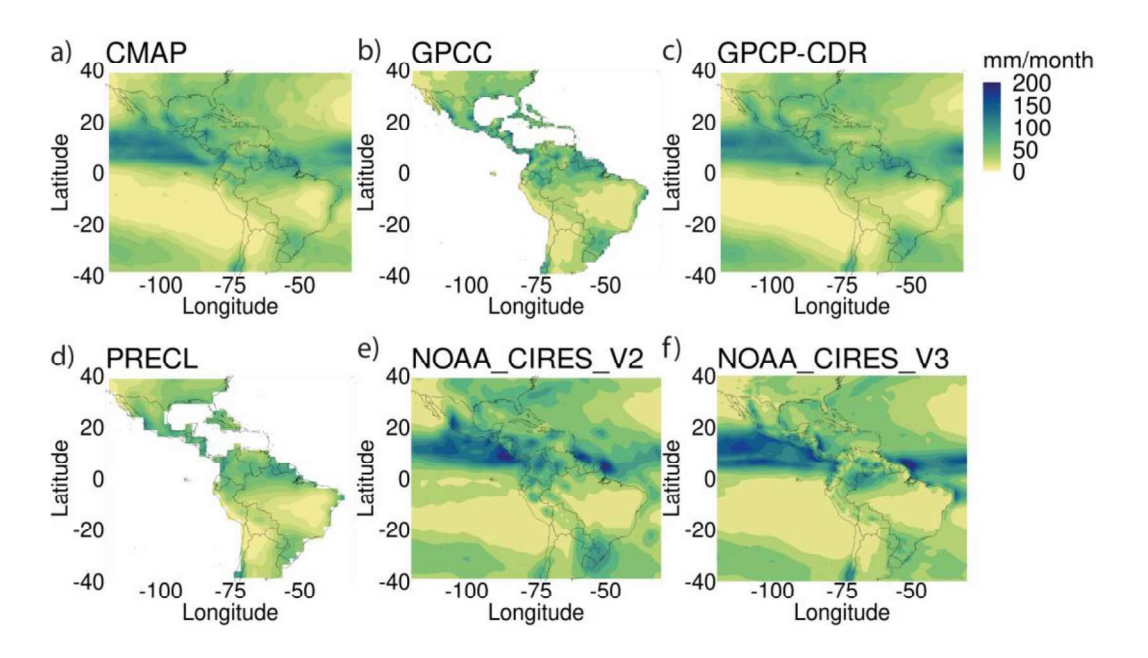


Figure S.4. JJA precipitation variability (SD) (mm/month), represented by observational and reanalysis datasets. a) CMAP, b) GPCC, c) GPCP-CDR, d) PRECL, e) NOAA_CIRES_V2, and f) NOAA_CIRES_V3. Reference period for anomalies: 1982 – 2012.

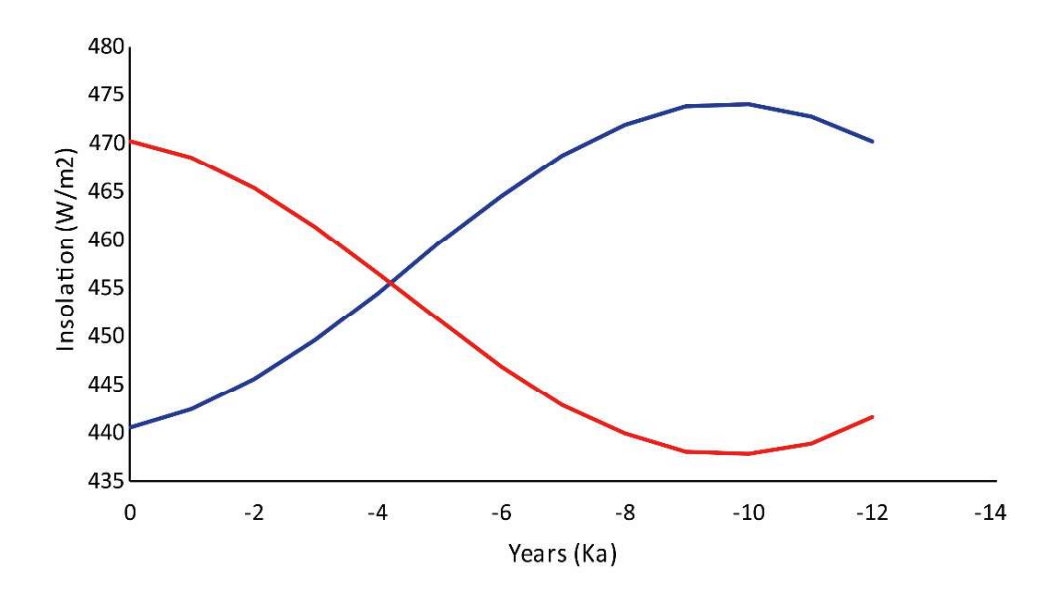


Figure S.5. Summer insolation in the Northern (blue line) (15°N) and Southern (red line) (15°S) Hemispheres of the last 12000 years. Data from Berger & Loutre (1991) and available at https://www.ncdc.noaa.gov/paleo-search/study/577.

More detailed analysis of Section 3.2.2

Results from the NA are shown in Figure 4 (the reader is referred to Section 2.2.3. for more details on the areas' domains). The annual cycle shows that precipitation varies between 0 and 65 mm/month in this region throughout the Holocene. DJF is more humid during EH (~61 mm/month) and this humidity decreases continuously during MH (~55 mm/month) and LH (~53 mm/month). JJA is also more humid during the EH (~29 mm/month) and this humidity decreases during the MH and LH, being very similar in these periods (~27 mm/month) (Figure 4. a). While this annual cycle shows a wet season between September and February, the annual cycle observed today shows the wet season occurring between June and October, with a precipitation increase during boreal summer (Comrie & Glenn, 1998; Mo & Schemm, 2008).

Precipitation anomaly in the NA varies approximately from -18 to 25 mm/month in DJF and from -4 to 18 mm/month in JJA. In DJF the EH has higher average values (~5 mm/month) that decreases along the MH until the end of this period, around 5,000 years (~0 mm/month). From that period on there is an increase in these values (~3 mm/month), which decreases again at the beginning of the LH, around 4,200 years, reaching negative values (~-3 mm/month) (Figure 4. b).

In JJA the EH has higher average values (~8 mm/month) that decreases with time, around 9,000 years there is an increase in these average values (~9 mm/month) followed by another decrease trend that prevails until the end of the MH (~4 mm/month). The LH has a trend of increasing mean values (up to 5 mm/month) with an abrupt decrease at the end of this period, reaching negative values (~-4 mm/month) (Figure 4. c.).

Results from the CA are shown in Figure 5. The annual cycle shows that precipitation varies between 0 and 140 mm/month in this region throughout the Holocene. DJF initiates the EH with lower precipitation (~18 mm/month) that increases during the MH (~90 mm/month), which is the wettest period in this region, dropping the LH (~15 mm/month) to values even lower than those of the beginning of the Holocene period. JJA initiates the EH with higher precipitation (~101 mm/month), when compared to DJF, which increases during the MH and LH being very similar in these periods (~135 mm/month) (Figure 5. a). This annual cycle has the same behavior as the annual cycle observed today for this region, with the wet season occurring between May and October, with a more pronounced increase in precipitation during boreal summer (Gamble & Curtis, 2008; Herrera et al., 2020; Singh, 1997).

Precipitation anomaly in the CA varies approximately from 0 to 17 mm/month in DJF and from -40 to 30 mm/month in JJA. In DJF the EH has an oscillation in the average values of the precipitation anomaly, which tends to decrease until the end of that period around 8000 years (8 to 2 mm/month). During the MH there is also an oscillation in the average of these values, which starts lower and tends to increase until approximately 5000 years (2 to 6 mm/month). Thereafter, there is a downward trend in the mean values of the precipitation anomaly for the rest of the MH and for most of the LH (6 to 2 mm/month), with even greater decrease at the end of this period (~0 mm/month) (Figure 5. b).

In JJA the EH has an oscillation in the average values of the precipitation anomaly, which starts with lower average values increase until the end of this period (-30 to -15 mm/month), around 9,000 years, when there is a decrease in these average values (~ -30 mm/month). During the MH there is also an oscillation in the average of these values, which starts lower and increase until about 6,000 years (increasing from -30 to 5 mm/month). Thereafter, there is a slight upward trend in mean values during the rest of MH and throughout LH (~10 mm/month) (Figure 5. c). At both seasons it is possible to observe abrupt changes in the precipitation anomaly related to the Younger Dryas (YD) at the beginning of the EH and the 8,200 years event.

Results from the NSA are shown in Figure 6. The annual cycle shows that precipitation varies between 0 and 160 mm/month in this region throughout the Holocene. DJF has more precipitation during EH (~90 mm/month) and precipitation decreases during MH (~88 mm/month) and continues to decrease during LH (~75 mm/month), being lower in this period when compared to the other two periods. JJA also has more precipitation during the EH (~135 mm/month) and this precipitation continues to decrease during MH (~126 mm/month) and LH (~117 mm/month) (Figure 6. a). While this annual cycle shows a wet season between March and August, the annual cycle observed today shows the wet season occurring between December and April, with a precipitation increase during DJF (Zeng, 1999).

Precipitation anomaly in the NSA varies approximately from -10 to 42 mm/month in DJF and from -18 to 32 mm/month in JJA. In DJF the EH has an oscillation in the average values of the precipitation anomaly, which starts to increase around 11,000 years until about 9,000 years (from 18 to 30 mm/month), when they decrease until the end of that period (~18 mm/month). The MH starts with these lower values that increase until about 7,000 years (~30 mm/month). Thereafter, there is a negative trend in the average values of the precipitation anomaly for the rest of the MH (~15 mm/month) and for the entire LH (until ~ -10 mm/month) (Figure 6. b).

In JJA the EH has higher average values that decreases around 10,000 years (from 18 to 8 mm/month) and increases again at the end of that period (~18 mm/month). The MH starts with these lower values until around 8,000 years, when there is a tendency for the average values of the precipitation anomaly to decrease throughout the rest of the MH (~0 mm/month) and throughout the LH (until ~ -18 mm/month) (Figure 6. c). At both seasons it is possible to observe abrupt changes in the precipitation anomaly related to the YD at the beginning of the EH and the 8,200 years event.

Results from the NESA are shown in Figure 7. The annual cycle shows that precipitation varies between 0 and 210 mm/month in this region throughout the Holocene. DJF has more precipitation during EH (~208 mm/month), that precipitation decreases a little during MH (~183 mm/month) and continues to decrease during LH (~169 mm/month). JJA has little variation in precipitation during the Holocene period when compared to the variation observed during DJF, however it was possible to observe that there is a small increase in humidity during the LH (~11 mm/month) when compared to the other periods (~10 mm/month) (Figure 7. a). This annual cycle has the same behavior

as the annual cycle observed today for this region, with the wet season occurring between January and May, with a precipitation increase during DJF (Hastenrath, 2006).

Precipitation anomaly in the NSA varies approximately from -40 to 75 mm/month in DJF and from -2.8 to 0 mm/month in JJA. In DJF the EH has an oscillation in the average values of the precipitation anomaly, which starts to decrease around 11,000 years until about 9,000 years (from 50 to 13 mm/month), when they increase until the end of that period (~60 mm/month). The MH starts with these highest values that decreases around 8,000 years (~10 mm/month) to increase again until about 7,000 years (~25 mm/month). Thereafter, there is a downward trend in the mean values of the precipitation anomaly for the rest of the MH and most of the LH (~ -5 mm/month), with a decrease at the end of this period (~ -25 mm/month) (Figure 7. b).

In JJA the EH also has an oscillation in the average values of the precipitation anomaly that decreases at the beginning of that period until around 11,500 years (from 0 to -1 mm/month) to increase again until around 11,000 years (~ -0.4 mm/month). After this period there is a tendency for these values to decrease until around 9,000 years (~ -1.6 mm/month), when these values increase again until the end of this period (~ -0.5 mm/month). The MH starts with these highest values which tend to decrease until about 6,000 years (~ 1.8 mm/month), when there is a tendency for these values to increase during the rest of the MH (~ -1 mm/month) and LH (~ -0.2 mm/month) (Figure 7. c). At both seasons it is possible to observe abrupt changes in the precipitation anomaly related to the YD at the beginning of the EH and the 8,200 years event.

Results from the CSA are shown in Figure 8. The annual cycle shows that precipitation varies between 0 and 245 mm/month in this region throughout the Holocene. DJF initiates the EH with precipitation ~240 mm/month, that decreases during the MH (~229 mm/month) and increases again during the LH (~242 mm/month). JJA has the same behavior, initiates the EH with a certain precipitation (~1.8 mm/month), that decreases during the MH (~1.7 mm/month) and increases again during the LH (~1.95 mm/month). In this region it can be observed that JJA is the wettest period in this region in all considered periods, and that during JJA this region has much lower precipitation than in any other season (-1.95 to 1.7 mm/month) (Figure 8. a). This annual cycle has the same behavior as the annual cycle observed today for this region, with the wet season occurring between October and March, with a precipitation increase during DJF (Butler et al., 2012; Gan et al., 2004; Prado et al., 2021).

Precipitation anomaly in the CSA varies approximately from -75 to 15 mm/month in DJF and from -1 to 0.75 mm/month in JJA. In DJF the EH has a tendency for the average values of the precipitation anomaly to decrease until around 9,000 years (decreasing from 0.25 to -0.5 mm/month), when these values increase until the end of that period (\sim -0.1 mm/month). The MH starts with these highest values which tend to decrease until about 6,000 years (\sim -31 mm/month). From there, there is a tendency for the average values of the precipitation anomaly to increase for the rest of the MH (\sim -29 mm/month) and for most of the LH (\sim 5 mm/month), with a decrease at the end of this period (from -5 to -15 mm/month) (Figure 8. b).

In JJA the EH has a tendency for the average values of the precipitation anomaly to decrease until around 9,000 years (from 0.25 to -0.5 mm/month), when these values increase until the end of that period (\sim -0.25 mm/month). The MH starts with these highest values which tend to decrease until about 6,000 years (\sim -0.6 mm/month). From there, there is a trend towards an increase in the mean values of the precipitation anomaly for the rest of the MH (\sim -0.2 mm/month) and LH (\sim 0.1 mm/month) (Figure 8. c). At both seasons it is possible to observe abrupt changes in the precipitation anomaly related to the 8,200 years event.

References

Ait Brahim, Y., Peros, M. C., Viau, A. E., Liedtke, M., Pajón, J. M., Valdes, J., Li, X., Edwards, R. L., Reinhardt, E. G., & Oliva, F. (2022). Hydroclimate variability in the Caribbean during North Atlantic Heinrich cooling events (H8 and H9). Scientific Reports, 12(1), 20719. https://doi.org/10.1038/s41598-022-24610-x

Akers, P. D., Brook, G. A., Railsback, L. B., Liang, F., Iannone, G., Webster, J. W., Reeder, P. P., Cheng, H., & Edwards, R. L. (2016). An extended and higher-resolution record of climate and land use from stalagmite MC01 from Macal Chasm, Belize, revealing connections between major dry events, overall climate variability, and Maya sociopolitical changes. Palaeogeography, Palaeoclimatology, Palaeoecology, 459, 268–288. https://doi.org/10.1016/j.palaeo.2016.07.007

- Anderson, L. (2011). Holocene record of precipitation seasonality from lake calcite δ18O in the central Rocky Mountains, United States. Geology, 39(3), 211–214. https://doi.org/10.1130/G31575.1
- Anderson, L. (2012). Rocky Mountain hydroclimate: Holocene variability and the role of insolation, ENSO, and the North American Monsoon. Global and Planetary Change, 92–93, 198–208. https://doi.org/10.1016/j.gloplacha.2012.05.012
- Apaéstegui, J., Cruz, F. W., Sifeddine, A., Vuille, M., Espinoza, J. C., Guyot, J. L., Khodri, M., Strikis, N., Santos, R. V., Cheng, H., Edwards, L., Carvalho, E., & Santini, W. (2014). Hydroclimate variability of the northwestern Amazon Basin near the Andean foothills of Peru related to the South American Monsoon System during the last 1600 years. Climate of the Past, 10(6), 1967–1981. https://doi.org/10.5194/cp-10-1967-2014
- Asmerom, Y., Polyak, V. J., Rasmussen, J. B. T., Burns, S. J., & Lachniet, M. (2013). Multidecadal to multicentury scale collapses of Northern Hemisphere monsoons over the past millennium. Proceedings of the National Academy of Sciences, 110(24), 9651–9656. https://doi.org/10.1073/pnas.1214870110
- Bahr, A., Kaboth-Bahr, S., Jaeschke, A., Chiessi, C., Cruz, F., Carvalho, L., Rethemeyer, J., Schefuß, E., Geppert, P., Albuquerque, A. L., Pross, J., & Friedrich, O. (2021). Late Holocene Precipitation Fluctuations in South America Triggered by Variability of the North Atlantic Overturning Circulation. Paleoceanography and Paleoclimatology, 36(9). https://doi.org/10.1029/2021PA004223
- Beal, S. A., Kelly, M. A., Stroup, J. S., Jackson, B. P., Lowell, T. V., & Tapia, P. M. (2014). Natural and anthropogenic variations in atmospheric mercury deposition

- during the Holocene near Quelccaya Ice Cap, Peru. Global Biogeochemical Cycles, 28(4), 437–450. https://doi.org/10.1002/2013GB004780
- Behling, H., Carlos Berrio, J., & Hooghiemstra, H. (1999). Late Quaternary pollen records from the middle Caquetá river basin in central Colombian Amazon. Palaeogeography, Palaeoclimatology, Palaeoecology, 145(1–3), 193–213. https://doi.org/10.1016/S0031-0182(98)00105-9
- Behling, H., & Lima da Costa, M. (2001). Holocene vegetational and coastal environmental changes from the Lago Crispim record in northeastern Pará State, eastern Amazonia. Review of Palaeobotany and Palynology, 114(3–4), 145–155. https://doi.org/10.1016/S0034-6667(01)00044-6
- Benson, L., Kashgarian, M., Rye, R., Lund, S., Paillet, F., Smoot, J., Kester, C., Mensing, S., Meko, D., & Lindström, S. (2002). Holocene multidecadal and multicentennial droughts affecting Northern California and Nevada. Quaternary Science Reviews, 21(4–6), 659–682. https://doi.org/10.1016/S0277-3791(01)00048-8
- Berger, A., & Loutre, M. F. (1991). Insolation values for the climate of the last 10 million years. Quaternary Science Reviews, 10(4), 297–317. https://doi.org/10.1016/0277-3791(91)90033-Q
- Bernal, J. P., Cruz, F. W., Stríkis, N. M., Wang, X., Deininger, M., Catunda, M. C. A., Ortega-Obregón, C., Cheng, H., Edwards, R. L., & Auler, A. S. (2016). High-resolution Holocene South American monsoon history recorded by a speleothem from Botuverá Cave, Brazil. Earth and Planetary Science Letters, 450, 186–196. https://doi.org/10.1016/j.epsl.2016.06.008
- Bhattacharya, T., Byrne, R., Böhnel, H., Wogau, K., Kienel, U., Ingram, B. L., & Zimmerman, S. (2015). Cultural implications of late Holocene climate change in the

- Cuenca Oriental, Mexico. Proceedings of the National Academy of Sciences, 112(6), 1693–1698. https://doi.org/10.1073/pnas.1405653112
- Bird, B. W., Abbott, M. B., Vuille, M., Rodbell, D. T., Stansell, N. D., & Rosenmeier, M. F. (2011). A 2,300-year-long annually resolved record of the South American summer monsoon from the Peruvian Andes. Proceedings of the National Academy of Sciences, 108(21), 8583–8588. https://doi.org/10.1073/pnas.1003719108
- Bird, B. W., Rudloff, O., Escobar, J., Gilhooly, W. P., Correa-Metrio, A., Vélez, M., & Polissar, P. J. (2018). Paleoclimate support for a persistent dry island effect in the Colombian Andes during the last 4700 years. The Holocene, 28(2), 217–228. https://doi.org/10.1177/0959683617721324
- Brugger, S. O., Gobet, E., van Leeuwen, J. F. N., Ledru, M.-P., Colombaroli, D., van der Knaap, W. O., Lombardo, U., Escobar-Torrez, K., Finsinger, W., Rodrigues, L., Giesche, A., Zarate, M., Veit, H., & Tinner, W. (2016). Long-term man–environment interactions in the Bolivian Amazon: 8000 years of vegetation dynamics. Quaternary Science Reviews, 132, 114–128. https://doi.org/10.1016/j.quascirev.2015.11.001
- Bush, M. B., Miller, M. C., De Oliveira, P. E., & Colinvaux, P. A. (2000). Two histories of environmental change and human disturbance in eastern lowland Amazonia. The Holocene, 10(5), 543–553. https://doi.org/10.1191/095968300672647521
- Bush, M. B., Silman, M. R., de Toledo, M. B., Listopad, C., Gosling, W. D., Williams,
 C., de Oliveira, P. E., & Krisel, C. (2007). Holocene fire and occupation in
 Amazonia: records from two lake districts. Philosophical Transactions of the Royal
 Society B: Biological Sciences, 362(1478), 209–218.
 https://doi.org/10.1098/rstb.2006.1980

- Butler, A., Meir, P., Saiz, G., Maracahipes, L., Marimon, B. S., & Grace, J. (2012). Annual variation in soil respiration and its component parts in two structurally contrasting woody savannas in Central Brazil. Plant and Soil, 352(1–2), 129–142. https://doi.org/10.1007/s11104-011-0984-7
- Carson, J. F., Mayle, F. E., Whitney, B. S., Iriarte, J., & Soto, J. D. (2016). Pre-Columbian ring ditch construction and land use on a 'chocolate forest island' in the Bolivian Amazon. Journal of Quaternary Science, 31(4), 337–347. https://doi.org/10.1002/jqs.2835
- Carson, J. F., Watling, J., Mayle, F. E., Whitney, B. S., Iriarte, J., Prümers, H., & Soto, J. D. (2015). Pre-Columbian land use in the ring-ditch region of the Bolivian Amazon. The Holocene, 25(8), 1285–1300. https://doi.org/10.1177/0959683615581204
- Carson, J. F., Whitney, B. S., Mayle, F. E., Iriarte, J., Prümers, H., Soto, J. D., & Watling, J. (2014). Environmental impact of geometric earthwork construction in pre-Columbian Amazonia. Proceedings of the National Academy of Sciences, 111(29), 10497–10502. https://doi.org/10.1073/pnas.1321770111
- Cassino, R. F., Ledru, M.-P., Santos, R. de A., & Favier, C. (2020). Vegetation and fire variability in the central Cerrados (Brazil) during the Pleistocene-Holocene transition was influenced by oscillations in the SASM boundary belt. Quaternary Science Reviews, 232, 106209. https://doi.org/10.1016/j.quascirev.2020.106209
- Cheng, H., Sinha, A., Cruz, F. W., Wang, X., Edwards, R. L., d'Horta, F. M., Ribas, C.
 C., Vuille, M., Stott, L. D., & Auler, A. S. (2013). Climate change patterns in
 Amazonia and biodiversity. Nature Communications, 4(1), 1411.
 https://doi.org/10.1038/ncomms2415

- Comrie, A., & Glenn, E. (1998). Principal components-based regionalization of precipitation regimes across the southwest United States and Northern Mexico, with an application to monsoon precipitation variability. Climate Research, 10, 201–215. https://doi.org/10.3354/cr010201
- Conroy, J. L., Overpeck, J. T., Cole, J. E., Shanahan, T. M., & Steinitz-Kannan, M. (2008). Holocene changes in eastern tropical Pacific climate inferred from a Galápagos lake sediment record. Quaternary Science Reviews, 27(11–12), 1166–1180. https://doi.org/10.1016/j.quascirev.2008.02.015
- Conroy, J. L., Thompson, D. M., Collins, A., Overpeck, J. T., Bush, M. B., & Cole, J. E. (2014). Climate influences on water and sediment properties of Genovesa Crater Lake, Galápagos. Journal of Paleolimnology, 52(4), 331–347. https://doi.org/10.1007/s10933-014-9797-z
- Cruz, F. W., Burns, S. J., Karmann, I., Sharp, W. D., & Vuille, M. (2006). Reconstruction of regional atmospheric circulation features during the late Pleistocene in subtropical Brazil from oxygen isotope composition of speleothems. Earth and Planetary Science Letters, 248(1–2), 495–507. https://doi.org/10.1016/j.epsl.2006.06.019
- Cruz, F. W., Vuille, M., Burns, S. J., Wang, X., Cheng, H., Werner, M., Lawrence Edwards, R., Karmann, I., Auler, A. S., & Nguyen, H. (2009). Orbitally driven east—west antiphasing of South American precipitation. Nature Geoscience, 2(3), 210–214. https://doi.org/10.1038/ngeo444
- Curtis, J. H., Brenner, M., Hodell, D. A., Balser, R. A., Islebe, G. A., & Hooghiemstra, H. (1998). A multi-proxy study of Holocene environmental change in the Maya Lowlands of Peten, Guatemala. Journal of Paleolimnology, 19(2), 139–159. https://doi.org/10.1023/A:1007968508262

- de Jong, R., von Gunten, L., Maldonado, A., & Grosjean, M. (2013). Late Holocene summer temperatures in the central Andes reconstructed from the sediments of high-elevation Laguna Chepical, Chile (32° S). Climate of the Past, 9(4), 1921–1932. https://doi.org/10.5194/cp-9-1921-2013
- De Toledo, M. B., & Bush, M. B. (2007). A mid-Holocene environmental change in Amazonian savannas. Journal of Biogeography, 34(8), 1313–1326. https://doi.org/10.1111/j.1365-2699.2006.01606.x
- Enters, D., Behling, H., Mayr, C., Dupont, L., & Zolitschka, B. (2010). Holocene environmental dynamics of south-eastern Brazil recorded in laminated sediments of Lago Aleixo. Journal of Paleolimnology, 44(1), 265–277. https://doi.org/10.1007/s10933-009-9402-z
- Evans, N. P., Bauska, T. K., Gázquez-Sánchez, F., Brenner, M., Curtis, J. H., & Hodell,
 D. A. (2018). Quantification of drought during the collapse of the classic Maya civilization. Science, 361(6401), 498–501. https://doi.org/10.1126/science.aas9871
- Fontes, D., Cordeiro, R. C., Martins, G. S., Behling, H., Turcq, B., Sifeddine, A., Seoane, J. C. S., Moreira, L. S., & Rodrigues, R. A. (2017). Paleoenvironmental dynamics in South Amazonia, Brazil, during the last 35,000 years inferred from pollen and geochemical records of Lago do Saci. Quaternary Science Reviews, 173, 161–180. https://doi.org/10.1016/j.quascirev.2017.08.021
- Fornace, K. L., Hughen, K. A., Shanahan, T. M., Fritz, S. C., Baker, P. A., & Sylva, S. P. (2014). A 60,000-year record of hydrologic variability in the Central Andes from the hydrogen isotopic composition of leaf waxes in Lake Titicaca sediments. Earth and Planetary Science Letters, 408, 263–271. https://doi.org/10.1016/j.epsl.2014.10.024

- Fornace, K. L., Whitney, B. S., Galy, V., Hughen, K. A., & Mayle, F. E. (2016). Late Quaternary environmental change in the interior South American tropics: new insight from leaf wax stable isotopes. Earth and Planetary Science Letters, 438, 75–85. https://doi.org/10.1016/j.epsl.2016.01.007
- Frugone-Álvarez, M., Latorre, C., Barreiro-Lostres, F., Giralt, S., Moreno, A., Polanco-Martínez, J., Maldonado, A., Carrevedo, M. L., Bernárdez, P., Prego, R., Delgado Huertas, A., Fuentealba, M., & Valero-Garcés, B. (2020). Volcanism and climate change as drivers in Holocene depositional dynamic of Laguna del Maule (Andes of central Chile 36° S). Climate of the Past, 16(4), 1097–1125. https://doi.org/10.5194/cp-16-1097-2020
- Gamble, D. W., & Curtis, S. (2008). Caribbean precipitation: review, model and prospect.

 Progress in Physical Geography: Earth and Environment, 32(3), 265–276.

 https://doi.org/10.1177/0309133308096027
- Gan, M. A., Kousky, V. E., & Ropelewski, C. F. (2004). The South America Monsoon Circulation and Its Relationship to Rainfall over West-Central Brazil. Journal of Climate, 17(1), 47–66. https://doi.org/10.1175/1520-0442(2004)017<0047:TSAMCA>2.0.CO;2
- Hardage, K., Street, J., Herrera-Silveira, J. A., Oberle, F. K. J., & Paytan, A. (2022). Late Holocene environmental change in Celestun Lagoon, Yucatan, Mexico. Journal of Paleolimnology, 67(2), 131–162. https://doi.org/10.1007/s10933-021-00227-4
- Hastenrath, S. (2006). Circulation and teleconnection mechanisms of Northeast Brazil droughts. Progress in Oceanography, 70(2–4), 407–415. https://doi.org/10.1016/j.pocean.2005.07.004

- Hermanowski, B., da Costa, M. L., & Behling, H. (2012). Environmental changes in southeastern Amazonia during the last 25,000 yr revealed from a paleoecological record. Quaternary Research, 77(1), 138–148. https://doi.org/10.1016/j.yqres.2011.10.009
- Hermanowski, B., Da Costa, M. L., & Behling, H. (2015). Possible linkages of palaeofires in southeast Amazonia to a changing climate since the Last Glacial Maximum. Vegetation History and Archaeobotany, 24(2), 279–292. https://doi.org/10.1007/s00334-014-0472-0
- Herrera, D. A., Ault, T. R., Carrillo, C. M., Fasullo, J. T., Li, X., Evans, C. P., Alessi, M. J., & Mahowald, N. M. (2020). Dynamical Characteristics of Drought in the Caribbean from Observations and Simulations. Journal of Climate, 33(24), 10773–10797. https://doi.org/10.1175/JCLI-D-20-0100.1
- Hiner, C. A., Kirby, M. E., Bonuso, N., Patterson, W. P., Palermo, J., & Silveira, E. (2016). Late Holocene hydroclimatic variability linked to Pacific forcing: evidence from Abbott Lake, coastal central California. Journal of Paleolimnology, 56(4), 299–313. https://doi.org/10.1007/s10933-016-9912-4
- Hodell, D. A., Brenner, M., & Curtis, J. H. (2005). Terminal Classic drought in the northern Maya lowlands inferred from multiple sediment cores in Lake Chichancanab (Mexico). Quaternary Science Reviews, 24(12–13), 1413–1427. https://doi.org/10.1016/j.quascirev.2004.10.013
- Horbe, A. M. C., Behling, H., Nogueira, A. C. R., & Mapes, R. (2011). Environmental changes in the western Amazônia: morphological framework, geochemistry, palynology and radiocarbon dating data. Anais Da Academia Brasileira de Ciências, 83(3), 863–874. https://doi.org/10.1590/S0001-37652011005000030

- Irion, G., Bush, M. B., Nunes de Mello, J. A., Stüben, D., Neumann, T., Müller, G., Morais de, J. O., & Junk, J. W. (2006). A multiproxy palaeoecological record of Holocene lake sediments from the Rio Tapajós, eastern Amazonia. Palaeogeography, Palaeoclimatology, Palaeoecology, 240(3–4), 523–535. https://doi.org/10.1016/j.palaeo.2006.03.005
- Jeske-Pieruschka, V., & Behling, H. (2012). Palaeoenvironmental history of the São Francisco de Paula region in southern Brazil during the late Quaternary inferred from the Rincão das Cabritas core. The Holocene, 22(11), 1251–1262. https://doi.org/10.1177/0959683611414930
- Jeske-Pieruschka, V., Pillar, V. D., De Oliveira, M. A. T., & Behling, H. (2013). New insights into vegetation, climate and fire history of southern Brazil revealed by a 40,000 year environmental record from the State Park Serra do Tabuleiro. Vegetation History and Archaeobotany, 22(4), 299–314. https://doi.org/10.1007/s00334-012-0382-y
- Kanner, L. C., Burns, S. J., Cheng, H., Edwards, R. L., & Vuille, M. (2013). High-resolution variability of the South American summer monsoon over the last seven millennia: insights from a speleothem record from the central Peruvian Andes.
 Quaternary Science Reviews, 75, 1–10.
 https://doi.org/10.1016/j.quascirev.2013.05.008
- Kirby, M. E., Feakins, S. J., Hiner, C. A., Fantozzi, J., Zimmerman, S. R. H., Dingemans, T., & Mensing, S. A. (2014). Tropical Pacific forcing of Late-Holocene hydrologic variability in the coastal southwest United States. Quaternary Science Reviews, 102, 27–38. https://doi.org/10.1016/j.quascirev.2014.08.005

- Kirby, M. E., Lund, S. P., Patterson, W. P., Anderson, M. A., Bird, B. W., Ivanovici, L., Monarrez, P., & Nielsen, S. (2010). A Holocene record of Pacific Decadal Oscillation (PDO)-related hydrologic variability in Southern California (Lake Elsinore, CA).
 Journal of Paleolimnology, 44(3), 819–839. https://doi.org/10.1007/s10933-010-9454-0
- Kirby, M. E., Zimmerman, S. R. H., Patterson, W. P., & Rivera, J. J. (2012). A 9170-year record of decadal-to-multi-centennial scale pluvial episodes from the coastal Southwest United States: a role for atmospheric rivers? Quaternary Science Reviews, 46, 57–65. https://doi.org/10.1016/j.quascirev.2012.05.008
- Kock, S. T., Schittek, K., Mächtle, B., Wissel, H., Maldonado, A., & Lücke, A. (2019).
 Late Holocene environmental changes reconstructed from stable isotope and geochemical records from a cushion-plant peatland in the Chilean Central Andes (27°S). Journal of Quaternary Science, 34(2), 153–164.
 https://doi.org/10.1002/jqs.3088
- Kock, S. T., Schittek, K., Wissel, H., Vos, H., Ohlendorf, C., Schäbitz, F., Lupo, L. C.,
 Kulemeyer, J. J., & Lücke, A. (2019). Stable Oxygen Isotope Records (δ18O) of a
 High-Andean Cushion Peatland in NW Argentina (24° S) Imply South American
 Summer Monsoon Related Moisture Changes During the Late Holocene. Frontiers in Earth Science, 7. https://doi.org/10.3389/feart.2019.00045
- Lachniet, M. S., Asmerom, Y., Burns, S. J., Patterson, W. P., Polyak, V. J., & Seltzer, G.
 O. (2004). Tropical response to the 8200 yr B.P. cold event? Speleothem isotopes indicate a weakened early Holocene monsoon in Costa Rica. Geology, 32(11), 957. https://doi.org/10.1130/G20797.1

- Lane, C. S., Horn, S. P., Mora, C. I., & Orvis, K. H. (2009). Late-Holocene paleoenvironmental change at mid-elevation on the Caribbean slope of the Cordillera Central, Dominican Republic: a multi-site, multi-proxy analysis. Quaternary Science Reviews, 28(23–24), 2239–2260. https://doi.org/10.1016/j.quascirev.2009.04.013
- Leonhardt, A., & Lorscheitter, M. L. (2010). The last 25,000 years in the Eastern Plateau of Southern Brazil according to Alpes de São Francisco record. Journal of South American Earth Sciences, 29(2), 454–463. https://doi.org/10.1016/j.jsames.2009.09.003
- Maezumi, S. Y., Power, M. J., Mayle, F. E., McLauchlan, K. K., & Iriarte, J. (2015). Effects of past climate variability on fire and vegetation in the cerrãdo savanna of the Huanchaca Mesetta, NE Bolivia. Climate of the Past, 11(6), 835–853. https://doi.org/10.5194/cp-11-835-2015
- Mark, S. Z., Abbott, M. B., Rodbell, D. T., & Moy, C. M. (2022). XRF analysis of Laguna Pallcacocha sediments yields new insights into Holocene El Niño development.

 Earth and Planetary Science Letters, 593, 117657. https://doi.org/10.1016/j.epsl.2022.117657
- Metcalfe, S. E., Jones, M. D., Davies, S. J., Noren, A., & MacKenzie, A. (2010). Climate variability over the last two millennia in the North American Monsoon region, recorded in laminated lake sediments from Laguna de Juanacatlán, Mexico. The Holocene, 20(8), 1195–1206. https://doi.org/10.1177/0959683610371994
- Mo, K. C., & Schemm, J. E. (2008). Droughts and Persistent Wet Spells over the United States and Mexico. Journal of Climate, 21(5), 980–994. https://doi.org/10.1175/2007JCLI1616.1

- Mosblech, N. A. S., Bush, M. B., Gosling, W. D., Hodell, D., Thomas, L., van Calsteren, P., Correa-Metrio, A., Valencia, B. G., Curtis, J., & van Woesik, R. (2012). North Atlantic forcing of Amazonian precipitation during the last ice age. Nature Geoscience, 5(11), 817–820. https://doi.org/10.1038/ngeo1588
- Nogueira, J., Evangelista, H., Valeriano, C. de M., Sifeddine, A., Neto, C., Vaz, G., Moreira, L. S., Cordeiro, R. C., Turcq, B., Aniceto, K. C., Neto, A. B., Martins, G., Barbosa, C. G. G., Godoi, R. H. M., & Shimizu, M. H. (2021). Dust arriving in the Amazon basin over the past 7,500 years came from diverse sources. Communications Earth & Environment, 2(1), 5. https://doi.org/10.1038/s43247-020-00071-w
- Obrist-Farner, J., & Rice, P. M. (2019). Nixtun-Ch'ich' and its environmental impact: Sedimentological and archaeological correlates in a core from Lake Petén Itzá in the southern Maya lowlands, Guatemala. Journal of Archaeological Science: Reports, 26, 101868. https://doi.org/10.1016/j.jasrep.2019.05.033
- Parsons, L. A., LeRoy, S., Overpeck, J. T., Bush, M., Cárdenes-Sandí, G. M., & Saleska, S. (2018). The Threat of Multi-Year Drought in Western Amazonia. Water Resources Research, 54(9), 5890–5904. https://doi.org/10.1029/2017WR021788
- Pessenda, L. C. R., Ledru, M. P., Gouveia, , S. E.MN., Aravena, R., Ribeiro, A. S., Bendashsollil, J. A., & Boulet, R. (2005). Holocene palaeoenvironmental reconstruction in norteastern Brazi inferred from polen,, charcoal and carboon isotope records. The Holocene, 15(6), 812–820. https://doi.org/10.1191/0959683605hl855ra
- Pires, G. L. P., Meyer, K. E. B., & Gomes, M. O. S. (2016). Palinologia da Vereda Juquinha/Cuba, Parque Estadual da Serra do Cabral, Minas Gerais, Brasil. Revista Brasileira de Paleontologia, 19(1), 95–110. https://doi.org/10.4072/rbp.2016.1.08

- Pollock, A. L., van Beynen, P. E., DeLong, K. L., Polyak, V., & Asmerom, Y. (2017). A speleothem-based mid-Holocene precipitation reconstruction for West-Central Florida. The Holocene, 27(7), 987–996. https://doi.org/10.1177/0959683616678463
- Prado, L. F., Wainer, I., Yokoyama, E., Khodri, M., & Garnier, J. (2021). Changes in summer precipitation variability in central Brazil over the past eight decades.
 International Journal of Climatology, 41(8), 4171–4186.
 https://doi.org/10.1002/joc.7065
- Raczka, M. F., De Oliveira, P. E., Bush, M., & McMichael, C. H. (2013). Two paleoecological histories spanning the period of human settlement in southeastern Brazil. Journal of Quaternary Science, 28(2), 144–151. https://doi.org/10.1002/jqs.2597
- Schittek, K., Forbriger, M., Mächtle, B., Schäbitz, F., Wennrich, V., Reindel, M., & Eitel, B. (2015). Holocene environmental changes in the highlands of the southern Peruvian Andes (14° S) and their impact on pre-Columbian cultures. Climate of the Past, 11(1), 27–44. https://doi.org/10.5194/cp-11-27-2015
- Schittek, K., Kock, S. T., Lücke, A., Hense, J., Ohlendorf, C., Kulemeyer, J. J., Lupo, L. C., & Schäbitz, F. (2016). A high-altitude peatland record of environmental changes in the NW Argentine Andes (24 ° S) over the last 2100 years. Climate of the Past, 12(5), 1165–1180. https://doi.org/10.5194/cp-12-1165-2016
- Shuman, B. N., Carter, G. E., Hougardy, D. D., Powers, K., & Shinker, J. J. (2014). A north-south moisture dipole at multi-century scales in the Central and Southern Rocky Mountains, U.S.A., during the late Holocene. Rocky Mountain Geology, 49(1), 33–49. https://doi.org/10.2113/gsrocky.49.1.33

- Sifeddine, A., Martin, L., Turcq, B., Volkmer-Ribeiro, C., Soubiès, F., Cordeiro, R. C., & Suguio, K. (2001). Variations of the Amazonian rainforest environment: a sedimentological record covering 30,000 years. Palaeogeography, Palaeoclimatology, Palaeoecology, 168(3–4), 221–235. https://doi.org/10.1016/S0031-0182(00)00256-X
- Singh, B. (1997). Climate changes in the greater and southern Caribbean. International Journal of Climatology, 17(10), 1093–1114. https://doi.org/10.1002/(SICI)1097-0088(199708)17:10<1093::AID-JOC187>3.0.CO;2-L
- Stansell, N. D., Abbott, M. B., Rull, V., Rodbell, D. T., Bezada, M., & Montoya, E. (2010). Abrupt Younger Dryas cooling in the northern tropics recorded in lake sediments from the Venezuelan Andes. Earth and Planetary Science Letters, 293(1–2), 154–163. https://doi.org/10.1016/j.epsl.2010.02.040
- Stansell, N. D., Polissar, P. J., Abbott, M. B., Bezada, M., Steinman, B. A., & Braun, C. (2014). Proglacial lake sediment records reveal Holocene climate changes in the Venezuelan Andes. Quaternary Science Reviews, 89, 44–55. https://doi.org/10.1016/j.quascirev.2014.01.021
- Stansell, N. D., Rodbell, D. T., Abbott, M. B., & Mark, B. G. (2013). Proglacial lake sediment records of Holocene climate change in the western Cordillera of Peru.

 Quaternary Science Reviews, 70, 1–14.

 https://doi.org/10.1016/j.quascirev.2013.03.003
- Stansell, N. D., Rodbell, D. T., Licciardi, J. M., Sedlak, C. M., Schweinsberg, A. D., Huss, E. G., Delgado, G. M., Zimmerman, S. H., & Finkel, R. C. (2015). Late Glacial and Holocene glacier fluctuations at Nevado Huaguruncho in the Eastern Cordillera of the Peruvian Andes. Geology, 43(8), 747–750. https://doi.org/10.1130/G36735.1

- Stansell, N. D., Steinman, B. A., Abbott, M. B., Rubinov, M., & Roman-Lacayo, M. (2013). Lacustrine stable isotope record of precipitation changes in Nicaragua during the Little Ice Age and Medieval Climate Anomaly. Geology, 41(2), 151–154. https://doi.org/10.1130/G33736.1
- Stansell, N. D., Steinman, B. A., Lachniet, M. S., Feller, J., Harvey, W., Fernandez, A., Shea, C. J., Price, B., Coenen, J., Boes, M., & Perdziola, S. (2020). A lake sediment stable isotope record of late-middle to late Holocene hydroclimate variability in the western Guatemala highlands. Earth and Planetary Science Letters, 542, 116327. https://doi.org/10.1016/j.epsl.2020.116327
- Strikis, N. M., Cruz, F. W., Cheng, H., Karmann, I., Edwards, R. L., Vuille, M., Wang, X., de Paula, M. S., Novello, V. F., & Auler, A. S. (2011). Abrupt variations in South American monsoon rainfall during the Holocene based on a speleothem record from central-eastern Brazil. Geology, 39(11), 1075–1078. https://doi.org/10.1130/G32098.1
- Thompson, D. M., Conroy, J. L., Collins, A., Hlohowskyj, S. R., Overpeck, J. T., Riedinger-Whitmore, M., Cole, J. E., Bush, M. B., Whitney, H., Corley, T. L., & Kannan, M. S. (2017). Tropical Pacific climate variability over the last 6000 years as recorded in Bainbridge Crater Lake, Galápagos. Paleoceanography, 32(8), 903–922. https://doi.org/10.1002/2017PA003089
- Turcq, B., Albuquerque, A. L. S., Cordeiro, R. C., Sifeddine, A., Simoes Filho, F. F. L.,
 Souza, A. G., Abrão, J. J., Oliveira, F. B. L., Silva, A. O., & Capitâneo, J. (2002).
 Accumulation of organic carbon in five Brazilian lakes during the Holocene.
 Sedimentary Geology, 148(1–2), 319–342. https://doi.org/10.1016/S0037-0738(01)00224-X

- Urrego, D. H., Bush, M. B., Silman, M. R., Niccum, B. A., De La Rosa, P., McMichael,
 C. H., Hagen, S., & Palace, M. (2013). Holocene fires, forest stability and human occupation in south-western Amazonia. Journal of Biogeography, 40(3), 521–533.
 https://doi.org/10.1111/jbi.12016
- Wahl, D., Byrne, R., & Anderson, L. (2014). An 8700 year paleoclimate reconstruction from the southern Maya lowlands. Quaternary Science Reviews, 103, 19–25. https://doi.org/10.1016/j.quascirev.2014.08.004
- Whitney, B. S., Mayle, F. E., Punyasena, S. W., Fitzpatrick, K. A., Burn, M. J., Guillen, R., Chavez, E., Mann, D., Pennington, R. T., & Metcalfe, S. E. (2011). A 45kyr palaeoclimate record from the lowland interior of tropical South America. Palaeogeography, Palaeoclimatology, Palaeoecology, 307(1–4), 177–192. https://doi.org/10.1016/j.palaeo.2011.05.012
- Winter, A., Zanchettin, D., Lachniet, M., Vieten, R., Pausata, F. S. R., Ljungqvist, F. C.,
 Cheng, H., Edwards, R. L., Miller, T., Rubinetti, S., Rubino, A., & Taricco, C.
 (2020). Initiation of a stable convective hydroclimatic regime in Central America
 circa 9000 years BP. Nature Communications, 11(1), 716.
 https://doi.org/10.1038/s41467-020-14490-y
- Wogau, K. H., Arz, H. W., Böhnel, H. N., Nowaczyk, N. R., & Park, J. (2019). High resolution paleoclimate and paleoenvironmental reconstruction in the Northern Mesoamerican Frontier for Prehistory to Historical times. Quaternary Science Reviews, 226, 106001. https://doi.org/10.1016/j.quascirev.2019.106001
- Wong, C. I., Banner, J. L., & Musgrove, M. (2015). Holocene climate variability in Texas, USA: An integration of existing paleoclimate data and modeling with a new, high-

- resolution speleothem record. Quaternary Science Reviews, 127, 155–173. https://doi.org/10.1016/j.quascirev.2015.06.023
- Wright, K. T., Johnson, K. R., Marks, G. S., McGee, D., Bhattacharya, T., Goldsmith, G. R., Tabor, C. R., Lacaille-Muzquiz, J.-L., Lum, G., & Beramendi-Orosco, L. (2023).
 Dynamic and thermodynamic influences on precipitation in Northeast Mexico on orbital to millennial timescales. Nature Communications, 14(1), 2279.
 https://doi.org/10.1038/s41467-023-37700-9
- Yuan, F., Koran, M. R., & Valdez, A. (2013). Late Glacial and Holocene record of climatic change in the southern Rocky Mountains from sediments in San Luis Lake, Colorado, USA. Palaeogeography, Palaeoclimatology, Palaeoecology, 392, 146– 160. https://doi.org/10.1016/j.palaeo.2013.09.016
- Yuan, F., Linsley, B. K., Lund, S. P., & McGeehin, J. P. (2004). A 1200 year record of hydrologic variability in the Sierra Nevada from sediments in Walker Lake, Nevada.
 Geochemistry, Geophysics, Geosystems, 5(3).
 https://doi.org/10.1029/2003GC000652
- Zeng, N. (1999). Seasonal cycle and interannual variability in the Amazon hydrologic cycle. JOURNAL OF GEOPHYSICAL RESEARCH, , 104, 9097–9106.

Appendix II

Supplementary Material

A fully calibrated and updated mid-Holocene climate reconstruction for Eastern South America

Iuri Gorenstein a, *, Luciana F. Prado a, b, Paula R. Bianchini b, Ilana Wainer a,

Michael L. Griffiths c, Francesco S.R. Pausata d, Elder Yokoyama b

Table S.1 - Compilation Table

No	Site	Lat.	Long.	Proxy	Qualit	Reference
		(°)	(°)	Type	\mathbf{y}	
103	Dom Helvecio	-19.68	-42.59	BI/PC	0.40	Turcq et al., 2002
	Lake					
104	Feia Lake	-15.57	-47.30	BI/PC	0.43	Turcq et al., 2002
105	Lagoa do Ca,c'o	-2.96	-43.42	IF/BI	0.60	Pessenda et al.,
						2005
106	Botucatu*	-22.85	-48.48	IF/BI	0.53	Scheel-Ybert et al.,
						2003
107	Jaguariu'na*	-22.67	-47.17	IF/BI	0.50	Scheel-Ybert et al.,
						2003
108	Anhembi*	-22.75	-47.97	IF/BI	0.37	Scheel-Ybert et al.,
						2003
109	Barreirinhas	-3.00	-45.00	IF/PC	0.47	Pessenda et al.,
						2004b
110	Curucutu	-23.93	-46.65	IF/BI/PC	0.43	Pessenda et al.,
						2009
11	Lagoa Serra	-18.95	-46.83	BI	0.10	Cassino, 1992
1	Negra*					
112	Lagoa dos	-19.38	-43.90	BI	0.10	Cassino, 1992
	Olhos*					
113	Crom´ınia*	-17.28	-49.42	BI	0.43	Vicentini &

^a Instituto Oceanogra fico, Universidade de Sa~o Paulo, Sa~o Paulo, Brazil

^b Instituto de Geoci[^]encias, Universidade de Brasília, Brasília, Brazil

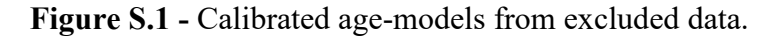
^c Department of Environmental Science, William Paterson University, Wayne, NJ, USA

^d Centre ESCER (Etude et la Simulation du Climat a` l'Echelle Regionale) and GEOTOP (Research Center on the Dynamics of the Earth System), Department of Earth and Atmospheric Sciences, University of Quebec in Montreal, Montreal, QC, Canada

						Labouriau, 1996
114	Paix~ao Cave	-12.63	-41.02	IF	4.00	Barreto, 2010
115	Tamboril	-16	-47	IF	0.74	Ward et al., 2019
116	Para'iso	-4	-55	IF	0.96	Ward et al., 2019
	Para'iso	-4	-55	IF	0.33	Wang et al., 2017
	Para'iso	-4	-55	IF	0.73	Wang et al., 2017
119	Jaragua	-21	-56	IF	0.89	Ward et al., 2019
120	Jaragua	-21	-56	IF	0.72	Novello et al.,
	8					2017
121	Botuver'a Caves	-27	-49	IF	1.17	Ward et al., 2019
122	Botuver'a Caves	-27	-49	IF	0.66	Bernal et al., 2016
123	Primeiro	-20.41	-41.66	BI	1.03	Pereira et al., 2012
	Rancho					
	Caparao'					
124	Ciama Serra do	-27.9	-48.87	BI	0.83	Jeske-Pieruschka et
	tabuleiro					al., 2013
125	Rinca~o das	-29.48	-50.57	BI	0.65	Jeske-Pieruschka &
	Cabritas					Behling, 2011
126	Sa~o Paulo Bight	t-18.3	-43.4	IF/BI/PC	21.17	Mahiques et al.,
	C					2009
127	Pinheiro Mire	-4.3	-63.2	IF/BI	0.43	Hora'k-Terra et al.,
						2020
128	Lago	-12.6	-65.6	PC/IF	0.38	Horbe et al., 2011
	Rogaguado					
129	Lago	-17	-69	BI	0.80	Brugger et al.,
	Rogaguado					2016
130	Lake Titicaca	-13.2	-63.31	IF/BI	0.40	Weide et al., 2017
131	Laguna Or'icore	-0.42	-72	IF/BI	0.41	Carson et al., 2014
132	Pantano de	-0.27	76.27	IF/BI	0.49	Behling et al.,
	Monica					1999
133	Rio Yasuni	-6.21	-50.23	IF/BI	0.47	Weng et al., 2002
134	Lagoa Da	-6.21	-50.24	IF/BI	0.44	Hermanowski et
	Cachoeira					al., 2015
135	Pantano da	-6.21	-50.24	IF/BI	0.52	Hermanowski et
	Mauritia					al., 2012
136	Porto Velho	-8.46	-63.56	IF/BI	0.40	Cohen et al., 2014
137	Laguna Granja	-13.15	-63.42	IF/BI	0.38	Carson et al., 2015
138	La Luna	-13.35	-63.34	IF/BI	0.55	Carson et al., 2016
139	Huanchaca	-14.32	-60.43	IF/BI/PC	C1.18	Maezumi et al.,
						2015
140	Vereda Juquinha	-17.56	-44.15	IBI	1.30	Pires et al., 2016
141	Lagoa Olhos	-19.38	-43.54	BI	0.56	Raczka et al., 2013
	D'′agua					
142	Lagoa dos	-19.39	-43.59	BI	0.50	Raczka et al., 2013
	Mares					
143	Colonia Crater	-23.52	-46.42	IF/BI	0.63	Ledru et al., 2009
144	1	-29.29	-50.37	IF/BI	0.46	Leonhardt &
	Francisco					Lorscheitter, 2010
145	Flona	-7.2	-39.25	IF/BI	0.93	Pessenda et al.,
						2010
146	Parna	-4.1	-41.37	IF/BI	0.73	Pessenda et al.,
						2010

147	Porto Velho - Humaita*	-8	-63.3	IF/BI	0.27	Freitas et al., 2001
148	Ariquemes*	-10.1	-62.49	IF/BI	0.10	Pessenda et al., 1998
149	Cerrada ^o - Pimenta Bueno*	-11.49	-61.1	IF/BI	0.17	Pessenda et al., 1998
150	Vilhena*	-12.42	-66.07	IF/BI	0.10	Pessenda et al., 1998
151	Laguna Sucuara	-16.49	-62.2	IF/BI/PC	C0.47	Zech et al., 2009
	Pau-de-fruta	-18.15		BI	0.45	Hora'k-Terra et al., 2015
153	Machado soil core	-21.4	-45.55	BI	0.45	Calegari et al., 2013
154	CPCN	-29.28	-50.1	IF/BI	0.43	Du"mig et al., 2008
155	Pampean Region	n-38.0	-60.0	IF/BI	0.33	Prado & Alberdi, 1999
156	Cariaco Basin	10	-65	PC	3.00	Haug et al., 2001
157	Tobago Basin	11	61	IF/BI	0.58	Reißig et al., 2019
158	Tobago Basin	11	61	IF/PC	0.73	Hoffmann et al., 2014
159	Mid Atlantic Ridge	-44	-14	IF/BI	0.59	Skinner et al., 2010
160	Sao Jos'e palm swamp	-17.04	-45.06	IF/BI	0.60	Cassino et al., 2018
161	Lagoa Feia	-15.34	-47.18	IF/BI	0.51	Cassino et al., 2020
162	P'e-de-Pato palm swamp*	-16.2	-49.3	PC	1.35	Ribeiro et al., 2003
163	Lago do Saci	-9.7	-56.16	IF/BI	0.10	Fontes et al., 2017
164	Santa ninha	-2.07	-55.49	IF/BI/PC	C0.80	Moreira et al., 2012
165	Viola~o Lake	-6.20	-50.25	IF/BI	0.73	Guimara~es et al., 2021
166	Serra Sul	-6.23	-50.22	IF/BI	0.46	Guimar aes et al., 2021
167	Serra do Tarzan	-6.19	-50.08	IF/BI	0.43	Guimara~es et al., 2021
168	Huma´ıta	-7.55	-63.04	IF/BI	0.40	Cohen et al., 2014
169	Cerro do Touro*	-26.25	-49.25	IF/BI/PC	C0.54	Oliveira et al., 2008a
170	Lago do Aquiri*	-3.17	-44.98	BI/PC	0.43	Behling & Costa, 1997
171	Tamandua' River*	-21.45	-47.60	PC	0.43	Turcq et al., 1997
172	Campo Alegre*	-26.25	-49.25	IF/BI/PC	C0.43	Oliveira et al., 2008b
173	Ang'elica Cave	-13.40	-46.23	IF	1.81	Wong et al., 2021
			1 /	1.1 .1		

Table S1: Complete proxy compilation with the number, study site, coordinates, proxy type and reference study. The paleo records that were calibrated in this study appear with an aster- isk next to the study site name.



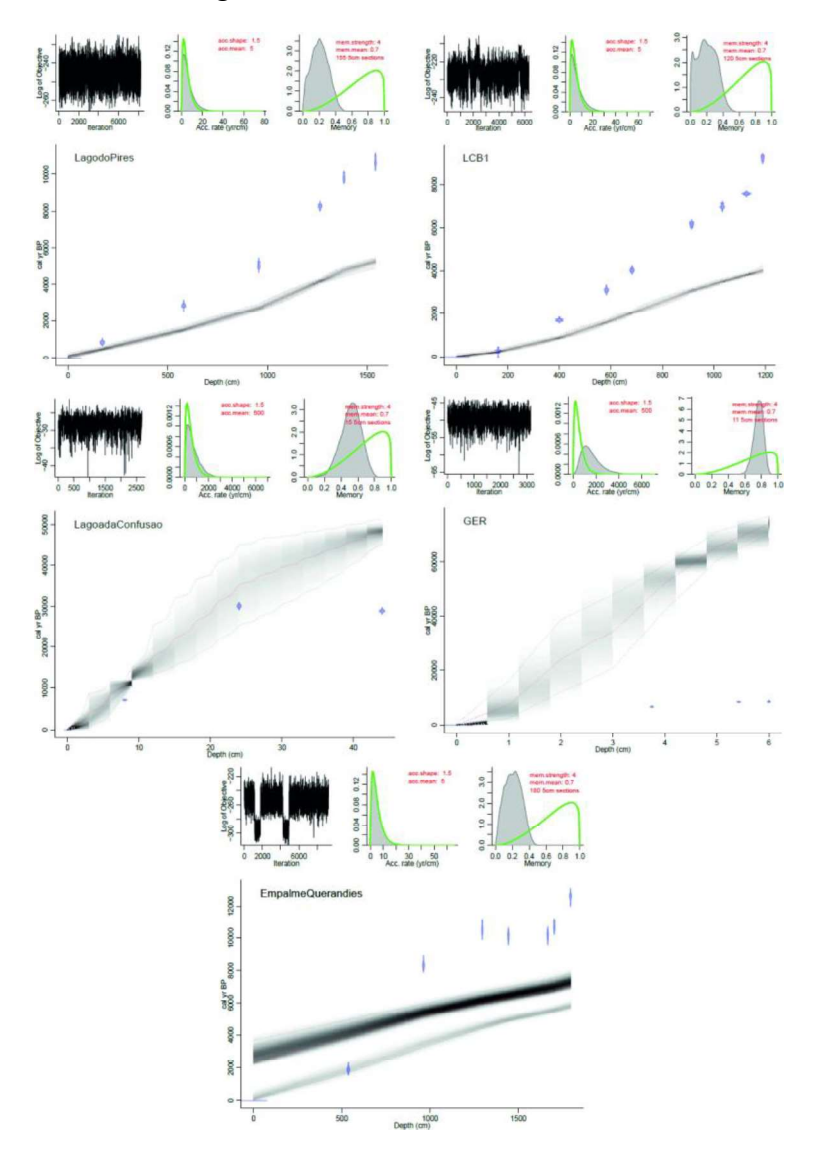


Figure S1. Calibrated 14C age models of the data excluded. Upper panels depict the Markov Chain Monte Carlo iterations (left panel), the prior (green curves) and posterior (grey histograms) distributions for the accumulation rate (middle panel) and memory (right panel). Bottom panel shows the calibrated 14C dates (transparent blue) and the agedepth model (Blaauw & Christen, 2013). It is possible to observe that the adjustment made to generate these age models present a certain discrepancy in relation to the uncalibrated ages of each age model.

Figure S.2 - Calibrated Data Locations.

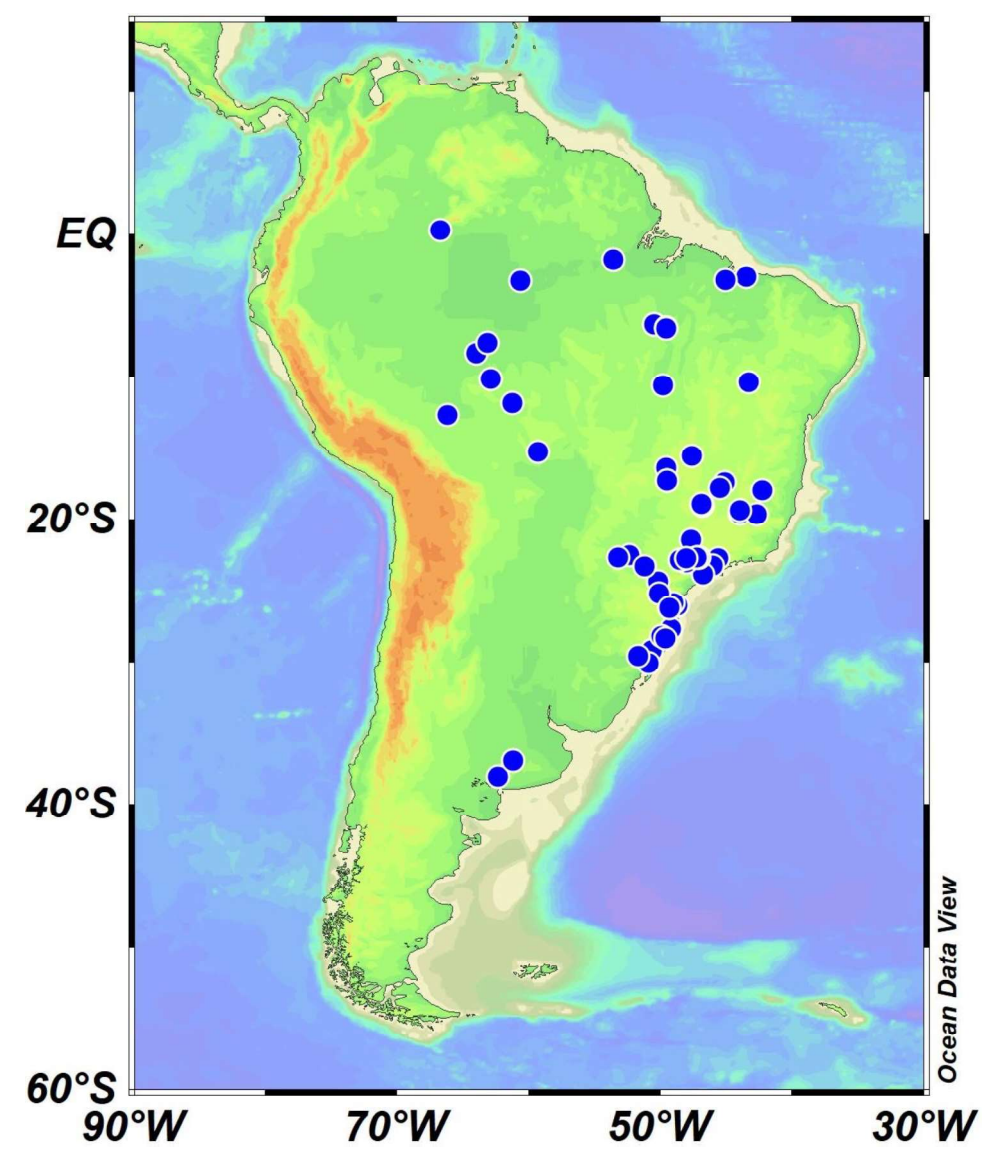


Figure S2. South America's map. The circles refer to the proxies calibrated by this article, specified in Table S1 by an asterisk next to the site's name.

Figure S.3 - All Data Locations.

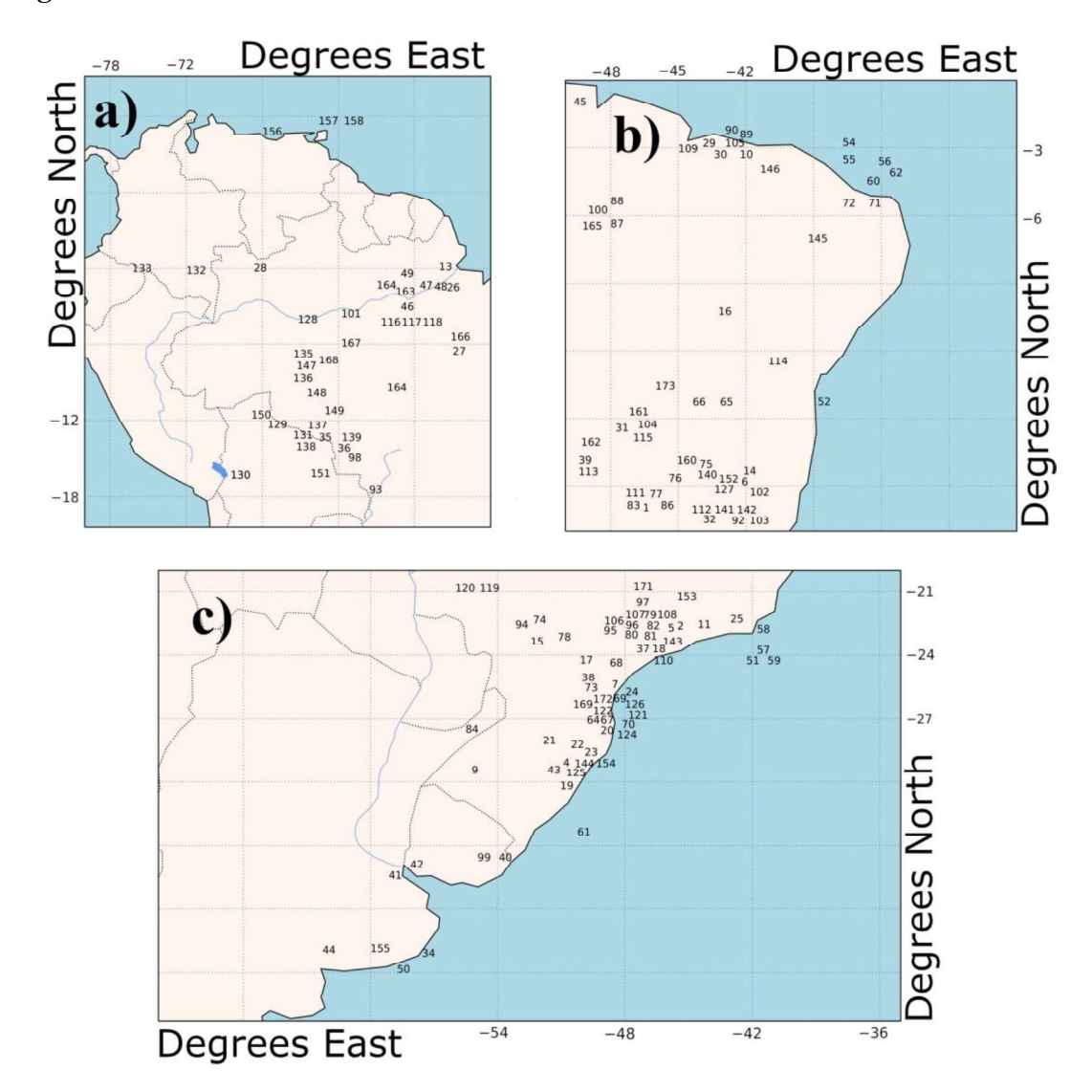


Figure S3. Locations from the compilation proxies in South America's map, numbers refer to the proxies exemplified in Table 2. a) Amazonia region. b) NE Brazil region. b) Southern SA region.

References

- Absy, M. L., Cleef, A., Fournier, M., L., M., M., S., Sifeddine, A., . . . Van Der Hammen, T. 1991. Mise en evidence de quatre phases d'ouverture de la foret dense dans de sud-est de l'amazonie au cours des 60000 dernieres ann'ees. premi'ere comparaison avec d'autres regions tropicales. Acad. Sci. Paris, 312, 673–678.
- Arz, H. W., Gerhardt, S., Patzold, & Rohl, U. 2001. Millennial-scale changes of surface-and deep-water flow in the western tropical atlantic linked to northern hemisphere high-latitude climate during the holocene. Geology, 29, 239–242. doi: 10.1130/0091-7613(2001)029(0239:MSCOSA)2.0.CO;2
- Arz, H. W., Patzold, J., & Wefer, G. 1998. Correlated millennial-scale changes in surface hydrography and terrigenous sediment yield inferred from last-glacial marine deposits off northeastern brazil. Quaternary Res., 50, 157–166. doi: 10.1006/gres.1998.1992
- Barberi, M., Salgado-Labouriau, M. L., & Suguio, K. 2000. Paleovegetation and paleoclimate of "vereda de aguas emendadas", central brazil. J. S. Am. Earth Sci., 13, 241–254. doi: 10.1016/S0895-9811(00)00022-5
- Barreto, E. A. S. 2010. Reconstituicao da pluviosidade da chapada diamantina (ba) durante o quaternario tardio atraves de registros isotopicos (o e c) em estalagmites. Butanta, S~ao Paulo SP, Brazil.
- Bauermann, S. G., Marques-Toigo, M., Behling, H., & Souza, P. A. 2003. Analises palinol'ogicas da turfeira de A'guas claras, plan'ıcie costeira do rio grande do sul, brasil, 9 ° congresso da associac, ao brasileira de estudos do quatern'ario.
- Behling, H. 1995b. A high resolution holocene pollen records from lago do pires, se brazil: vegetation, climate and fire history. J. Paleolimnol., 14, 253–268.
- Behling, H. 1997b. Late quaternary vegetation, climate and fire history of the arau-caria forest and campos region from serra campos gerais, parana state (south brazil). Rev. Palaeobot. Palyno., 97. doi: 10.1016/S0034-6667(96)00065-6
- Behling, H. 2001. Late quaternary environmental changes in the lagoa da curuca region (eastern amazonia, brazil) and evidence of podocarpus in the amazon lowland. Veg. Hist. Archaeobot., 10, 175–183. doi: 10.1007/PL00006929

- Behling, H. 2003. Late glacial and holocene vegetation, climate and fire history inferred from lagoa nova in the southeastern brazilian lowland. Veg. Hist. Ar- chaeobot., 12, 263–270. doi: 10.1007/s00334-003-0020-9
- Behling, H. 2007. Late quaternary vegetation, fire and climate dynamics of serra do arac atuba in the atlantic coastal mountains of parana state, southern brazil.
- Veg. Hist. Archaeobot., 16, 77–85. doi: 10.1007/s00334-006-0078-2
- Behling, H., Bauermann, S. G., & Neves, P. C. P. 2001a. Holocene environmental changes in the sao francisco de paula region, southern brazil. J. S. Am. Earth Sci., 16, 631–639. doi: 10.1016/S0895-9811(01)00040-2
- Behling, H., Carlos Berrio, J., & Hooghiemstra, H. 1999. Late quaternary pollen records from the middle caquet'a river basin in central colombian amazon.
- Palaeogeography, Palaeoclimatology, Palaeoecology, 145 (1), 193-213. Retrieved from https://www.sciencedirect.com/science/article/pii/ S0031018298001059 doi: https://doi.org/10.1016/S0031-0182(98)00105-9
- Behling, H., & Costa, M. L. 1997. Studies on holocene tropical vegetation man- grove and coast environments in the state of maranhao, ne brazil. J. Quat. S. Am. A., 10, 93–118. doi: 10.1002/jqs.3268
- Behling, H., & Costa, M. L. 1997a. Studies on holocene tropical vegetation mangrove and coast environments in the state of maranhao, ne brazil. J. Quat. S. Am. A., 10, 93–118.
- Behling, H., & Costa, M. L. 2000. Holocene environmental changes from the rio curu'a record in the caxiuan a region, eastern amazon basin. Quaternary Res., 53, 369–377. doi: 10.1006/gres.1999.2117
- Behling, H., & Costa, M. L. 2001. Holocene vegetational and coastal environmental changes from the lago crispim record in northeastern para state, eastern amazonia. Rev. Palaeobot. Palyno., 114, 145–155. doi: 10.1016/S0034-6667(01)00044-6
- Behling, H., & Negrelle, R. B. 2001. Tropical rain forest and climate dynamics of the atlantic lowland southern brazil, during the late quaternary. Quaternary Res., 56, 383–389. doi: 10.1006/qres.2001.2264

- Behling, H., Pillar, V. D., Orloci, L., & Bauermann, S. G. 2004. Late quaternary araucaria forest, grassland (campos), fire and climate dynamics, studied by high-resolution pollen, charcoal and multivariate analysis of the cambar'a do sul core in southern brazil. Palaeogeogr. Palaeocl., 203, 277–297. doi: 10.1016/S0031-0182(03)00687-4
- Behling, H., Pillar, V. D. P., & Bauermann, S. G. 2005. Late quaternary grassland (campos), gallery forest, fire and climate dynamics, studied by pollen, char-coal and multivariate analysis of the sao francisco de assis core in western rio grande do sul (southern brazil). Rev. Palaeobot. Palyno., 133, 235–248. doi: 10.1016/j.revpalbo.2004.10.004
- Behling, H., & Safford, H. D. 2010. Late-glacial and holocene vegetation, climate and fire dynamics in the serra dos org~aos, rio de janeiro state, southeastern brazil. Glob. Change Biol., 16, 1661–1671. doi: 10.1111/j.1365-2486.2009.02029.x
- Bernal, J., W.Cruz, F., M.Str'ıkis, N., Wang, X., Deininger, M., Catunda, M. C. A., . . . Auler, A. S. 2016. High-resolution holocene south american monsoon history recorded by a speleothem from botuver'a cave, brazil. Earth and Planetary Science Letters, 450, 186-196. doi: 10.1016/j.epsl.2016.06.008
- Blaauw, M., & Christen, J. 2013. Bacon manual v2. 3.3.
- Brugger, S. O., Gobet, E., van Leeuwen, J. F., Ledru, M.-P., Colombaroli, D., van der Knaap, W., . . . Tinner, W. 2016. Long-term man–environment inter- actions in the bolivian amazon: 8000 years of vegetation dynamics. Quaternary Science Reviews, 132, 114–128. doi: 10.1016/j.quascirev.2015.11.001
- Bush, M. B., Miller, M. C., De Oliveira, P. E., & Colinvaux, P. 2000. Two histories of environmental change and human disturbance in eastern lowland amazonia. The Holocene, 10, 543–553. doi: 10.1191/095968300672647521
- Bush, M. B., Silman, M. R., De Toledo, M. B., Listopad, C., Gosling, W. D., Williams,
 C., . . . Krisel, C. 2007. Holocene fire and occupation in amazo- nia: records from two lake districts. Philos. T. Roy. Soc. B., 362, 209–218. doi: doi:10.1098/rstb.2006.1980
- Calegari, M. R., Madella, M., Vidal-Torrado, P., Pessenda, L. C. R., & Marques, F. A. 2013. Combining phytoliths and δ13c matter in holocene palaeoenvironmental

- studies of tropical soils: An example of an oxisol in brazil. Quaternary International, 287, 47-55. Retrieved from https://www.sciencedirect.com/science/article/pii/S1040618211006525 (Comprehensive Perspectives on Phytolith Studies in Quaternary Research) doi: https://doi.org/10.1016/j.quaint.2011.11.012
- Carson, J. F., Mayle, F. E., Whitney, B. S., Iriarte, J., Pru'mers, H., & Soto, J. D. 2016. Pre-columbian ring ditch construction and land use on a 'choco- late forest island' in the bolivian amazon. J Quat Sci, 31, 337–347. doi: 10.1002/jqs.2835
- Carson, J. F., Watling, J., Mayle, F. E., Whitney, B. S., Iriarte, J., Pru"mers, H., & Soto, J. D. 2015. Pre-columbian land use in the ring-ditch region of the boli-vian amazon. The Holocene, 2, 1285-1300. doi: 10.1177/0959683615581204
- Carson, J. F., Whitney, B. S., Mayle, F. E., Iriarte, J., Pru"mers, H., Soto, J. D., & Watling, J. 2014. Environmental impact of geometric earthwork con-struction in pre-columbian amazonia. PNAS 111, 29, 10497-10502. doi: 10.1073/pnas.1321770111
- Cassino, R. F. 1992. A palynological record of late quaternary vegetational and cli-matic change in southeastern brazil. 281 W Lane Ave, Columbus, OH 43210, United States.
- Cassino, R. F. 2011. Reconstitui cao da vegeta cao e do clima do chapada dos gerais durante o holoceno, a partir da analise palinologica da vereda la cador. Av. Pres. Antônio Carlos, 6627 Pampulha, Belo Horizonte MG, Brazil.
- Cassino, R. F., Ledru, M.-P., de Almeida Santos, R., & Favier, C. 2020. Vegetation and fire variability in the central cerrados (brazil) during the Pleistocene holocene transition was influenced by oscillations in the sasm boundary belt.
- Quaternary Science Reviews, 232. doi: 10.1016/j.quascirev.2020.106209 Cassino, R. F., Martinho, C. T., & Caminha, S. A. S. 2018. A late quaternary palynological record of a palm swamp in the cerrado of central brazil inter- preted using modern analog data. Palaeogeogr. Palaeocl., 490, 1–16. doi: 10.1016/j.palaeo.2017.08.036
- Chiessi, C. M., Mulitza, S., Patzold, J., & Wefer, G. 2010. How different proxies record precipitation variability over southeastern south america. IOP Conf. Series: Earth and Environmental Science, 9. doi: 10.1088/1755-1315/9/1/012007

- Cohen, M., Rossetti, D., Pessenda, L., Friaes, Y., & Oliveira, P. 2014. Late pleistocene glacial forest of humait'a western amazonia. Palaeogeography, Palaeoclimatology, Palaeoecology, 41, 37-47. Retrieved from https://www.sciencedirect.com/science/article/pii/S0031018213005622 (Continental and Coastal Marine Records of Centennial to Millennial
- Changes in South American Climate since the Last Glacial Maximum) doi: https://doi.org/10.1016/j.palaeo.2013.12.025
- Colinvaux, P. A., De Oliveira, P. E., Moreno, J. E., Miller, M. C., & Bush, M. B. 1996.A long pollen record from lowland amazonia: forest and cooling in glacial times. Science, 274, 85–88. doi: 10.1126/science.274.5284.85
- Cruz, F. W., Vuille, M., Wang, X., Cheng, H., Werner, M., Lawrence Edwards, R., . . . Nguyen, H. 2009. Orbitally driven east-west antiphasing of south american precipitation. Nat. Geosci., 2, 210–214. doi: 10.1038/NGEO444
- Cruz Jr., F. W., Burns, S. J., Jercinovic, M., Karmann, I., Sharp, W. D., & Vuille, M. 2007. Evidence of rainfall variations in southern brazil from trace element ratios (mg/ca and sr/ca) in late pleistocene stalagmite. Geochim. Cosmochim. Ac., 71, 2250–2263. doi: 10.1016/j.gca.2007.02.005
- Cruz Jr., F. W., Burns, S. J., Karmann, I., Sharp, W. D., & Vuille, M. 2006a. Reconstruction of regional atmospheric circulation features during the late pleistocene in subtropical brazil from oxygen isotope composition of speleothems. Earth Planet. Sc. Lett., 248, 495–507. doi: 10.1016/j.epsl.2006.06.019 Cruz Jr., F. W., Burns, S. J., Karmann, I., Sharp, W. D., Vuille, M., Cardoso,
- A. O., . . . Viana Jr., O. 2005. Insolation-driven changes in atmospheric cir- culation over the past 116,000 years in subtropical brazil. Nature, 434, 63–66. doi: 10.1029/2010PA001949
- Cruz Jr., F. W., Burns, S. J., Karmann, I., Sharp, W. D., Vuille, M., & Ferrari, J. A. 2006b. A stalagmite record of changes in atmospheric circulation and soil processes in the brazilian subtropics during the late pleistocene. Quaternary Sci. Rev., 25, 2749–2761. doi: 10.1016/j.quascirev.2006.02.019
- Du'mig, A., Schad, P., Rumpel, C., Dignac, M.-F., & K'ogel-Knabner, I. 2008.

 Araucaria forest expansion on grassland in the southern brazilian highlands as

- revealed by 14c and δ13c studies. Geoderma, 145 (1), 143-157. Retrieved from https://www.sciencedirect.com/science/article/pii/ S0016706107001681 doi: https://doi.org/10.1016/j.geoderma.2007.06.005
- Enters, D., Behling, H., Mayr, C., Dupont, L., & Zolitschka, B. 2010. Holocene environmental dynamics of south-eastern brazil recorded in laminated sediments of lago aleixo. J. Paleolimnol., 44, 265–277. doi: 10.1007/s10933-009-9402-z
- Fontes, D., Cordeiro, R., Martins, G., Behling, H., Turcq, B., Sifeddine, A., Ro drigues, R. 2017. Paleoenvironmental dynamics in south amazonia, brazil, during the last 35,000 years inferred from pollen and geochemical records of lago do saci. *Quaternary Science Reviews*, 173, 161-180. Retrieved from https://www.sciencedirect.com/science/article/pii/S0277379117301026 doi: https://doi.org/10.1016/j.quascirev.2017.08.021
- Freitas, H. A. D., Pessenda, L. C. R., Aravena, R., Gouveia, S. E. M., de Souza Ribeiro, A., & Boulet, R. 2001. Late quaternary vegetation dynamics in the southern amazon basin inferred from carbon isotopes in soil organic matter. Quaternary Research, 5, 39-46. doi: 10.1006/qres.2000.2192
- Garcia, M. J., De Oliveira, P. E., Siqueira, E., & Fernandes, R. 2004. A holocene vegetational and climatic record from the atlantic rainforest belt of coastal state of sao paulo, se brazil. Rev. Palaeobot. Palyno., 131, 181–199. doi: 10.1016/j.revpalbo.2004.03.007
- Gouveia, S. E. M., Pessenda, L. C. R., Aravena, R., Boulet, R., Scheel-Ybert, R., Bendassoli, J. A., . . . Freitas, H. A. 2002. Carbon isotopes in charcoal and soils in studies of paleovegetation and climate changes during the late pleis- tocene and the holocene in the southeast and centerwest regions of brazil.
- Global Planet. Change, 33, 95–106. doi: 10.1016/S0921-8181(02)00064-4 Groeneveld, J., & Chiessi, C. M. 2011. Mg/ca of globorotalia inflata as a recorder of permanent thermocline temperatures in the south atlantic. Paleoceanography, 26, 2203. doi: 10.1029/2010PA001949
- Guimar aes, J. T. F., Sahoo, P. K., Figueiredo, M. M. J. C. D., da Silva Lopes, K., Gastauer, M., Ramos, S. J., ... Rodrigues, T. M. 2021. Lake sedimentary

- processes and vegetation changes over the last 45k cal a bp in the uplands of southeastern amazonia. Paleolimnol, 36, 255-272. doi: 10.1002/jqs.3268
- Hassan, G. S., Espinosa, M. A., & Isla, F. I. 2009. Diatom-based inference model for paleosalinity reconstructions in estuaries along the northeastern coast of argentina. Palaeogeogr. Palaeocl., 275, 77–91. doi: 10.1016/j.palaeo.2009.02.020
- Haug, G. H., Hughen, K. A., Sigman, D. M., Peterson, L. C., & R"ohl, U. 2001. Southward migration of the intertropical convergence zone through the holocene. Science, 293, 1304-1308. doi: 10.1126/science.1059725
- Hermanowski, B., Da Costa, M., & Behling, H. 2012. Environmental changes in southeastern amazonia during the last 25,000 years revealed from a paleoecological record. Quat Res, 7, 138–148. doi: 10.1016/j.yqres.2011.10.009
- Hermanowski, B., Da Costa, M., & Behling, H. 2015. Possible linkages of palaeofires in southeast amazonia to a changing climate since the last glacial maximum. Veget Hist Archaeobot, 24, 279–292. doi: 10.1007/s00334-014-0472-0
- Hoffmann, J., Bahr, A., Voigt, S., Sch"onfeld, J., Nu"rnberg, D., & Rethemeyer, J. 2014. Disentangling abrupt deglacial hydrological changes in Northern south america: Insolation versus oceanic forcing. Geology, 4, 79–582. doi: 10.1130/G35562.1
- Horbe, A. M., Behling, H., Nogueira, A. C., & Mapes, R. 2011. Environmental changes in the western amazˆonia: morphological framework, geochemistry, palynology and radiocarbon dating data. An. Acad. Bras. Ciˆenc., 83, 863-874. doi: 10.1590/S0001-37652011005000030
- Hor'ak-Terra, I., Mart'ınez Cortizas, A., da Luz, C. F. P., Rivas L'opez, P., Silva, A. C., & Vidal-Torrado, P. 2015. Holocene climate change in central–eastern brazil reconstructed using pollen and geochemical records of pau de fruta mire (serra do espinha, co meridional, minas gerais). Palaeogeography, Palaeoclimatology, Palaeoecology, 437, 117-131. Retrieved from https://www.sciencedirect.com/science/article/pii/S0031018215003946 doi: https://doi.org/10.1016/j.palaeo.2015.07.027
- Hor'ak-Terra, I., Cortizas, A. M., Luz, C. F. P. D., Silva, A. C., Mighall, T., Ca-margo, P. B. D., . . . Vidal-Torrado, P. 2020. Late quaternary vegetation and climate

- dynamics in central-eastern brazil: insights from a 35k cal a bp peat record in the cerrado biome. JQS. doi: 10.1002/jqs.3209
- Iriarte, J. 2006. Vegetation and climate change since 14,810 14c yr b.p. in southeastern uruguay and implications for the rise of early formative societies. Quaternary Res., 65, 20–32. doi: 10.1016/j.yqres.2005.05.005
- Iriarte, J., Holst, I., Marozzi, O., Listopad, C., Alonso, E., Rinderknecht, A., & Montana, J. 2004. Evidence for cultivar adoption and emerging complexity during the mid-holocene in the la plata basin. Nature, 43, 614–617. doi: 10.1038/nature02983
- Irion, G., Bush, M. B., Nunes de Mello, J. A., Stuben, D. N., Muller, G., Morais de, J. O., & Junk, J. W. 2006. A multi proxy palaeoecological record of holocene lake sediments from the rio tapajos, eastern amazonia. Palaeogeogr. Palaeocl., 240, 523–535. doi: doi:10.1016/j.palaeo.2006.03.005
- Jacob, J., Disnar, J., Boussafir, M., Sifeddine, A., Albuquerque, A. L. S., & Turcq, B. 2004. Major environmental changesrecorded by lacustrine sedimentary organic matter sincethe last glacial maximum near the equator (lagoa do caco, ne brazil). Palaeogeogr. Palaeocl., 205, 183–197. doi: 10.1016/j.palaeo.2003.12.005
- Jaeschke, A., Ruhlemann, C., Arz, H., G., H., & Lohmann, G. 2007. Coupling of millennial-scale changes in sea surface temperature and precipitation off northeastern brazil with high-latitude climate shifts during the last glacial period. Paleoceanography, 22, 4206. doi: 10.1029/2006PA001391
- Jeske-Pieruschka, V., & Behling, H. 2011. Palaeoenvironmental history of the s^{*}ao francisco de paula region in southern brazil during the late quaternary in- ferred from the rinc^{*}ao das cabritas core. The Holocene, 22, 1251-1262. doi: 10.1177/0959683611414930
- Jeske-Pieruschka, V., Pillar, V. D., Oliveira, M. A. T. D., & Behling, H. 2013. New insights into vegetation, climate and fire history of southern brazil revealed by a 40,000 year environmental record from the state park serra do tabuleiro. Veget Hist Archaeobot, 22, 299–314. doi: 10.1007/s00334-012-0382-y
- Leal, M. G., & Lorscheitter, M. L. 2007. Plant succession in a forest on the lower northeast slope of serra geral, rio grande do sul, and holocene palaeoenvironments,

- southern brazil. Acta Bot. Bras., 21, 1–10. doi: http://dx.doi.org/
- Ledru, M., Rousseau, D., Cruz Jr., F. W., Riccomini, C., Karmann, I., & Martin, L. 2005. Paleoclimate changes during the last 100,000 yr from a record in the brazilian atlantic rainforest region and interhemispheric comparison. Quater- nary Res., 64, 444–450. doi: 10.1016/j.yqres.2005.08.006
- Ledru, M.-P. 1993. Late quaternary environmental and climatic changes in central brazil. Quaternary Researche, 39, 90-98. doi: 10.1006/qres.1993.1011
- Ledru, M.-P., Ceccantini, G., Gouveia, S. E. M., Lopez-S'aez, J. A., Pessenda, L. C. R., & Ribeiro, A. S. 2006. Millennial-scale climatic and veg- etation changes in a northern cerrado (northeast, brazil) since the last glacial maximum. Quaternary Sci. Rev., 25, 1110–1126. doi: 10.1016/j.quascirev.2005.10.005
- Ledru, M.-P., Cordeiro, R. C., Dominguez, J. M. L., Martin, L., Mourguiart, P., Sifeddine, A., & Turcq, B. 2001. Late-glacial cooling in amazonia inferred from pollen at lagoa do cac,o, northern brazil. Quaternary Res., 55, 47–56. doi: 10.1006/gres.2000.2187
- Ledru, M.-P., Mourguiart, P., Ceccantini, G., Turcq, B., & Sifeddine, A. 2002. Tropical climates in the game of two hemispheres revealed by abrupt climatic change. Geology, 30, 275–278. doi: 10.1130/0091-7613(2002)030(0275: TCITGO)2. 0.CO:2
- Ledru, M.-P., Mourguiart, P., & Riccomini, C. 2009. Related changes in biodiversity, insolation and climate in the atlantic rainforest since the last inter-glacial. Palaeogeography, Palaeoclimatology, Palaeoecology, 271 (1), 140-152. Retrieved from https://www.sciencedirect.com/science/article/pii/S0031018208005786 doi: https://doi.org/10.1016/j.palaeo.2008.10.008
- Leonhardt, A., & Lorscheitter, M. L. 2010. The last 25,000 years in the Eastern plateau of southern brazil according to alpes de s~ao francisco record. Journal of South American Earth Sciences, 29 (2), 454-463. Retrieved from https://www.sciencedirect.com/science/article/pii/S089598110900145X doi: https://doi.org/10.1016/j.jsames.2009.09.003

- Lorente, F. L., Meyer, K. E. B., & Horn, A. H. 2010. Analise palinologica de vereda da fazenda urbano, municipio de buritizeiro, minas gerais, brasil. Geonomos, 18, 57–72. doi: 10.18285/geonomos.v18i2.73
- Maezumi, S. Y., Power, M. J., Mayle, F. E., McLauchlan, K. K., & Iriarte, J. 2015. Effects of past climate variability on fire and vegetation in the cerr^{*}ado sa- vanna of the huanchaca mesetta, ne bolivia. Clim. Past, 11, 835–853. doi: 10.5194/cp-11-835-2015
- Mahiques, M. M., Wainer, I. K. C., Burone, L., Nagai, R., de Mello e Sousa, S. H., Figueira, R. C. L., . . . Øyvind Hammer 2009. A high-resolution holocene record on the southern brazilian shelf: Paleoenvironmental implications. Quaternary International, 206, 52–61. doi: 10.1016/j.quaint.2008.09.010
- Mayle, F. E., Burbridge, R., & Killeen, T. J. 2000. Millennial-scale dynamics of southern amazonian rain forests. Science, 290, 2291–2294. doi: doi:10.1126/science.290.5500.2291
- Moreira, L. S., Moreira-Turcq, P., Turcq, B., Caquineau, S., & Cordeiro, R. C. 2012. Paleohydrological changes in an amazonian floodplain lake: Santa ninha lake. Paleolimnol, 48, 339–350. doi: 10.1007/s10933-012-9601-x
- Moro, R. S., Bicudo, C. E. M., Melo, M. S., & Schmitt, J. 2004. Paleoclimate of the late pleistocene and holocene at lagoa dourada, parana state, southern brazil. Quatern. Int., 114, 87–99. doi: 10.1016/S1040-6182(03)00044-2
- Nagai, R. H., Sousa, S. H. M., Burone, L., & Mahiques, M. M. 2009. Paleoproductivity changes during the holocene in the inner shelf of cabo frio, southeastern brazilian continental margin: benthic foraminifera and sedimentological proxies. Quatern. Int., 206, 62–71. doi: 10.1016/j.quaint.2008.10.014
- Novello, V. F., Cruz, F. W., Vuille, M., Str'ıkis, N. M., Edwards, R. L., Cheng, H., . . . Santos, R. V. 2017. A high-resolution history of the south american mon-soon from last glacial maximum to the holocene. Sci Rep, 7, 44267. doi: 10.1038/srep44267
- Oliveira, M. A., Behling, H., & Pessenda, L. C. 2008a. Late-pleistocene and midholocene environmental changes in highland valley head areas of santa catarina state, southern brazil. Journal of South American Earth Sciences, 26 (1), 55-67.

- Retrieved from https://www.sciencedirect.com/science/article/pii/S0895981108000333 doi: https://doi.org/10.1016/j.jsames.2008.03.001
- Oliveira, M. A., Behling, H., Pessenda, L. C. R., & de Lima, G. L. 2008b. Stratig- raphy of near-valley head quaternary deposits and evidence of climate-driven slope-channel processes in southern brazilian highlands. CATENA, 75 (1), 77-92. Retrieved from https://www.sciencedirect.com/science/article/pii/S034181620800043X (Environmental change, geomorphic processes and land degradation in tropical highlands) doi: https://doi.org/10.1016/j.catena.2008.04.003
- Oliveira, P. E. d., Barreto, A. M. F., & Suguio, K. 1999. Late pleistocene/holocene climatic and vegetational history of the brazilian caatinga: the fossil dunes of the middle sao francisco river. Palaeogeogr. Palaeocl., 152, 319–337. doi: 10.1016/S0031-0182(99)00061-9
- Parizzi, M. G., Salgado-Labouriau, M. L., & Kohler, H. C. 1998. Genesis and environment history of lagoa santa, southeastern brazil. The Holocene, 8, 311–321. doi: 10.1191/095968398670195708
- Parolin, M., Medeanic, S., & Stevaux, J. C. 2006. Registros palinologicos e mudanc, as ambientais durante o holoceno de taquarussu (ms). Rev. Bras. Paleontol., 9, 137–148.
- Pereira, N. V., Safford, H. D., Behling, H. F., L., S., Bianchi, M. M., & Bennett, K. D. 2012. Holocene vegetation and fire history of the serra do capara'o, se brazil. The Holocene, 22, 1243-1250. doi: 10.1177/0959683612437864
- Pessenda, L., Gouveia, S., Gomes, B., Aravena, R., Ribeiro, a., & Boulet, R. 1998. The carbon isotope record in soils along a forest-cerrado ecosystem transect: implications for vegetation changes in the rondonia state, southwestern brazilian amazon region. The Holocene, 8, 599-603. doi: 10.1191/095968398673187182
- Pessenda, L., Gouveia, S., Ribeiro, A., De Oliveira, P., & Aravena, R. 2010.

 Late pleistocene and holocene vegetation changes in northeastern brazil determined from carbon isotopes and charcoal records in soils. Palaeogeography,

 Palaeoclimatology, Palaeoecology, 297 (3), 597-608. Retrieved from

- https:// www.sciencedirect.com/science/article/pii/S0031018210005584 doi: https://doi.org/10.1016/j.palaeo.2010.09.008
- Pessenda, L. C. R., Aravena, R., Melfi, A. J., Telles, E. C. C., Boulet, R., Valencia, E. P. E., & Tomazello, M. 1996. The use of carbon isotopes (13c, 14c) in soil to evaluate vegetation changes during the holocene in central brazil. Radiocarbon, 38, 191–201. doi: 10.1017/S0033822200017562
- Pessenda, L. C. R., De Oliveira, P. E., Mofatto, M., Medeiros, V. B., Garcia, R. J. F., Aravena, R., . . . Etchebehere, M. L. 2009. The evolution of a tropical rainforest/grassland mosaic in southeastern brazil since 28,000 14c yr bp based on carbon isotopes and pollen records. Quaternary Res., 71, 437–452. doi: 10.1016/j.ygres.2009.01.008
- Pessenda, L. C. R., Gouveia, S. E. M., Aravena, R., Boulet, R., & Valencia, E. P. E. 2004a. Holocene fire and vegetation changes in southeastern brazil as deduced from fossil charcoal and soil carbon isotope. s, Quatern. Int., 114, 35–43. doi: 10.1016/S1040-6182(03)00040-5
- Pessenda, L. C. R., Ledru, M.-P., Gouveia, S. E. M., Aravena, R., Ribeiro, A. S., Bendassolli, J. A., & Boulet, R. 2005. Holocene palaeoenvironmental reconstruction in northeastern brazil inferred from pollen, charcoal and carbon isotope records. The Holocene, 15, 812–820. doi: 10.1191/0959683605hl855ra
- Pessenda, L. C. R., Ribeiro, A. S., Gouveia, S. E. M., Aravena, R., Boulet, R., & Bendassolli, J. A. 2004b. Vegetation dynamics during the late pleistocene in the barreirinhas region, maranhao state, northeastern brazil, based on carbon isotopes in soil organic matter. Quaternary Res., 62, 183–193. doi: 10.1016/j.yqres.2004.06.003
- Pires, G., Meyer, K., & Gomes, M. 2016. Palinologia da vereda juquinha/cuba, par- que estadual da serra do cabral, minas gerais, brasil. Rev. Bras. Palaontol., 19, 95-110. doi: 10.4072/rbp.2016.1.08
- Pivel, M. A. G., Toledo, F. A. L., & Costa, K. B. 2010. Foraminiferal record of changes in summer monsoon precipitation at the southeastern brazilian continental margin since the last glacial maximum. Rev. Bras. Paleontol., 13, 79–88. doi: 10.4072/rbp.2010.2.01

- Prado, J. L., & Alberdi, M. T. 1999. The mammalian record and climatic change over the last 30,000 years in the pampean region, argentina. Quaternary Inter- national, 57-58, 165-174. Retrieved from https://www.sciencedirect.com/science/article/pii/S1040618298000573 doi: https://doi.org/10.1016/ S1040-6182(98)00057-3
- Prieto, A. R. 1996. Late quaternary vegetational and climatic changes in the pampa grassland of argentina. Quaternary Res., 45, 75–88. doi: 10.1006/qres.1996.0007
- Prieto, A. R., Blasi, A. M., De Francesco, C. G., & Fernandez, C. 2004.

 Environmental history since 11,000 14c yr b.p. of the northeastern pampas, argentina, from alluvial sequences of the lujan river. Quaternary Res., 60, 146–161. doi:10.1016/j.yqres.2004.04.006
- Raczka, M. F., Oliveira, P. E. D., Bush, M., & McMichael, C. H. 2013. Two paleoecological histories spanning the period of human settlement in southeastern brazil. JQS. doi: 10.1002/jqs.2597
- Reißig, S., Nu"rnberg, D., Bahr, A., Poggemann, D., & Hoffmann, J. 2019.
 Southward displacement of the north atlantic subtropical gyre circulation system during north atlantic cold spells. Paleoceanography and Paleoclimatology, 34, 866-885. doi: 10.1029/2018PA003376
- Ribeiro, M. d. S. L., Barberi, M., & Rubin, J. 2003. ReconstruC, A o da composiC, A o flor Istica no decorrer dos U Itimos 32.000 anos ap em A reas de cerrados da bacia hidrogra fica do rio meia ponte, goia s, brasil. II Congresso sobre Planejamento e Gesta o das Zonas Costeiras dos Parises de Expressa o Portuguesa. IX Congresso da Associa, cão Brasileira de Estudos do Quatern ario. II Congresso
- do Quatern'ario dos Pa'ises de L'ingua Ib'ericas.
- Salgado-Labouriau, M. L., Casseti, V., Ferraz-Vicentini, K. R., Martin, L., Soubies, F., Suguio, K., & Turcq, B. 1997. Late quaternary vegetational and climatic changes in cerrado and palm swamp from central brazil. Palaeogeogr. Palaeocl., 128, 215–226. doi: 10.1016/S0031-0182(96)00018-1
- Scheel-Ybert, R., Gouveia, S. E. M., Pessenda, L. C. R., Aravena, R., Coutinho, L. M., & Boulet, R. 2003. Holocene palaeoenvironmental evolution in the sao paulo state

- (brazil), based on anthracology and soil d13c analysis. The Holocene, 13, 73–81. doi: 10.1191/0959683603hl596rp
- Servant, M., Maley, J., Turcq, B., Absy, M. L., Brenac, P., Fournier, M., & Ledru, M. 1993. Tropical forest changes during the late quaternary in african and south american lowlands. Global Planet. Change, 7, 25–40. doi: 10.1016/0921-8181(93)90038-P
- Sifeddine, A., Bertrand, P., Fournier, M., Martin, L., Servant, M., Soubies, F., . . . Turcq, B. 1994. La sedimentation organique lacustre en milieu tropical humide (carajas, amazonie orientale, bresil): relation avec les changements climatiques au cours des 60,000 dernieres annees. Bull. Soc. Geol. France, 165, 613–621.
- Sifeddine, A., Martin, L., Turcq, B., Volkmer-Ribeio, C., Soubies, F., Cordeiro, R. C., & Suguio, K. 2001. Variations of the amazonian rainforest environment: a sedimentological record covering 30,000 years. Palaeogeogr. Palaeocl., 168, 221–235. doi: 10.1016/S0031-0182(00)00256-X
- Sifeddine, A., Wirrmann, D., Albuquerque, A. L. S., Turcq, B., Cordeiro, R. C., & Gurgel, M. H. 2004. Bulk composition of sedimentary organic matter used in palaeoenvironmental reconstructions: examples from the tropical belt of south america and africa. Palaeogeogr. Palaeocl., 214, 41–53. doi: 10.1016/j.palaeo.2004.06.012
- Skinner, L. C., Fallon, S., Waelbroeck, C., Michel, E., & Barker, S. 2010. Ven-tilation of the deep southern ocean and deglacial co2 rise. Science, 328, 1147-1151. doi: 10.1126/science.1183627
- Smith, C. B., Cohen, M. C. L., Pessenda, L. C. R., Franc, a, M. C., Guimaraes, J. T. F., Rossetti, D. F., & Lara, R. J. 2011. Holocene coastal vegetational changes at the mouth of the amazon river. Rev. Palaeobot. Palyno., 168, 21–30. doi: 10.1016/j.revpalbo.2011.09.008
- Stevaux, J. C. 2000. Climatic events during the late pleistocene and holocene in the upper parana river: correlation with ne argentina and south-central brazil. Quatern. Int., 72, 73–85. doi: 10.1016/S1040-6182(00)00023-9
- Str'ıkis, N. M., Cruz, F. W., Cheng, H., Karmann, I., Lawrence Edwards, M., R. and Vuille, Wang, X., . . . Auler, A. S. 2011. Abrupt variations in south american

- monsoon rainfall during the holocene based on a speleothems record from central-eastern brazil. Geology, 39, 1075–1078. doi: 10.1029/2010PA001949
- Toledo, F. A. L., Costa, K. B., & Pivel, M. A. G. 2007. Salinity changes in the western tropical south atlantic during the last 30 kyr. Global Planet. Change, 57, 383–395. doi: 10.1016/j.gloplacha.2007.01.001
- Toledo, F. A. L., Costa, K. B., Pivel, M. A. G., & Campos, E. J. D. 2008.

 Tracing past circulation changes in the western south atlantic based on planktonic foraminifera. Rev. Bras. Paleontol, 11, 169–178. doi: 10.4072/rbp.2008.3.03
- Toledo, M. B. d., & Bush, M. B. 2007. A mid-holocene environmental change in amazonian savannas. J. Biogeogr., 34, 1313–1326. doi: 10.1111/j.1365-2699.2006.01606.x
- Turcq, B., Albuquerque, A. L. S., Cordeiro, R. C., Sifeddine, A., Simoes Filho, F. F. L., Souza, A. G., . . . Capitaneo, J. 2002. Accumulation of organic car- bon in five brazilian lakes during the holocene. Sediment.Geol., 148, 319–342. doi: 10.1016/S0037-0738(01)00224-X
- Turcq, B., Pressinotti, M. M., & Martin, L. 1997. Paleohydrology and paleoclimate of the past 33,000 years at the tamandu'a river, central brazil. Quaternary Research, 47 (3), 284-294. Retrieved from https://www.sciencedirect.com/science/article/pii/S0033589497918809 doi: https://doi.org/10.1006/qres.1997.1880
- Vicentini, K. R. F., & Labouriau, M. L. S. 1996. Palynological analysis of a palm swamp in central brazil. J. S. Am. Earth Sci., 9, 207–219. doi: 10.1016/0895-9811(96)00007-7
- Vilanova, I., Prieto, A. R., & Espinosa, M. 2006. Palaeoenvironmental evolution and sea-level fluctuations along the southeastern pampa grasslands coast of argentina during the holocene. J. Quaternary Sci., 21, 227–242. doi: 10.1002/jqs.953
- Wang, X., Augusto, R. L. E., Auler, S., Cheng, H., Kong, X., Wang, Y., . . . Chiang, H. W. 2017. Hydroclimate changes across the amazon lowlands over the past 45,000 years. Nature, 541, 204–207. doi: 10.1038/nature20787

- Wang, X., Auler, A. S., Edwards, R. L., Cheng, H., Ito, E., Wang, Y., . . . Solheid, M. 2007. Millennial-scale precipitation changes in southern brazil over the past 90,000 years. Geophys. Res. Lett., 34, L23701. doi: 10.1029/2007GL031149
- Wang, X., Auler, A. S., Lawrence Edwards, R., Cheng, H., Ito, E., & Solheid, M. 2006. Interhemispheric anti-phasing of rainfall during the last glacial period. Quaternary Sci. Rev., 25, 3391–3403. doi: 10.1016/j.quascirev.2006.02.009
- Ward, B. M., Wong, C. I., Novello, V. F., Gee, D. M., Santos, R. V., Silva, L. C. R., . . . Chengh, H. 2019. Reconstruction of holocene coupling between the south american monsoon system and local moisture variability from speleothem δ180 and 87sr/86sr records. Quaternary Science Reviews, 210, 51-63. doi: 10.1016/j.quascirev.2019.02.019
- Weide, D. M., Fritz, S. C., Hastorf, C. A., Bruno, M. C., Baker, P. A., Guedron, S., & Salenbiend, W. 2017. A 6000 yr diatom record of mid- to late holocene fluctuations in the level of lago win~aymarca, lake titicaca (peru/bolivia). Quaternary Research, 88, 1–14. doi: 10.1017/qua.2017.49
- Weldeab, S., Schneider, R. R., & Kolling, M. 2006. Deglacial sea surface temperature and salinity increase in the western tropical atlantic in synchrony with high latitude climate instabilities. Earth Planet. Sci. Lett., 241, 699–706. doi: 10.1016/j.epsl.2005.11.012
- Weng, C., Bush, M. B., & Athens, J. 2002. Holocene climate change and hydrarch succession in lowland amazonian ecuador. Review of Palaeobotany and Palynology, 120 (1), 73-90. Retrieved from https://www.sciencedirect.com/science/article/pii/S0034666701001488 doi: https://doi.org/10.1016/S0034-6667(01)00148-8
- Whitney, B. S., Mayle, F. E., Punyasena, S. W., Fitzpatrick, K. A., Burn, M. J., Guillen,
 R., . . . Metcalfe, S. E. 2011. A 45 kyr palaeoclimate record from the lowland interior of tropical south america. Palaeogeogr. Palaeocl., 307, 177–192. doi: 10.1016/j.palaeo.2011.05.012
- Wong, Wang, X., Latrubesse, E. M., He, S., & Bayer, M. 2021. Variations in the south atlantic convergence zone over the mid-to-late holocene inferred from speleothem δ180 in central brazil. Quaternary Science Reviews, 270, 107178.

Retrieved from https://www.sciencedirect.com/science/article/pii/S0277379121003851 doi: https://doi.org/10.1016/j.quascirev.2021.107178

Zech, W., Zech, M., Zech, R., Peinemann, N., Morras, H. J. M., Moretti, L., . . . Glaser, B. 2009. Late quaternary palaeosol records from subtropical (38° s) to tropical (16° s) south america and palaeoclimatic implications. Quatern. Int., 196, 107–120. doi: 10.1016/j.quaint.2008.01.005

Appendix III

Supplementary Material

Long-and shor-term vegetation change and inferred climate dynamics and anthropogenic activity in the central Cerrado during the Holocene

KATERINE ESCOBAR-TORREZ,^{1,2*} MARIE-PIERRE LEDRU,¹ RAQUEL FRANCO CASSINO,² PAULA RIBEIRO BIANCHINI³ and ELDER YOKOYAMA³

Table S1. Ecological classification of the pollen taxa identified in the LFB1 core based on phytosociological surveys (Araújo et al., 2002, 2011; Assunção and Felfili, 2004; Bridgewater et al., 2004; Bueno et al. 2013, 2018; Carvalho and Martins, 2009; Felfili, 1995, 1997; Felfili et al, 2004; Rossi et al, 1998; Silva Junior et al, 1998, Silva and Felfili, 1998).

			Ecological
Family	Taxon	Life form	classification
Acanthaceae	Justicia	Herb	cerrado
Amaranthaceae	Gomphrena	Herb	cerrado
Amaranthaceae	Althernantera	Herb	cerrado
Amaranthaceae	Am/Cheno	Herb	cerrado
Anacardiaceae	Astronium	Tree	cerrado (cerradão)
Anacardiaceae	Cyrtocarpa	Tree	cerrado (cerradão)
Anacardiaceae	Tapirira	Tree	gallery forest
Anacardiaceae	Thyrsodium type	Tree	gallery forest/cerradão
Apiaceae	Apium	Herb	gallery forest
Apocynaceae	Aspidosperma	Tree	gallery forest/cerradão
Aquifoliaceae	Ilex	Tree	gallery forest
Araceae	Spatiphyllum	Herb	gallery forest
Araliaceae	Schefflera	Tree	cerrado (cerradão)

¹Institut des Sciences de l'Evolution de Montpellier (ISEM), Université de Montpellier-CNRS-IRD-EPHE, France

²Departamento de Geologia, Universidade Federal de Ouro Preto, Brazil

³Instituto de Geociências, Universidade de Brasília, Brazil

		1	gallery forest/lake
Arecaceae	Euterpe type	Treepalm	margin
Asteraceae	Baccharis	Herb/shrub	cerrado
Asteraceae	Vernonia	Herb	cerrado
Bignoniaceae	Jacaranda	Tree	cerrado (cerradão)
Bignoniaceae	Tabebuia	Tree	cerrado (cerradão)
Boraginaceae	Cordia	Herb	gallery forest/cerradão
Boraginaceae	Echium Echium	Herb	cerrado
Boraginaceae	Heliotrophium	Herb	cerrado/antropic
Burseraceae	Protium	Tree	gallery forest/cerradão
Cannabaceae	Celtis	Tree	gallery forest
Camadaccac	Cellis	Ticc	gallery forest/lake
Cannabaceae	Trema	Tree	margin
Caryocaraceae	Caryocar	Tree	cerrado
Celasteraceae	Plenckia	Tree	cerrado
Celasteraceae	Celasteraceae	Tree	gallery forest/cerradão
		Tree	1 -
Chrysobalanaceae Cleomaceae	Licania type Cleome	Herb	gallery forest/cerradão cerrado
Clethraceae	Clethra	Tree	
		Tree	gallery forest
Connaraceae Convolvulaceae	Connarus Evolvulus	Herb	gallery forest/cerradão cerrado
Cunnoniaceae	Lamanonia	Tree	gallery forest
Dillenaceae	Curatella	Tree	cerrado
Elaeocarpaceae	Sloanea	Tree	gallery forest
F.:	E	C11.	gallery forest/lake
Ericaceae	Ericaceae	Shrub	margin
Erythroxilaceae	Erythroxylum	Tree	cerrado (cerradão)
Euphorbiaceae	Chamaesyce	Shrub	cerrado
Euphorbiaceae	Euphorbia	Shrub	cerrado
Euphorbiaceae	Sapium	Shrub	cerrado
Euphorbiaceae	Sebastiana	Shrub	cerrado
Euphorbiaceae	Acalypha	Herb	gallery forest/cerradão
Euphorbiaceae	Alchornea	Tree	gallery forest
Euphorbiaceae	Euphorbiaceae	All	various
Fabaceae	Fabaceae	All	various
Fabaceae			1 (12)
(caesalpiniaceae)	Ateleia	Tree	cerrado (cerradão)
Fabaceae	D. 1	_	1 / 12 >
(caesalpiniaceae)	Diplotropis	Tree	cerrado (cerradão)
Fabaceae			
(caesalpiniaceae)	Caesalpinea type	Tree	cerrado (cerradão)
Fabaceae		_	
(caesalpiniaceae)	Cassia type	Tree	Gallery forest

Fabaceae		1	
(caesalpiniaceae)	Copaifera	Tree	cerrado (cerradão)
Fabaceae			()
(caesalpiniaceae)	Crotalaria	Shrub	cerrado
Fabaceae			
(caesalpiniaceae)	Senna	Tree	gallery forest/cerradão
Fabaceae	Serina	1100	gainery rerest certains
(caesalpiniaceae)	Peltogyne	Tree	cerrado
Fabaceae	1 chogyne	1100	Cerrado
(caesalpiniaceae)	Pterogyne	Tree	cerrado (cerradão)
Fabaceae (mimosaceae)	Anadenanthera	Tree	gallery forest
Fabaceae (mimosaceae)	Mimosa	Shrub	cerrado
Fabaceae (mimosaceae)	Piptadenia	Tree	gallery forest
Fabaceae (mmosaceae)		1100	ganery forest
(papilonaceae)	Andira	Tree	gallery forest/cerradão
Fabaceae	Anuiru	Ticc	gariery forest/cerradao
(papilonaceae)	Apuleia	Tree	gallery forest
Fabaceae	Аршеш	Ticc	galicity forest
(papilonaceae)	Cuatulia typo	Shrub	cerrado
Fabaceae	Cratylia type	Siliub	Cerrado
	Dalhavaia	Tree	cerrado
(papilonaceae) Fabaceae	Dalbergia	1166	Cerrado
	Dint on we true	Tree	aamada (aamadãa)
(papilonaceae)	Dipteryx type	Tree	cerrado (cerradão)
Fabaceae	Facilities a	Turk	1. (12 .)
(papilonaceae)	Erythrina	Tree Subshrub/shr	cerrado (cerradão)
Fabaceae			1. (12 .)
(papilonaceae)	Glyzyrrhiza type	ub	cerrado (cerradão)
Fabaceae	1.6.1	T	1 (1~)
(papilonaceae)	Machaerium	Tree	cerrado (cerradão)
Fabaceae	14	TT 1	1
(papilonaceae)	Macroptilium	Herb	cerrado
Fabaceae	D. 1		1
(papilonaceae)	Pterodon	Tree	cerrado
Fabaceae	D '1	4.11	
(papilonaceae)	Papilonaceae	All	various
Fabaceae	Rhynchosia	Herb	cerrado
Humiricacae	Vantanea	Tree	gallery forest
Icacinaceae	Villarezia	Tree	gallery forest
Lamiaceae	Aegiphila	Tree	gallery forest/cerradão
Lamiaceae	Hyptis	Herb	cerrado
Loranthaceae	Psittacanthus	Herb	cerrado
Lythraceae	Cuphea	Herb	cerrado/lake margin
Lythraceae	Lafoensia	Tree	cerrado
Malvaceae	Apeiba	Tree	gallery forest

Malphigiaceae	Banisteriopsis	Vine	gallery forest
Malphigiaceae	Byrsonima	Tree	cerrado
Malphigiaceae	Malpighia type	Herb/vine	gallery forest
1 &	Ceiba speciosa		
Malvaceae	type	Herb	cerrado
		Herb/subshru	
Malvaceae	Byttneria	ь	cerrado
Malvaceae	Helicteres type	Shrub	cerrado
Malvaceae	Eriotheca	Tree	cerrado (cerradão)
Melastomataceae	Melastomataceae	Tree	various
Meliaceae	Cedrela	Tree	gallery forest
			gallery forest/lake
Meliaceae	Guarea type	Tree	margin
Menispermaceae	Abuta type	Shrub	cerrado
Moraceae	Moraceae	Tree	gallery forest
Myrtaceae	Myrtaceae	Tree	various
Nyctaginaceae	Pisonia	Tree	gallery forest/cerradão
Ochnaceae	Ouratea	Tree	cerrado (cerradão)
Ochnaceae	Sauvagesia	Herb	cerrado/lake margin
Pentaphylacacées	Ternstroemia	Tree	semideciduos forest
Phytolaccaceae	Gallesia	Tree	gallery forest
Piperaceae	Peperomia	Herb	gallery forest
-			gallery forest/lake
Piperaceae	Piper	Shrub	margin
Plumbaginaceae	Plumbago type	Subshrub	gallery forest
Poaceae	Poaceae	Herb	cerrado
Podocarpaceae	Podocarpus	Tree	gallery forest
Portulacaceae	Portulaca	Herb	cerrado
Primulaceae	Cybianthus	Tree	gallery forest/cerradão
			gallery forest/lake
Primuliaceae	Myrsine	Tree	margin
Rhamnaceae	Ziziphus	Tree	gallery forest
Rhamnaceae	Colubrina	Tree	gallery forest
Rubiaceae	Borreria	Herb	cerrado
Rubiaceae	Didymaea type	Herb	cerrado
Rubiaceae	Alibertia	Shrub	cerrado (cerradão)
Rubiaceae	Sabiceae	Shrub/herb	cerrado (cerradão)
Rubiaceae	Citrus	Tree	cerrado
Rubiaceae	Psychotria	Shrub	gallery forest
Rubiaceae	Amaiuoa	Tree	gallery forest
Rubiaceae	Coussarea	Tree	gallery forest/cerradão
Rubiaceae	Guettarda	Tree	gallery forest/cerradão
Rubiaceae	Rubiaceae type	All	various
Rutaceae	Esenbenckia	Shrub	cerrado
	. 102	•	•

Rutaceae	Zanthoxylum	Tree	cerrado (cerradão)
Salicaceae	Casearia	Tree	cerrado (cerradão)
Sapindaceae	Diatenopterix	Shrub	cerrado/gallery forest
Salicaceae	Neosprucea	Tree	cerrado
Sapindaceae	Paullinia	Herb	gallery forest
Sapindaceae	Matayba	Tree	gallery forest/cerradão
Sapotaceae	Chrysophyllum	Treelet	cerrado (cerradão)
Sapotaceae	Diploon	Tree	gallery forest/cerradão
Sapotaceae	Pouteria	Tree	gallery forest/cerradão
Simaroubaceae	Simaruba	Tree	gallery forest/cerradão
Smilaceae	Smilax	Herb	gallery forest
Solanaceae	Solanum	Shrub	cerrado/gallery forest
			gallery forest/lake
Urticaceae	Cecropia	Tree	margin
Verbenaceae	Lantana	Shrub	cerrado/gallery forest
Verbenaceae	Lippia	Shrub	cerrado/lake margin
Vochysiaceae	Vochysia	Tree	cerrado/cerradão
Winteraceae	Drimys	Tree	gallery forest
Xyridaceae	Xyris	Herb	cerrado/lake margin
			5
Cyperaceae	Cyperaceae	Herb	various
Alismataceae	Echinodorus	Herb	lake margin
Alismataceae Alismataceae	Echinodorus Sagittaria	Herb Herb	lake margin lake margin
			\
Alismataceae	Sagittaria	Herb	lake margin
Alismataceae Arecaceae	Sagittaria Mauritia type	Herb Treepalm	lake margin lake margin/aquatic
Alismataceae Arecaceae Cabombaceae	Sagittaria Mauritia type Cabomba	Herb Treepalm Herb	lake margin/aquatic lake margin/aquatic
Alismataceae Arecaceae Cabombaceae Eriocaulaceae	Sagittaria Mauritia type Cabomba Eriocaulon	Herb Treepalm Herb Herb	lake margin/aquatic lake margin/aquatic lake margin
Alismataceae Arecaceae Cabombaceae Eriocaulaceae Haloragaceae	Sagittaria Mauritia type Cabomba Eriocaulon Myriophyllum	Herb Treepalm Herb Herb Herb	lake margin/aquatic lake margin/aquatic lake margin/aquatic lake margin aquatic
Alismataceae Arecaceae Cabombaceae Eriocaulaceae Haloragaceae Lentibulariaceae	Sagittaria Mauritia type Cabomba Eriocaulon Myriophyllum Utricularia	Herb Treepalm Herb Herb Herb Herb	lake margin lake margin/aquatic lake margin/aquatic lake margin aquatic lake margin
Alismataceae Arecaceae Cabombaceae Eriocaulaceae Haloragaceae Lentibulariaceae Lythraceae	Sagittaria Mauritia type Cabomba Eriocaulon Myriophyllum Utricularia Crenea	Herb Treepalm Herb Herb Herb Herb Herb	lake margin/aquatic lake margin/aquatic lake margin/aquatic lake margin aquatic lake margin lake margin/aquatic
Alismataceae Arecaceae Cabombaceae Eriocaulaceae Haloragaceae Lentibulariaceae Lythraceae Nymphaeaceae	Sagittaria Mauritia type Cabomba Eriocaulon Myriophyllum Utricularia Crenea Nymphaea	Herb Treepalm Herb Herb Herb Herb Herb Herb	lake margin/aquatic lake margin/aquatic lake margin aquatic lake margin aquatic lake margin lake margin/aquatic aquatic
Alismataceae Arecaceae Cabombaceae Eriocaulaceae Haloragaceae Lentibulariaceae Lythraceae Nymphaeaceae Onagraceae	Sagittaria Mauritia type Cabomba Eriocaulon Myriophyllum Utricularia Crenea Nymphaea Ludwigia	Herb Treepalm Herb Herb Herb Herb Herb Herb Shrub	lake margin/aquatic lake margin/aquatic lake margin/aquatic lake margin aquatic lake margin lake margin/aquatic aquatic lake margin/aquatic
Alismataceae Arecaceae Cabombaceae Eriocaulaceae Haloragaceae Lentibulariaceae Lythraceae Nymphaeaceae Onagraceae Plantaginaceae	Sagittaria Mauritia type Cabomba Eriocaulon Myriophyllum Utricularia Crenea Nymphaea Ludwigia Stemodia type	Herb Treepalm Herb Herb Herb Herb Herb Herb Herb Herb	lake margin/aquatic lake margin/aquatic lake margin aquatic lake margin lake margin/aquatic aquatic lake margin/aquatic aquatic lake margin
Alismataceae Arecaceae Cabombaceae Eriocaulaceae Haloragaceae Lentibulariaceae Lythraceae Nymphaeaceae Onagraceae Plantaginaceae Polygalaceae	Sagittaria Mauritia type Cabomba Eriocaulon Myriophyllum Utricularia Crenea Nymphaea Ludwigia Stemodia type Polygalaceae	Herb Treepalm Herb Herb Herb Herb Herb Herb Herb Herb	lake margin/aquatic lake margin/aquatic lake margin/aquatic lake margin aquatic lake margin/aquatic aquatic lake margin/aquatic aquatic lake margin lake margin
Alismataceae Arecaceae Cabombaceae Eriocaulaceae Haloragaceae Lentibulariaceae Lythraceae Nymphaeaceae Onagraceae Plantaginaceae Polygalaceae Polygonaceae	Sagittaria Mauritia type Cabomba Eriocaulon Myriophyllum Utricularia Crenea Nymphaea Ludwigia Stemodia type Polygalaceae Polygonum	Herb Treepalm Herb Herb Herb Herb Herb Herb Herb Herb	lake margin/aquatic lake margin/aquatic lake margin/aquatic lake margin aquatic lake margin/aquatic aquatic lake margin/aquatic aquatic lake margin lake margin lake margin
Alismataceae Arecaceae Cabombaceae Eriocaulaceae Haloragaceae Lentibulariaceae Lythraceae Nymphaeaceae Onagraceae Plantaginaceae Polygalaceae Polygonaceae Pontederiaceae	Sagittaria Mauritia type Cabomba Eriocaulon Myriophyllum Utricularia Crenea Nymphaea Ludwigia Stemodia type Polygalaceae Polygonum Eichornia	Herb Treepalm Herb Herb Herb Herb Herb Herb Herb Herb	lake margin/aquatic lake margin/aquatic lake margin/aquatic lake margin aquatic lake margin/aquatic aquatic lake margin/aquatic aquatic lake margin lake margin lake margin lake margin aquatic
Alismataceae Arecaceae Cabombaceae Eriocaulaceae Haloragaceae Lentibulariaceae Lythraceae Nymphaeaceae Onagraceae Plantaginaceae Polygalaceae Polygonaceae Pontederiaceae Potamogetaceae	Sagittaria Mauritia type Cabomba Eriocaulon Myriophyllum Utricularia Crenea Nymphaea Ludwigia Stemodia type Polygalaceae Polygonum Eichornia Potamogeton	Herb Treepalm Herb Herb Herb Herb Herb Herb Herb Herb	lake margin/aquatic lake margin/aquatic lake margin/aquatic lake margin aquatic lake margin/aquatic aquatic lake margin lake margin lake margin lake margin lake margin aquatic aquatic aquatic

Table S2. Principal Component Analysis (PCA) of the pollen taxa and their contribution to the temporal variability.

Taxon	PC1	PC2	PC3	PC4	PC5
Myrtaceae	0.0016	4.18E+00	1.53E+01	3.71E-01	1.06E-01
Melastomataceae	1.179555	9.39E-01	4.80E-02	4.28E-01	6.18E+00
Ilex	0.790575	2.14E+00	6.53E+00	4.26E-02	4.08E-01
Trema	1.402998	1.13E-01	5.64E-01	1.94E+00	1.68E+00
Guarea	0.008116	3.25E-01	1.39E-01	1.11E+00	4.05E+00
Myrsine	5.787764	3.21E-01	4.36E-01	1.37E-02	1.81E-01
Cecropia	5.454394	1.11E-01	6.56E-01	2.99E+00	7.49E-01
Euterpe	0.741225	1.25E+00	1.46E+00	4.21E-02	3.14E+00
Tapirira	2.838768	7.98E-02	3.29E-01	3.02E-02	2.84E-01
Celtis	6.514203	1.90E+00	1.89E-03	9.86E-02	3.21E+00
Clethra	0.030433	6.68E-01	3.62E-02	1.38E+00	9.27E-01
Lamanonia	3.87372	1.02E+00	3.69E-02	1.93E+00	1.33E-03
Sloanea	0.511929	3.26E-03	2.72E+00	2.02E-01	2.48E-03
Alchornea	1.795179	3.66E-01	2.77E-01	1.05E-01	7.44E+00
Apuleia	1.789067	2.63E+00	1.65E-01	1.09E+01	7.93E-01
Anadenanthera	1.361225	2.09E-01	4.76E-02	4.27E-01	2.98E-01
Piptadenia	1.383366	1.73E-06	1.14E-02	1.41E-01	1.90E+00
Vantanea	1.456087	3.65E+00	5.69E-02	1.39E+01	1.37E-01
Villarezia	0.00212	6.72E-01	1.63E-01	1.73E-01	1.03E+00
Apeiba	0.664419	1.76E-01	6.34E-01	7.08E-02	7.95E+00
Cedrela	0.053749	2.83E+00	7.97E+00	5.87E-01	6.90E-01
Moraceae	5.905101	7.39E-01	1.18E-02	1.06E+00	8.53E-02
Gallesia	0.370934	9.15E-02	6.24E-01	1.82E-03	4.11E+00
Podocarpus	0.087041	1.09E+00	4.32E-01	1.30E+00	9.35E-03
Rosaceae	0.001568	1.33E+00	5.42E-02	1.41E-05	7.25E-02
Ziziphus	0.432087	3.34E+00	2.85E-01	2.02E-02	9.02E-03
Colubrina	2.372129	7.57E-01	4.17E-03	3.11E+00	2.14E+00
Amaiuoa	0.001871	4.38E-01	8.29E-05	1.75E-01	6.12E-01
Drymis	0.07726	2.59E-02	1.37E-03	3.45E-02	1.55E+00
Banisteriopsis	0.053486	2.46E+00	1.40E+01	5.23E-01	3.18E-03
Poaceae	5.870007	3.69E-02	1.29E-01	9.43E-01	7.74E-01
Cassia type	0.311777	7.81E-01	2.87E-01	1.54E-01	1.43E-01
Senna	0.720932	3.90E+00	2.07E+00	2.07E+00	1.51E-02
Andira type	0.078293	1.01E-01	7.02E-02	1.46E+01	8.68E-01
Pisonia	0.36167	5.85E-03	7.45E-02	5.60E-01	5.23E-01
Cybianthus	3.035126	4.22E-01	3.75E-01	6.79E-01	3.08E-01
Rhamnaceae	0.043932	3.59E-05	1.02E-03	2.72E-02	1.10E-02
Coussarea	0.603992	5.49E+00	1.83E+00	3.23E-02	8.98E-01
Guettarda	3.281143	2.29E+00	6.99E-01	4.07E-01	1.63E-01

Matayba	2.751269	2.17E+00	2.87E+00	6.16E-01	1.33E-04
Samaba/Simaruba	0.041321	1.39E-02	1.94E-01	1.08E-02	2.03E-01
Protium	0.74764	5.92E-01	2.75E-01	1.30E+00	6.73E-01
Aspidosperma type	0.05617	1.43E+00	7.61E+00	6.67E-01	1.69E-02
Thyrsodium type	0.718029	3.43E+00	6.21E-01	1.33E+00	1.37E-03
Erythrina	0.122823	4.17E-02	4.98E-02	1.48E-01	6.34E-03
Ternstroemia	0.145183	2.11E+00	1.11E+00	3.12E-03	8.27E+00
Pterogyne	0.094572	2.93E+00	3.90E-01	6.00E-03	9.29E-01
Ateleia	0.032263	1.32E-02	2.81E-01	8.44E-01	3.45E+00
Diplotropis	0.086668	1.56E-01	1.31E-02	1.22E-01	6.45E-03
Licania type	0.138436	1.94E+00	1.27E+01	1.58E-01	1.59E-01
Connarus type	0.48735	4.76E-01	3.15E-01	2.35E-01	3.07E-01
Aegiphila	0.123962	5.15E-04	4.68E-03	3.25E-03	7.77E-01
Celasteraceae type	0.163682	3.32E+00	5.24E-01	2.77E+00	1.74E+00
Diploon	2.40457	4.47E+00	2.20E-01	3.76E+00	2.02E-02
Pouteria	1.792844	1.28E+00	6.30E-01	9.57E-03	2.14E+00
Astronium	4.430871	1.88E-01	3.80E-01	4.56E-01	2.11E+00
Schefflera	5.924555	6.70E-01	6.31E-03	2.65E-01	2.01E-01
Copaifera	3.411755	3.25E-02	1.52E-01	9.01E-01	3.58E-01
Eriotheca	0.966714	2.14E+00	2.56E-03	9.67E-01	2.53E+00
Zanthoxylum	0.04248	1.12E+00	1.24E-01	6.56E-02	2.72E+00
Casearia	1.872353	6.42E-02	1.06E+00	7.22E-03	3.45E+00
Chrysophyllum	0.063083	3.45E-02	1.47E-01	1.68E+00	4.25E-05
Vochysia	0.009194	2.89E-01	7.17E-01	1.12E-01	2.26E-01
Ouratea	0.289571	1.75E-02	1.66E-02	1.33E-01	2.73E+00
Cyrtocarpa	1.467075	5.73E-01	1.21E-01	3.76E-02	1.73E+00
Jacaranda	0.403733	8.87E-01	2.54E+00	1.92E+00	8.58E-03
Tabebuia	1.012926	7.05E+00	1.02E+00	2.99E-01	5.16E-01
Erythroxilum	1.273246	4.04E+00	2.01E+00	4.01E-01	1.15E+00
Caesalpinea type	0.186274	6.28E-01	2.04E-01	1.50E-01	5.10E-02
Dalbergia	0.077493	3.50E-03	1.29E-01	2.71E-01	1.07E-03
Dipteryx type	0.222771	7.62E-01	2.87E+00	5.03E-03	2.28E-01
Machaerium	0.025338	1.29E-01	1.20E-02	1.46E-01	3.05E-01
Byrsonima	3.848225	8.85E-01	3.68E-02	2.17E+00	2.06E-01
Peltogyne	0.032795	5.77E+00	1.01E+00	4.48E-02	8.90E-03
Caryocar	0.123721	4.71E-02	2.08E-01	1.67E-01	4.18E-01
Plenckia	0.187918	7.40E-01	2.16E-01	1.20E+01	1.53E-01
Curatella	1.665836	9.96E-01	2.36E-01	6.00E-02	2.19E+00
Pterodon	0.112336	9.95E-04	6.79E-02	1.67E-01	1.48E+00
Lafoensia	0.008988	9.33E-01	1.72E-02	4.36E-01	1.39E+00
Citrus	0.655789	6.51E-02	1.85E-01	2.41E-02	3.55E+00
Neosprucea	0.529339	6.51E-01	1.78E-01	2.60E+00	1.62E-01

Table S3. Results of the PCA analysis showing the eigenvalues of each component and the significance as a percentage, and the contribution of Poaceae, cerrado tree taxa and gallery forest taxa. Bold numbers show the contribution of important taxa in each component.

	PC1	PC2	PC3
Eigenvalue	4.0720421	2.2171906	1.9753245
% of variance	20.360211	11.085953	9.876623
Cumulative % of variance	20.360211	31.44616	41.32279
Variable contribution			
Alchornea	0.015606	0.477148	5.833479
Anadenanthera	3.077405	0.110325	4.029714
Apeiba	5.513804	8.668668	7.532887
Astronium	10.3359	1.096979	6.5464
Banisteropsis	2.953117	14.38045	0.692803
Byrsonima	6.169119	0.42987	0.543156
Casearia	0.199846	14.40314	0.004718
Cecropia	9.185715	2.078618	3.580463
Celtis	11.24933	1.655514	3.258701
Euterpe type	0.160955	11.48573	1.565791
Ilex	10.70556	4.836976	0.10812
Melastomataceae	0.200181	2.718896	25.27243
Moraceae	10.10654	0.001396	2.318473
Myrsine	5.923308	0.195154	13.17908
Myrtaceae	3.90931	23.25632	0.036048
Ouratea	0.023185	2.980759	1.503758
Poaceae	8.930181	1.534874	8.595117
Tapirira	2.372401	1.015388	1.806671
Ternstroemia	3.213703	8.524285	13.55841
Trema	5.754831	0.149508	0.033776

Table S4. Classification of pollen taxa according to life form (LF), pollination syndromes (PS), ecology (stratum = S, light exposition = L and habitat). t=tree, h=herb, e=entomophilous, a=anemophilous, ls=lower storey (< 10 m), ms=medium storey (~ 15 m), us=upper storey (> 20 m), st=shade tolerant, ld=light demanding. The pollination syndrome was based on: Deus et al., 2014; Martins and Batalha, 2006; Pereira et al., 2022; Rios and Sousa-Silva, 2017. Life form and ecology are from: Rossi et al., 1998; Silva Junior et al., 1998; Araujo et al., 2011; Felfili et al., 2007; Oliveira-Filho and Ratter, 1995; Assunção and Felfili, 2004; Araujo et al., 2002; Carvalho and Martins, 2009; Felfili et al., 2004; Bridgewater, 2004; Silva and Felfili, 1998; Bueno et al., 2013 and 2018, Durigan et al., 2022.

Family	Pollen taxa	L F	P S	S-L	Habitat
Gallery forest					
Anacardiaceae	Tapirira	t	e	ms-st	Commonly found in moist soils that can tolerate a reduction in humidity
Aquifoliaceae	Ilex	t	e	ls-st	When present and well established can support low humidity. Can be present in montane forest and in floodplain or swampy gallery forest
Arecaceaea	Euterpe	t	e	ls-st	Moist soils and/or increase in precipitation
Cannabaceae	Celtis	t	e	ls	Moist soils, when present in gallery forest can support periodic flooding
Cannabaceae	Trema	t	ae	ls-ld	Found in humid soils, but can growth in inundated areas. Pioneer tree
Euphrobiaceae	Alchornea	t	a	us-ld	Along river banks and alluvial plains
Fabaceae (mim)	Anadenanther a	t	e	md- ld	Fertile soils with resistance to water deficiency
Malphigiaceae	Banisteropsis	t	e	ls-ld	Inside gallery forest and dry forest
Malvaceae	Apeiba	t	e	ms	Moist soils with low resistance to water deficiency
Melastomatace ae	Melast-Comb	t	e	ls	Fertile and moist soils. Can be found associated with the edge of swamps and marshes
Moraceae	Mor-Urt	t	ae	ls	Well-drained soils in moist forest, common in rainforest
Myrtaceae	Myrtaceae	t	e	ls	Moist soils, adapted to reduction in water availability. Can tolerate less humid conditions
Primulaceae	Myrsine	t	e	us-ld	Usually found in forest (gallery forest, dry forest and cerradão), tolerant to reduced water availability
Urticaceae	Cecropia	t	ae	ls-ld	Moist soils. Pioneers with rapid growth: re- establishes woodland physiognomies
Cerrado					
Poaceae	Poaceae	t	a	f	Most species C4 plants, dominant on open cerrado physiognomies

Anacardiaceae	Astronium	t	e	ls	Commonly found in rocky and dry soils, with a
					preference for fertile soils, and can tolerate
					reduction in humidity
Dillenaceae	Curatella	t	e	ls	Adapted to dry soils; drought tolerant and slow
					growth
Fabaceae (pap)	Dalbergia	t	e	ls-st	Fertile soils; adapted to dry conditions and
					reduced water availability
Malphigiaceae	Byrsonima	t	e	ls	Well-drained soils, adapted to reduced water
					availability
Ochnaceae	Ouratea	t	e	ls,	Well-drained soils, can tolerate dry conditions.
				lm-ld	Found in transition zones from open to closed
					physiognomies, usually in Cerrado sensu stricto
					and cerradão
Pentaphylacea	Ternstroemia	t	e	ls	Fertile soils; when established can tolerate
e					drought
Salicaceae	Casearia	t	e	ls	Found in moist soils; tolerates reduced water
					availability. Natural pioneer trees, observed
					after burn episodes. Commonly found near river
					banks, in the upper area, and in transition zones
					from grassland to arboreal vegetation

Figure S1. Pollen diagram of core LFB1 with, from left to right, radiocarbon dates, depth scale, AP/NAP frequency, 28 selected pollen taxa frequency, total pollen influx (PAR) of the terrestrial (Tpollen) and water level-related taxa (Apollen), macrocharcoal concentration (mm2/cm3) and cluster diagram with the five pollen zones. The red bars on the left show the samples with less than 300 pollen grains in the total pollen sum.

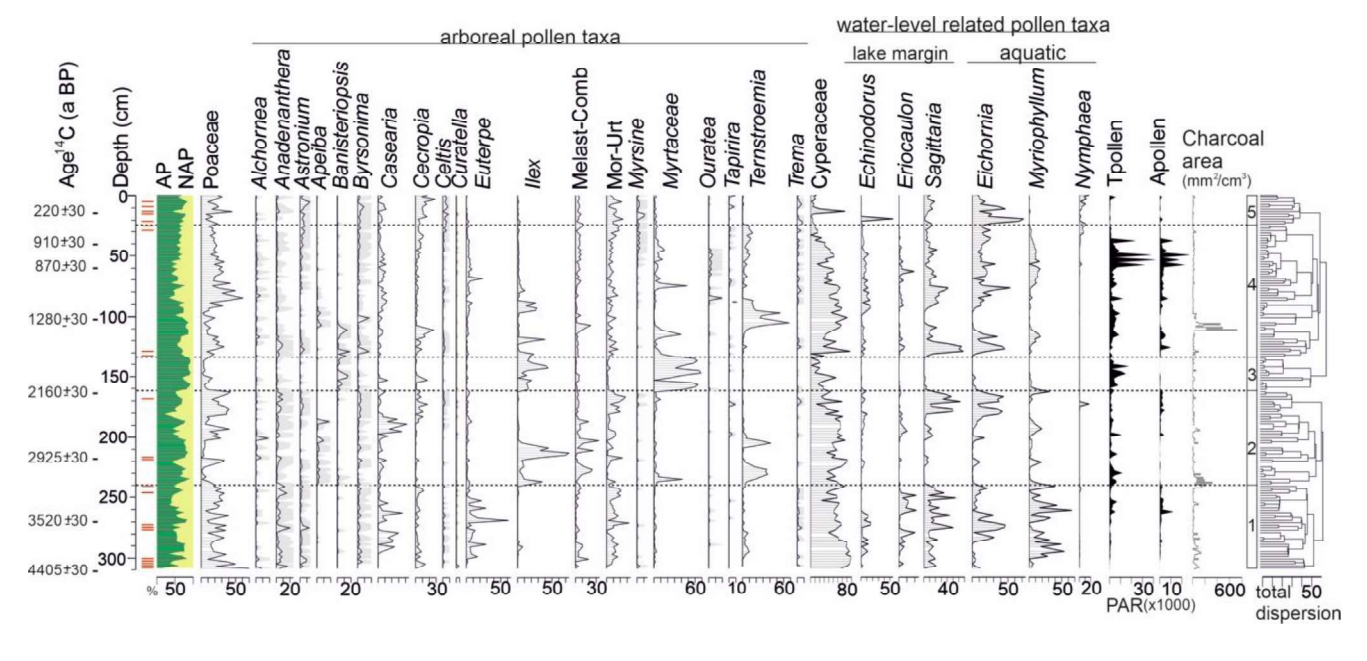


Figure S2. A) PCA of selected pollen taxa representing the first and second components. The groups suggest a relation to water availability: high (green), intermediate (red), and low (yellow) dependance. B) Values of z-scores for each variable contributing in PC1, pollen taxa in bold have contributed >5% in the temporal changes for the first component.

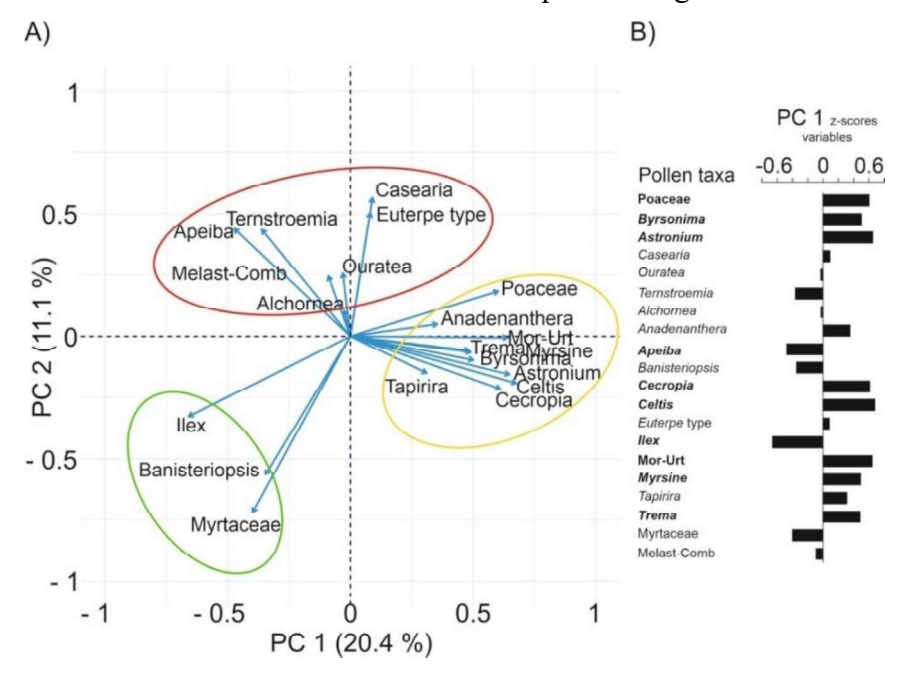


Figure S3. Pollen diagram of water level-related taxa (8) fern spores (6), and non-palynomorphs (algae and fungal spores) (15) of core LFB-1 presented along a depth scale and showing the pollen zones.

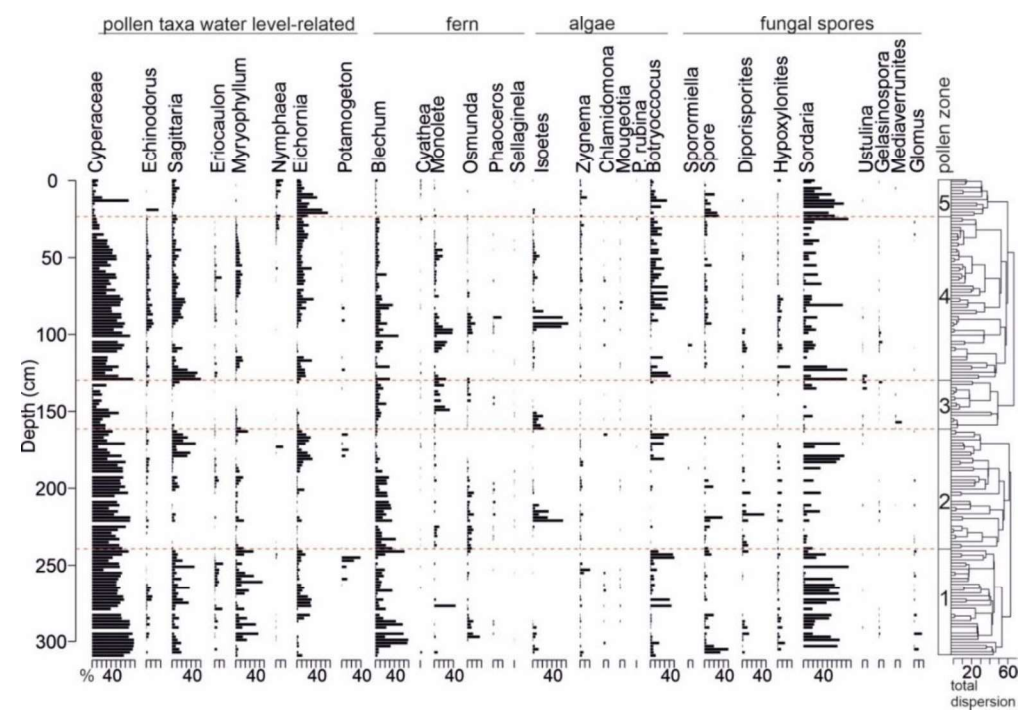
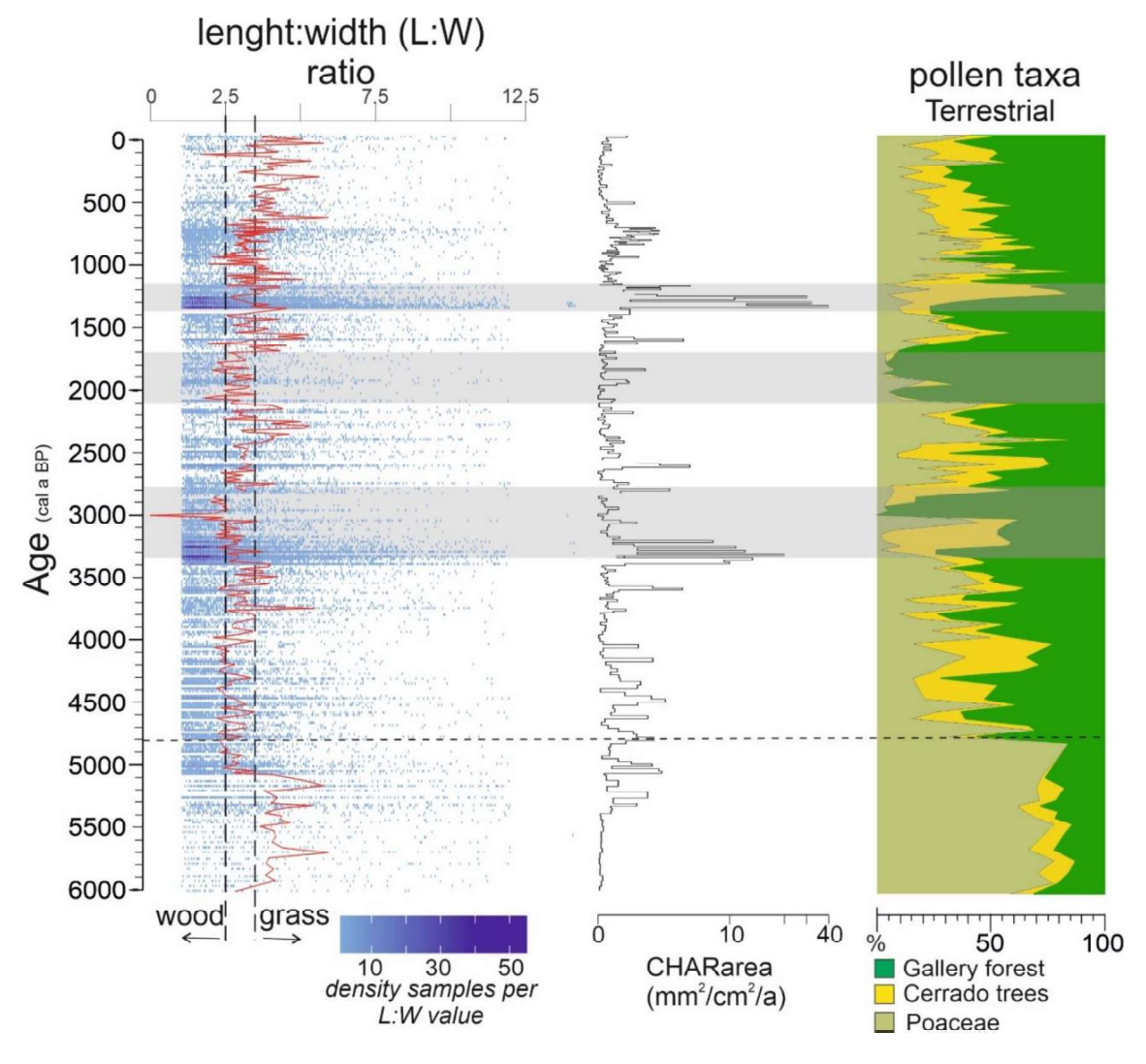


Figure S4. Changes in fire activity at Lake Feia during the last 6000 years, showing, from left to right, the time scale (cal a BP), L:W ratio, charcoal influx (CHARarea; mm2/cm2/a), a summary pollen diagram for the three main ecological groups. The dashed vertical lines shows the division between wood (<2.5)/grass (>3.5) origin of the charcoal particles (from Vachula et al., 2021), the dashed horizontal line shows when the vegetation cover changed from an open to a woody cerrado, and the gray bands show the dry intervals as identified by the palynological analysis.



References

- Araujo GM, Barbosa AAA, Arantes AA, Amaral AF. 2002. Composição floristica de veredas no Municipio de Uberlândia, MG. Revista Brassil. Bot. 25(4), 475-493.
- Araujo GM, Nascimento ART, Lopes SF, Rodrigues RF, Ratter JA. 2011. Structure and floristic of the arboreal components of dystrophic Cerradão and comparison with other Cerradões in Central Brazil. Edinburg Journal of Botany, 68(3), 401-418.
- Assunção SL, Feilfili JM. 2004. Fitossociologia de um fragmento de cerrado sensu stricto na APA do Paranoa, DF, Brasil. Acta bot. bras. 18 (4), 903-909.
- Bridgewater et al. 2004. Biogeographic patterns, B-diversity and dominnce in the cerrado biome of Brazil. Biodiversity and Conservation, 13, 2295-2318.
- Bueno ML, Neves DM, Souza AF, Junior EO, Damasceno Junior GA, Pontara V, Laura VA, Ratter JA. 2013. Influence of edaphic factors in the floristic composition of an area of cerradão in the Brazilian central-west. Acta Botanica Brazilica, 27(2),: 445 45.
- Bueno ML, Dexter KG, Pennington TR, Pontara V, Neves DM, Ratter JA, Oliveira-Filho AT. 2018. The environmental triangle of the Cerrado Domain: Ecological factors driving shifts in tree species composition between forest and savannas. Journal of Ecology, 12 p. doi: 10.1111/1365-2745.12969
- Carvalho DA, Martins RF. 2009. Shrub and tree species composition I n the Cerrados of southwest Minas Gerais. Cerna, Lavra 15(2), 142-154.
- Deus FF, Vale VS, Schia Vini I, Oliveira PE. 2014. Dyversity of reproductive ecological groups in semideciduous seasonal forests. Ûberlandia, 30(6), 1885 1902.
- Durigan G, Munhoz, CB, Zakia, MJB, Oliveira RS, Pilon NA, do Valle RST, Walter BMT, Honda EA, Pott A. 2022. Cerrado wetlands: multiple ecosystems deserving legal protection as a unique and irreplaceable treasure. Perspectives in ecology and conservation, 20 (3), 185-196.
- Felfili JM. 1995. Diversity, structure and dynamics of a gallery forest in central Brazil. VegatatioVegetatio, 117, 1-15.

- Felfili JM. 1997. Diameter and height distributions in a gallery forset tree community and some of its main species in central Brazil over a six-year period (1985-1991). Revista Brasileira de Botânica, 20(2),155-162.
- Felfili JM, da Silva Junior MC, Sevilha AC, Fagg CW, Walter BMT, Nogueira PE, Rezende AV. 2004. Diversity, floristic and structural patterns of cerrado vegetation in Central Brazil. Plant Ecology, 175, 37-46.
- Felfili JM, Silva Junior MC, Mendoça RC, Fagg WC, Filgueiras TS, Mecenas V. 2007. Composição floristica da estação ecologica de àguas Emendadas no Distrito Federal. Heringeriana, 1(2), 25-85.
- Martins FQ, Batalha MA. 2006. Pollination systems and floral traits in cerrado woody species of the upper Taquari region (central Brazil). Braz. J. Biol., 66 (2A), 543-552.
- Oliveira-Filho, A.T. and Ratter, J.A. 1995. A study of the origin of Central Brazilian forests by the analysis of plant species distribution patterns. Edinburg Journal of Botany, 52(2), 141-194.
- Pereira CC, Arruda DM, Soares FFS, Fonseca RS. 2022. The importance of pollination and dispersal syndromes for the conservation of Cerrado Rupestre fragments on ironstone outcrops immersed in an agricultural landscape. Neotropical Biology and Concervation, 17, 87 102.
- Rios MNS, Sousa-Silva JC. 2017. Grupos funcionais em áreas com histórico de queimadas em Cerrado sentido restrito no Distrito Federal. Brazilian Journal of Forestry Research, 37 (91), 285-298.
- Rossi CV, Silva Junior MC, Nacimento CE. 1998. Fitossociologia do estrato arboreo do Cerrado (sensu stricto) no parque Ecologico Norte, Brasilia -DF. Bol.Herb. Ezechias Paulo Hering. 2, 49-56
- Silva Junior JM, Nogueira PE, Felfili JJ. 1998. Flora lenhosa das mata de Galeria no Brasil Central. Bol.Herb. Ezechias Paulo Hering, 2, 57-76.
- Silva, M.C.J., and Felfili, J.M. 1998. A vegetação de Estação Ecologica de Aguas Emendadas. Brasilia DF

Vachula RS, Sae-Lim J, Li R. 2021. A critical of charcoal morphometry as a paleofire fuel type proxy. Quaternary Science Review, 262, 106979.